



TECHNISCHE
UNIVERSITÄT
DRESDEN

Statistical mechanics of time-periodic quantum systems

Dissertation
zur Erlangung des akademischen Grades
Doctor rerum naturalium

vorgelegt von

Waltraut Wustmann
geboren am 04.10.1982 in Dresden

Institut für Theoretische Physik
Fachrichtung Physik
Fakultät für Mathematik und Naturwissenschaften
Technische Universität Dresden
2010

Eingereicht am 3. Februar 2010

1. Gutachter: Prof. Dr. Roland Ketzmerick

2. Gutachter: Prof. Dr. Martin Holthaus

Verteidigt am _____

Abstract

The asymptotic state of a quantum system, which is in contact with a heat bath, is strongly disturbed by a time-periodic driving in comparison to a time-independent system. In this thesis an extensive picture of the asymptotic state of time-periodic quantum systems is drawn by relating it to the structure of the corresponding classical phase space. To this end the occupation probabilities of the Floquet states are analyzed with respect to their semiclassical property of being either regular or chaotic. The regular Floquet states are occupied with exponential weights $e^{-\beta_{\text{eff}} E^{\text{reg}}}$ similar to the canonical weights $e^{-\beta E}$ of time-independent systems. The regular energies E^{reg} are defined by the quantization of the time-periodic system, whose classical properties also determine the effective temperature $1/\beta_{\text{eff}}$. In contrast, the chaotic Floquet states acquire almost equal probabilities, irrespective of their time-averaged energy. Beyond these semiclassical properties the existence of avoided crossings in the spectrum is an intrinsic quantum property of time-periodic systems. Avoided crossings can strongly influence the entire occupation distribution. As an impressive application a novel switching mechanism is proposed in a periodically driven double well potential coupled to a heat bath. By a weak variation of the driving amplitude its asymptotic state is switched from the ground state in one well to a state with higher average energy in the other well.

Zusammenfassung

Der asymptotische Zustand eines Quantensystems, das in Kontakt mit einem Wärmebad steht, wird durch einen zeitlich periodischen Antrieb gegenüber einem zeitunabhängigen System nachhaltig verändert. In dieser Arbeit wird ein umfassendes Bild über den asymptotischen Zustand zeitlich periodischer Quantensysteme entworfen, indem es diesen zur Struktur des zugehörigen klassischen Phasenraums in Beziehung setzt. Dazu werden die Besetzungswahrscheinlichkeiten der Floquet-Zustände hinsichtlich ihrer semiklassischen Eigenschaft analysiert, nach welcher sie entweder regulär oder chaotisch sind. Die regulären Floquet-Zustände sind mit exponentiellen Gewichten $e^{-\beta_{\text{eff}} E^{\text{reg}}}$ ähnlich der kanonischen Verteilung $e^{-\beta E}$ zeitunabhängiger Systeme besetzt. Dabei sind die reguläre Energien E^{reg} durch die Quantisierung des Systems vorgegeben, dessen klassische Eigenschaften auch die effektive Temperatur $1/\beta_{\text{eff}}$ bestimmen. Die chaotischen Zustände dagegen haben fast einheitliche Besetzungswahrscheinlichkeiten, welche unabhängig von ihrer mittleren Energie sind. Über diese semiklassischen Eigenschaften hinaus ist das Auftreten von vermiedenen Kreuzungen im Spektrum eine intrinsisch quantenmechanische Eigenschaft zeitlich periodischer Systeme. Diese können die gesamte Besetzungsverteilung nachhaltig beeinflussen und finden eine eindrucksvolle Anwendung in Form eines neuartigen Schaltmechanismus in einem harmonisch modulierten Doppelmuldenpotential in Kontakt mit einem Wärmebad. Der asymptotische Zustand kann unter geringer Variation der Antriebsamplitude vom Grundzustand der einen Mulde in einen Zustand höherer mittlerer Energie in der anderen Mulde geschaltet werden.

Contents

1	Introduction	1
2	Time-periodic systems	7
2.1	Floquet theory	8
2.1.1	Floquet states and their properties	8
2.1.2	Extended phase space and composite Hilbert space	9
2.1.3	Methods of solution	12
2.2	Quantum maps: One-dimensional periodically kicked systems	13
2.2.1	Kicked rotor	14
2.2.2	Quantization on the torus	16
2.2.3	Husimi representation	18
2.3	Semiclassical quantization for the regular islands	20
2.3.1	Single island	20
2.3.2	Island chain of a nonlinear resonance	23
3	Statistical mechanics of time-periodic systems	27
3.1	Floquet-Markov master equation	28
3.1.1	Microscopic dissipation model	29
3.1.2	Equation of motion for $\rho(t)$ and Born-Markov approximation	30
3.1.3	Floquet-Markov master equation	33
3.2	Effective rate R^{ac} at avoided crossings	36
3.2.1	Diabatic states of the avoided crossing	37
3.2.2	Diabatic representation of the rate equation	38
3.3	Displaced signatures of avoided crossings due to Lamb shifts	42
3.4	Diffusion in the extended zone scheme	44
3.4.1	Random walk	44
3.4.2	Energy absorption	50
4	Statistical mechanics of time-periodic systems with a mixed phase space	53
4.1	Occupations of regular and chaotic Floquet states	55
4.1.1	Driven quartic oscillator	55
4.1.2	Kicked rotor	57
4.1.3	Rate matrix	59
4.2	Regular states	60
4.2.1	Quality of the exponential fits	61
4.2.2	Effective temperature $1/\beta_{\text{eff}}$	62
4.2.3	Quality of the detailed balance assumption	68
4.2.4	Dependence of β_{eff} on the winding number ν	70

4.3	Additional classical phase-space structures	73
4.3.1	Independent islands	73
4.3.2	Nonlinear resonances	74
4.3.3	Beach states	79
4.3.4	Hierarchical States	79
4.4	Chaotic states	82
4.4.1	Distribution of the chaotic Floquet occupations	82
4.4.2	A random-rate model for the chaotic occupations	87
4.4.3	Influence of dynamical localization	90
4.5	System-bath interaction and symmetry	94
5	Occupations at avoided crossings and bath-induced switching	99
5.1	Switching in a double well potential	100
5.1.1	Inspection of the Floquet occupations	101
5.1.2	Explanation based on the effective rate R^{ac}	103
5.1.3	Switching efficiency and parameter study	104
5.1.4	Displaced signatures of avoided crossings	110
5.2	General occupation characteristics at avoided crossings	113
5.3	Switching between independent islands	116
5.4	Analytical model for the signatures of avoided crossings	118
6	Summary and outlook	121
A	The harmonic oscillator heat bath	125
A.1	Quantum Langevin equation	125
A.2	Correlation function	127
B	Derivation of the Floquet-Markov master equation and its asymptotics	130
B.1	Evolution of the density operator	130
B.2	Born-Markov approximation	132
B.3	Master equation in Floquet representation	135
B.4	Rate equations for the asymptotic state	138
B.5	Some properties of Eqs. (B.47) and (B.56)	140
C	Lamb shifts in the Floquet-Markov master equation	142
D	Rate equations at avoided crossings	145
E	Rate equations at avoided crossings including Lamb shifts	150
F	Rate balance among the resonance states	152

1 Introduction

The response of a dynamical system to a time-periodic driving force is ubiquitous in both classical and quantum mechanics and plays a fundamental role in many physical and technical applications. Examples of classical motion under time-periodic driving include the action of varying electromagnetic fields on single particles or in electrical circuits, being a cornerstone of information processing. Besides, almost all spectroscopic techniques are based on the application of oscillating fields. Since the invention of the laser and its application to such diverse microscopic systems, e.g. in quantum optics and quantum chemistry, the interest in the response of quantum systems to time-periodic forces steadily increased. It opened the field for the coherent control of atoms and molecules [1–4], the optimal control of chemical reactions [5–7], or the manipulation of semiconductor-nanodevices and heterostructures in solids [8–10], and also fostered the development of theoretical concepts and computational methods.

Under realistic, non-idealized conditions real physical systems interact with their environment. The hypothesis of isolated systems then often fails and leaves the task to either determine the full dynamics of the composite system or, if this is not viable due to the vast number of external degrees of freedom, to interpret the system as an open subsystem in mutual contact with a heat bath. To evaluate the reduced dynamics of the subsystem two main alternative strategies are conventionally utilized: firstly, a quantum stochastic Schrödinger equation is written for the state vector of the subsystem [11–13] in analogy to the classical Langevin equation, or alternatively a quantum master equation is established for the reduced density operator ρ , which corresponds classically to a Fokker-Planck equation. To evaluate the evolution of ρ for an open quantum system in a time-varying, strong external field, where the competing forces of the coherent quantum evolution and the incoherent damping are further enriched by the external driving force, is a nontrivial task, as it is permanently driven out of equilibrium. For only very few systems exact analytical solutions of the damped dynamics are feasible, in particular a driven two-level system [14,15] and a harmonic oscillator driven by an additive periodic force [16] or by periodic variation of a parameter [17]. In other examples the exactly solvable time-evolution of ρ follows as an immediate consequence of a quantum nondemolition coupling to the heat bath [18], where the interaction term commutes with the system Hamiltonian and which is known to inhibit relaxation to an equilibrium state [19].

The relaxation process of the reduced density operator ρ , where quantum-mechanical signatures are made transient by the interaction with the environment and gradually fade out, has been studied extensively, e.g. with focus on tunneling, see Ref. [20] and references therein. Especially in the regime of weak interaction with the environment, standard methods, originally established for time-independent quantum systems, have been adapted to the demands of time-periodic systems [21–25], but also strongly damped systems have been

investigated [26, 27].

Beyond the transient phenomena, however, the final state of the relaxation process has not received comparable attention in the literature, although this can be ranked as even more fundamental and is in fact a core question of statistical mechanics. The usual thermodynamic concepts for the equilibrium state of time-independent systems are not applicable, such as the canonical distribution of Boltzmann weights, reached in the stationary limit of a time-independent system, that is weakly coupled to a heat bath. The Boltzmann weights $e^{-\beta E_n}$ of the eigenstates are unique functions of the eigenenergy with the temperature $1/\beta = k_B T$ of the heat bath as the only relevant parameter, whereas microscopic details of the weak coupling play no role. Such a stationary limit, in the sense of convergence to time-independent values for all dynamical variables, is not encountered in a periodically driven system, where energy is permanently pumped into the system and is eventually absorbed by the environment. In place of the stationary state of time-independent systems the relaxation process finally leads to an asymptotic state that adopts the periodicity of the driving. In general it depends on the microscopic details of the coupling. The goal of this study is to contribute to the understanding of the asymptotic state in time-periodic quantum systems.

The density operator of the time-periodic subsystem is best represented in the Floquet state basis. The Floquet states are quasi-periodic solutions of the Schrödinger equation for the time-periodic Hamiltonian. They can be factorized into a product $e^{-i\varepsilon t/\hbar}|u(t)\rangle$ of a periodic state $|u(t + \tau)\rangle = |u(t)\rangle$ with the period τ of the Hamiltonian and a phase factor with the quasienergy ε . The Floquet states, which in some sense take the place of the eigenstates of time-independent systems, form an orthonormal basis at all times t . In this Floquet basis the evolution equation for the density matrix takes a similar form as in time-independent systems. It can be approximated within the *Floquet-Markov* approach [21–25] by a Markovian quantum master equation, that is of second-order in the system-bath coupling and local in time. The dynamics in the long-time limit of the evolution is then described by a system of rate equations for the constant asymptotic density matrix. In this thesis, such rate equations are used to determine the statistical weights of the Floquet states, i.e. the probabilities with which they are asymptotically occupied. Beyond the sole numerical evaluation of such a master equation, an intuitive understanding of these Floquet occupations is still lacking. An analysis with respect to appropriate classical or quantum-mechanical quantities of the underlying isolated system would therefore help the interpretation or even the prediction of the Floquet occupations. In the special, non-generic case of an additively driven harmonic oscillator, where also the Floquet problem is exactly solvable [28, 29], the evolution and asymptotic state of ρ can be related to a classical trajectory and limit cycle [16]. This thesis aims to shed some further light in that direction, by establishing a relation of the Floquet occupations in the time-periodic system to the phase-space structure of the corresponding classical system.

In periodically driven systems generically regular and chaotic motion coexist. This coexistence is most clearly reflected in phase space, where on the one hand regular trajectories evolve on invariant tori in a stable, predictable motion, whereas in contrast the erratic motion of chaotic trajectories depends sensitively on the initial conditions: chaotic trajectories, that are initially neighboring in phase space, separate exponentially when evolving in time. The phase-space structure is a key to the understanding not only of classical properties, but also of properties inherent to the quantum regime. The reason is, according to the semiclassical eigenfunction hypothesis [30–32], that the classical distinction of regular vs. chaotic motion is reflected in the quantum regime: almost all Floquet states can be classified as either regular or chaotic, provided that the corresponding phase-space areas are larger than Planck’s constant. The regular states localize on the regular regions of phase space and the chaotic states typically spread out over the whole chaotic area. A further signature of the mixed classical phase space is observed in the level spacing distribution of the Floquet eigenphases, which are of fundamentally different character for the two subsets of regular and chaotic Floquet states [33, 34].

Are the ubiquitous signatures of the classical phase space reflected also in the density matrix of the Floquet states? Studies on a driven particle in a box [23] give evidence for an answer in the affirmative: the Floquet occupations of regular and chaotic states follow different statistical distributions. The regular states carry almost Boltzmann weights, whereas all chaotic states have nearly the same occupation probability. In this thesis, these findings are investigated in further detail for typical Floquet systems with either continuous or kicked type of time-dependence. In contrast to the studies in Ref. [23], where the regular states differ only slightly from the eigenstates of the undriven system, we concentrate on situations characteristic for strong driving, where both phase space and Floquet states are strongly perturbed compared to the originally time-independent system. We demonstrate that the Floquet occupations of the states in a regular island under these conditions deviate considerably from the Boltzmann result. In many cases, however, their distribution can be well approximated by weights of the Boltzmann type $e^{-\beta_{\text{eff}} E^{\text{reg}}}$. This involves the definition of the *regular energies* E^{reg} , which are semiclassical invariants of the quantizing tori in the regular islands. The parameter $1/\beta_{\text{eff}}$ is the corresponding temperature and is an approximate function of the winding number in the regular island. Furthermore, we give an overview and interpretation for the implications of some of the most prevailing features in a mixed phase space, such as resonance island chains, stickiness, and partial barriers.

The Floquet states do not diagonalize the density operator once the strength of the system-bath coupling grows larger than the minimal quasienergy spacing. In fact, this situation is generic for Floquet systems even for arbitrary small, but finite coupling strength, since the quasienergies are bounded within a finite interval, $0 \leq \varepsilon < \hbar\omega$, and, as a consequence, the number of avoided crossings grows without limit for increasing Hilbert space

dimension [35,36]. It is therefore instructive to ask, how ρ behaves especially at such points of near degeneracy. As shown in Ref. [25], the reduced density operator is not affected by a small avoided crossing, provided that it is smaller than a specific effective coupling parameter and so is not ‘resolved’ by the heat bath. These findings justify the truncation of the, in general, infinite Hilbert dimension of the time-periodic system. In this thesis we focus on the opposite limit, where the quasienergy spacing at the avoided crossing exceeds the effective coupling strength, and demonstrate how this affects not only the occupations of the two involved Floquet states, but changes the whole character of the occupation distribution. This phenomenon can be exploited for a switching mechanism in driven quantum systems, as we demonstrate for a particle in a bistable system. By a weak periodic driving, that is in fact even much weaker than the asymmetry of the static system, a practically complete probability transfer from the lower to the upper well is induced [37]. An intuitive explanation of this impressive phenomenon is based on Ref. [25], where the authors introduce a set of effective rate equations with an additional rate R^{ac} for the Floquet occupations at an avoided crossing.

The back action of the heat bath on the system in general leads to a renormalization of the system energies, usually paraphrased as the *Lamb shifts* in reference to quantum optics. Although these can cause deviations from the canonical distribution even in the framework of time-independent systems [38,39], their contribution is often disregarded, like also in the Floquet-Markov master equation. Concluding from our previous studies, the Floquet occupations are particularly sensitive to the exact values of the involved quasienergies in the vicinity of an avoided crossing, and the Lamb shifts are therefore expected to become important especially there. We introduce a modified Floquet-Markov master equation, now also including the Lamb shift contributions. By their presence, the switching effect can be displaced, i.e. the switching can take place at a parameter value far away from the actual position of the avoided crossing. Again, an intuitive explanation is possible with the help of a new rate R^{ac} , now also accounting for the Lamb shifts.

This thesis is organized as follows: basic properties of isolated systems with periodic time-dependence are outlined in chapter 2, starting with the Floquet theory (Section 2.1). Section 2.2 introduces quantum kicked systems as particularly advantageous model systems. We also briefly review basic characteristics of the classical phase space as well as the quantization procedure in these systems. We conclude the chapter with a survey of the semiclassical quantization in time-periodic systems (Section 2.3).

Chapter 3 continues to develop the models, now taking into account the interaction with a heat bath. It starts with a brief sketch of the Floquet-Markov theory of open time-periodic systems in Section 3.1. A more detailed derivation can be found in Appendix B. It eventually leads to the rate equations (3.26) for the asymptotic density matrix ρ_{ij} in Floquet representation, which is employed as the central means of our numerical as well

as analytical studies. An approximation of the rate equation with the effective rate R^{ac} can be employed in the vicinity of an isolated avoided crossing in the quasienergy spectrum (Section 3.2 and Appendix D). In order to study the effect of Lamb shifts on ρ_{ij} , we include those into a modified version of the Floquet-Markov master equation and derive the corresponding approximate rate equation at avoided crossings (Section 3.3). Technical details are deferred to Appendices C and E. In Section 3.4 it is intended to complement the Floquet-Markov approach by another method which is based on a random walk in the space of the quasienergies. Within this model we relate the dissipation process to a biased diffusion on the energy axis and evaluate drift and diffusion constants.

Chapter 4 is the first of the two central chapters of this thesis. In Section 4.1, we survey the general properties of the asymptotic Floquet occupations $p_i \equiv \rho_{ii}$ and characterize them with respect to signatures of the classical phase space. The occupations of the regular states are analyzed as functions of the regular energy in Section 4.2 and we derive an approximation for their distribution in terms of Boltzmann-like weights. Furthermore, we investigate the implications of additional phase-space structures in Section 4.3 and of the chaotic states in Section 4.4. The chapter is closed by a brief inspection of alternative models for the system-bath coupling operator.

The next chapter, Chapter 5, combines studies related to avoided crossings in the quasienergy spectrum. In Section 5.1 we demonstrate a bath-induced switching mechanism in a periodically driven bistable system based on the presence of an avoided crossing. Sections 5.2-5.4 use these findings to explain the effect of avoided crossings in the Floquet occupations of quantum kicked systems and establish a simplified, analytically solvable model. Finally, a summary of the thesis and future perspectives are given in Chapter 6.

2 Time-periodic systems

In this chapter basic properties of time-periodic systems are outlined. Quantum systems in external time-dependent fields are intensively studied in physics and chemistry. Strong driving can induce completely new signatures in the dynamics of the quantum system. Photoionization or induced chemical reactions are frequently encountered examples. A more subtle example is the coherent destruction of tunneling [2, 40], where the internal tunneling dynamics can be stalled almost completely by a coherent driving.

Starting with the application to the periodically driven two-level system [41], quantum-mechanical systems interacting with intense oscillating fields have been successfully analyzed on the basis of Floquet's theory for linear differential equations with periodic coefficients [42]. The Floquet formalism ensures a non-perturbative treatment of the system's dynamics. The driving field is treated classically without explicit field quantization, a description that is possible for intense fields with negligible fluctuations in the photon number. A brief survey of the Floquet formalism is presented in Section 2.1.

Generic time-periodic systems are non-integrable, i.e. there exist fewer constants of motion than degrees of freedom N . In contrast to one-dimensional autonomous systems, which are always integrable, the resulting chaotic or mixed regular-chaotic dynamics is already seen in time-periodic systems with only one degree of freedom, like one-dimensional kicked systems, where a δ -kick potential acts on the system only once in a period for an infinitesimally short time span. This reduced dimensionality together with the numerical simplicity makes them an attractive means of study in the fields of nonlinear dynamics and quantum chaos, see e.g. Refs. [43–45]. Their classical dynamics is completely determined by a stroboscopic map. The numerical treatment of the quantum mechanical evolution is comparably simple, as the time-evolution operator splits into a product of a kinetic and a potential contribution. We sketch general properties of kicked systems as well as their quantization in Section 2.2.

Due to the perturbed integrability, not all trajectories in a time-periodic system are confined to N -dimensional invariant tori. Nonetheless, in the generic case regular regions in phase space with prevailing invariant tori still exist. These may support regular states, which together with their associated quasienergies can be approximated within a semiclassical quantization. In Section 2.3 we give a short summary on the semiclassical quantization in time-periodic systems and introduce the regular energies E^{reg} used later in this thesis.

Before starting, it is helpful to mention that all quantities throughout this thesis are understood to be dimensionless. To this end we introduce the dimensionless quantities $\tilde{x} = x/x_0$, $\tilde{H} = H/V_0$, $\tilde{p} = p/p_0$ with $p_0 = \sqrt{mV_0}$, $\tilde{t} = t \cdot p_0/(x_0m)$, and $\tilde{\omega} = \omega \cdot (x_0m)/p_0$, based on the system-typical values x_0 , V_0 and t_0 . The corresponding effective Planck constant $\tilde{h} = h/(x_0p_0)$ is the ratio of Planck's constant to a typical phase space area and $\tilde{h} = 2\pi\tilde{h}$. Since all quantities are dimensionless, we omit the tilde and no explicit notation for the dimensionless variables is employed.

2.1 Floquet theory

2.1.1 Floquet states and their properties

The dynamics of a nonrelativistic quantum system is ruled by the time-dependent Schrödinger equation

$$i\hbar \frac{\partial}{\partial t} |\psi(t)\rangle = H(t) |\psi(t)\rangle \quad (2.1)$$

for the state vector $|\psi(t)\rangle$. Its formal solution $|\psi(t)\rangle = U(t, t_0)|\psi(t_0)\rangle$, introduces the time evolution operator

$$U(t, t_0) = \hat{\mathcal{T}} \exp \left(-\frac{i}{\hbar} \int_{t_0}^t dt' H(t') \right) , \quad (2.2)$$

which itself is a solution of the Schrödinger equation, $i\hbar \partial_t U(t, t_0) = H(t)U(t, t_0)$, with the initial condition $U(t_0, t_0) = \mathbb{1}$. The time-ordering operator $\hat{\mathcal{T}}$ accounts for the possible non-commutativity of $H(t)$ at different times t .

If the Hamiltonian $H(t)$ is explicitly time-dependent the separation $|\psi_n(t)\rangle = e^{-iE_n t/\hbar} |\varphi_n\rangle$ into a time-dependent phase-factor and the stationary state $|\varphi_n\rangle$ in general fails. Energy is no longer a conserved quantity since $H(t)$ is not invariant under an arbitrary shift in time. A special case is a time-periodic Hamiltonian, which is invariant under the particular time shift of the period τ ,

$$H(t + \tau) = H(t) . \quad (2.3)$$

According to the Floquet theorem [42, 46, 47], the Schrödinger equation (2.1) with a periodic Hamiltonian has a complete set of solutions $|\psi_i(t)\rangle$, that are separable into a product of a phase factor $e^{-i\varepsilon_i t/\hbar}$ and a time-periodic state vector $|u_i(t + \tau)\rangle = |u_i(t)\rangle$, i.e.

$$|\psi_i(t)\rangle = e^{-i\varepsilon_i(t-t_0)/\hbar} |u_i(t)\rangle . \quad (2.4)$$

The real-valued phases ε_i are called *quasienergies*, reflecting the formal analogy of the *Floquet states* (2.4) to the Bloch eigenstates $\phi_{nk}(x + a) = e^{ika} \phi_{nk}(x)$ of spatially periodic quantum systems with the quasimomentum k . Likewise, the Floquet states are quasi-periodic in time,

$$|\psi_i(t + \tau)\rangle = e^{-i\varepsilon_i \tau/\hbar} |\psi_i(t)\rangle . \quad (2.5)$$

Inserting the Floquet solutions (2.4) into the Schrödinger equation yields an equation for the periodic components $|u_i(t)\rangle$,

$$\left(H(t) - i\hbar \frac{\partial}{\partial t} \right) |u_i(t)\rangle = \varepsilon_i |u_i(t)\rangle . \quad (2.6)$$

The factorization (2.4) of the Floquet state is not unique, but has infinitely many equivalent realizations: the transformation $|u_i(t)\rangle \rightarrow |u_i^{(q)}(t)\rangle = e^{iq\omega t} |u_i(t)\rangle$ with $q \in \mathbb{Z}$ conserves

the time-periodicity of the states $|u_i^{(q)}(t)\rangle$ and leaves the Floquet state $|\psi_i(t)\rangle$ unchanged if it is accompanied by the shift $\varepsilon_i \rightarrow \varepsilon_i^{(q)} = \varepsilon_i + q\hbar\omega$ of the associated quasienergy. In this thesis we understand $|u_i(t)\rangle \equiv |u_i^{(0)}(t)\rangle$ with the quasienergy $\varepsilon_i \equiv \varepsilon_i^{(0)}$ lying in the first ‘Brillouin zone’, $\varepsilon_i \in [0, \hbar\omega)$, again an expression borrowed from the Bloch theory.

For the time-periodic Hamiltonian (2.3) the one-period propagator $U(t_0 + \tau, t_0)$ is of particular significance. Expressed in terms of the Floquet solutions (2.4) it reads

$$U(t_0 + \tau, t_0) = \sum_i e^{-i\varepsilon_i\tau/\hbar} |u_i(t_0 + \tau)\rangle \langle u_i(t_0)| = \sum_i e^{-i\varepsilon_i\tau/\hbar} |u_i(t_0)\rangle \langle u_i(t_0)|, \quad (2.7)$$

where the second equality uses the time-periodicity of states $|u_i(t)\rangle$. Its eigenvectors are recognized as the Floquet states $|\psi_i(t_0)\rangle$, as they are identical to the $|u_i(t_0)\rangle$ at t_0 and evolve quasi-periodically in time,

$$|\psi_i(t_0 + \tau)\rangle = U(t_0 + \tau, t_0)|\psi_i(t_0)\rangle = e^{-i\varepsilon_i\tau/\hbar}|\psi_i(t_0)\rangle. \quad (2.8)$$

While the energy is not a conserved quantity for an explicitly time-dependent Hamiltonian, it is sometimes convenient to introduce the cycle-averaged energy $\langle E_i \rangle_\tau$ of a Floquet state,

$$\langle E_i \rangle_\tau := \frac{1}{\tau} \int_t^{t+\tau} dt' \langle u_i(t') | H(t') | u_i(t') \rangle \quad (2.9)$$

$$\stackrel{(2.6)}{=} \varepsilon_i + \frac{1}{\tau} \int_t^{t+\tau} dt' \langle u_i(t') | i\hbar \frac{\partial}{\partial t} | u_i(t') \rangle, \quad (2.10)$$

i.e. the energy averaged over the period τ . It can be evaluated as

$$\langle E_i \rangle_\tau = \varepsilon_i - \sum_K \hbar\omega K \langle u_i(K) | u_i(K) \rangle \quad (2.11)$$

from the Fourier decomposition of the periodic states

$$|u_i(t)\rangle = \sum_K e^{iK\hbar\omega t} |u_i(K)\rangle. \quad (2.12)$$

2.1.2 Extended phase space and composite Hilbert space

In classical mechanics, an explicitly time-dependent system is equivalent to an autonomous system with an additional degree of freedom. In the *extended phase space* $\{(x, t, p, p_t)\}$, where the time t is treated as an additional coordinate with the conjugate momentum p_t , the generalized Hamiltonian function

$$\mathcal{H}(x, p, t, p_t) := H(x, p, t) + p_t \quad (2.13)$$

takes over the role of a the the Hamiltonian function $H(t)$ of the conventional phase space. The Hamiltonian flow generated by $\mathcal{H}(x, p, t, p_t)$ is parametrized in terms of a new variable s and the equations of motion in the extended phase space read

$$\frac{dp}{ds} = -\frac{\partial\mathcal{H}}{\partial x} = -\frac{\partial H}{\partial x} \quad (2.14)$$

$$\frac{dx}{ds} = \frac{\partial\mathcal{H}}{\partial p} = \frac{\partial H}{\partial p} \quad (2.15)$$

$$\frac{dp_t}{ds} = -\frac{\partial\mathcal{H}}{\partial t} = -\frac{\partial H}{\partial t} \quad (2.16)$$

$$\frac{dt}{ds} = \frac{\partial\mathcal{H}}{\partial p_t} = 1. \quad (2.17)$$

\mathcal{H} is a conserved quantity under this flow, $d\mathcal{H}/ds = \partial\mathcal{H}/\partial s = 0$, although the Hamiltonian function $H(t)$ is not a conserved quantity of the time-evolution in the conventional phase space.

For a time-periodic system, this extension to a higher-dimensional space is particularly advantageous. In this context the generalized Hamiltonian function (2.13) is sometimes termed the *Floquet function*. In the integrable case, all trajectories evolve on τ -periodic vortex tubes Λ^{N+1} , that are invariant under the flow and that are embedded in a quasienergy-shell $\{(x, t, p, p_t) \mid \mathcal{H}(x, t, t, p_t) = \varepsilon\}$. Here, Λ^{N+1} denotes a non-compact $(N+1)$ -dimensional cylinder that is based on a N -torus \mathbb{T}^N in the conventional phase space \mathbb{R}^{2N} .

Corresponding to the extension of the coordinate space in classical mechanics, the Hilbert space \mathcal{R} of the quantum-mechanical states $|\psi_i(t)\rangle$ can be extended to a composite Hilbert space $\mathcal{R} \otimes \mathcal{T}$ [41, 48]. \mathcal{T} is the Hilbert space of τ -periodic functions $a(t) = a(t + \tau)$ that have a finite norm $\|a\|_\tau^2 = \langle a|a\rangle_\tau$ with respect to the inner product

$$\langle a|b\rangle_\tau := \frac{1}{\tau} \int_0^\tau dt a^*(t) b(t). \quad (2.18)$$

The set of states $|K\rangle_\tau$ ($K = 0, \pm 1, \pm 2, \dots$) with $\langle t|K\rangle_\tau = e^{iK\omega t}$ constitutes a complete and orthonormal basis in \mathcal{T} . The inner product of the states $|u\rangle_\tau, |v\rangle_\tau$ in the composite Hilbert space is then defined in a natural way by

$$\langle\langle u|v\rangle\rangle_\tau := \frac{1}{\tau} \int_0^\tau dt \langle u(t)|v(t)\rangle \quad (2.19)$$

with $|u(t)\rangle = \langle t|u\rangle_\tau$ and $|v(t)\rangle = \langle t|v\rangle_\tau$. Note, that in later sections we will omit the double bracket for the inner product, when the assignment to the composite Hilbert space is evident. A complete and orthonormal basis in the composite Hilbert space is constituted by the set of product states $|nK\rangle_\tau := |n\rangle \otimes |K\rangle_\tau$, composed of the basis states $|n\rangle$ ($n = 0, 1, 2, \dots$) in \mathcal{R} and the basis states $|K\rangle_\tau$ ($K = 0, \pm 1, \pm 2, \dots$) in \mathcal{T} .

The correspondence $p \rightarrow -i\hbar\partial/\partial x$ and $p_t \rightarrow -i\hbar\partial/\partial t$ translates the Floquet func-

tion (2.13) into the *Floquet operator* \mathcal{H} , with the coordinate-time representation

$$\mathcal{H}(t) = H(t) - i\hbar \frac{\partial}{\partial t} . \quad (2.20)$$

It is Hermitian, i.e. it fulfills $\langle\langle u|\mathcal{H}v \rangle\rangle_\tau = \langle\langle \mathcal{H}u|v \rangle\rangle_\tau$ for any states $|u\rangle_\tau, |v\rangle_\tau$ in the extended Hilbert space $\mathcal{R} \otimes \mathcal{T}$, and acts as the generator of the evolution

$$i\hbar \frac{\partial}{\partial s} |\psi(s)\rangle\rangle_\tau = \mathcal{H} |\psi(s)\rangle\rangle_\tau \quad (2.21)$$

with the formal solution

$$|\psi(s)\rangle\rangle_\tau = e^{-i\mathcal{H}\cdot(s-s_0)/\hbar} |\psi(s_0)\rangle\rangle_\tau . \quad (2.22)$$

When evaluating the state (2.22) on the cut $s = t$ with $\partial s/\partial t = 1$, it is projected down to the conventional Hilbert space,

$$|\psi(t)\rangle = \langle t|\psi(s)\rangle\rangle_\tau \Big|_{s=t} , \quad (2.23)$$

and is a solution of the Schrödinger equation there:

$$\begin{aligned} i\hbar \frac{\partial}{\partial t} |\psi(t)\rangle &= i\hbar \frac{\partial}{\partial t} \langle t|\psi(s)\rangle\rangle_\tau \Big|_{s=t} \\ &= \left(i\hbar \frac{\partial}{\partial t} + i\hbar \frac{\partial s}{\partial t} \frac{\partial}{\partial s} \right) \langle t|\psi(s)\rangle\rangle_\tau \Big|_{s=t} \\ &\stackrel{(2.21)}{=} \left(i\hbar \frac{\partial}{\partial t} + \mathcal{H}(t) \right) \langle t|\psi(s)\rangle\rangle_\tau \Big|_{s=t} \\ &= H(t) |\psi(t)\rangle . \end{aligned} \quad (2.24)$$

The comparison of the Floquet operator (2.20) with Eq. (2.6) shows that its eigenequation is equivalent to the Schrödinger equation (2.1) with a time-periodic Hamiltonian (2.3) and is solved by the time-periodic parts $|u_i(t)\rangle$ of the Floquet states,

$$\mathcal{H}(t) |u_i(t)\rangle = \varepsilon_i |u_i(t)\rangle . \quad (2.25)$$

Being the eigenvalues of the Hermitian operator \mathcal{H} , the quasienergies ε_i are real-valued, and the eigenstates $|u_i(t)\rangle$ constitute a complete and orthonormal basis in $\mathcal{R} \otimes \mathcal{T}$. That in turn means that the time-periodic states $|u_i(t)\rangle$ form also in \mathcal{R} a complete orthonormal basis at any time t .

The formulation of the Schrödinger equation in the composite Hilbert space is advantageous, as it allows to make use of methods and concepts from autonomous quantum systems. In fact, using the analogy between the eigenequation (2.25) on the one hand and the conventional time-independent Schrödinger equation on the other hand, quantum-mechanical

theorems can be extended to time-periodic systems [48], such as the variational principle or the Hellmann-Feynman theorem. The states $|u_i(t)\rangle$ adopt the role of the stationary states of time-independent systems. A further advantage is the possible application of the evolution equation (2.21) to non-periodic drivings, e.g. for chirped laser pulses with varying frequency, since it separates the different time scales: the coordinate time t is associated with the short time scale of the driving itself, whereas the parameter time s accounts for the longer time scale of changes of the driving parameters. This separation of time scales allows on the one hand for a very efficient numerical solution by means of the (t, t') -method, see below. On the other hand, it provides the means for the formulation of an adiabatic theorem similar to its equivalent in time-independent systems [49].

2.1.3 Methods of solution

A. Floquet matrix method

The Floquet operator \mathcal{H} can be diagonalized numerically by an expansion in an appropriate basis set $|nK\rangle_\tau = |n\rangle \otimes |K\rangle_\tau$ ($n = 0, 1, 2, \dots$, $K = 0, \pm 1, \pm 2, \dots$) with the Fourier states $|K\rangle_\tau$. The corresponding representation of the Floquet operator reads

$$\begin{aligned} \langle\langle nK | \mathcal{H} | mL \rangle\rangle_\tau &= \frac{1}{\tau} \int_0^\tau dt \langle K | t \rangle_\tau \left(\langle n | H(t) | m \rangle - i\hbar \frac{\partial}{\partial t} \delta_{nm} \right) \langle t | L \rangle_\tau \\ &= \frac{1}{\tau} \int_0^\tau dt \langle n | H(t) | m \rangle e^{i(L-K)\omega t} + L\hbar\omega \delta_{KL} \delta_{nm}, \end{aligned} \quad (2.26)$$

e.g. for the dipole interaction with a monochromatic field, $H(t) = H^{(0)} + x \cdot A \cos(\omega t)$,

$$\langle\langle nK | \mathcal{H} | mL \rangle\rangle_\tau = H_{nm}^{(0)} \delta_{LK} + x_{nm} \cdot \frac{A}{2} (\delta_{L, K+1} + \delta_{L, K-1}) + L\hbar\omega \delta_{KL} \delta_{nm}. \quad (2.27)$$

In this representation, Eq. (2.25) translates into the eigenequation

$$\sum_{m,L} \left(H_{nm}(L-K) + L\hbar\omega \delta_{nm} \delta_{K,L} \right) \langle m | u_i(L) \rangle = \varepsilon_i \langle n | u_i(K) \rangle \quad (2.28)$$

for the coefficients $\langle n | u_i(K) \rangle = \langle nK | u_i \rangle_\tau$ in the Fourier expansion of the time-periodic states $|u_i(t)\rangle = \sum_K e^{iK\omega t} |u_i(K)\rangle$.

B. Propagator methods

Apart from the diagonalization of the Floquet operator \mathcal{H} , the Floquet states can be equally determined as the eigenstates of the propagator $U(t_0 + \tau, t_0)$. The most simple way to set up $U(t_0 + \tau, t_0)$ is a factorization of $U(t_0 + \tau, t_0)$ into a kinetic and a potential part. This split operator method is exact for kicked quantum systems, considered in Section 2.2. It is,

however, in general an inadequate approximation for continuously driven systems due to the non-commutativity of the kinetic and potential operator parts of $H(t)$. A more appropriate approximation is the unitary expansion

$$U(t + \delta, t) = \left(1 + \frac{i}{2\hbar} H(t)\delta\right)^{-1} \left(1 - \frac{i}{2\hbar} H(t)\delta\right) + \mathcal{O}(\delta^3) . \quad (2.29)$$

The period τ may be divided into N_t intervals of length $\delta = \tau/N_t$ and, using the semi-group property

$$U(t_2, t_1) = U(t_2, t')U(t', t_1) , \quad (2.30)$$

the propagator factorizes into a series of short-time propagators,

$$U(t_0 + \tau, t_0) = U(t_0 + N_t\delta, t_0 + (N_t - 1)\delta) \cdots U(t_0 + 2\delta, t_0 + \delta) \cdot U(t_0 + \delta, t_0) , \quad (2.31)$$

for each of which the approximation (2.29) may be utilized.

A very efficient method to solve the eigenequation for $U(t_0 + \tau, t_0)$ is the (t, t') -method [50, 51]. As indicated by the name, it relies on the separation of different time scales in the composite Hilbert space. The propagator $e^{-i\mathcal{H}\cdot(s-s_0)/\hbar}$ in $\mathcal{R} + \mathcal{T}$ is expanded in the $|nK\rangle_{\tau}$ -basis and projected to the conventional Hilbert space. For the propagator $U(t, t_0)$ in \mathcal{R} , this basically amounts to the Fourier expansion of the matrix elements,

$$U_{nm}(t, t_0) = \sum_K e^{iK\omega t} \langle\langle nK | e^{-i\mathcal{H}\cdot(t-t_0)/\hbar} | m0 \rangle\rangle_{\tau} . \quad (2.32)$$

The Fourier expansion accounts for the dependence of \mathcal{H} on the coordinate time t with the expansion coefficients $\langle\langle nK | \mathcal{H} | mL \rangle\rangle_{\tau}$ of Eq. (2.26). Only the parameter time appears explicitly in the exponent. That is why each of the short-time propagators $U(t + \delta, t)$ for time intervals of the same length δ ,

$$U_{nm}(t + \delta, t) = \sum_K e^{iK\omega(t+\delta)} \langle\langle nK | e^{-i\mathcal{H}\cdot\delta/\hbar} | m0 \rangle\rangle_{\tau} , \quad (2.33)$$

is based on the same expansion with the coefficients $\langle\langle nK | \mathcal{H} | mL \rangle\rangle_{\tau}$, which therefore have to be computed only once. For sufficiently small δ the infinite Fourier basis for \mathcal{H} can be truncated to only a few contributions [51], e.g. $|K| \leq 5$ with reasonably small error.

2.2 Quantum maps: One-dimensional periodically kicked systems

One-dimensional periodically kicked systems are attractive to study in the field of nonlinear dynamics and quantum chaos. They feature all essential phase-space characteristics of non-integrable systems, but are considerably simpler to deal with, compared e.g. to two-dimensional autonomous systems, due to the reduced number of degrees of freedom. They

allow for a comparably simple numerical treatment, independent of the kick strength, while in contrast continuously driven quantum systems usually require a numerical effort that increases with the driving strength.

The dynamics of a kicked system is generated by the Hamiltonian

$$H(t) = T(p) + V(x) \cdot \tau \sum_n \delta(t - n\tau), \quad (2.34)$$

with the kick period $\tau = 1$, the kinetic energy $T(p)$ and a spatially periodic potential, $V(x + x_0) = V(x)$, the latter acting solely at the times $n\tau$ ($n \in \mathbb{Z}$) of the kicks. By the choice of $T(p)$ and $V(x)$, there is scope to tune the structure of the phase space to a certain desired appearance (“phase space design”).

The classical equations of motion can be reduced to the *stroboscopic Poincaré-map* from the position $x_n = x(t = n\tau + 0^+)$ and momentum $p_n = p(t = n\tau + 0^+)$ after the n -th kick to the evolved variables x_{n+1} , p_{n+1} after the subsequent kick

$$\begin{pmatrix} x_n \\ p_n \end{pmatrix} \mapsto \begin{pmatrix} x_{n+1} \\ p_{n+1} \end{pmatrix} = \begin{pmatrix} x_n + \tau T'(p_n) \\ p_n - \tau V'(x_{n+1}) \end{pmatrix}. \quad (2.35)$$

It determines the evolution of an orbit in the *stroboscopic Poincaré-section* of the phase space, $\{(x(t), p(t)) \mid t = n\tau + 0^+, n \in \mathbb{Z}\}$ at integer multiples of τ .

2.2.1 Kicked rotor

As a paradigmatic model for a driven system with a mixed phase space we consider the kicked rotor [52, 53] with the Hamiltonian

$$H(t) = \frac{p^2}{2} + \frac{\kappa}{(2\pi)^2} \cos(2\pi x) \sum_n \delta(t - n). \quad (2.36)$$

The corresponding classical map (2.35) is widely known as the standard map. Due to the spatial periodicity of $V'(x)$ the classical map (2.35) is invariant under an appropriate shift $p \mapsto p + 1$ of the momentum. Hence, the classical dynamics may be represented in a single unit cell, e.g. $(x, p) \in [0, 1) \times [-1/2, 1/2)$. To this end periodic boundary conditions are imposed on the map: the coordinates x and $x + k$ ($k \in \mathbb{Z}$) are identified with each other, as well as the momenta p and $p + l$ ($l \in \mathbb{Z}$). Thereby, the classical dynamics takes place on the two-torus $\mathbb{T}^2 = \mathbb{R}/\mathbb{Z}$ and the map on this torus reads

$$\begin{pmatrix} x_n \\ p_n \end{pmatrix} \mapsto \begin{pmatrix} x_{n+1} \\ p_{n+1} \end{pmatrix} = \begin{pmatrix} (x_n + p_n) \pmod{1} \\ (p_n + \frac{\kappa}{2\pi} \sin(2\pi x_{n+1}) + \frac{1}{2}) \pmod{1 - \frac{1}{2}} \end{pmatrix}. \quad (2.37)$$

The kicked rotor is the prototype of an originally integrable system, whose integrability

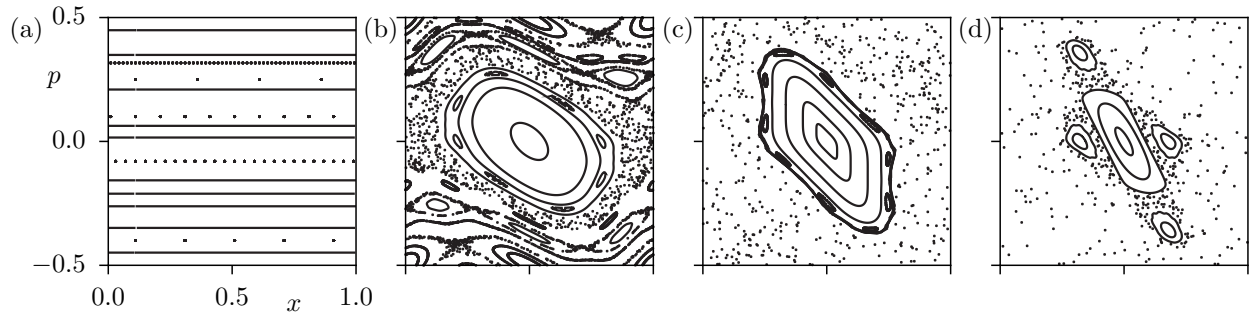


Figure 2.1: Stroboscopic Poincaré-section of phase space for the standard map (2.37) with (a) $\kappa = 0$, (b) $\kappa = 1.0$, (c) $\kappa = 2.0$, and (d) $\kappa = 2.5$.

is destroyed by the periodic driving [44, 52]. Due to the numerical simplicity it is often used to investigate signatures of chaos in classical or quantum mechanics instead of higher-dimensional non-integrable systems. The figures 2.1(a)-(d) demonstrate the dynamics generated by the map (2.37) for four different values of κ . At $\kappa = 0$, the dynamics is integrable. All orbits lie on invariant tori in phase space, which constitute lines with conserved momentum $p_n = p_0$ in the stroboscopic Poincaré-section.

The dynamics is no longer integrable once the perturbation parameter takes a finite value $\kappa > 0$. Nonetheless, at small values of κ , invariant tori still exist, though distorted. These surviving tori are the deformed remnants of the formerly invariant tori at irrational values of p_0 . This is the essence of the famous Kolmogorov-Arnol'd-Moser (KAM) theorem. To the contrary, the formerly invariant tori with rational $p_0 = s/r$ are resonant in the following sense: they break up into an alternating series of stable elliptic and unstable hyperbolic fixed points in the stroboscopic Poincaré-section (Poincaré-Birkhoff theorem). The stable elliptic fixed points are the stroboscopic reductions of s equivalent stable periodic trajectories of period r . They are surrounded by regular islands and a thin chaotic layer at their boundary, altogether forming a so-called nonlinear $r:s$ -resonance chain. For increasing κ it grows in size and, once two such resonances overlap, their phase-space area is dominated by the chaotic layer (see Fig. 2.1(b) for $\kappa = 1.0$). The chaotic dynamics is reflected by a sensitive dependence on the initial conditions: two orbits initially situated infinitesimally close in phase space separate exponentially fast in the course of time. A typical orbit that is initialized in a chaotic phase-space region spreads and eventually fills the chaotic layer densely.

Figure 2.1(c) shows the stroboscopic Poincaré-section at an intermediate value, $\kappa = 2.0$, where one dominant regular island still exists around the central fixed point at $(x_c, p_c) = (1/2, 0)$, embedded in the so-called chaotic sea. Apart from the dominant regular island innumerable further tiny regular structures exist, but are not visible in the figure. Also the regular island itself features substructures of small resonances that typically become prevailing at the transition region to the chaotic sea.

As mentioned above, the series of stable fixed points of a periodic trajectory of period r supports a chain of r regular islands. In Fig. 2.1(d) such a nonlinear 4:1-resonance chain

appears around the periodic fixed points of period 4, separated from the main island. If r and s are coprime all islands are dynamically connected, i.e. a trajectory initialized on one of those iterates from island to island and returns to the initial island after r iterations. Otherwise, there exists a family of s independent island chains, each consisting of r/s islands. When considering the r -fold iterated map instead of the map itself, the trajectory always remains on one and the same island.

2.2.2 Quantization on the torus

The stroboscopic evolution of the quantum kicked system is mediated by the one-period propagator $U(\tau, 0)$ with the Floquet eigenstates $|\psi_i(t)\rangle$. It factorizes into a potential and a kinetic part

$$U(\tau, 0) = e^{-i\tau V(x)/\hbar} e^{-i\tau T(p)/\hbar} . \quad (2.38)$$

To see this, one may consider $U(\tau, 0) = \lim_{\delta \rightarrow 0} U(\tau + \delta, 0 + \delta)$ and use the semigroup property of the propagator to split the period τ into the time span of purely free evolution and the infinitesimal span enclosing the kick,

$$U(\tau + \delta, 0 + \delta) = U(\tau + \delta, \tau - \delta) \cdot U(\tau - \delta, 0 + \delta) \quad (2.39)$$

$$= \hat{T} \exp\left(-\frac{i}{\hbar} \int_{\tau-\delta}^{\tau+\delta} dt H(t)\right) \cdot \hat{T} \exp\left(-\frac{i}{\hbar} \int_{0+\delta}^{\tau-\delta} dt H(t)\right) \quad (2.40)$$

$$= \hat{T} e^{-i(\tau V(x) + 2\delta T(p))/\hbar} \cdot e^{-i(\tau - 2\delta)T(p)/\hbar} \quad (2.41)$$

$$\rightarrow e^{-i\tau V(x)/\hbar} e^{-i\tau T(p)/\hbar} \quad (2.42)$$

According to Bloch's theorem, a wave function, whose time evolution is determined by a spatially periodic Hamiltonian like the kick Hamiltonian (2.34), is quasi-periodic in the coordinate representation. By the requirement, that the quantum dynamics takes place on the same space as the classical motion, i.e. on the two-torus \mathbb{T}^2 , periodic boundary conditions in p -direction are additionally imposed. The wave function then becomes also quasi-periodic with respect to the momentum representation. Hence, the action of an integer shift translation operator in x - or p -direction on the wave function amounts merely to a phase shift with the Bloch phases θ_x and θ_p ,

$$\langle x + 1 | \psi \rangle = e^{2\pi i \theta_x} \langle x | \psi \rangle \quad (2.43)$$

$$\langle p + 1 | \psi \rangle = e^{-2\pi i \theta_p} \langle p | \psi \rangle . \quad (2.44)$$

Note, that since the kinetic energy $T(p)$ is not a periodic function of p with period 1, the phase θ_x is fixed to the value $\theta_x = 0$ ¹. By that a smooth boundary condition at the borders

¹If the unit cell is extended to the momentum interval $[-M_p/2, M_p/2)$, further values $\theta_x = \nu/M_p$ ($\nu = 0, 1, \dots, M_p - 1$) are allowed.

$p = \pm 1/2$ of the unit cell is ensured [54, 55]. We set $\theta_x = \theta_p = 0$ throughout this thesis unless stated otherwise.

On the two-torus \mathbb{T}^2 with a unit cell of size 1×1 the effective Planck constant cannot assume arbitrary values, but is restricted to the discrete values [56]

$$h = 2\pi\hbar = \frac{1}{N} \quad (N \in \mathbb{Z}) . \quad (2.45)$$

We recall the convention that h does not denote Planck's constant itself, but instead its dimensionless counterpart measured in units of the phase space area. Condition (2.45) can be seen as a consequence of the non-commutativity of the translation operators in position and momentum [55]. It is also known as the quantum resonance condition [53, 56], where the propagator $U(\tau, 0)$ commutes with the group of integer momentum translations, provided that θ_x is rational. That means that the quantum kicked rotor like its classical equivalent behaves, as if it were periodic in momentum space with the lattice constant 1.

By its quasi-periodicity in x -direction, the momentum representation of a wave function has only a finite number of grid points, at the fixed p -values

$$p_k = \frac{1}{N}(\theta_x + k + k_0^{(p)}), \quad k = 0, 1, \dots, N-1; \quad k_0^{(p)} = \lceil Np_{\min} - \theta_x \rceil . \quad (2.46)$$

In the same fashion, the quasi-periodicity in p -direction allows only the grid of the fixed x -values

$$x_l = \frac{1}{N}(\theta_p + l + l_0^{(x)}), \quad l = 0, 1, \dots, N-1; \quad l_0^{(x)} = \lceil Nx_{\min} - \theta_p \rceil \quad (2.47)$$

for the coordinate representation of the wave function. The parameters x_{\min} , p_{\min} denote the freedom to shift the lower borders of the unit cell, here $x_{\min} = 0$, $p_{\min} = -1/2$, giving rise to the off-set integers $l_0^{(x)}$, $k_0^{(p)}$.

The propagator (2.38), evaluated on the grid (2.47), becomes

$$U_{kl} = \langle q_k | U | q_l \rangle = \sum_m \langle q_k | U_V | q_m \rangle \langle q_m | U_T | q_l \rangle = e^{-i\tau V(q_k)/\hbar} \langle q_k | U_T | q_l \rangle \quad (2.48)$$

$$= e^{-i\tau V(q_k)/\hbar} \sum_m \langle q_k | p_m \rangle \langle p_m | q_l \rangle e^{-i\tau T(p_m)/\hbar} \quad (2.49)$$

$$= \frac{1}{N} e^{-i\tau V(q_k)/\hbar} \sum_m e^{\frac{2\pi i}{N}(\theta_x + m + m_0^{(p)})} e^{-i\tau T(p_m)/\hbar} e^{i\frac{2\pi i}{N}(k-l)(\theta_x + m + m_0^{(p)})} , \quad (2.50)$$

where the second (third) line makes use of the fact, that $U_V(U_T)$ is diagonal in the position (momentum) representation. The last step is based on the representation of the plane waves

$$\langle q_k | p_m \rangle = \frac{1}{\sqrt{N}} e^{\frac{2\pi i}{N}(\theta_p + k + k_0^{(x)})} e^{i\frac{2\pi i}{N}(\theta_x + m + m_0^{(p)})} . \quad (2.51)$$

Note, that the invariance of the classical dynamics is fulfilled for general integer shifts

$x \mapsto x + M_x$ and $p \mapsto p + M_p$. If the quantization is correspondingly adapted to the extended unit cell $[0, M_x) \times [-M_p/2, M_p/2)$, a generalization of the above criteria is required: instead of the condition (2.45) the adapted resonant values of the effective Planck constant are

$$h = 2\pi\hbar = \frac{M_x M_p}{N} \quad (N \in \mathbb{Z}) \quad (2.52)$$

and the quantization grids (2.46) and (2.47) become, now with $p_{\min} = -M_p/2$,

$$p_k = \frac{M_p}{N}(\theta_x + k + k_0^{(p)}), \quad k = 0, 1, \dots, N-1; \quad k_0^{(p)} = \left\lceil \frac{N}{M_p} p_{\min} - \theta_x \right\rceil \quad (2.53)$$

$$x_l = \frac{M_x}{N}(\theta_p + l + l_0^{(x)}), \quad l = 0, 1, \dots, N-1; \quad l_0^{(x)} = \left\lceil \frac{N}{M_x} x_{\min} - \theta_p \right\rceil. \quad (2.54)$$

2.2.3 Husimi representation

In the spirit of the quantum-classical correspondence a comparison between the classical phase-space structure of the driven system and the Floquet states is desirable. This can be established by the Husimi representation [57], which serves to visualize a wave function $\phi(x)$ and to compare it with the classical phase space. It is constructed as the projection

$$H_\phi(x, p) = |\langle \alpha_{x,p} | \phi \rangle|^2 = \left| \int_{-\infty}^{\infty} dx' \alpha_{x,p}^*(x') \phi(x') \right|^2 \quad (2.55)$$

of the wave functions onto the coherent states $|\alpha_{x,p}\rangle$ centered at the points (x, p) in phase-space,

$$\alpha_{x,p}(x') = \langle x' | \alpha_{x,p} \rangle = \left(\frac{1}{2\pi\sigma_x^2} \right)^{1/4} \exp\left(-\frac{(x' - x)^2}{4\sigma_x^2} \right) \exp\left(\frac{i}{\hbar} p(x' - x) \right). \quad (2.56)$$

In contrast to the Wigner function, the most prominent phase space representation [58], it is by construction positive definite and may be interpreted as a Gaussian-smoothed probability density in phase space.

The Husimi representation (2.55) refers to the infinite range $-\infty < x < \infty$. To account for the periodic boundary conditions on the two-torus \mathbb{T}^2 the integration in (2.55) can be split into the contributions of each of the intervals $[\nu, \nu + 1)$. This is equivalent to restricting the integration in (2.55) to the grid (2.47) on the torus and simultaneously projecting to the periodized coherent states $|\bar{\alpha}_{x,p}\rangle$,

$$\bar{\alpha}_{x,p}(x') = \langle x' | \bar{\alpha}_{x,p} \rangle \quad (2.57)$$

$$= \left(\frac{1}{2\pi\sigma_x^2} \right)^{1/4} \sum_{\nu=-\infty}^{\infty} \exp\left(-\frac{(x' + \nu - x)^2}{4\sigma_x^2} \right) \exp\left(\frac{i}{\hbar} p(x' + \nu - x) \right) \quad (2.58)$$

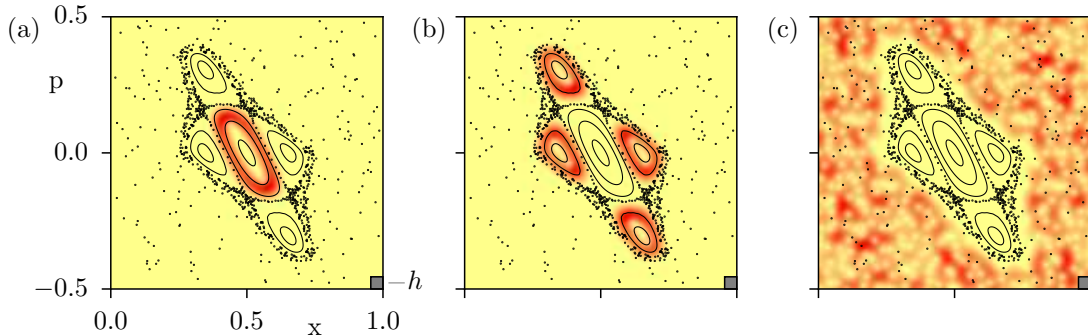


Figure 2.2: Husimi representations for three Floquet states of the kicked rotor (2.36) with $\kappa = 2.35$. The smallness of the effective Planck constant $h = 2\pi\hbar = 1/500$ compared to the area of the dominant regular islands allows to classify the Floquet states as (a) regular, (b) regular resonant and (c) chaotic.

instead of the ordinary coherent states [56]. Practically, such a periodization can also be done by extending the wave function $\phi(x)$ to the neighboring phase space cells $x \pm \nu$, where the additional phase factors $e^{\pm 2\pi i \theta x}$ according to Eq. (2.43) have to be taken into account, and then projecting it to the ordinary coherent states (2.56).

Figures 2.2(a)-(c) show the Husimi representations for three eigenstates of the propagator (2.50) for the kick strength $\kappa = 2.35$, contrasted with the underlying classical phase space to visualize the quantum-classical correspondence. According to the *semiclassical eigenfunction hypothesis* [30–32] almost all Floquet states can be classified as either regular or chaotic, provided that the effective Planck constant h is sufficiently small, $h < A_{\text{reg}}$, to resolve the area A_{reg} of regular structures in phase space. The regular states are localized on the regular island and suggest a natural order by a quantum number m . Figure 2.2(a) shows the Husimi representation of the regular state $m = 13$ of the central island. As h is even smaller than the islands of the surrounding 4:1-resonance island chain, these islands also support localized states. There are 4 equivalent resonance Floquet states with equal weight in each of the dynamically connected islands, like the one in Fig. 2.2(b). The chaotic states, as the one in Fig. 2.2(c), typically extend over the entire chaotic phase-space area and irregularly fluctuate in phase and amplitude.

2.3 Semiclassical quantization for the regular islands

In this section, the semiclassical quantization for time-periodic systems with one degree of freedom is surveyed, based on Refs. [59,60], where more profound presentations can be found. Equivalent approaches specialized to area preserving maps are presented e.g. in Refs. [61,62].

2.3.1 Single island

At first, we ask for a quantization rule for a regular island around a period-one fixed point in the stroboscopic Poincaré-section. In integrable autonomous systems it is provided by the EBK-quantization conditions [43] and analogous conditions are applicable to the invariant regular tori of non-integrable systems [63,64]. To this end the authors of Ref. [59] apply a canonical operator method, introduced by Maslov and Fedoriuk [63], which serves to generalize the EBK-quantization to the invariant regular tori of non-integrable systems. This method is also appropriate in the context of time-periodic systems, when applied to the flow-invariant vortex tubes Λ^{1+1} in the extended phase space \mathbb{R}^{2+2} of the autonomized system. Figure 2.3 illustrates the situation.

A unique quantization in the extended phase space requires two quantization conditions. The first condition on the action integral

$$I_1 = \frac{1}{2\pi} \oint_{\gamma_1} (p dx + p_t dt) = \hbar \left(m + \frac{\mu_1}{4} \right) \quad m = 0, 1, 2, \dots \quad (2.59)$$

is analogous to the EBK-quantization condition of integrable systems and ensures single-valuedness of a wave function projected from the vortex tube Λ^{1+1} to the extended configuration space $\{(x, t)\}$. The closed path γ_1 , which has to satisfy condition (2.59), is chosen to lie in the surface of section $\{(x, t, p, p_t) \mid t = 0\}$. For the librational motion under consideration the path γ_1 contains two turning points which give rise to the Maslov index $\mu_1 = 2$ in Eq. (2.59). We do not consider the case $\mu_1 = 0$ here, which applies for rotational motion. By the specific choice of γ_1 , the integration in Eq. (2.59) is restricted to the conventional phase space and the integrand to the Poincaré-Cartan form $\omega^1 = p dx - H dt$ on \mathbb{R}^{2+1} ,

$$I_1 = \frac{1}{2\pi} \oint_{\gamma_1} \omega^1. \quad (2.60)$$

The quantum number m in (2.59) specifies the quantizing torus in the surface of section $\{(x, t, p, p_t) \mid t = 0\}$. By the evolution of this manifold under the Hamiltonian flow in \mathbb{R}^{2+2} the quantizing vortex tube Λ_m^{1+1} is generated.

The second quantization condition

$$I_2 = \frac{1}{2\pi} \int_{\gamma_2} (p dx + p_t dt) = K \hbar \quad K = 0, \pm 1, \pm 2, \dots \quad (2.61)$$

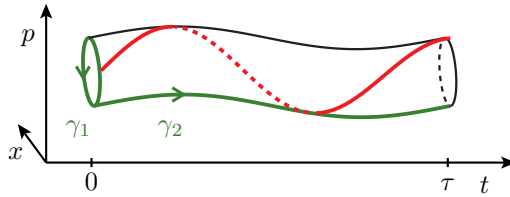


Figure 2.3: Sketch of a τ -periodic vortex tube Λ^{1+1} in the extended phase $\{(x, t, p, p_t)\}$, originating from an invariant torus in the conventional phase space $\{(x, p)\}$. The red line represents a trajectory evolving on Λ^{1+1} . The paths $\gamma_{1,2}$ on Λ^{1+1} are topologically independent.

accounts for the periodicity in t by identification of the times t and $t + \tau$. The path γ_2 lies on the quantizing vortex tube Λ_m^{1+1} predefined by the first condition (2.59) and connects a point (x, p) at time $t = 0$ with the same point at time $t = \tau$. The Maslov index μ_2 is zero, since γ_2 does not contain a turning point. As the vortex tube Λ_m^{1+1} is part of the quasienergy shell $\varepsilon = H(x, p, t) + p_t$, the second quantization condition (2.61) likewise translates to the conventional phase space with the Poincaré-Cartan form ω^1 ,

$$I_2 = \frac{1}{2\pi} \int_{\gamma_2} (p dx - H dt + \varepsilon dt) = \frac{1}{2\pi} \int_{\gamma_2} \omega^1 + \varepsilon \frac{\tau}{2\pi}. \quad (2.62)$$

Using the condition (2.61) this determines the semiclassical quasienergy

$$\varepsilon_{m,K} = -\frac{1}{\tau} \int_{\gamma_2} \omega^1 + K \hbar \omega. \quad (2.63)$$

In order to establish a link between the two conditions (2.59) and (2.61) a trajectory on Λ_m^{1+1} is considered. It is characterized by the two frequencies ω_1 and ω_2 which are related to the advance of the evolving trajectory projected to the paths γ_1 and γ_2 , respectively. Of course, $\omega_2 = \omega$ is fixed by the external frequency. The action $I(k_2\tau)$ of a trajectory evolving for the time span $k_2\tau$ can be represented as a combination of the actions I_1 and I_2 along the two paths,

$$I(k_2\tau) = \frac{1}{2\pi} \int_0^{k_2\tau} \underbrace{(p\dot{x} - H)}_{=L(x,\dot{x},t)} dt + \frac{k_2\tau}{2\pi} \varepsilon = k_1 I_1 + k_2 I_2. \quad (2.64)$$

Herein, the ratio k_1/k_2 ($k_1, k_2 \in \mathbb{Z}$) of both contributions is fixed by the winding number

$$\nu := \frac{\omega_1}{\omega_2} = \frac{k_1}{k_2} \quad (2.65)$$

of the trajectory or, if the frequencies are incommensurable, by a rational approximate $\nu \simeq k_1/k_2$ of ν . The error in (2.64) approaches zero for $k_1, k_2 \rightarrow \infty$ and $k_1/k_2 \rightarrow \nu$. The quasienergy is thus determined by the actions $I_{1,2}$ and the long-time average $\langle L \rangle$ of the

Lagrangian $L(x, \dot{x}, t) = p\dot{x} - H(x, p(x, \dot{x}), t)$ of the trajectory,

$$\varepsilon = \lim_{k_1, k_2 \rightarrow \infty} \left[\frac{k_1}{k_2} \omega I_1 + \omega I_2 - \frac{1}{k_2 \tau} \int_0^{k_2 \tau} L(x, \dot{x}, t) dt \right] = \nu \omega I_1 + \omega I_2 - \langle L \rangle. \quad (2.66)$$

Inserting the quantization conditions (2.59) and (2.61), the semiclassical quasienergy finally reads

$$\varepsilon_{m,K} = \hbar \omega \nu_m \left(m + \frac{1}{2} \right) + \hbar \omega K - \langle L \rangle_m \quad (2.67)$$

with the winding number ν_m and the Lagrangian $\langle L \rangle_m$ of the m -th quantizing vortex tube Λ_m^{1+1} .

Inside a stable island the winding number ν as well as $\langle L \rangle$ vary only slowly and smoothly. Special cases are harmonic-oscillator like islands with elliptic tori and a constant winding number. As can be inferred from the virial theorem, also $\langle L \rangle$ is constant in such islands. These properties often serve to approximate the behavior of a generic regular island in a limited region around its center.

In kicked systems, where the winding number ν is defined only up to additive integers, it is usually chosen in the interval $[-1/2, 1/2]$, but continued smoothly if it varies beyond the interval boundaries. Note, that an integer shift of $\nu \rightarrow \nu + q$ ($q \in \mathbb{Z}$) results in a new set of regular energies whose mutual spacing is enlarged by the additional term $q\hbar\omega$.

To determine ν we have applied the frequency map analysis [65]. It is based on an iterative Fourier transformation of the complex variable $z_n = x_n + ip_n$ composed of the stroboscopic iterates x_n, p_n on the regular torus. In each recursion step k of the frequency map analysis, at first the contribution of the preceding fundamental frequency $\nu^{(k-1)}$ is subtracted and the new fundamental frequency $\nu^{(k)}$ is evaluated thereafter from the Fourier expansion of the resulting quantity $z_n^{(k)}$. The winding number ν of the torus can be determined from the frequencies $\nu^{(k)}$, which are integer combinations $\nu^{(k)} = \omega \left(m_2^{(k)} + m_1^{(k)} \nu \right)$ of $\omega_2 = \omega$ and $\omega_1 = \nu\omega$.

The quantum number K , reflecting the equivalence of all Brillouin zones, has to be chosen appropriately if the quasienergies are required to lie in a certain Brillouin zone, e.g. in $[0, \hbar\omega)$. The quasienergies $\varepsilon_{m,K}$ from the family (2.67) are associated with the semiclassical periodic states $|u_{m,K}(t)\rangle = e^{iK\omega t} |u_m(t)\rangle$, each of which leads to the unique Floquet state

$$|\psi_m(t)\rangle = e^{-i\varepsilon_{m,K}t/\hbar} |u_{m,K}(t)\rangle = e^{-iE_m^{\text{reg}}t/\hbar} |u_m(t)\rangle. \quad (2.68)$$

We have introduced the regular energies

$$E_m^{\text{reg}} := \hbar \omega \nu_m \left(m + \frac{1}{2} \right) - \langle L \rangle_m, \quad (2.69)$$

which are implicitly defined in (2.67) and coincide with the semiclassical quasienergies

$\varepsilon_{m,K} = E_m^{\text{reg}} + K\hbar\omega$ upon projection to the first Brillouin zone, $(E_m^{\text{reg}} - \varepsilon_{m,K}) \bmod \hbar\omega = 0$. These energies may be regarded as the eigenenergies of a time-independent system, whose quantizing tori in the stroboscopic Poincaré-section are indistinguishable from those of the time-periodic system.

2.3.2 Island chain of a nonlinear resonance

Apart from the islands centered at stable elliptic fixed points of period one also chains consisting of r regular islands are found in phase space around the fixed points of period r . These are generated at nonlinear resonances with a rational winding number $\nu = s/r$ [52]. A trajectory on the secondary tori in the $r:s$ -resonance islands is not confined to a single island but passes from one island to another during each period τ and returns to the initial island after r periods. As illustrated in Fig. 2.4, the cylindrical vortex tube originating from a torus in one of the resonance islands is connected to the equivalent tori in the other islands and closes after r periods, provided that s and r are coprime. That is why, to perform the semiclassical quantization as in the previous section, the periodic boundary condition in the coordinate t has to be extended from τ to $r \cdot \tau$, such that the path γ_2 connects the point (x, p) at time $t = 0$ with the same point at time $r \cdot \tau$ [66]. This equates to considering the dynamics in the modified stroboscopic Poincaré-section of period $r \cdot \tau$, $\{(x(t), p(t)) \mid t = nr \cdot \tau, n \in \mathbb{Z}\}$. For a kicked system this means the r -fold iterated map instead of the original stroboscopic map itself.

The action along the path γ_1 is not affected by this extension, $I_1^{(r)} = \frac{1}{2\pi} \oint_{\gamma_1} \omega^1 = I_1 = \hbar(m + \frac{1}{2})$. The path γ_2 , on the contrary, is prolonged and, if the resonance vortex tube twines around a central periodic trajectory along the t -direction, additional turning points arise in the projection to the (x, p) -plane. The number of twists is s and increases the number μ_1 of turning points that already exist along γ_1 by the factor s , i.e. $\mu_2 = s\mu_1 = 2s$

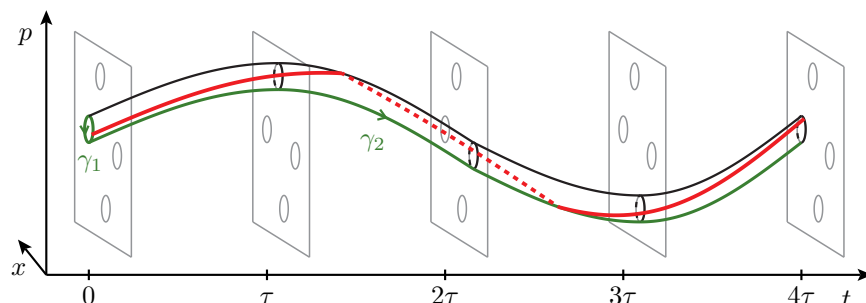


Figure 2.4: Sketch of a $4 \cdot \tau$ -periodic vortex tube Λ^{1+1} around a periodic trajectories of winding number $s/r = 1/4$ in the extended phase space $\{(x, t, p, p_t)\}$, originating from an invariant torus of a resonance island in the conventional phase space $\{(x, p)\}$. The three other equivalent vortex tubes are not shown. The red line represents a trajectory evolving on Λ^{1+1} . The paths $\gamma_{1,2}$ on Λ^{1+1} are topologically independent.

for librational motion. The action along the path γ_2 thus reads

$$I_2^{(r)} = \frac{1}{2\pi} \int_{\gamma_2} \omega^1 + \varepsilon \frac{r\tau}{2\pi} = \hbar \left(K' + \frac{s}{2} \right) \quad K' = 0, \pm 1, \pm 2, \dots \quad (2.70)$$

The action of a trajectory on Λ_m^{1+1} during the time span $k_2 r \tau$ is approximately

$$I(k_2 r \tau) = \frac{1}{2\pi} \int_0^{k_2 r \tau} L(x, \dot{x}, t) dt + k_2 \frac{r\tau}{2\pi} \varepsilon = k_1 I_1^{(r)} + k_2 I_2^{(r)} \quad (2.71)$$

and the quasienergy becomes

$$\varepsilon = \lim_{k_1, k_2 \rightarrow \infty} \left[\frac{k_1 \omega}{k_2 r} I_1^{(r)} + \frac{\omega}{r} I_2^{(r)} - \frac{1}{k_2 r \tau} \int_0^{k_2 r \tau} L(x, \dot{x}, t) dt \right] \quad (2.72)$$

$$= \frac{\nu^{(r)}}{r} \hbar \omega \left(m + \frac{1}{2} \right) + \frac{1}{r} \hbar \omega \left(K' + \frac{s}{2} \right) - \langle L \rangle. \quad (2.73)$$

With the substitution $K' = rK + sl$ ($K, K' \in \mathbb{Z}, l = 0, \dots, r-1$) the semiclassical quasienergy of a state on a quantizing torus finally reads

$$\varepsilon_{(ml),K} = \frac{\nu_m^{(r)}}{r} \hbar \omega \left(m + \frac{1}{2} \right) + \frac{s}{r} \hbar \omega \left(l + \frac{1}{2} \right) + \hbar \omega K - \langle L \rangle_m. \quad (2.74)$$

The multi-index (ml) denotes the combined principal quantum number m and the counting index l . The notation $\nu_m^{(r)}$ points out that the winding number is interpreted with respect to the period $r \cdot \tau$, i.e. $\nu^{(r)} := \omega_1 / \omega'_2 = r\omega_1 / \omega$. It can exceed the above-mentioned range $[-1/2, 1/2]$, but under the rescaling $\nu = \nu^{(r)} / r$ to the actual driving period τ falls again in this interval. Likewise, the semiclassical quasienergy $\varepsilon_{(ml),K}$ can be regarded as referring to an auxiliary system of period $r \cdot \tau$ instead of τ . The associated first Brillouin zone is $[0, \hbar\omega/r)$, where the r quasienergies $l = 0, \dots, r-1$ of fixed principal quantum number m are degenerate. Interpreted with respect to the actual τ -periodic system these are equidistant in $[0, \hbar\omega)$ with mutual spacing $\hbar\omega/r$.

Analogously to Def. (2.69) we introduce the regular energies

$$E_m^{\text{reg}} := \hbar \omega \frac{\nu_m^{(r)}}{r} \left(m + \frac{1}{2} \right) + \hbar \omega \frac{s}{2r} - \langle L \rangle_m \quad (2.75)$$

which coincide with the semiclassical quasienergies $\varepsilon_{(ml),K} = E_m^{\text{reg}} + K\hbar\omega + sl\hbar\omega/r$ upon projection to $[0, \hbar\omega/r)$:

$$(E_m^{\text{reg}} - \varepsilon_{(ml),K}) \bmod \left(\frac{\hbar\omega}{r} \right) = 0. \quad (2.76)$$

The same property is fulfilled e.g. for the quantities $E_m^{\text{reg}} + (ls/r)\hbar\omega$, which give an l -dependent off-set to the energy. However, as l plays the role of a mere counting index and is not related

to a measurable quantity, we omit its contribution to the semiclassical quasienergies in Def. (2.75).

In the semiclassical approximation the periodic parts of the resonance Floquet states are an equally weighted linear combination

$$|u_m(t)\rangle = \sum_{j=0}^{r-1} |\tilde{u}_m^{(j)}(t)\rangle \quad (2.77)$$

of the r semiclassical states $|\tilde{u}_m^{(j)}(t)\rangle$, which are initially localized on the m -th quantizing torus in the j -th island of the resonance chain. The states $|\tilde{u}_m^{(j)}(t)\rangle$ evolve with the period $r \cdot \tau$ on the quantizing vortex tube Λ^{1+1} . They are not independent, but cyclically connected according to

$$|\tilde{u}_m^{(j)}(t + \tau)\rangle = |\tilde{u}_m^{(j+1)}(t)\rangle, \quad (2.78)$$

thus ensuring the periodicity of the states $|u_m(t)\rangle$ with period τ . The index j needs to be interpreted modulo r . In order to represent the τ -periodic semiclassical states $|u_{(ml),K}(t)\rangle$, the $|\tilde{u}_m^{(j)}(t)\rangle$ have to be linearly combined with appropriate phase factors:

$$|u_{(ml),K}(t)\rangle = \left(\sum_{j=0}^{r-1} |\tilde{u}_m^{(j)}(t)\rangle e^{i2\pi jls/r} \right) e^{i(ls/r+K)\omega t}. \quad (2.79)$$

These semiclassical states indeed have the period τ ,

$$|u_{(ml),K}(t + \tau)\rangle = \left(\sum_{j=0}^{r-1} |\tilde{u}_m^{(j)}(t + \tau)\rangle e^{i2\pi jls/r} \right) e^{i(ls/r+K)\omega t} e^{i2\pi(ls/r+K)} \quad (2.80)$$

$$\stackrel{(2.78)}{=} \left(\sum_{j'=0}^{r-1} |\tilde{u}_m^{(j')}(t)\rangle e^{i2\pi j'ls/r} \right) e^{i(ls/r+K)\omega t} \quad (2.81)$$

$$= |u_{(ml),K}(t)\rangle, \quad (2.82)$$

and together with the associated phase factor form the unique semiclassical Floquet state

$$|\psi_{(ml)}(t)\rangle = e^{-i\varepsilon_{(ml),K}t/\hbar} |u_{(ml),K}(t)\rangle = e^{-iE_m^{\text{reg}}t/\hbar} \left(\sum_{j=0}^{r-1} |\tilde{u}_m^{(j)}(t)\rangle e^{i2\pi jls/r} \right). \quad (2.83)$$

3 Statistical mechanics of time-periodic systems

Under realistic, non-idealized conditions a real physical system is not isolated, but interacts with its environment. It can be considered as an open part of a larger Hamiltonian system comprised of the system itself and the environment. The state of the subsystem is characterized by the reduced density operator $\rho(t)$, which contains no direct information about the environment, but whose evolution is influenced by the latter. In many applications, where the number of external degrees of freedom exceeds the internal degrees by far, the environment can be modelled as a heat bath of constant temperature $1/\beta$. If the system under consideration is time-independent and interacts only weakly with the heat bath, it relaxes in the long-time limit to a unique equilibrium state. Its eigenstates $|i\rangle$ are occupied with probabilities p_i governed by the rate balance

$$0 = \sum_j p_j R_{ji} - p_i \sum_j R_{ij}. \quad (3.1)$$

The ratio between a rate R_{ij} and the rate R_{ji} of the reverse process is $R_{ij}/R_{ji} = e^{\beta(E_i - E_j)}$. It is a unique function of the energy difference with only the temperature $1/\beta$ as a parameter, whereas details of the coupling to the heat bath do not play a role. Beyond the global balance (3.1), the detailed balance $p_i R_{ij} = p_j R_{ji}$ is fulfilled between any two states and allows to infer the Boltzmann weights $e^{-\beta E_i}$ as the stationary solutions for the occupations p_i . Note, that the true equilibrium state of even a time-independent system, even in the lowest perturbation order, can deviate from this canonical form, if e.g. the back action of the bath on the system energies (*Lamb shifts*) is taken into account [38, 39].

The derivation of the canonical Boltzmann-distribution from the equation of motion for $\rho(t)$ is a standard technique [67–69]. In the limit of a weak coupling between the system and the heat bath the coupling strength γ is treated as a perturbation parameter, with expansions usually performed to the second order $\mathcal{O}(\gamma^2)$. Moreover, the *Markov approximation* is employed. This approximation requires a rapid decay of bath correlations compared to the typical relaxation time of the system. The resulting master equation for $\rho(t)$ has been generalized for time-periodic quantum systems by the Floquet-Markov approach [20–25], where the density operator is conveniently expressed in the basis of the time-periodic parts of the Floquet states, $\rho_{ij}(t) = \langle u_i(t) | \rho(t) | u_j(t) \rangle$. The Floquet formalism ensures a non-perturbative treatment of the driven system’s coherent dynamics. In the long-time limit of the evolution, when the system has reached an asymptotic state, the density operator is time-periodic with the period τ of the driving. The Floquet density matrix elements ρ_{ij} are then approximately the solutions of a linear system of time-independent rate equations. The following section, Section 3.1, contains a survey of the Floquet-Markov method and a brief derivation of the rate equations for the asymptotic Floquet density matrix elements ρ_{ij} . A more detailed

derivation is deferred to Appendix B.

As a side note, we point out that also the alternative approach to dissipative dynamics, the stochastic evolution of an ensemble of state vectors, can make use of the Floquet representation of the time-periodic system. This is similar to the extension of the conventional master equation of time-independent systems to the Floquet-Markov master equation. Such an approach is presented in Ref. [13], but is not followed here.

It is instructive to ask, how the Floquet densities ρ_{ij} behave especially at avoided crossings. These are ubiquitous in Floquet systems, as the quasienergies are bounded within a finite interval, $0 \leq \varepsilon < \hbar\omega$, and typically form a dense point spectrum [35,36]. The authors of Ref. [25] derive an approximate rate equation for the asymptotic Floquet densities ρ_{ij} at an isolated avoided crossing. This approximate rate equation is addressed in Section 3.2, and in more detail in Appendix D.

The back action of the heat bath on the system in general leads to a renormalization of the system energies, usually paraphrased as the *Lamb shifts* in reference to quantum optics. In principle, these can cause deviations from the canonical distribution even in the framework of time-independent dissipative systems [38,39]. A sufficiently small coupling strength γ provided, their tiny contribution is often disregarded, like also in the Floquet-Markov master equation. However, concluding from our previous studies, the Floquet occupations are particularly sensitive to the exact values of the involved quasienergies in the vicinity of an avoided crossing, and the Lamb shifts are therefore expected to become important especially there. That is why we extend the Floquet-Markov master equation by the Lamb shift contributions and derive in Section 3.3 an approximate rate equation for its asymptotic solution at avoided crossings. The technical details are deferred to Appendices C and E.

In a further section of this chapter, Section 3.4, we complement the Floquet-Markov approach by an alternative method based on a random walk along the energy axis. It reveals the diffusive character of the dissipation process in time-periodic systems, which is caused by the interplay of the driving and the damping force: energy is permanently pumped into the system by the driving and eventually absorbed by the heat bath. We evaluate the drift and diffusion constants for this process and relate the resonant enhancement of these quantities to the rate of energy dissipation in a classical oscillator.

3.1 Floquet-Markov master equation

The microscopic model for dissipation in a quantum system is based on the Hamiltonian

$$H_{\text{tot}}(t) = H_s(t) + H_{sb} + H_b, \quad (3.2)$$

which governs the dynamics of the composite system. The system of interest itself, equipped with the Hamiltonian $H_s(t)$, is coupled via H_{sb} to an, in practice normally unknown, en-

environment with the Hamiltonian H_b . The interaction term H_{sb} is usually understood as a weak perturbation of the uncoupled system, $H_0(t) = H_s(t) + H_b$. We study the case, where the system of interest is subject to a periodic driving, $H_s(t + \tau) = H_s(t)$, whereas its thermal environment remains unaffected by that driving. This situation is certainly present for an environment in the sense of a heat bath, i.e. a reservoir possessing a much larger number of degrees of freedom in comparison to the system itself. In most cases the system has only a few degrees of freedom and sometimes it even has a finite-dimensional Hilbert space, e.g. a spin-system or a quantum map on the two-torus \mathbb{T}^2 as introduced in Section 2.2. The interaction between system and heat bath is assumed weak in the sense of perturbation theory. At the same time, the large reservoir is assumed to be in equilibrium at all times and to give rise to a fast decay of correlations originating from the interaction, in particular faster than the driving period τ . Under these circumstances any minor modification in the heat bath – may it stem from an interaction with the system itself or from the driving – is suppressed that fast that no information about it can return to the system. Another option, where the driving force exclusively acts on the system but not on the heat bath, would be due to different coupling mechanisms to the driving on the one hand and to the heat bath on the other hand. A molecule, which is coupled via a permanent or induced electric dipole moment to the heat bath and is at the same time subject to a driving force via a magnetic degree of freedom, is an example.

3.1.1 Microscopic dissipation model

A standard microscopic description for the heat bath is an ensemble of non-interacting harmonic oscillators with the Hamiltonian

$$H_b = \sum_n \left(\frac{p_n^2}{2m_n} + \frac{m_n \omega_n^2}{2} x_n^2 \right). \quad (3.3)$$

It is the idealized form of a reservoir with energetically more or less equidistant modes. Such a boson bath is particularly suited to describe phonon modes in a lattice or the electromagnetic background in quantum optics. Strictly speaking, the bath needs to have infinitely many degrees of freedom in order to generate truly irreversible instead of quasi-periodic dynamics, which otherwise occurs due to the the Hamiltonian nature of the composite system (3.2).

The presumed weak interaction between the system and the individual modes of the heat bath is appropriately described by the bilinear coupling term

$$H_{sb} = -x \sum_n c_n x_n. \quad (3.4)$$

The linearity of H_{sb} in the bath coordinates x_n as well as in the system coordinate x is adapted to the presumed weak interaction between the system and the bath modes. The

coupling constants c_n measure the individual strength of the interaction with the n -th bath mode. In order to remove a coupling-induced renormalization of the energy [69, 70], H_{sb} can be supplemented by the term $x^2 \sum_n c_n^2 / (2m_n \omega_n^2)$. The resulting Hamiltonian of the composite system

$$H_{\text{tot}} = \frac{p^2}{2} + V(x) + \sum_n \left(\frac{p_n^2}{2m_n} + \frac{m_n \omega_n^2}{2} \left(x_n - \frac{c_n}{m_n \omega_n^2} x \right)^2 \right) \quad (3.5)$$

then also correctly preserves the translational invariance of a free quantum Brownian particle ($V(x) = 0$) immersed in the oscillator bath.

The model Hamiltonian (3.5) has been used extensively to study dissipation, see e.g. the list of references in [69]. It is widely known as the Caldeira-Leggett model [71], although similar model Hamiltonians have been used earlier. As explicated in Appendix A, the associated Heisenberg equation of motion for the system coordinate x reproduces a quantum Langevin equation [70, 72, 73]. Therein, the bilinear coupling (3.4) can generate a damping term of the Stokes type, i.e. velocity-proportional with the damping coefficient as proportionality factor. If the system Hamiltonian $H_s = p^2/2 + V(x)$ allows a conceptual reduction to a two-level system, this is known as the spin-boson model. We apply the Caldeira-Leggett model to a system with a time-periodic potential $V(x, t)$. The evaluation follows the Floquet-Markov approach of Refs. [20–25]. In the following section it is outlined only in a few steps, with further details given in Appendix B.

3.1.2 Equation of motion for $\rho(t)$ and Born-Markov approximation

For an open quantum system one is generally not interested in the Hamiltonian, i.e. deterministic, time-reversible, and phase-space preserving dynamics of the composite system comprising the degrees of freedom of both the system and the reservoir. This would amount to finding the solutions of the the *Liouville-von Neumann equation* of the density operator $\rho_{\text{tot}}(t)$ of the composite system

$$i\hbar \frac{\partial}{\partial t} \rho_{\text{tot}}(t) = [H_{\text{tot}}(t), \rho_{\text{tot}}(t)] \quad (3.6)$$

and is typically not feasible, simply due to the vast number of degrees of freedoms in the composite system. Instead, the uninteresting degrees of freedom in the Hilbert space of the heat bath are traced out, leaving statistical information about the relevant system degrees of freedom in the reduced density operator

$$\rho(t) := \text{Tr}_b(\rho_{\text{tot}}(t)) . \quad (3.7)$$

The reduced density $\rho_b = \text{Tr}_s(\rho_{\text{tot}}(t))$ of the heat bath is of the canonical form $\rho_b \sim e^{-\beta H_b}$, assuming that the heat bath remains permanently in thermodynamic equilibrium at the temperature $1/\beta$. The complicated equation of motion for $\rho(t)$ is not solvable in practical applications. Usually, if the interaction $H_{sb} \sim \gamma$ between system and heat bath is weak with respect to the energy scales of the uncoupled system, $H_0(t) = H_s(t) + H_b$, a perturbation expansion of Eq. (3.6) can be performed with the characteristic interaction strength γ as perturbation parameter. Note, that for convenience the global interaction strength γ is here factored out of the individual interaction strengths c_n in H_{sb} of Eqs. (3.4) and (3.5), by which the latter are now redefined according to $c_n = c_n/\gamma$. Terminating the perturbation expansion after the second order $\mathcal{O}(\gamma^2)$ by virtue of the *Born approximation* and requiring that the evolution at the time t depends only on the current state $\rho(t)$, but not on its history (*Markov approximation*), leads to the master equation²

$$\begin{aligned} \frac{\partial}{\partial t}\rho(t) = & -\frac{i}{\hbar}[H_s(t), \rho(t)] \\ & -\frac{\gamma^2}{\hbar^2} \int_0^\infty dt' \left(G(t') \left(x(t)\tilde{x}(t-t', t)\rho(t) - \tilde{x}(t-t', t)\rho(t)x(t) \right) \right. \\ & \left. + G^*(t') \left(\rho(t)\tilde{x}(t-t', t)x(t) - x(t)\rho(t)\tilde{x}(t-t', t) \right) \right). \end{aligned} \quad (3.8)$$

It describes the evolution of the reduced density operator $\rho(t)$ under the influence of the weak damping force, which is exerted by the heat bath via the interaction term H_{sb} with the characteristic correlation function $G(t)$. The tilde serves to denote the interaction picture representation of an operator.

The heat bath, due to its immense number of degrees of freedoms, has a short-time memory limited by the correlation time τ_c . It is estimated by the characteristic decay time of the correlation function

$$G(t-t') := \text{Tr}_b \left(\sum_{n,m} c_n c_m \tilde{x}_n(t) \tilde{x}_m(t') \rho_b \right) \quad (3.9)$$

for the component of the interaction operator (3.4) that acts in the Hilbert space of the heat bath. Note, that Def. (3.9) together with Eq. (3.8) are equivalent to the expressions (B.21) and (B.29) in Appendix B, if the general coupling operators A, B of $H_{sb} = \gamma AB$ are specified to the according operators $A = -x$ and $B = \sum_n c_n x_n$ of the Caldeira-Leggett model. According to Ref. [25], the criterion for validity of Eq. (3.8), i.e. of the Born-Markov approximation for time-periodic systems, is

$$\tau_c \Gamma^{(2)} := \frac{\gamma^2}{\hbar^2} \tau_c^2 \langle x^2 \rangle \langle (\sum_n c_n x_n)^2 \rangle \ll 1. \quad (3.10)$$

²Compare Eq. (B.29) in Appendix B.

Roughly speaking, the Markov approximation requires, that changes in $\tilde{\rho}(t)$ take place on a time scale much larger than the characteristic memory time τ_c of the heat bath. The characteristic rate $\Gamma^{(2)}$ gives an estimate for this relaxation time as $1/\Gamma^{(2)}$, and $\tau_c\Gamma^{(2)}$ hence implicitly defines an effective, dimensionless coupling strength between system and heat bath.

The correlation function (3.9) is influenced by the density of spectral modes ω_n present in the heat bath, each weighted with the individual coupling strength. This dependence is subsumed in the definition of the spectral density

$$J(\omega) := \frac{\pi}{2} \sum_n \frac{c_n^2}{m_n \omega_n} \left(\delta(\omega - \omega_n) - \delta(\omega + \omega_n) \right). \quad (3.11)$$

In the continuum limit, presuming an infinite number of bath oscillators with continuously distributed frequencies, $J(\omega)$ can be modelled as a smooth function. In Appendix A, containing a derivation of a quantum Langevin equation starting from the microscopic model (3.5), the idealized Ohmic form

$$J_o(\omega) = \eta \omega \quad (3.12)$$

is motivated by the correspondence to the classical Langevin equation. Presuming $J_o(\omega)$, the damping force in the Langevin equation is velocity-proportional with the frequency-independent damping constant $\gamma^2 \eta$. We can set $\eta = 1$, as by our previous construction its role is already taken by γ^2 . In order to avoid the influence of unphysical, extremely high frequencies of the unbounded spectral density (3.12), a cut-off beyond the spectral mode ω_c is usually assumed,

$$J(\omega) = \omega e^{-|\omega|/\omega_c}, \quad (3.13)$$

or equivalent forms like the Drude regularization [69]. The spectral density $J(\omega)$ according to Eq. (3.13) is employed throughout this thesis.

Invoking Def. (3.11) of the spectral density $J(\omega)$, the Fourier-transformed correlation function evaluates to

$$g(E) := \frac{1}{2\pi\hbar} \int_{-\infty}^{\infty} dt G(t) e^{-iEt/\hbar} \quad (3.14)$$

$$= \frac{1}{\pi} n_\beta(E) J(E/\hbar) \quad (3.15)$$

with the thermal occupation number $n_\beta(E) = (e^{\beta E} - 1)^{-1}$ of the oscillator bath, see Appendix A. The correlation function $g(E)$ has the property

$$g(-E) = \frac{1}{\pi} (n_\beta(E) + 1) J(E/\hbar) = e^{\beta E} g(E). \quad (3.16)$$

Since ω_c is a roughly upper frequency bound of $J(\omega)$, the correlation time τ_c of the heat

bath can be inferred to be roughly $\tau_c \simeq 1/\omega_c$ from the inverse Fourier transformation of Eq. (3.15). For very low temperatures, however, the correlation time is rather limited by the temperature, $\tau_c \simeq \hbar\beta$.

3.1.3 Floquet-Markov master equation

Adapted to the relevant degrees of freedom of the isolated Floquet system with the time-periodic Hamiltonian $H_s(t)$, the density operator $\rho(t)$ is now represented in the complete orthonormal basis of the time-periodic parts $|u_i(t)\rangle$ of the Floquet states (2.4). The equation of motion for the Floquet density matrix $\rho_{ij}(t)$ takes the form (compare Eq. (B.47) in Appendix B)

$$\left(\frac{\partial}{\partial t} + \frac{i}{\hbar}\varepsilon_{ij}\right)\rho_{ij}(t) = -\frac{1}{2}\sum_{k,l}\left(\rho_{lj}(t)R_{ik;lk}(t) + \rho_{il}(t)R_{jk;lk}^*(t) - \rho_{kl}(t)\left(R_{lj;ki}(t) + R_{ki;l j}^*(t)\right)\right) \quad (3.17)$$

with the short-hand notation $\varepsilon_{ij} = \varepsilon_i - \varepsilon_j$. This is a coupled system of linear first order differential equations with the complex-valued rates

$$R_{lj;ki}(t) := \sum_L R_{lj;ki}(L)e^{iL\omega t} \quad \text{with} \quad (3.18)$$

$$R_{lj;ki}(L) := \sum_K R_{lj;ki}^{(K)}(L) = 2\pi\frac{\gamma^2}{\hbar}\sum_K x_{lj}(K+L)x_{ki}^*(K)g(\varepsilon_{ik} - K\hbar\omega) \quad (3.19)$$

($L, K \in \mathbb{Z}$), which describe bath-induced probability flows between the individual Floquet states and decoherence processes. They are based on the Fourier coefficients

$$x_{ij}(K) = \frac{1}{\tau}\int_0^\tau dt e^{-i\omega Kt} x_{ij}(t) \quad (3.20)$$

of the time-periodic matrix elements

$$x_{ij}(t) = \langle u_i(t) | x | u_j(t) \rangle . \quad (3.21)$$

We now restrict the analysis to the limit of large times, larger than the relaxation time, $t \gg 1/\Gamma^{(2)}$. Inferring from the Floquet theorem on one hand and general properties of density matrices on the other hand, the asymptotic solution of Eq. (3.17) must be time-periodic

$$\rho_{ij}(t) = \sum_K \rho_{ij}(K)e^{iK\omega t} \quad (3.22)$$

and its Fourier components are governed by the equations

$$\begin{aligned} \frac{i}{\hbar} (K\hbar\omega + \varepsilon_{ij}) \rho_{ij}(K) = & -\frac{1}{2} \sum_{k,l,L} \left(\rho_{lj}(K-L) R_{ik;lk}(L) + \rho_{il}(K-L) R_{jk;lk}^*(-L) \right. \\ & \left. - \rho_{kl}(K-L) \left(R_{lj;ki}(L) + R_{ki;lj}^*(-L) \right) \right). \end{aligned} \quad (3.23)$$

In the spirit of the weak-coupling assumption the rates $R_{lj;ki}(t)$ on the rhs, being of the order $\mathcal{O}(\gamma^2)$, are small with respect to the relevant rates of change in the isolated system. In particular, we take them to be small compared to the driving frequency ω on the lhs, under the assumption that dissipative effects occur on a time scale $1/\Gamma^{(2)}$ larger than the period $\tau = 2\pi/\omega$. Consequently, the leading Fourier coefficients

$$\rho_{ij} := \rho_{ij}(K=0) \quad (3.24)$$

dominate all other contributions $\rho_{ij}(K \neq 0)$, which account for small oscillations about the average value ρ_{ij} . Neglecting those, the summation over L on the rhs of Eq. (3.23) becomes equivalent to taking the cycle-average of the rates

$$R_{lj;ki} := R_{lj;ki}(L=0) = \frac{1}{\tau} \int_0^\tau dt R_{lj;ki}(t) = 2\pi \frac{\gamma^2}{\hbar} \sum_K x_{lj}(K) x_{ki}^*(K) g(\varepsilon_{ik} - K\hbar\omega). \quad (3.25)$$

A system of homogeneous linear equations for the time-independent densities ρ_{ij}

$$0 = \frac{1}{2} \sum_{k,l} \left(\rho_{lj} R_{ik;lk} + \rho_{il} R_{jk;lk}^* - \rho_{kl} (R_{lj;ki} + R_{ki;lj}^*) \right) + \frac{i}{\hbar} \varepsilon_{ij} \rho_{ij} \quad (3.26)$$

remains. Of course, the density operator $\rho(t) = \sum_{i,j} |u_i(t)\rangle \rho_{ij} \langle u_j(t)|$ is still periodic in time because of the inherent time-dependence of the $|u_i(t)\rangle$. In a short-hand matrix notation, Eqs. (3.17) and (3.26) can be written

$$\dot{\rho}_{ij}(t) = - \sum_{k,l} M_{ij;kl}(t) \rho_{kl}(t) \quad \text{and} \quad (3.27)$$

$$0 = \sum_{k,l} M_{ij;kl} \rho_{kl}, \quad (3.28)$$

respectively, with the coefficient matrix

$$M_{ij;kl} := \frac{1}{2} \left(\sum_m R_{im;km} \delta_{jl} + \sum_m R_{jm;lm}^* \delta_{ik} - R_{lj;ki} - R_{ki;lj}^* \right) + \frac{i}{\hbar} \varepsilon_{ij} \delta_{ik} \delta_{jl}. \quad (3.29)$$

It should be emphasized, that this reduction of the differential equations (3.17) to the rate equations (3.26) for its long-time behavior does not require the rates to be small with

respect to all quasienergy spacings ε_{ij}/\hbar [25]. Note also, that Eq. (3.26) could be also obtained directly from Eq. (3.17), when the time-dependent rates $R_{lj;ki}(t)$ are immediately replaced by their cycle-averages $R_{lj;ki}(K=0)$. The stationary solution ρ_{ij} of the resulting differential equation with time-independent coefficients is then determined by Eq. (3.26). This *moderate rotating wave approximation* [74,75] is to be contrasted with the full *rotating wave approximation*, where instead of the average over the driving period τ an average is performed over a longer time scale, given by the maximum value of $\hbar/(K\hbar\omega + \varepsilon_i - \varepsilon_j)$. This approximation requires the rates to be small with respect to *all* quasienergy spacings. For a generic Floquet system this premise can be fulfilled only in a finite-dimensional Hilbert space.

Considering the case, where all rates in Eq. (3.26) are small compared to a certain quasienergy spacing ε_{ij}/\hbar , the corresponding non-diagonal density ρ_{ij} must be likewise small, since the coherent term ε_{ij}/\hbar is independent of the other terms in Eq. (3.26), which involve the rates. The non-diagonal ρ_{ij} might therefore be neglected and, if this can be done even for the smallest quasienergy spacing, a reduced rate equation

$$0 = p_i \sum_k R_{ik} - \sum_k p_k R_{ki} \quad (3.30)$$

for the diagonal densities $p_i := \rho_{ii}$ remains. The herein appearing rates with the short-hand notation

$$R_{ik} := R_{ik;ik} = 2\pi \frac{\gamma^2}{\hbar} \sum_K |x_{ik}(K)|^2 g(\varepsilon_{ki} - K\hbar\omega) \quad (3.31)$$

are real-valued. Again, the full-rotating wave approximation can be applied directly to Eq. (3.17) [21,68,75], resulting in a set of differential equations for the diagonal density matrix elements $\rho_{ii}(t)$, which are then decoupled from those of the non-diagonal density matrix elements $\rho_{ij}(t)$ ($i \neq j$). The latter relax mutually independent,

$$\begin{aligned} \dot{\rho}_{ii} &= -\rho_{ii} \sum_k R_{ik} + \sum_k \rho_{kk} R_{ki} &= -\sum_k M_{ii;kk} \rho_{kk} \\ \dot{\rho}_{ij} &= -\frac{1}{2} \left(\sum_k R_{ik} + R_{jk} - R_{jj;ii} - R_{ii;jj}^* \right) \rho_{ij} - \frac{i}{\hbar} \varepsilon_{ij} \rho_{ij} &= -M_{ij;ij} \rho_{ij} \end{aligned} \quad (3.32)$$

3.2 Effective rate R^{ac} at avoided crossings

The coefficient matrix $M_{ij;kl}$ (3.29) of Eq. (3.28) contains two independent contributions: on the one hand the contributions of the rates and on the other hand the spectral term expressing the coherent dynamics of the isolated Floquet system. It is assumed that Floquet occupations crucially depend on the ratio between those two terms. As an immediate example, the reduction of Eq. (3.26) to Eq. (3.30) is feasible only for very weak system-bath coupling, where the rate term is small compared to all quasienergy spacings. For a Floquet system this is a highly restrictive condition, since the spectrum is bounded within the finite interval $[0, \hbar\omega)$. When approximating the Hilbert space of the Floquet system by a finite number N of basis states and considering the limit $N \rightarrow \infty$, the spectrum typically approaches a dense point spectrum [35, 36] and the number of near degeneracies grows without limit. For a fixed value of the coupling strength γ a critical value of N necessarily exists, above which quasienergy spacings smaller than any of the rates occur, and a transition between the relative strength of the rate contributions on the one hand and the coherent contributions on the other hand can be studied.

Besides, upon variation of a parameter avoided level crossings emerge and give rise to the hybridization of the involved Floquet states. Eventually in the limit $N \rightarrow \infty$, adiabatic transitions between individual Floquet states may not be supported anymore, i.e. any tiny parameter variation will hybridize infinitely many Floquet states in a complex way. This effect has its origin in the intriguing property of Floquet systems, that in any finite interval of the parameter space there exists a dense parameter subset, for which the Floquet states of the N -dimensional basis have an arbitrarily small overlap with any of those corresponding to a larger basis [36]. As argued in Ref. [25], such pathologies are resolved if one takes into account the ubiquitous influence of a heat bath: all near degeneracies that are smaller than a certain effective coupling strength to the bath do not influence the Floquet occupations apart from the trivial hybridization effect. The density operator ρ itself is then not affected by the avoided crossing. This allows to sort the Floquet states via their occupations, thus defining a hierarchical order, which is stable against parameter fluctuations and justifies a truncation of the Floquet basis to a finite number N . Although the Hilbert space may be infinite, the dimension of the Floquet system becomes effectively finite, spanned only by the set of dominantly occupied Floquet states.

In this section, the opposite limit is studied, where a single isolated avoided crossing affects the entire set of Floquet occupations. To begin with, essential steps from Ref. [25] are retraced, resulting in an approximate rate equation with a new, effective rate R^{ac} . For simplicity of notation the time-dependence of the Floquet states is omitted in this section, assuming a fixed time.

3.2.1 Diabatic states of the avoided crossing

Avoided crossings are a generic property of spectra in the absence of symmetries, especially for Floquet spectra with their confined domain $[0, \hbar\omega)$. They emerge under variation of a parameter A , when two quasienergies ε_a and ε_b approach and repel each other (Fig. 3.1). The Floquet solutions $|u_a\rangle$ and $|u_b\rangle$ hybridize and are eventually interchanged.

The states $|u_{a,b}\rangle$ of the avoided crossing can be approximately expressed as a linear combination of the *diabatic* states $|\bar{u}_{1,2}\rangle$, which remain almost invariant throughout the avoided crossing and would correspond to an exact crossing of the asymptotic branches $\bar{\varepsilon}_1$ and $\bar{\varepsilon}_2$ at $A = A_0$. The situation is modelled [48,76] by the Floquet operator in the subspace of the avoided crossing

$$\mathcal{H}^{\text{ac}} = \begin{pmatrix} \bar{\varepsilon}_1(A) & \Delta/2 \\ \Delta/2 & \bar{\varepsilon}_2(A) \end{pmatrix}, \quad (3.33)$$

represented in the A -independent basis of the diabatic states $|\bar{u}_{1,2}\rangle$. Far away from the center A_0 of the avoided crossing, where the Floquet states are almost identical to their diabatic approximates, the quasienergies are presumed to be linear functions of A ,

$$\bar{\varepsilon}_{1,2}(A) = \varepsilon_0 + \sigma_{1,2} \cdot (A - A_0). \quad (3.34)$$

By virtue of the finite coupling term $\mathcal{H}_{12}^{\text{ac}} = \mathcal{H}_{21}^{\text{ac}} = \Delta/2$ the eigenvalues

$$\varepsilon_{a,b} = \frac{\bar{\varepsilon}_1 + \bar{\varepsilon}_2}{2} \pm \frac{1}{2} \sqrt{(\bar{\varepsilon}_1 - \bar{\varepsilon}_2)^2 + \Delta^2} \quad (3.35)$$

of \mathcal{H}^{ac} repel each other, where the minimal splitting is Δ . The corresponding eigenstates $|u_{a,b}\rangle$ are

$$|u_{a,b}\rangle = \frac{1}{\sqrt{2}} \begin{pmatrix} \sqrt{1 \pm \frac{d}{\sqrt{1+d^2}}} \\ \pm \sqrt{1 \mp \frac{d}{\sqrt{1+d^2}}} \end{pmatrix}, \quad (3.36)$$

where the dimensionless ratio

$$d := \frac{(\bar{\varepsilon}_1 - \bar{\varepsilon}_2)}{\Delta} = \frac{(\sigma_1 - \sigma_2)}{\Delta} (A - A_0) \quad (3.37)$$

measures the distance from the center A_0 of the avoided crossing. They arise from $|\bar{u}_{1,2}\rangle$ by the rotation

$$|u_a\rangle = \alpha |\bar{u}_1\rangle + \beta |\bar{u}_2\rangle \quad (3.38a)$$

$$|u_b\rangle = \beta |\bar{u}_1\rangle - \alpha |\bar{u}_2\rangle \quad (3.38b)$$

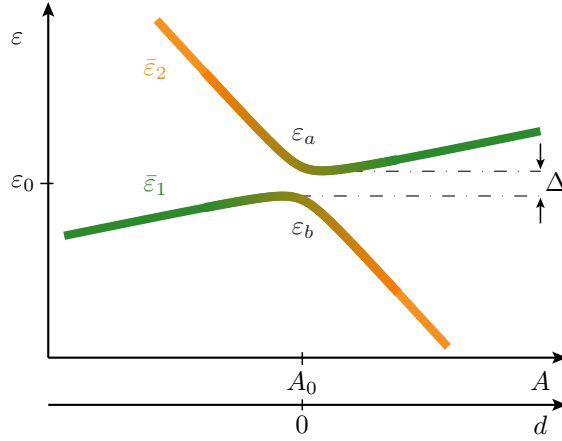


Figure 3.1: Avoided crossing between quasienergies ε_a and ε_b with the minimal splitting $\Delta = \varepsilon_a(A_0) - \varepsilon_b(A_0)$ vs. parameter A . The dimensionless distance d to the avoided crossing is defined by Def. (3.37). The asymptotic quasienergy branches $\bar{\varepsilon}_1$ and $\bar{\varepsilon}_2$ cross exactly in the center A_0 of the avoided crossing.

with the coefficients

$$\alpha = \frac{1}{\sqrt{2}} \sqrt{1 + \frac{d}{\sqrt{1+d^2}}} \quad (3.39)$$

$$\beta = \frac{1}{\sqrt{2}} \sqrt{1 - \frac{d}{\sqrt{1+d^2}}} \quad (3.40)$$

which satisfy $\alpha^2 + \beta^2 = 1$, as well as the relations $d = (\alpha^2 - \beta^2) / (2\alpha\beta)$ and $\varepsilon_{ab} = \varepsilon_a - \varepsilon_b = \Delta\sqrt{1+d^2} = \Delta/(2\alpha\beta)$. The diabatic states are evaluated from the true Floquet solutions $|u_a\rangle$ and $|u_b\rangle$ by the inverse transformation of Eq. (3.38),

$$|\bar{u}_1\rangle = \alpha |u_a\rangle + \beta |u_b\rangle \quad (3.41a)$$

$$|\bar{u}_2\rangle = \beta |u_a\rangle - \alpha |u_b\rangle. \quad (3.41b)$$

In opposition to the *diabatic* states $|\bar{u}_{1,2}\rangle$, the eigenstates of the Floquet operator $|u_{a,b}\rangle$ may be denoted as the *adiabatic* states³. We point out, that the entire Floquet basis $\{|u_i\rangle\} = \{|u_a\rangle, |u_b\rangle, |u_i\rangle \mid i \neq a, b\}$ is in the following denoted as the adiabatic basis, whereas the term diabatic basis refers to the set of states $\{|\bar{u}_1\rangle, |\bar{u}_2\rangle, |u_i\rangle \mid i \neq a, b\}$. All quantities represented in the diabatic basis are indicated by an overbar.

3.2.2 Diabatic representation of the rate equation

In order to remove the trivial parameter dependence of the Floquet basis originating from the hybridization of the adiabatic states, we aim to find the analog of the rate equation (3.26)

³We use these expressions, as they are termed in the context of the Born-Oppenheimer approximation for the Schrödinger equation of molecules.

in the local diabatic basis of the avoided crossing. In the subspace of the avoided crossing the diabatic density matrix elements are related to the adiabatic density matrix elements via

$$\bar{\rho}_{11} = \alpha^2 \rho_{aa} + \beta^2 \rho_{bb} + 2\alpha\beta \operatorname{Re}\rho_{ab} \quad (3.42a)$$

$$\bar{\rho}_{22} = \beta^2 \rho_{aa} + \alpha^2 \rho_{bb} - 2\alpha\beta \operatorname{Re}\rho_{ab} \quad (3.42b)$$

$$\operatorname{Re}\bar{\rho}_{12} = \alpha\beta(\rho_{aa} - \rho_{bb}) - (\alpha^2 - \beta^2) \operatorname{Re}\rho_{ab} \quad (3.42c)$$

$$\operatorname{Im}\bar{\rho}_{12} = -\operatorname{Im}\rho_{ab}. \quad (3.42d)$$

Here we outline only a few steps of the derivation and focus on the result. A more detailed derivation is explicated in Appendix D. The starting point is the equation of motion (3.8) for $\rho(t)$, already in Born-Markov approximation, but still independent of a certain representation. The following assumptions are made:

- (i) Almost all quasienergy spacings are larger than the effective coupling strength to the heat bath, with the exception of the single quasienergy spacing ε_{ab} .
- (ii) The deviations between $\varepsilon_{a,b}$ and their asymptotic approximates $\bar{\varepsilon}_{1,2}$ as well as the spacings ε_{ab} and $|\bar{\varepsilon}_{12}|$ are tiny compared to the mean quasienergy spacing. All of them are then treated as equal, $\varepsilon_a \approx \varepsilon_b \approx \bar{\varepsilon}_1 \approx \bar{\varepsilon}_2$, in the arguments of the correlation function $g(E)$. The error takes its maximum value, Δ , at A_0 . Provided that the correlation function does not vary strongly on the scale Δ , i.e. $\Delta \ll \hbar/\tau_c$, the approximation is not critical. This is automatically satisfied, since we here restrict ourselves to cases $\hbar/\tau_c > \hbar\omega$.
- (iii) The derivation of the desired rate equation further relies on a different spatial structure of the states $|\bar{u}_1\rangle$ and $|\bar{u}_2\rangle$, as can be established e.g. if these arise from energetically widely separated states of the undriven system. In this case the avoided crossing is very small at the same time.

When representing Eq. (3.8) in the diabatic basis instead of the Floquet basis, it can be shown with the help of the approximation (ii), that the rhs of Eq. (3.17) is reproduced form invariant. Therein, out of all the rates involving the state $|\bar{u}_1\rangle$, eventually only the real-valued rates \bar{R}_{11} , $\bar{R}_{1i} = \bar{R}_{i1}$, $\bar{R}_{1i;i1}$, $\bar{R}_{i1;1i}$ remain as a consequence of the approximations (iii). The same holds for the accordant quantities referring to the state $|\bar{u}_2\rangle$, and also $\bar{R}_{11;22}$ and $\bar{R}_{22;11}$ are in general non-negligible. Finally, the approximation (i) allows an almost complete separation of the non-diagonal density matrix elements in the manner of the reduction from Eq. (3.26) to the diagonal form (3.30), with the exception of the remaining elements $\bar{\rho}_{12}$, $\bar{\rho}_{21}$.

The finally resulting system of rate equations for the long-time limit of the evolution presents itself in the following way: The rates \bar{R}_{ik} in the diabatic representation, which are

defined equivalently to the original rates (3.31) of the Floquet basis, are invariant under the variation of the parameter A . The internal rates of the avoided crossing, which under the above assumptions are negligible, $\bar{R}_{12} \approx \bar{R}_{21} \approx 0$, have to be replaced by the effective rate

$$R^{\text{ac}} := \frac{\Gamma}{(\hbar\Gamma/\Delta)^2 + 4d^2}. \quad (3.43)$$

This rate explicitly depends on the parameter $d \sim (A - A_0)$. The composite rate

$$\Gamma := \sum_k (\bar{R}_{1k} + \bar{R}_{2k}) - 2\text{Re}\bar{R}_{11;22} \quad (3.44)$$

accounts basically for all transitions that depopulate the states of the avoided crossing. Like all other rates, it is proportional to γ^2 with a factor that is specific to the individual avoided crossing. Note, that we have assumed $\text{Im}\bar{R}_{11;22} = 0$ in the above definition of R^{ac} , which is exact for symmetric driving, $H_s(-t) = H_s(t)$, as shown in Appendix D. Otherwise, the definition (3.43) has to be slightly modified by the shift $2d \rightarrow 2d + \hbar\text{Im}\bar{R}_{11;22}/\Delta$ (compare Eq. (D.18)). The rate equations for the diagonal densities $\bar{p}_i = \bar{\rho}_{ii}$ formally adopt the identical structure as the reduced rate system (3.30),

$$0 = \bar{p}_i \sum_k \bar{R}_{ik} - \sum_k \bar{p}_k \bar{R}_{ki}, \quad (3.45)$$

but here the negligible rates $\bar{R}_{12}, \bar{R}_{21}$ are substituted by R^{ac} ,

$$\bar{R}_{12}, \bar{R}_{21} \rightarrow R^{\text{ac}}. \quad (3.46)$$

Besides, in contrast to Eq. (3.30), the non-diagonal density matrix element $\bar{\rho}_{12}$

$$\bar{\rho}_{12} = \frac{2d + i\hbar\Gamma/\Delta}{(\hbar\Gamma/\Delta)^2 + 4d^2} (\bar{p}_1 - \bar{p}_2) = \left(2d + i\frac{\hbar\Gamma}{\Delta}\right) \frac{R^{\text{ac}}}{\Gamma} (\bar{p}_1 - \bar{p}_2) \quad (3.47)$$

exists, though decoupled from the rate equations (3.45) for the diagonal elements.

As a side note we remark that we have for simplicity assumed real-valued non-diagonal elements $\mathcal{H}_{12}^{\text{ac}} = \mathcal{H}_{21}^{\text{ac}} = \Delta/2$ of the Floquet operator \mathcal{H}^{ac} . In general, an additional phase factor χ had to be taken into account, $\mathcal{H}_{12}^{\text{ac}} = (\mathcal{H}_{21}^{\text{ac}})^* = \chi^* \Delta/2$, reflecting that the eigenstates of the Floquet operator are only defined up to a phase factor. In contrast to the other parameters of \mathcal{H}^{ac} in (3.33), χ cannot be determined from the avoided crossing itself. It can be shown that the additional phase factor χ has an effect only on the non-diagonal density $\bar{\rho}_{12}$, which is modified by that phase via $\bar{\rho}_{12} \rightarrow \chi^* \bar{\rho}_{12}$ compared to the result (3.47).

The additional rate R^{ac} in (3.45) measures the effective probability flow between the states $|\bar{u}_1\rangle$ and $|\bar{u}_2\rangle$ of the avoided crossing. The main advantage of the diabatic representation

is, that exclusively the rate R^{ac} is affected when tuning the distance d from the avoided crossing. It has the shape of a Lorentzian with the full width at half maximum of $\hbar\Gamma/\Delta$ and the maximum value of $(\Delta/\hbar)^2\Gamma^{-1}$.

If R^{ac} is only small compared to other relevant rates in Eq. (3.45), its influence is certainly negligible. This happens either for $|d| \gg 1$, or independent of d , under the condition that the effective coupling strength is larger than the minimal spacing Δ , $\hbar\Gamma \gg \Delta$. On the contrary, if $\hbar\Gamma \ll \Delta$, R^{ac} dominates against Γ in the center $d = 0$ of the avoided crossing. For the moment we regard the coupling strength γ as a tunable parameter, although this is usually not the case in practice. In the limit $\gamma \rightarrow 0$ the effective coupling strength $\hbar\Gamma$ eventually falls below the spacing Δ of the avoided crossing, and then $R^{\text{ac}} > \Gamma$ is fulfilled around $d = 0$. Allowing γ to decrease further, R^{ac} becomes dominant compared to all other rates in Eq. (3.45), whose solution can thus be changed severely. In Chapter 5 we study such effects, first of all a remarkable application in a bistable potential (Section 5.1). Note, that R^{ac} diverges at $d = 0$ for $\gamma = 0$. From the equation for $i = 1$ in Eq. (3.45)

$$0 = \bar{p}_1 \sum_{k \neq 1,2} \bar{R}_{1k} + \bar{p}_1 R^{\text{ac}} - \sum_{k \neq 1,2} \bar{p}_k \bar{R}_{k1} - \bar{p}_2 R^{\text{ac}} \quad (3.48)$$

follows that a divergent R^{ac} enforces equality of the occupations \bar{p}_1 and \bar{p}_2 , and therefore the divergence of R^{ac} is not critical.

To summarize these considerations, we interpret Γ , defined in Eq. (3.44), as the characteristic coupling strength of the avoided crossing under consideration. The question, whether an avoided crossing can change the state ρ or not, is decided by the parameter $\hbar\Gamma/\Delta$. If the criterion $\hbar\Gamma/\Delta \ll 1$ is satisfied, ρ changes around $d = 0$. Examples, where the avoided crossing induces prominent changes of the asymptotic state, will be studied in Chapter 5. However, a conclusion about the range of influence around $d = 0$ cannot be established by a general criterion. This intricate question would require to identify certain relevant rates in Eq. (3.45), to which R^{ac} had to be put in relation. For example, the naive guess, that the range of impact is estimated by the condition $R^{\text{ac}} > \Gamma$, falls often short. If for example the components $\sum_{k \neq 1} \bar{R}_{1k}$ and $\sum_{k \neq 2} \bar{R}_{2k}$ differ by orders of magnitude, the influence range of R^{ac} around $d = 0$ can appear considerably enlarged. Such a behavior will be illustrated in an example of Section 5.1.3.

3.3 Displaced signatures of avoided crossings due to Lamb shifts

In the previous section the rate equations for the asymptotic state ρ have been analyzed at an avoided level crossing, where two quasienergies $\varepsilon_{a,b}$ as function of a parameter A approach each other up to a minimal spacing Δ . The influence of the avoided crossing on ρ depends crucially on the characteristic parameters Δ and $\sigma_{1,2}$ of the avoided crossing, as the definition (3.43) of the rate R^{ac} indicates. We therefore expect that already small perturbations of the spectrum in the vicinity of the avoided crossing can give rise to severe deviations from the solution predicted by Eq. (3.45). Such a perturbation comes along with the coupling to the heat bath itself: the back action of the bath on the system in general leads to a renormalization of the system energies. Instead of the unperturbed spectrum, the bath experiences a slightly modified spectrum, owing to the interaction with the system⁴. In quantum optics the deviation between the effective and the unperturbed spectrum are paraphrased as the *Lamb shifts*. The Lamb shifts arise from the principal value integrals (B.41) of the bath correlation function $g(E)$, which are usually disregarded in the derivation of the Born-Markov master equation, although they can cause deviations from the canonical distribution even in the framework of time-independent systems [38, 39].

We address the question, how the Lamb shifts influence the solutions of Eq. (3.26) in the vicinity of avoided crossings. To this end, we include the Lamb shifts into the original Floquet-Markov master equation and derive from this a modified version of the rate equation system for its asymptotic solutions

$$0 = \frac{1}{2} \sum_{k,l} \left(\rho_{lj} \hat{R}_{ik;lk} + \rho_{il} \hat{R}_{jk;lk}^* - \rho_{kl} (\hat{R}_{lj;ki} + \hat{R}_{ki;lj}^*) \right) + \frac{i}{\hbar} \varepsilon_{ij} \rho_{ij} . \quad (3.49)$$

The derivation is explicated in Appendix C. This rate equation has the identical form as the original rate equation, Eq. (3.26), but involves modified rates

$$\hat{R}_{lj;ki} := R_{lj;ki} - i S_{lj;ki} , \quad (3.50)$$

where the original rates $R_{lj;ki}$ of Defs. (3.18) and (3.19) are extended by the additional contributions

$$S_{lj;ki}(t) := \sum_L S_{lj;ki}(L) e^{iL\omega t} \quad \text{with} \quad (3.51)$$

$$S_{lj;ki}(L) := 2\gamma^2 \sum_K x_{lj}(K+L) x_{ki}^*(K) \left(\Delta'(-\varepsilon_{ki} - K\hbar\omega) - \Delta_1(\varepsilon_{ki} + K\hbar\omega) \right)$$

($L, K \in \mathbb{Z}$). In Eq. (3.49) again only the cycle-averages $S_{lj;ki} := S_{lj;ki}(L=0)$ of these terms are relevant, in analogy to the rates $R_{lj;ki}$ of Def. (3.25). The quantities $\Delta'(E)$ and $\Delta_1(E)$

⁴This effect is best demonstrated for a time-independent two-level system [77].

are based on principal value integrals of the correlation function $g(E)$, see Eq. (C.5).

To answer the above question, we analyze the modified Floquet-Markov rate equations at an avoided crossing. We take Eq. (3.49) as starting point and, following the lines of Section 3.2 and Appendix D, transform it into the diabatic basis of the avoided crossing. The detailed derivation is deferred to Appendix E and eventually leads to the approximate rate equations

$$0 = \bar{p}_i \sum_k \bar{R}_{ik} - \sum_k \bar{p}_k \bar{R}_{ki}, \quad (3.52)$$

where instead of the negligible rates \bar{R}_{12} and \bar{R}_{21} again an effective rate R^{ac} occurs,

$$\bar{R}_{12}, \bar{R}_{21} \rightarrow R^{\text{ac}} := \frac{\Gamma}{(\hbar\Gamma/\Delta)^2 + (2d - \hbar\Sigma/\Delta)^2}. \quad (3.53)$$

The composite rate $\Sigma = \sum_k (\bar{S}_{1k} - \bar{S}_{2k}) - 2\text{Im}\bar{R}_{11,22}$ is defined in analogy to Γ in Def. (3.44). Interestingly, the original rates \bar{R}_{ik} (in the diabatic basis) are recovered in Eq. (3.52) instead of the modified rates $\hat{\bar{R}}_{ik}$, and it is therefore identical to Eq. (3.45). The only novelty is encountered in the effective rate R^{ac} , which according to Def. (3.53) now reaches its maximum value at $d = d^* := \hbar\Sigma/(2\Delta)$ instead of $d = 0$ in the original definition (3.43). This indicates that the parameter value of maximum occupation change, indicating the maximum influence of the avoided crossing, is displaced away from its actual position.

This phenomenon, although non-intuitive at the first glance, is qualitatively in line with the interpretation of the Lamb shifts as the deviations between the unperturbed quasi-energy spectrum and the effective spectrum experienced by the bath. Since the influence of an avoided crossing on the \bar{p}_i depends sensitively on its characteristic parameters Δ and $\sigma_{1,2}$, one can expect that any spectral changes, of the unperturbed or the effective system, can drastically change the occupations \bar{p}_i . If the unperturbed spectrum, apart from the quasienergies $\varepsilon_{a,b}$ at $d = 0$, changes only slightly within the range $|d| \lesssim |d^*|$, the solution of Eq. (3.52) at a parameter value d might be associated with the original solution of Eq. (3.45), but at the shifted parameter value $d - d^*$.

The value d^* estimates the displacement of the avoided crossing in the effective spectrum. Since the rate Σ scales with γ^2 , a notable displacement d^* is expected only for a relatively strong system-bath coupling. At the same time, as discussed in the previous section, the avoided crossing can only cause strong changes in the \bar{p}_i for sufficiently small γ , where $\hbar\Gamma < \Delta$ is fulfilled. Hence, a severe effect of the avoided crossing away from its center is restricted to the range $\hbar\Gamma < \Delta \lesssim \hbar\Sigma$, where both Γ and Σ are proportional to γ^2 . In Section 5.1 an example of such a remarkable displacement is studied in a driven bistable potential.

As a side note, we recall that even without the Lamb shifts a displacement effect might occur, if $\Sigma = -2\text{Im}\bar{R}_{11,22}$ takes a finite value. For $H_s(-t) = H_s(t)$ it vanishes, as shown in Appendix D.

3.4 Diffusion in the extended zone scheme

In this section a complementary approach to the asymptotic dynamics of driven dissipative systems is introduced. We relate the dissipative process of the driven system to a random walk in the ‘extended zone scheme’. By that term, which is again borrowed from the Bloch theory of solids, we mean the division of the energy axis into the Brillouin zones. The characteristic quantities underlying this stochastic process are borrowed from the microscopic model of Section 3.1. We would like to point out, that this section is rather detached from the remaining parts of the thesis and the method introduced herein, though interesting in itself, will not be used elsewhere in the thesis.

3.4.1 Random walk

As mentioned in Section 2.1, the Floquet states $|\psi_i(t)\rangle$ have infinitely many equivalent time-periodic representations $|u_i^{(e)}(t)\rangle$, each associated with a quasienergy $\varepsilon_i^{(e)}$, that is situated in the e -th Brillouin zone, $(e-1)\hbar\omega \leq \varepsilon_i^{(e)} \leq e\hbar\omega$. In this section, instead of choosing a single representation $\{|u_i(t)\rangle, \varepsilon_i\} \equiv \{|u_i^{(0)}(t)\rangle, \varepsilon_i^{(0)}\}$ out of the family of Floquet representations, we treat the $|u_i^{(e)}(t)\rangle$ as independent states of the extended basis set, denoted by the multi-index (i, e) . The Brillouin zone indices $e \in \mathbb{Z}$ measure the energy in integer units of $\hbar\omega$.

The probabilistic character of the transitions between the states (i, e) can be described by a random walk on the grid of the multi-indices (i, e) in the extended zone scheme, see the illustration in Fig. 3.2. A trajectory (i_t, e_t) passes from a site (i, e) to another site $(k, e - K)$ with a characteristic transition probability $R_{ik}^{(K)}$. We quantify these transition probabilities in terms of the Floquet rates

$$R_{ik}^{(K)} := 2\pi \frac{\gamma^2}{\hbar} |x_{ik}(K)|^2 g(\varepsilon_{ki} - K\hbar\omega), \quad (3.54)$$

defined according to Eqs. (3.19) and (3.31) of the microscopic model. The Fourier index K is limited within a band, $|K| \leq K_{\max}$, where K_{\max} is chosen such that matrix elements $x_{ik}(|K| > K_{\max})$ are negligible. The transition probabilities $R_{ik}^{(K)}$ do not depend on initial and final Brillouin zones e and e' , but only on their distance $e' - e$. This approach does not account for the rates $R_{lj;ki}^{(K)}$ with $l \neq k$ or $j \neq i$, nor for the higher order Fourier contributions $R_{ik}^{(K)}(L \neq 0)$.

The random walk of a single trajectory on the energy axis is implemented in the following way, known as the *Gillespie algorithm* [78]:

- (i) The trajectory (i_t, e_t) is initialized at the time $t = 0$ on a site $(i_0, e_0 = 0)$.
- (ii) Since the rates $R_{ik}^{(K)}$ can differ by many orders of magnitude, it is not suitable to predefine time steps of fixed size and perform a transition in each of them. It would then take too many iterations for a transition with only a tiny rate to occur. Besides,

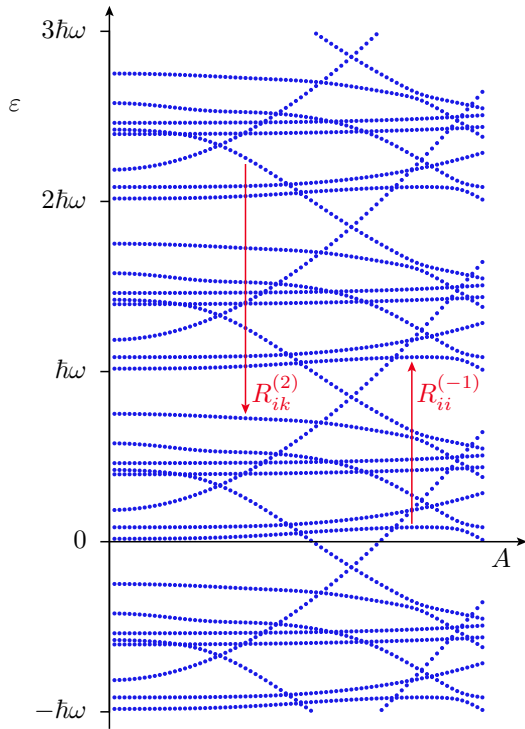


Figure 3.2: Quasienergies $\varepsilon_i^{(e)}$ in four Brillouin zones of the extended zone scheme vs. a parameter A . The arrows indicate two of the transition rates $R_{ik}^{(K)}$.

this type of random walk is not describable by a master equation [79]. Instead, the trajectory remains at a given site (i, e) for a time Δ_t , that is chosen as a random number from an exponential distribution $p(\Delta_t) = e^{-\Delta_t/t_{(i,e)}} / t_{(i,e)}$, expressing a generic decay law. The characteristic dwell time $t_{(i,e)} = 1/R_{i,\Sigma}$ at the site (i, e) is determined as the inverse of the total rate

$$R_{i,\Sigma} := \sum_{k,K} R_{ik}^{(K)} - R_{ii}^{(0)} \quad (3.55)$$

of all transitions leading away from the present site. The contribution of the rate $R_{ii}^{(0)}$ to the sum has to be subtracted, as it induces no transition in the extended zone scheme. This rate has in general finite values, but cancels in the rate equation (3.26) of the Floquet-Markov formalism.

- (iii) The second step is to determine the target site. We divide the interval $[0, 1]$ into $N \cdot (2K_{\max} + 1)$ disjoint intervals, such that their respective widths are proportional to $R_{ik}^{(K)}$. Accordingly, a random number from a uniform distribution in $[0, 1]$ uniquely determines the active rate $R_{ik}^{(K)}$ and the trajectory undergoes the transition $(i, e) \rightarrow (k, e - K)$. The interval corresponding to the rate $R_{ii}^{(0)}$ is set zero. The reason is, that the process associated with the transition probability $R_{ii}^{(0)}$ leaves the trajectory at its present site (i, e) , in contradiction to the elapsed dwell time Δ_t , after which a transition takes place by definition of step (ii).

For an ensemble of evolving trajectories of this stochastic process the density of trajec-

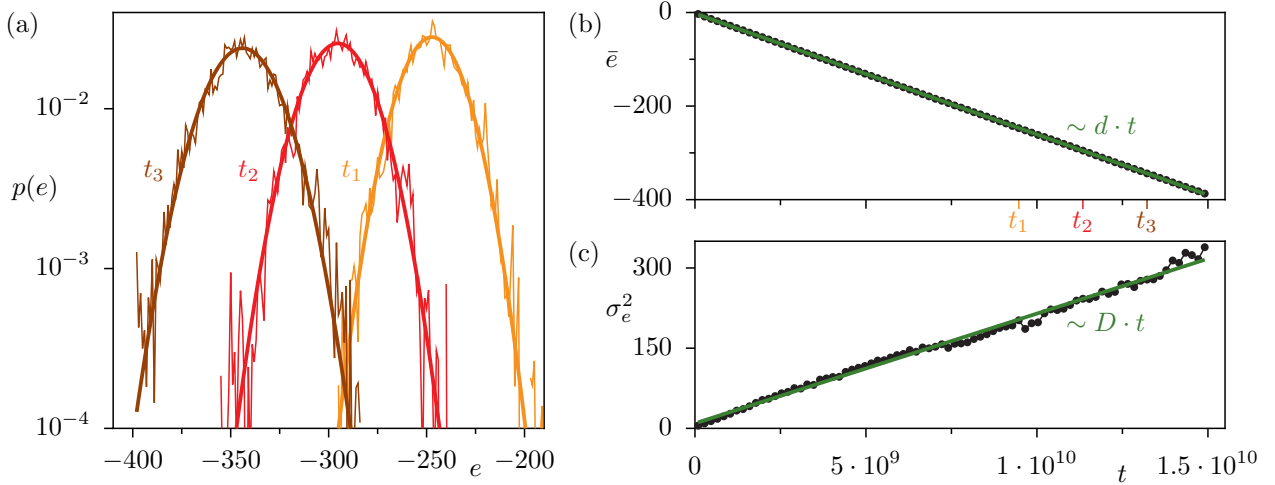


Figure 3.3: (a) Probability distribution $p(e)$ of 1000 trajectories at three different times of the random walk, indicated on the abscissa of (b), and corresponding Gaussian fits $p_f(e) = (\sqrt{2\pi}\sigma_e)^{-1}e^{-(e-\bar{e})^2/(2\sigma_e^2)}$. Time evolution of (b) the Gaussian mean $\langle e \rangle = \bar{e}$ and (c) the variance $\sigma_e^2 = \langle (e - \langle e \rangle)^2 \rangle$, each with linear fit $\bar{e} = d \cdot t$ and $\sigma_e = D \cdot t$. The random walk is based on the rates $R_{ik}^{(K)}$ between the three lowest Floquet states of the driven system (3.59) with $\mu = 0.09$, $A = 0.005$, $\hbar\omega = 0.212$, $\hbar = 0.13$, $\beta = 40$, $\eta = 4 \cdot 10^{-6}$, and $\omega_c/\omega = 100$.

jectories at a site (i, e) determines its occupation probability $p_i(e)$. It evolves according to the master equation

$$\frac{dp_i(e)}{dt} = -p_i(e) \sum_{k,K} R_{ik}^{(K)} + \sum_{k,K} p_k(e+K) R_{ki}^{(K)}. \quad (3.56)$$

By construction of the transition rates (3.54), the random walk eventually leads the probabilities $p_i := \sum_e p_i(e)$ to a time-independent state, satisfying Eq. (3.30), i.e. to the Floquet occupations. The reduced probabilities p_i and $p(e) := \sum_i p_i(e)$ are then independent, $p_i(e) = p_i \cdot p(e)$. The reduced weights $p(e)$ characterize the distribution of the energy on a coarse-grained level, that does not resolve the substructure of the Brillouin zones, i.e. the individual quasienergies ε_i . As the distribution is then stationary with respect to i , $\dot{p}_i = 0$, the master equation becomes

$$p_i \dot{p}(e) = -p_i p(e) \sum_{k,K} R_{ik}^{(K)} + \sum_{k,K} p_k p(e+K) R_{ki}^{(K)} \quad (3.57)$$

$$\stackrel{(3.30)}{=} \sum_{k,K} p_k R_{ki}^{(K)} (p(e+K) - p(e)), \quad (3.58)$$

where the second line makes use of the asymptotic balance (3.30) of the Floquet occupations.

To analyze the random walk and to determine the distributions p_i and $p(e)$ from an ensemble of evolving trajectories, the total evolution time is divided into equispaced time intervals. In each interval $[t_1, t_2]$ only those trajectories are considered, which contain at least one transition event. The occupation probabilities $p_i|_{t_1}^{t_2}$ and $p(e)|_{t_1}^{t_2}$ of a certain site (i, e) are

determined from the frequency of occurrence of i and e within $[t_1, t_2]$, each weighted with the respective time, which the trajectory dwells there. Finally, an average is taken over the ensemble of trajectories. The time spans $t_2 - t_1$ should be large enough to contain on average some incidents even of the least probable sites. Note, that the characteristic dwell times $t_{(i,e)}$ are of the order $\mathcal{O}(\gamma^{-2})$ and especially exceed the driving period τ , such that $t_2 - t_1 \gg \tau$ is naturally required.

The random walk in the extended zone scheme is a diffusive process and the distribution $p(e)$ of an ensemble of trajectories eventually becomes Gaussian. Figure 3.3(a) shows an example of the distribution at three times during the evolution of the random walk, each with fitted Gaussians $p_f(e) = (\sqrt{2\pi}\sigma_e)^{-1}e^{-(e-\bar{e})^2/(2\sigma_e^2)}$ with the mean \bar{e} and the variance σ_e^2 . To allow a straightforward interpretation, the rates $R_{ik}^{(K)}$ of this example are taken from a low-dimensional system, consisting of the Floquet states that originate from the three lowest eigenstates in the asymmetric double well potential

$$H(t) = \frac{\hbar^2}{2} \frac{\partial^2}{\partial x^2} + x^4 - x^2 + x(\mu + A \cos \omega t) . \quad (3.59)$$

The temperature is chosen sufficiently small, such that the truncation to a three-level system is appropriate, with $\beta(E_2 - E_0) \approx 8$. The trajectories of the random walk start from an initial distribution $p_i(e) \sim \delta_{e,0}$ in the first Brillouin zone. Note, that the probabilities p_i , which are not shown in Fig. 3.3, converge on a much shorter time scale to their asymptotic values, identical to the Floquet occupations. As Fig. 3.3(b) suggests that the random walk in the extended zone scheme is biased: the trajectories evolve on average with a constant drift velocity d , giving rise to the linear drift of the mean value $\langle e \rangle = d \cdot t$. The diffusive character of the stochastic process is confirmed in Fig. 3.3(c) by the linearly increasing variance $\langle (e - \langle e \rangle)^2 \rangle = D \cdot t$.

Figures 3.4(a) and (b) present the drift d and the diffusion constant D , respectively (green), vs. the driving frequency ω . Both parameters reveal a very similar and distinct resonant enhancement, occurring at the parameter positions of near degeneracies in the quasienergy spectrum, see Fig. 3.4(c). These near degeneracies are avoided crossings, which can be related to the resonance frequencies $\omega_{10} = (E_1 - E_0)/\hbar$, ω_{21} , ω_{20} , and $\omega_{20}/2$ of the three-level system. For a higher-dimensional system with a denser spectrum the behavior of d and D would become increasingly structured. The identification of the individual avoided crossings in terms of the resonance frequencies of the undriven system is particularly clear in the chosen example, since the system is weakly driven. We restrict the discussion to this relatively clear case, whereas in general a more detailed analysis is required.

The characteristic parameters d and D of the diffusion process in the extended zone

scheme are already determined by the underlying microscopic model:

$$d = \frac{d}{dt} \langle e \rangle = \frac{d}{dt} \sum_{i,e} p_i(e) e = \sum_{i,e} p_i \dot{p}(e) e \quad (3.60)$$

$$\stackrel{(3.58)}{=} \sum_{k,i,K} p_k R_{ki}^{(K)} \sum_e [p(e+K) - p(e)] e = \sum_{k,i,K} p_k R_{ki}^{(K)} \sum_e p(e) [e - K - e] \quad (3.61)$$

$$= - \sum_{k,i,K} p_k R_{ki}^{(K)} K \quad (3.62)$$

and

$$D = \frac{d}{dt} (\langle e^2 \rangle - \langle e \rangle^2) = \frac{d}{dt} \sum_{i,e} p_i(e) e^2 - 2 \langle e \rangle \frac{d}{dt} \langle e \rangle \quad (3.63)$$

$$\stackrel{(3.62)}{=} \sum_{i,e} p_i \dot{p}(e) e^2 + 2 \langle e \rangle \sum_{k,i,K} p_k R_{ki}^{(K)} K \quad (3.64)$$

$$\stackrel{(3.58)}{=} \sum_{k,i,K} p_k R_{ki}^{(K)} \sum_e [p(e+K) - p(e)] e^2 + 2 \langle e \rangle \sum_{k,i,K} p_k R_{ki}^{(K)} K \quad (3.65)$$

$$= \sum_{k,i,K} p_k R_{ki}^{(K)} \sum_e p(e) [(e-K)^2 - e^2 + 2eK] \quad (3.66)$$

$$= \sum_{k,i,K} p_k R_{ki}^{(K)} K^2. \quad (3.67)$$

In Figs. 3.4(a) and (b) the corresponding values for the drift d and the diffusion constant D , respectively, are indicated by the black circles. The estimate (3.62) for the drift constant d is identical to the fit parameter of the random walk (green). The estimate (3.67) for the diffusion constant D qualitatively also agrees with the respective fit parameter of the random walk. However, quantitatively there are considerable deviations, whose origin is open.

The observed strong correlation between d and D can be explained by means of Eqs. (3.62) and (3.67), in combination with the circumstance of weak driving: if the driving is harmonic and only weak, the rates $R_{ik}^{(K)}$ are strongly peaked at specific Fourier contributions K_{ik}^* . For the moment we assume the limiting case $R_{ik}^{(K)} = R_{ik}^* \delta(K - K_{ik}^*)$, which would result from the specific coupling matrix $A_{ik}(t) = A_{ik} e^{iK_{ik}^* \omega t}$. Further assuming, that the K_{ik}^* are even identical for each of the pairs (i, k) , the sums in Eqs. (3.62) and (3.67) simplify to the approximate values $d \approx -K^* \sum_{k,i} p_k R_{ki}^{(K^*)}$ and $D \approx (K^*)^2 \sum_{k,i} p_k R_{ki}^{(K^*)}$, which are related by $D = -K^* d$. In the present case, the ratio D/d is of the order -1 , but with fluctuations, that indicate the deviations from the rather restrictive approximation for very weak driving.

The existence of finite drift and diffusion constants indicates the failure of the detailed balance $p_i R_{ik} = p_k R_{ki}$. As a counterexample we again assume rates of the type $R_{ik}^{(K)} =$

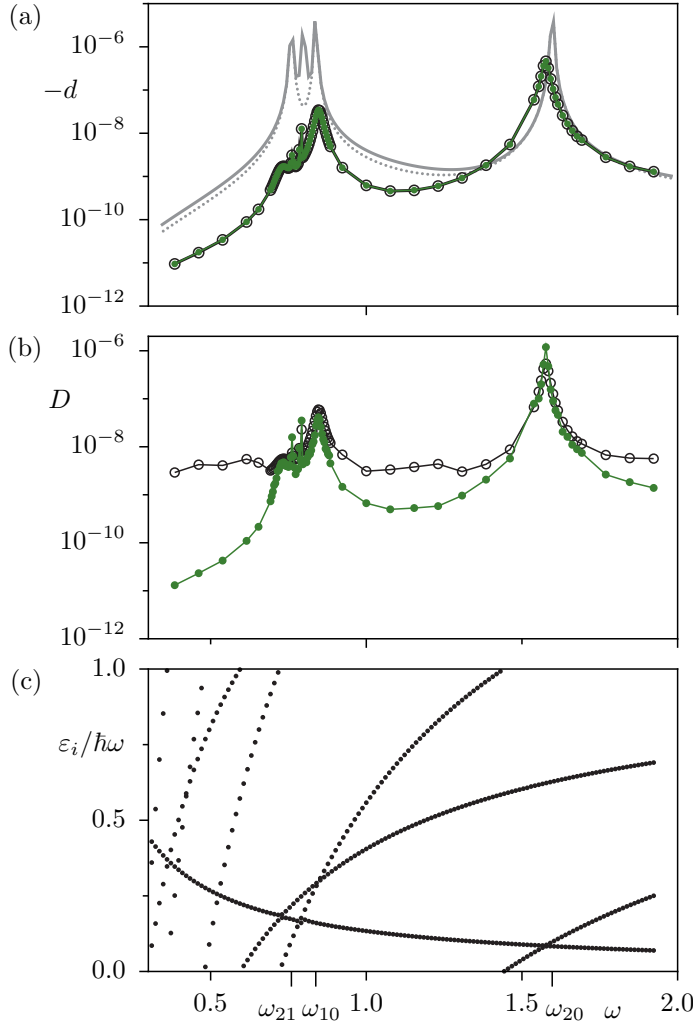


Figure 3.4: (a) Drift constant d and (b) diffusion constant D vs. driving frequency ω , determined as slopes from the linear fits of $\bar{\epsilon}(t)$ and $\sigma_e^2(t)$ (green), compare Figs. 3.3(b) and (c), in comparison to the estimates by Eqs. (3.62) and (3.67) based on the microscopic model (black circles). (c) Quasienergies ϵ_i of the underlying three-level system, normalized with $\hbar\omega$. The gray lines in (a) are two different evaluations of the approximation d_I according to Eq. (3.78), with the leading order resonance frequencies $\omega_{10} \approx 0.84$, $\omega_{21} \approx 0.76$ and $\omega_{20} \approx 1.60$ alone (dotted line), indicated on the abscissa of (c), and additionally including the higher order resonance frequency $\omega_{20}/2 \approx 0.80$ (solid line). For parameters see Fig. 3.3.

$R_{ik}^* \delta(K - K_{ik}^*)$. In this case the ratio between a rate and its reverse rate reduces to

$$\frac{R_{ik}}{R_{ki}} = \frac{\sum_K R_{ik}^{(K)}}{\sum_K R_{ki}^{(K)}} = \frac{R_{ik}^*}{R_{ki}^*} = e^{\beta(\epsilon_{ik} + K_{ik}^* \hbar\omega)} \quad (3.68)$$

and detailed balance $p_i R_{ik} = p_k R_{ki}$ is then fulfilled. On the other hand, it is obvious from Eq. (3.62), that the drift must vanish, if detailed balance is fulfilled:

$$-d = \sum_{k,i,K} p_k R_{ki}^{(K)} K = \sum_{k,i} p_k R_{ki}^* K_{ki}^* \stackrel{\text{det. bal.}}{=} \sum_{k,i} p_i R_{ik}^* K_{ki}^* \quad (3.69)$$

$$\stackrel{i \leftrightarrow k}{=} \sum_{i,k} p_k R_{ki}^* K_{ik}^* = - \sum_{k,i} p_k R_{ki}^* K_{ki}^* = d, \quad (3.70)$$

where in the next to last step the property $K_{ik}^* = -K_{ki}^*$ according to the assumed $A_{ik}(t) = A_{ik} e^{iK_{ik}^* \omega t}$ has been used. Furthermore, inferring from the reasoning above, D would then vanish together with d .

A further remark refers to the sign of d : although it is tempting to assume $d \leq 0$, and

although we have not observed counterexamples, we can not ascertain this assumption from Eq. (3.62) in full generality. A negative sign of d means that energy is permanently absorbed into the heat bath but is not retransferred from the heat bath into the driven system. This is certainly a self-evident assumption in view of the assumed huge heat bath. The unlikely events of a reversed energy flow from the bath into the system, though quite observable at certain times in the evolution of individual trajectories, is not reflected in d as this quantity measures the cumulative dynamics of many trajectories.

3.4.2 Energy absorption

The drift d is a measure for the rate, with which the system absorbs energy from the external driving and eventually transfers it to the heat bath. The *dissipation function*

$$F := \frac{1}{2}\eta\dot{x}^2 \quad (3.71)$$

of a classical damped oscillator [80, 81] with the damping constant η measures this rate of energy dissipation, $dE/dt = -2F$. Note, that $\eta = \gamma^2$ ensures consistency with the notation of Sec. 3.1 and the definition of the rates R_{ik} in Eqs. (3.19) and (3.31). We evaluate this quantity for a paradigmatic model of classical mechanics, the periodically driven, damped oscillator with the classical equation of motion

$$\ddot{x} + \eta\dot{x} + \omega_0^2 x = A \cos(\omega t) . \quad (3.72)$$

Its underdamped solution ($\eta \ll \omega_0$) is

$$x(t) = C_0 e^{-\eta t/2} \cos(\Omega t + \delta_0) + C \cos(\omega t + \delta) \quad (3.73)$$

with integration constants C_0 and δ_0 depending on the initial state, with $\Omega = \sqrt{\omega^2 - \eta^2/4}$ and $C = A((\omega^2 - \omega_0^2)^2 + \eta^2\omega^2)^{-1/2}$ and $\tan \delta = \eta\omega/(\omega^2 - \omega_0^2)$. After relaxation to its steady state, the particle oscillates with the external frequency, $x(t) = C \cos(\omega t + \delta)$, and the dissipation function becomes $F = (\eta/2)C^2\omega^2 \sin^2(\omega t + \delta)$. The average dissipation rate becomes

$$I(\omega) := - \left\langle \frac{dE}{dt} \right\rangle = 2\langle F \rangle = \frac{\eta}{2} C^2 \omega^2 = \frac{A^2}{2} \frac{\eta \omega^2}{(\omega^2 - \omega_0^2)^2 + \eta^2 \omega^2} \quad (3.74)$$

and for the near resonant case with $|\omega/\omega_0 - 1| \ll 1$

$$I(\omega) \simeq \frac{A^2}{8} \frac{\eta}{(\omega - \omega_0)^2 + \eta^2/4} . \quad (3.75)$$

To establish a link to the diffusion process in the extended zone scheme, we argue, that the quantity $\hbar\omega\langle e \rangle$ measures the energy, that is on average absorbed from the driving and

eventually transferred into the heat bath, and therefore set

$$I(\omega) = - \left\langle \frac{dE}{dt} \right\rangle \stackrel{!}{=} -\hbar\omega \frac{d}{dt} \langle e \rangle(t). \quad (3.76)$$

Together with the observation of the constant drift $\langle e \rangle \simeq d \cdot t$, this leads us to the prediction

$$d_I^{HO} := -\frac{I(\omega)}{\hbar\omega} = -\frac{A^2}{2\hbar\omega} \frac{\eta\omega^2}{(\omega^2 - \omega_0^2)^2 + \eta^2\omega^2} \simeq -\frac{A^2}{8\hbar\omega} \frac{\eta}{(\omega - \omega_0)^2 + \eta^2/4} \quad (3.77)$$

for the drift constant d of the damped driven harmonic oscillator. This analytical form describes the enhanced drift at the resonance and accords indeed very accurately with the values of d obtained from the random walk for the driven harmonic oscillator. Deviations only occur directly at the resonance $\omega \rightarrow \omega_0$. Note, that in the harmonic oscillator example with the analytical form (3.77) the negative semi-definiteness $d_I^{HO} \leq 0$ is indeed fulfilled.

Furthermore, we attempt to apply the analytical form (3.77) also to other driven systems by superimposing resonance terms of the type (3.77), with the relevant system frequencies $\omega_{ij} = (E_i - E_j)/\hbar$ of the system instead of the harmonic oscillator frequency ω_0 :

$$d_I := -\frac{A^2}{2\hbar\omega} \sum_{i,j} \frac{\eta\omega^2}{(\omega^2 - \omega_{ij}^2)^2 + \eta^2\omega^2} \simeq -\frac{A^2}{8\hbar\omega} \frac{\eta}{(\omega - \omega_{ij}^2)^2 + \eta^2/4} \quad (3.78)$$

Figure 3.4(a) compares this analytical form d_I (dotted gray line), comprising the system leading order resonances ω_{10} , ω_{21} and ω_{20} , to the drift d obtained from the random walk (green points) and Eq. (3.62) (black circles). The other, solid gray line refers to an extension of Eq. (3.78), including also the higher order frequency $\omega_{20}/2$ in addition to the leading order resonance frequencies. Equation (3.78) gives a rough estimate for the resonantly enhanced drift d . The correspondence of this analytical prediction d_I to the numerically determined d is here possible, because the considered system is only weakly driven. However, quantitatively Eq.(3.78) shows considerable deviations from d , as it does not take into account the quantum-mechanical matrix elements $x_{ij}(K)$ of the system-bath coupling operator, which are essential in the definition of the rates $R_{ij}^{(K)}$. Besides, Eq. (3.78) involves the eigenenergies E_i of the undriven system instead of the quasienergies.

To summarize this section, the description in the extended zone scheme gives insight into the process of energy absorption in time-periodic systems in contact with a heat bath. The nature of this process is diffusive, with a finite drift bias. The diffusion on the energy axis illustrates the non-equilibrium situation which is maintained even in the asymptotic state: although the probabilities p_i eventually converge to the time-independent Floquet occupations, the distribution $p(e)$ continues to drift without a limit and diffusively spreads over the Brillouin zones. The diffusion is completely quantified by the drift constant d and

the diffusion constant D , which both reflect the resonantly enhanced dissipation of energy at avoided crossings. These parameters can be estimated directly from the microscopic model and related to the classical dissipation function.

4 Statistical mechanics of time-periodic systems with regular and chaotic states

The interplay of the periodic driving on the one hand and the interaction with a thermal reservoir on the other hand modifies the transient dynamics of a quantum system and beyond that enriches the long-time evolution with new fascinating facets. In place of the stationary state of time-independent systems the relaxation process finally leads to an asymptotic state that adopts the periodicity of the driving. It depends in general on the microscopic details of the system-bath interaction.

As sketched in Section 3.1, the asymptotic state is best expressed by the density matrix in the basis of the time-periodic Floquet solutions $|u_i(t)\rangle$. The Floquet representation ensures a non-perturbative treatment of the driven systems coherent dynamics, valid in principle for arbitrary values of the driving amplitude. The Floquet density matrix elements ρ_{ij} are determined by the linear system of rate equations (3.26), provided that the weakness of the system-bath interaction allows to employ the Born-Markov approximation and to neglect small temporal oscillations about the cycle-averaged asymptotic density ρ_{ij} . Beyond their sole numerical evaluation from such rate equations, the Floquet density matrix elements ρ_{ij} still lack an intuitive understanding. In order to shed some further light in that direction, a relation of the Floquet occupations $p_i \equiv \rho_{ii}$ to the phase-space structure of the underlying classical system is established in this chapter. We study the Floquet occupations p_i for typical examples from two classes of time-periodic systems: firstly an additively driven anharmonic oscillator as representative of a continuously driven system, and secondly the quantum kicked rotor from the class of kicked systems.

Note, that the kicking type of the periodic driving in principle allows for an alternative approach: Since the kicks act during infinitesimal time spans and, according to the premises, exclusively on the system itself, but not on the heat bath, one might neglect the system-bath interaction during the kicks. The time evolution of the density operator is then split into the time span of the free but damped evolution and in the infinitesimal time step containing the action of the kicks on the system, which is then considered to be decoupled from the heat bath. Such a strategy has been followed in Ref. [18] in order to study entropy production in the open quantum kicked rotor. The authors consider the momentum p as the coupling operator of the system-bath interaction, which is then of nondemolition type, i.e. the interaction term and the Hamiltonian of the system commute. Consequently, also the time-evolution of ρ is exactly solvable, provided that the time-evolution of the isolated system is known [19]. However, the diagonal elements of ρ do not change in time under such a nondemolition coupling and the system does not reach thermodynamic equilibrium. We do not follow this approach.

Firstly, in Section 4.1 we demonstrate that the Floquet occupations of regular and chaotic

Floquet states follow tremendously different distributions. Similar observations have been made for a driven quantum particle in a box [23]. The authors report that the regular states carry Boltzmann-like weights $p_m \sim e^{-\beta \langle E_m \rangle \tau}$ as functions of their cycle-averaged energies $\langle E_m \rangle \tau$, whereas the chaotic states have nearly the same occupation probability. However, in this particular example the regular region is almost identical to the undriven system, leading to Boltzmann weights for the regular states by the following reasoning: the regular states of the driven box potential emerge from the highly excited eigenstates of the undriven box and still strongly resemble those. They change only slightly during the driving period $\tau = 2\pi/\omega$ and single out one dominant Fourier contribution K^* in the coupling matrix elements, $x_{nm}(K) \approx 0$ for $K \neq K^*$. In this situation the ratio between a rate R_{nm} , defined in Eq. (3.31), and its reverse rate R_{mn} simplifies to $R_{nm}/R_{mn} = e^{\beta(\varepsilon_{nm} + K^* \hbar \omega)}$. In combination with the fact, that their cycle-averaged energies are close to the eigenenergies in the undriven potential, this property is responsible for the occupations being close to the Boltzmann weights. For the lowest regular states, however, these properties are not satisfied very accurately and deviations from the stated Boltzmann-behavior are clearly visible in Fig. (1) of Ref. [23]. These deviations are quite plausible as a consequence of rates occurring between the regular and the chaotic Floquet states. As we will substantiate in this chapter, deviations from the Boltzmann behavior can be even much stronger in generic situations.

In contrast to Ref. [23], we concentrate here on situations characteristic for strong driving, where the phase-space structure and the Floquet states are strongly perturbed compared to the original time-independent system. This is in particular the case for the considered kicked systems, whose time-independent counterpart is simply a freely evolving particle. The strong driving allows to study the Floquet occupations far from the thermodynamic equilibrium situation encountered in the time-independent system and at the same time having dominant regular structures present in the classical phase space. Under such circumstances we report significant deviations of the regular occupations from the Boltzmann result. In many cases the distribution of the regular occupations can still be approximated by weights of the Boltzmann type $p_m \sim e^{-\beta_{\text{eff}} E_m^{\text{reg}}}$ as functions of the regular energies E_m^{reg} , introduced in Section 2.3. For the effective temperature $1/\beta_{\text{eff}}$ we derive an approximation as a function of the winding number in the regular island (Section 4.2). Beyond the characterization of regular and chaotic occupations we give an overview about the implications of further important features in a mixed phase space, such as resonance island chains and hierarchical regions (Section 4.3). The chapter is closed by an analysis of the chaotic occupations in the semi-classical limit in comparison to a random rate model (Section 4.4) and a short supplementary section about the role of symmetry in the system-bath interaction (Section 4.5).

Starting from the familiar perspective of time-independent quantum systems, where the occupation probabilities of the eigenstates in a canonical ensemble are functions of their eigenenergies, the analysis of the Floquet occupations in terms of a suited energy is desirable.

For lack of energy conservation in the time-periodic systems, an adapted measure for the energy of the Floquet states is identified by the cycle-averaged energy

$$\langle E_i \rangle_\tau := \frac{1}{\tau} \int_t^{t+\tau} dt' \langle u_i(t') | H(t') | u_i(t') \rangle - E_0, \quad (4.1)$$

where we have introduced an energy shift by a value E_0 for later convenience. It is determined by the classical periodic orbit at the center of the regular island, such that there the mean energy is set to zero. The cycle-averaged energy allows to order the Floquet states in a natural way, at least for moderate driving strengths and with the exception of states involved in an avoided crossing.

4.1 Occupations of regular and chaotic Floquet states

4.1.1 Driven quartic oscillator

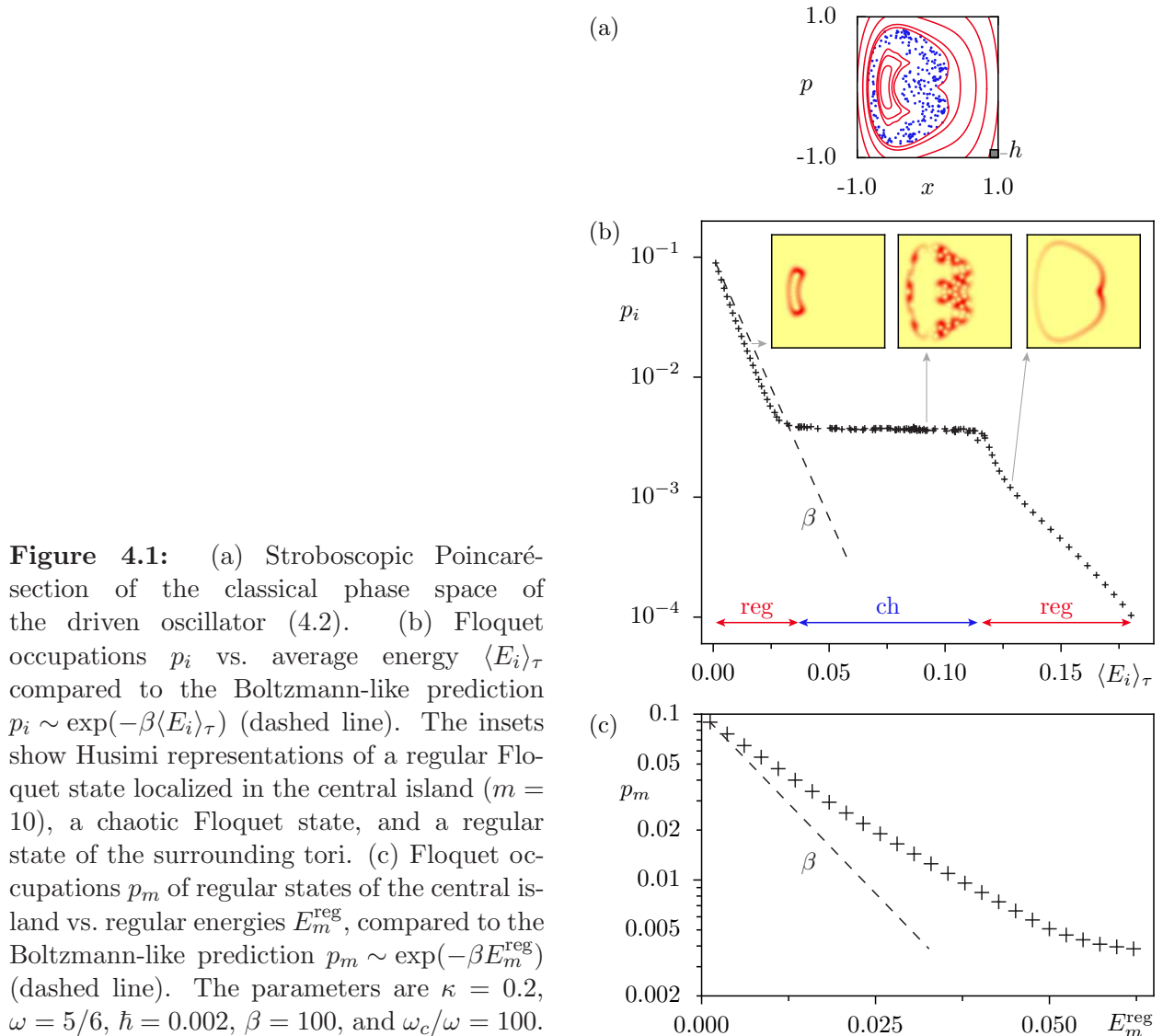
As an example of a continuously driven system we consider the additively driven quartic oscillator with the Hamiltonian

$$H(t) = \frac{p^2}{2} + x^4 + Ax \cos(\omega t) \quad (4.2)$$

with dimensionless variables and parameters. The system has two independent parameters, the driving amplitude A and the driving frequency $\omega = 2\pi/\tau$.

The stroboscopic Poincaré-section of the phase space referring to the Hamiltonian (4.2) is shown in Fig. 4.1(a) for $\kappa = 0.2$ and $\omega = 5/6$, where it features a chaotic domain at low energies and besides two distinct regular regions: firstly the highly excited tori, that are only slightly influenced by the driving, and secondly a regular island embedded in the chaotic sea. The Poincaré-section, which maps the phase space only stroboscopically, depends on the choice of the initial time $0 \leq t_0 < \tau$, here $t_0 = 0$. In particular, under the variation of t_0 the regular island rotates around the central point $(x, p) = (0, 0)$.

The periodic parts $|u_i(t)\rangle$ of the Floquet states are determined from the Floquet eigenequation (2.25), which is solved numerically with the help of the (t, t') -technique [50, 51] and using the truncated eigenstate basis $\{|n\rangle : n = 0, 1, \dots, N_{\mathcal{R}} - 1\}$ of the undriven system. Using a basis of $N_{\mathcal{R}} = 300$ eigenstates, we consider the $N = 145$ Floquet states of lowest mean energy (4.1). With the chosen $N_{\mathcal{R}}$ it is ensured that these Floquet states $i = 0, 1, \dots, N - 1$ have negligible overlap $\langle n | u_i(t) \rangle$ with the eigenstates $n \geq N_{\mathcal{R}}$. Whether the number N of Floquet states is chosen sensible, in principle turns out only once the Floquet occupations p_i are determined: a truncation of the Floquet basis is justified if the occupations of all Floquet states $i > N$ fall below a critical small value. However, also the exponentially decreasing occupations $p_n \sim e^{-\beta E_n}$ of the eigenstates $|n\rangle$ in the undriven system already give a reasonable estimate for N . The issue of the truncation of the Floquet basis size N has been already



addressed in the introduction of Section 3.2 and is in detail responded in Ref. [25].

According to the semiclassical eigenfunction hypothesis [30–32], almost all Floquet states can be classified as either regular or chaotic if the effective Planck constant \hbar takes a sufficiently small value. As mentioned before, we denote with \hbar a dimensionless parameter that measures the size of Planck’s constant relative to the unit area of the phase space, i.e. relative to the typical value of the classical action. We have chosen the small value $\hbar = 0.002$, indicated in the corner of Fig. 4.1(a), such that the small central island of size $A_{\text{reg}} \approx 0.33$ hosts $N_{\text{reg}} = 26$ regular states. Besides, there are several chaotic states, whose number is however restricted due to the finite size of the chaotic region. It is surrounded by regular tori, on which further, highly-excited regular states are localized. The insets in Fig. 4.1(b) show the Husimi representations (2.55) for one state out of each of these three classes.

The average energies $\langle E_i \rangle_\tau$ of these three different types of Floquet states are found in distinct intervals on the real axis \mathbb{R} with only small overlaps, as indicated by the arrows in Fig. 4.1(b). The regular states of the central island are lowest in energy, followed by the

chaotic states and finally the highly excited regular states of the surrounding tori.

The oscillator in a weak interaction with a heat bath is analyzed within the framework of the Floquet-Markov theory, following the lines of Section 3.1. We restrict the consideration to the weak coupling limit that is well described in terms of the reduced rate-balance (3.30) for the diagonal density matrix elements, i.e. the Floquet occupations $p_i \equiv \rho_{ii}$. In Fig. 4.1(b) the resulting Floquet occupations p_i are shown as function of the $\langle E_i \rangle_\tau$, by means of which the three types of Floquet states are well-separated into distinct intervals. The monotonously falling occupations at low values of $\langle E_i \rangle_\tau$ belong to the central regular island. At intermediate values of $\langle E_i \rangle_\tau$ one finds the occupations of the chaotic states, which fluctuate around a mean value \bar{p}_{ch} with a very small variance compared to the range of occupations of the regular states. At high values of $\langle E_i \rangle_\tau$ there are again monotonously falling occupations belonging to the regular states of the surrounding tori.

Figure 4.1(b) also clearly demonstrates The observed characteristics of the occupations p_i is in contrast to the naive expectation $p_i \sim e^{-\beta \langle E_i \rangle_\tau}$ motivated by the Boltzmann weights of equilibrium thermodynamics. Note, that even the occupations of the low-energy states in the central island notably differ from the Boltzmann result. The latter is indicated by the dashed line in Fig. 4.1(b). A quantitative analysis of these observations will be done in Section 4.2 for the numerically and analytically more convenient kicked rotor.

4.1.2 Kicked rotor

Kicked quantum systems feature all essential phase-space characteristics of periodically driven systems. They allow for a simplified numerical and conceptual treatment at the same time. Besides, kicked systems offer a further advantage in the context of these studies: at moderately high values of the kick strength, $\kappa \gtrsim 1$, their phase-space structure is completely unrelated to that of the corresponding unperturbed, time-independent system. For the kicked rotor this is simply the free particle. In contrast, for systems with an additive continuous driving force the emerging phase space remains structurally similar to that of the originally autonomous system, at least for a moderate driving amplitude.

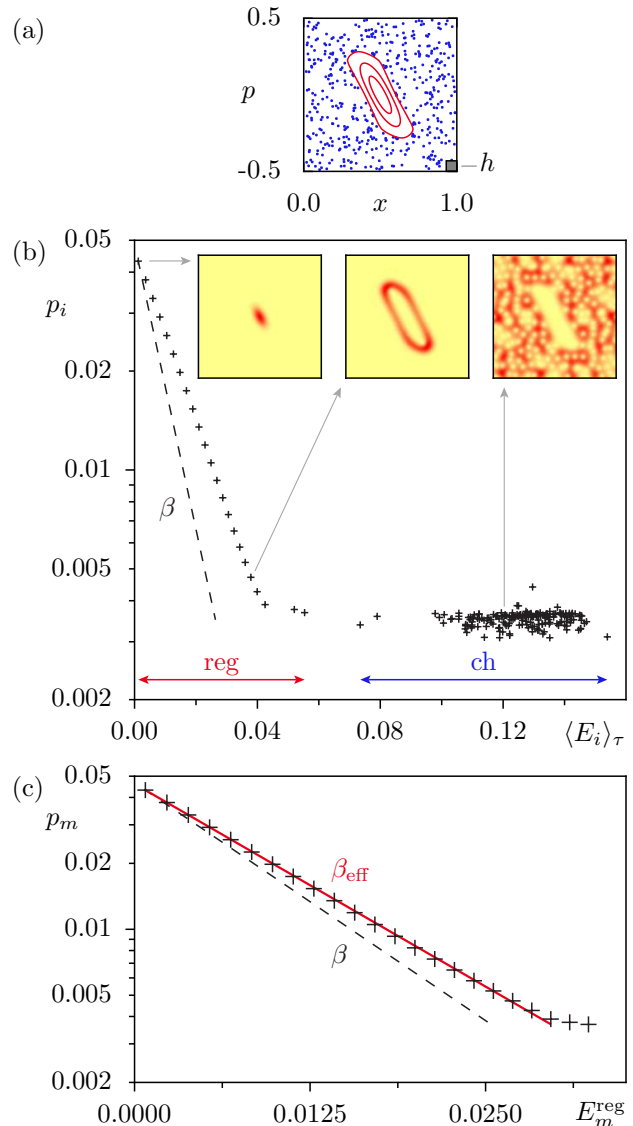
As a paradigmatic model for a kicked system with a mixed phase space we consider here the kicked rotor

$$H(t) = \frac{p^2}{2} + \frac{\kappa}{(2\pi)^2} \cos(2\pi x) \sum_n \delta(t - n), \quad (4.3)$$

as introduced in Section 2.2. Compared to the driven oscillator (4.2) it has a reduced number of independent parameters, the kick strength κ alone. The driving frequency is fixed, $\omega = 2\pi$, as a speciality of the kicking type of the periodic driving. In an intermediate regime of κ the stroboscopic Poincaré-section of phase space features a large regular island embedded in the chaotic sea, see Fig. 4.2(a) for $\kappa = 2.9$.

The Floquet states $|\psi_i(t)\rangle$ are evaluated as eigenstates of the time evolution operator

Figure 4.2: (a) Stroboscopic Poincaré-section of the classical phase space of the kicked rotor (4.3). (b) Floquet occupations p_i vs. average energy $\langle E_i \rangle_\tau$ compared to the Boltzmann-like prediction $p_i \sim \exp(-\beta \langle E_i \rangle_\tau)$ (dashed line). The insets show Husimi representations of two regular ($m = 0$ and $m = 18$) and a chaotic Floquet state. (c) Floquet occupations p_m of regular states vs. regular energies E_m^{reg} , compared to the Boltzmann-like prediction $p_m \sim \exp(-\beta E_m^{\text{reg}})$ (dashed line) and the analytical prediction from Eqs. (4.36) and (4.38) with the effective temperature β_{eff} (solid line). The parameters are $\kappa = 2.9$, $h = 1/210$, $\beta = 100$, and $\omega_c/\omega = 100$.



$U(\tau, 0)$. As explicated in Section 2.2, this factorizes into a potential and a kinetic contribution, Eq. (2.38), and is evaluated in position representation, Eq. (2.50). The quantization on the compact phase space, the two-torus \mathbb{T}^2 , makes the Hilbert space dimension N finite and relates it to \hbar by the condition $h = 2\pi\hbar = 1/N$. The area of the regular island is $A_{\text{reg}} \approx 0.11$ and supports $N_{\text{reg}} = 23$ regular states for $N = 210$.

The asymptotic state of the kicked rotor, when weakly coupled to a heat bath, is again determined from the reduced rate-balance (3.30). The resulting Floquet occupations p_i are shown in Fig. 4.2(b) vs. average energy $\langle E_i \rangle_\tau$, with $E_0 = -\kappa/(2\pi)^2$. The regular and chaotic states are again ordered with respect to this quantity, as indicated by the arrows in Fig. 4.2(b). The regular states have small values of $\langle E_i \rangle_\tau$, since both kinetic and potential energy are minimal in the center of the regular island, whereas the chaotic states spread over the high-energetic regions of phase space. Similarly as for the driven oscillator, the regular occupations depend monotonously on $\langle E_i \rangle_\tau$, while the occupations of the chaotic states form a plateau with only weak fluctuations about a mean value \bar{p}_{ch} and seem uncorrelated with

the average energies $\langle E_i \rangle_\tau$. This example for the kicked rotor again demonstrates that the observed occupation characteristics is not appropriately described in terms of the Boltzmann-like weights $p_i \sim e^{-\beta \langle E_i \rangle_\tau}$, which are indicated by the dashed line in Fig. 4.2(b).

4.1.3 Rate matrix

The Floquet rate matrix R_{ij} determines the Floquet occupations via Eq. (3.30). In Fig. 4.3 we show R_{ij} , or more precisely $R_{ij} - R_{ii}\delta_{ij}$, for both (a) the driven oscillator of Fig. 4.1 and (b) for the kicked rotor of Fig. 4.2. Again employing $\langle E_i \rangle_\tau$ as the ordering parameter for the entries i, j , the regular and chaotic parts are well-separated, revealing a distinct block structure of the matrix. There are only few rates between the regular and the chaotic subspace. Similarly, the rates between the two different regular subspaces in the case of the driven oscillator (a) are practically zero. Also by virtue of the chosen ordering, the regular domains feature a band-structure with particular dominance of the first off-diagonals (nearest-neighbor rates). The rates in the subspace of the chaotic states on the contrary fluctuate randomly.

One can thus record a close relation between the structure of the rate matrix R_{ij} and the resulting set of occupations. Firstly, the almost independent behavior of the occupation sets of regular states on the one hand and chaotic states on the other hand originates from the relatively weak rates R_{ij} connecting the corresponding subspaces, i.e. with the two indices pointing to different subspaces. Furthermore, the random character of the chaotic rate submatrix gives rise to the equally random character of the set of chaotic Floquet occupations. A further investigation of the chaotic occupations is deferred to Section 4.4, where these are studied in the semiclassical limit, $\hbar \rightarrow 0$, in comparison to the solutions of a random rate matrix model.

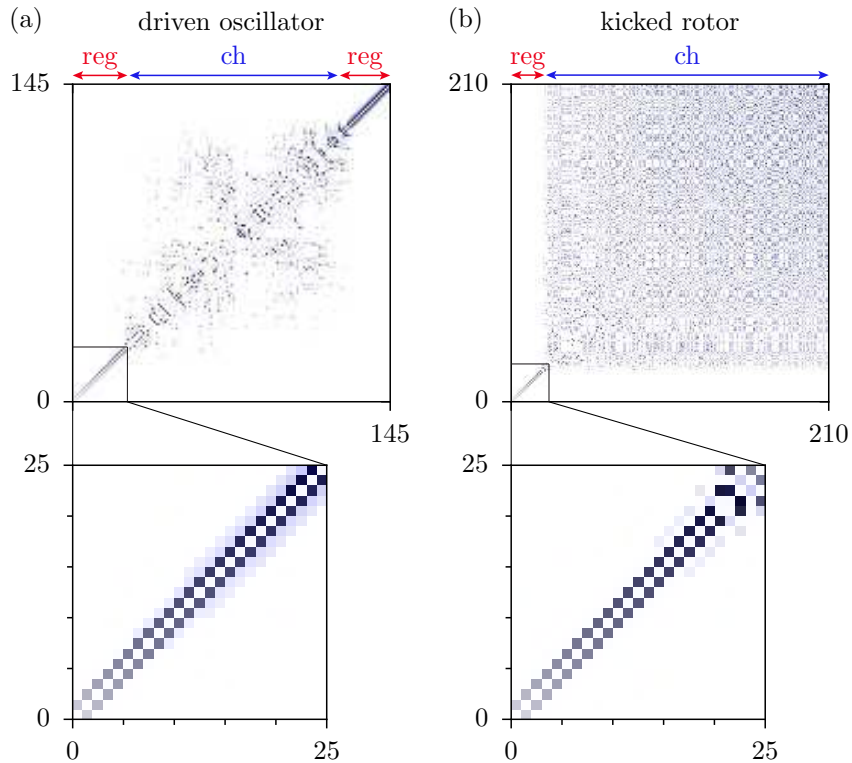


Figure 4.3: Rate matrix R_{ij} , with entries $i \neq j$ sorted by increasing $\langle E_i \rangle_\tau$, for (a) the driven oscillator (4.2) and (b) the kicked rotor (4.3), with magnified domain of the regular states in the regular island. For parameters see Figs. 4.1 and 4.2, respectively.

4.2 Regular states

The observations of Figs. 4.1 and 4.2 indicate that the asymptotic state of a time-periodic system in weak interaction with a heat bath carries signatures of the classical phase-space structure. The Floquet occupations of the regular and the chaotic states behave very differently, e.g. as functions of the average energies $\langle E_i \rangle_\tau$. In this section we focus on the asymptotic occupations of the regular states. These follow a distinct hierarchy, for which Figs. 4.1(b) and 4.2(b) suggest a roughly exponential dependence for the regular occupations p_m as functions of the average energies $\langle E_m \rangle_\tau$. However, the regular occupations are different from the Boltzmann-like weights $e^{-\beta \langle E_m \rangle_\tau}$ with the true inverse bath temperature β . In fact, there is no physical reason for a coincidence with the Boltzmann distribution when expressed in terms of the, qualitatively suitable but arbitrary, energy measure $\langle E_m \rangle_\tau$ [24]. In the following sections we make therefore use of an alternative energy measure for the regular states, the regular energy E_m^{reg} that is introduced in Section 2.3. With the help of E_m^{reg} the regular occupations p_m can be consistently parametrized by exponential weights.

In order to avoid confusion with the indices, we continue to denote the Floquet states in general, as well as all quantities referring to the entire Floquet basis by the indices i, j . The indices m, n are reserved for the regular states and all quantities referring only to those.

4.2.1 Quality of the exponential fits

Figure 4.2(c) shows the occupations p_m of the regular states of the kicked rotor as function of the regular energies E_m^{reg} . Likewise, Fig. 4.1(c) shows p_m vs. E_m^{reg} for the regular states of the central island in the driven oscillator (4.2). The functional dependence of the p_m is close to exponential, but different from the Boltzmann-like weights $e^{-\beta E_m^{\text{reg}}}$. However, the assumption of an exponential dependence of p_m vs. E_m^{reg} is fulfilled far better than vs. $\langle E_m \rangle_\tau$. This is demonstrated in Fig. 4.4, where the deviation factors

$$w_m := \frac{p_m}{p_0 e^{-\beta_{\text{fit}}(e_m - e_0)}} \quad (4.4)$$

between the occupations p_m and the respective exponential fit is shown for e_m being the regular energy E_m^{reg} (red circles) on the one hand and the cycle-averaged energy $\langle E_m \rangle_\tau$ (black diamonds) on the other hand. The fit involves the parameter

$$\beta_{\text{fit}} := \frac{\ln p_1 - \ln p_0}{e_0 - e_1}. \quad (4.5)$$

For the kicked rotor (Fig. 4.4(a)) these factors w_m for $e_m = E_m^{\text{reg}}$ are close to 1 for the majority of regular states, whereas the w_m for $e_m = \langle E_m \rangle_\tau$ systematically deviate from 1 already for smaller values of the quantum number m . This indicates, that the exponential scaling is far better fulfilled by using the regular energies E_m^{reg} .

For the driven oscillator (Fig. 4.4(b)) the quality of the fit with respect to E_m^{reg} is only marginally better as with respect to $\langle E_m \rangle_\tau$. The comparably poorer performance of a detailed balance approximation is likely responsible for this, as discussed later in Section 4.2.3. In other examples of continuously driven systems, e.g. for a driven double well potential, we again record a better quality of the fit with respect to E_m^{reg} , similar to the situation in Fig. 4.4(a).

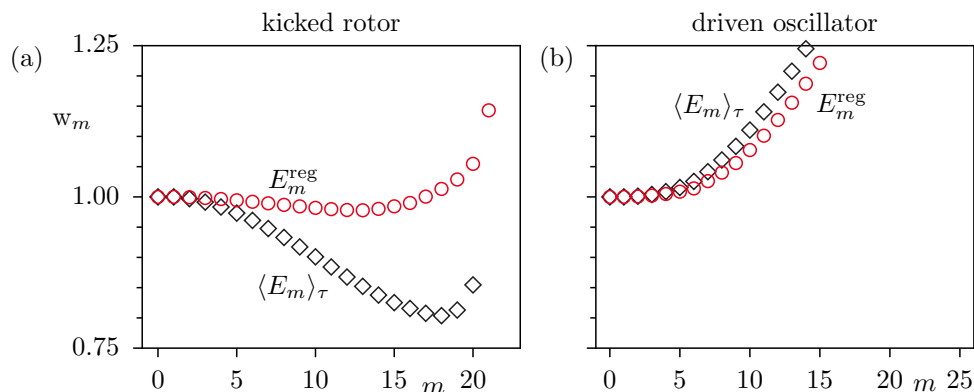


Figure 4.4: Factors w_m between the regular occupations p_m and an exponential fit for (a) the kicked rotor (4.3) and (b) the continuously driven oscillator (4.2) based on the average energies $e_m = \langle E_m \rangle_\tau$ (diamonds) and the regular energies $e_m = E_m^{\text{reg}}$ (circles). For parameters see Figs. 4.2 and 4.1, respectively.

4.2.2 Effective temperature $1/\beta_{\text{eff}}$

In this section, the ratio of the reverse rates $R_{m,m+1}$ and $R_{m+1,m}$ between two neighboring regular states m and $m+1$ is analyzed. We demonstrate that it is closely related to the regular energy E_m^{reg} , introduced in Section 2.3. With the help of an approximate detailed balance condition, the occupations p_m can be parametrized by the function $e^{-\beta_{\text{eff}} E_m^{\text{reg}}}$. The new parameter $1/\beta_{\text{eff}}$ takes the role of an effective temperature and we observe that it can deviate considerably from the actual temperature $1/\beta$ of the heat bath.

In the lower part of Fig. 4.3(a) the rate matrix R_{ij} for the regular subspace is shown. We recall that the indices i are ordered by increasing $\langle E_i \rangle_\tau$, coinciding with the natural order of growing quantum number m . Figure 4.3(a) illustrates that the nearest-neighbor rates $R_{m,m\pm 1}$ are dominant among the regular states. The next-nearest neighbor rates $R_{m,m\pm 2}$ between the regular states m and $m\pm 2$ are zero for symmetry reasons, an aspect that is discussed in further detail in Section 4.5.

The rates R_{mn} with $|m-n| \geq 2$ also vanish exactly in the case of a harmonic oscillator-like island with constant winding number and elliptic regular tori. To see this, one may employ a set of adapted creation and annihilation operators a^+ and a , which yield an algebra $a^+|m\rangle = \sqrt{m+1}|m+1\rangle$ and $a|m\rangle = \sqrt{m}|m-1\rangle$ for the regular states of the island at any fixed time t . The coupling operator x is a linear combination of the operators $\mathbb{1}$, a^+ and a , with linear coefficients $c_{0,1,2}$ depending on the island center, the rotation angle and the squeezing factor (the ratio of the normal axes) of the elliptic island. Using the harmonic oscillator algebra, the only non-vanishing matrix elements of the coupling operator x are the diagonal terms and the contributions of the neighboring regular states: $x_{mn}(t) = \langle m(t)|x|n(t)\rangle = c_0(t)\delta_{m,n} + c_1(t)\sqrt{m+1}\delta_{n,m+1} + c_2(t)\sqrt{m}\delta_{n,m-1}$. This property is passed to the rates and the above-stated ‘selection rule’ thus becomes evident.

Even in the generic case the coupling operator $A = x$ to the heat bath leads to dominant rates between those states that are localized nearby in phase space. In the following analysis of this section we neglect higher order rates. Using this approximation, the total rate balance among the regular states is that of a linear chain and can be reduced to the detailed balance condition

$$\frac{p_{m+1}}{p_m} = \frac{R_{m,m+1}}{R_{m+1,m}} \quad (4.6)$$

between two neighboring regular states m and $m+1$.

The ratio R_{ij}/R_{ji} of the rates between the Floquet states i, j is

$$\frac{R_{ij}}{R_{ji}} = \frac{\sum_K |x_{ij}(K)|^2 g(\varepsilon_{ji} - K\hbar\omega)}{\sum_K |x_{ji}(K)|^2 g(\varepsilon_{ij} - K\hbar\omega)} = \frac{\sum_K |x_{ij}(K)|^2 g(\varepsilon_{ij} + K\hbar\omega) e^{\beta(\varepsilon_{ij} + K\hbar\omega)}}{\sum_K |x_{ij}(K)|^2 g(\varepsilon_{ij} + K\hbar\omega)}, \quad (4.7)$$

where Def. (3.31) and the properties $x_{ij}(K) = x_{ji}^*(-K)$ and $g(E) = g(-E)e^{-\beta E}$ have been used.

If there were just a single Fourier component $x_{ij}(K^*)$, which is approximately the case for a weak harmonic driving, then the rate ratio simplifies to $R_{ij}/R_{ji} = e^{\beta(\varepsilon_{ij} + K^*\hbar\omega)}$ and leads to Boltzmann-like occupations. In general, however, several components K have to be considered. We factor out a so far unspecified Fourier component K_0 in the summations of Eq. (4.7), giving

$$\frac{R_{ij}}{R_{ji}} = e^{\beta\zeta_{ijK_0}} \frac{\sum_L \frac{|x_{ij}(K_0+L)|^2}{|x_{ij}(K_0)|^2} \frac{g(\zeta_{ijK_0} + L\hbar\omega)}{g(\zeta_{ijK_0})} e^{\beta L\hbar\omega}}{\sum_L \frac{|x_{ij}(K_0+L)|^2}{|x_{ij}(K_0)|^2} \frac{g(\zeta_{ijK_0} + L\hbar\omega)}{g(\zeta_{ijK_0})}} \quad (4.8)$$

with the short-hand notation

$$\zeta_{ijK_0} := \varepsilon_{ij} + K_0\hbar\omega. \quad (4.9)$$

When explicitly evaluating the correlation function $g(\zeta_{ijK_0} + L\hbar\omega)$ according to its definition (3.15) for an oscillator bath and with the spectral density $J(\omega)$ according to Eq. (3.13), the g -ratios appearing in Eq. (4.8) become

$$\frac{g(\zeta_{ijK_0} + L\hbar\omega)}{g(\zeta_{ijK_0})} = \frac{\zeta_{ijK_0} + L\hbar\omega}{\zeta_{ijK_0}} \frac{e^{\beta\zeta_{ijK_0}} - 1}{e^{\beta(\zeta_{ijK_0} + L\hbar\omega)} - 1} \cdot \exp\left(\frac{|\zeta_{ijK_0}| - |\zeta_{ijK_0} + L\hbar\omega|}{\hbar\omega_c}\right) \quad (4.10)$$

$$= \left(1 + \frac{L\hbar\omega}{\zeta_{ijK_0}}\right) \frac{e^{\beta\zeta_{ijK_0}} - 1}{e^{\beta(\zeta_{ijK_0} + L\hbar\omega)} - 1} \cdot C_L\left(\frac{\zeta_{ijK_0}}{\hbar\omega}, \frac{\omega_c}{\omega}\right) \quad (4.11)$$

with the factors

$$C_L(z, z_c) = \exp\left(\frac{|z| - |z + L|}{z_c}\right) = \exp\left(\frac{|z|}{z_c} \left(1 - \left|1 + \frac{L}{z}\right|\right)\right). \quad (4.12)$$

The parameter ω_c is the approximate upper bound of the spectral modes in $J(\omega)$. We show below, that $|K_0| \leq 1$ and that only small integers L contribute significantly to the sums in Eq. (4.8), and in the case $\omega_c \gg \omega$ the factors are therefore close to 1.

In the following steps we restrict the analysis of (4.8) to the regular states of a kicked system with the Hamiltonian (2.34), e.g. the kicked rotor (4.3). In a kicked system the evolution of the coupling matrix $x_{ij}(t)$ can be expressed explicitly due to the factorization of the time evolution operator $U(\tau, 0)$ into a pure kinetic and a pure potential part: the commutation relations of the coupling operator x with the respective factors are

$$[x, e^{-iV(x)\tau/\hbar}] = 0 \quad (4.13)$$

$$[x, e^{-iT(p)t/\hbar}] = t \frac{dT(p)}{dp} e^{-iT(p)t/\hbar}, \quad (4.14)$$

based on which the matrix elements $\langle u_i(t) | x | u_j(t) \rangle$ can be expressed as

$$x_{ij}(t) = e^{-i\varepsilon_{ij}t/\hbar} (x_{ij}^0 + tT'(p_{ij}^0)) \quad (0 \leq t \leq \tau) \quad (4.15)$$

with the initial matrix elements

$$x_{ij}^0 := \langle u_i(0) | x | u_j(0) \rangle \quad (4.16)$$

$$p_{ij}^0 := \langle u_i(0) | p | u_j(0) \rangle . \quad (4.17)$$

In detail, the individual steps to obtain Eq. (4.15) are the following:

$$x_{ij}(t) = \langle u_i(t) | x | u_j(t) \rangle \quad (4.18)$$

$$= e^{-i\varepsilon_{ij}t/\hbar} \langle \psi_i(0) | U^{-1}(t, 0) x U(t, 0) | \psi_j(0) \rangle \quad (4.19)$$

$$\stackrel{(4.13)}{=} e^{-i\varepsilon_{ij}t/\hbar} \langle \psi_i(0) | e^{iT(p)t/\hbar} x e^{-iT(p)t/\hbar} | \psi_j(0) \rangle \quad (4.20)$$

$$\stackrel{(4.14)}{=} e^{-i\varepsilon_{ij}t/\hbar} \langle \psi_i(0) | x + tT'(p) | \psi_j(0) \rangle = e^{-i\varepsilon_{ij}t/\hbar} \langle u_i(0) | x + tT'(p) | u_j(0) \rangle \quad (4.21)$$

$$= e^{-i\varepsilon_{ij}t/\hbar} (x_{ij}^0 + tT'(p_{ij}^0)) . \quad (4.22)$$

As a consequence of the time-periodicity, i.e.

$$x_{ij}^0 = \langle u_i(0) | x | u_j(0) \rangle \quad (4.23)$$

$$\stackrel{!}{=} \langle u_i(\tau) | x | u_j(\tau) \rangle = x_{ij}(\tau) = e^{-i\varepsilon_{ij}\tau/\hbar} (x_{ij}^0 + \tau T'(p_{ij}^0)) \quad (4.24)$$

these matrix elements are not independent, but fulfill

$$\tau T'(p_{ij}^0) = (e^{i\varepsilon_{ij}\tau/\hbar} - 1) x_{ij}^0 . \quad (4.25)$$

Thus, the matrix elements $x_{ij}(t)$ of Eq. (4.15) become

$$x_{ij}(t) = x_{ij}^0 e^{-i\varepsilon_{ij}t/\hbar} \left(1 + \frac{t}{\tau} (e^{i\varepsilon_{ij}\tau/\hbar} - 1) \right) \quad (0 \leq t \leq \tau) \quad (4.26)$$

and have the Fourier coefficients

$$x_{ij}(K) = \frac{x_{ij}^0}{2\pi^2} \left(\frac{\varepsilon_{ij}}{\hbar\omega} + K \right)^{-2} \left(1 - \cos \left(2\pi \frac{\varepsilon_{ij}}{\hbar\omega} \right) \right) . \quad (4.27)$$

We have used $\int_0^\tau dz e^{az} (b + cz) = (b/a - c/a^2)(e^{a\tau} - 1) + (c/a)\tau e^{a\tau}$ with $a = -i(\varepsilon_{ij} + K\hbar\omega)/\hbar$, $b = x_{ij}^0$, and $c = T'(p_{ij}^0)$. With these and the ζ_{ijK_0} from Eq. (4.9) the ratio of the matrix elements in Eq. (4.8) finally adopts the form

$$\frac{|x_{ij}(K_0 + L)|^2}{|x_{ij}(K_0)|^2} = \left(1 + \frac{L\hbar\omega}{\zeta_{ijK_0}} \right)^{-4} . \quad (4.28)$$

Caution with respect to the premised linear coupling operator $A = x$ of the Caldeira-Leggett model is required in the case of a kicked quantum map or other spatially periodic

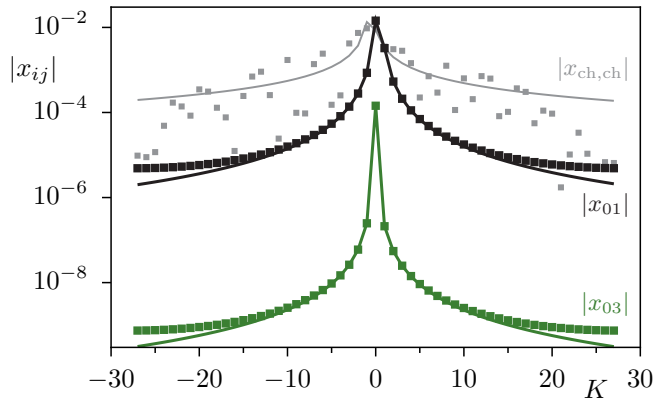


Figure 4.5: Fourier coefficients $|x_{ij}(K)|$ of the coupling matrix elements (points) compared to the approximation by Eq. (4.27), in particular for the regular states $i = m = 0, j = m + 1 = 1$ (black) and $i = m = 0, j = m + 3 = 3$ (green), as well as for the two chaotic states $i = 100, j = 101$ (gray). The parameters are $\kappa = 2.9$ and $h = 1/210$.

systems. The unbound linear coupling operator breaks the spatial periodicity of the quantum map and is therefore not uniquely defined on the torus. However, in the Floquet representation of the quantum kicked system the matrix elements of x are indistinguishable from the matrix elements of its periodized counterpart $x' = (x \bmod 1)$, because the Floquet states are evaluated only on a finite grid x_l in the unit cell $0 \leq x_l < 1$, Eq. (2.47). A more detailed discussion about the role of the coupling operator can be found in Section 4.5. We emphasize, that the explicitly time-dependent expressions (4.15) and (4.26) on the contrary are correct only for the unbound linear coupling operator x . That is why Eqs. (4.15) and (4.26) do in general not consistently describe the time evolution of the matrix elements $x_{ij}(t)$. However, the discrepancy is resolved, as we apply Eqs. (4.15) and (4.26) exclusively to the regular states. Being localized in the center of the phase-space unit-cell, these have exponentially small weights at its borders and are therefore not sensitive to the deviations of Eqs. (4.15) and (4.26) from the coupling matrix (4.18). Accordingly, if restricted to the regular states, the explicit expression (4.26) is a good approximation for the $x_{ij}(t)$ and so is Eq. (4.27) for $x_{ij}(K)$. This is illustrated in Fig. 4.5, where the approximations (4.27) are in good agreement with the $x_{ij}(K)$ in the subspace of the regular states, $x_{mn}(K)$, e.g. for $x_{01}(K)$ (black) or $x_{03}(K)$ (green), at least for the dominant contributions to the Fourier expansion. In contrast, the Fourier coefficients $x_{ij}(K)$ of matrix elements that involve at least one chaotic state, e.g. $i = 100, j = 101$ (gray), are not approximated well by Eq. (4.27).

Finally, inserting Eqs. (4.10) and (4.28) into the rate ratio of Eq. (4.8) yields

$$\frac{R_{ij}}{R_{ji}} = e^{\beta\zeta_{ij}K_0} \cdot f\left(\frac{\zeta_{ij}K_0}{\hbar\omega}, \beta\zeta_{ij}K_0\right) \quad (4.29)$$

with the function

$$f(z, b) := e^{-b} \cdot \frac{\sum_L (L-z)^{-3} (e^{(L-z)b/z} - 1)^{-1} C_L(-z, z_c)}{\sum_L (L+z)^{-3} (e^{(L+z)b/z} - 1)^{-1} C_L(z, z_c)}. \quad (4.30)$$

Upon an energy shift by integer multiples of $\hbar\omega$, $\zeta_{ijK_0} \rightarrow \zeta_{ijK_0} + k\hbar\omega$ ($k \in \mathbb{Z}$), it transforms like

$$f(z+k, b + \beta k \hbar\omega) = e^{-\beta k \hbar\omega} f(z, b), \quad (4.31)$$

demonstrating that expression (4.29) for the rate ratio is independent of the particular choice of K_0 . To see this, one has to use the property

$$C_L(z+k, z_c) = e^{(|z+k|-|z+k+L|)/z_c} = e^{(|z+k|-|z|)/z_c} e^{(|z|-|z+L+k|)/z_c} \quad (4.32)$$

$$= e^{(|z+k|-|z|)/z_c} C_{L+k}(z, z_c), \quad (4.33)$$

where the L -independent factor $e^{(|z+k|-|z|)/z_c}$ cancels in Eq. (4.30).

With the Boltzmann distribution of time-independent systems in mind, we now express the relative occupation of two neighboring regular states as a function of the spacing

$$E_{m,m+1}^{\text{reg}} := E_m^{\text{reg}} - E_{m+1}^{\text{reg}} \quad (4.34)$$

of their regular energies (2.69). We recall from Sec. 2.3 that this quantity is closely related to the quasienergy spacing: because of $E_m^{\text{reg}} \bmod \hbar\omega = \varepsilon_m$ the energy spacing and the quasienergy spacing can differ only by an integer multiple of $\hbar\omega$, i.e. $E_{m,m+1}^{\text{reg}} = \varepsilon_{m,m+1} + K\hbar\omega$. We can now choose the index K_0 in Def. (4.9) such that $\zeta_{m,m+1,K_0} = \varepsilon_{m,m+1} + K_0\hbar\omega = E_{m,m+1}^{\text{reg}}$ is fulfilled and the rate ratio in Eq. (4.29) becomes a function of the regular energy spacing,

$$\frac{R_{m,m+1}}{R_{m+1,m}} = e^{\beta E_{m,m+1}^{\text{reg}}} f\left(\frac{E_{m,m+1}^{\text{reg}}}{\hbar\omega}, \beta E_{m,m+1}^{\text{reg}}\right). \quad (4.35)$$

By requiring $\frac{R_{0,1}}{R_{1,0}} = e^{\beta E_{0,1}^{\text{reg}}} f\left(\frac{E_{0,1}^{\text{reg}}}{\hbar\omega}, \beta E_{0,1}^{\text{reg}}\right) \stackrel{!}{=} e^{\beta_{\text{eff}} E_{0,1}^{\text{reg}}}$ for the two lowest regular states $m = 0, 1$ we define a rescaled, effective temperature $1/\beta_{\text{eff}}$ with

$$\frac{\beta_{\text{eff}}}{\beta} := 1 + \frac{\ln f\left(\frac{E_{0,1}^{\text{reg}}}{\hbar\omega}, \beta E_{0,1}^{\text{reg}}\right)}{\beta E_{0,1}^{\text{reg}}}. \quad (4.36)$$

In Fig. 4.6 this parameter is shown as a function of the winding number ν_0 of the lowest regular state, where we assume for simplicity $\nu_0 \simeq -E_{0,1}^{\text{reg}}/(\hbar\omega)$, see Def. (2.69) of E_m^{reg} and the associated discussion in Section 2.3. This is fulfilled if the winding number is constant or slowly varying and the variation of $\langle L \rangle_m$ can likewise be neglected. The parameter β_{eff}/β takes values smaller than 1 and is symmetric in ν_0 . A substantial deviation from the true

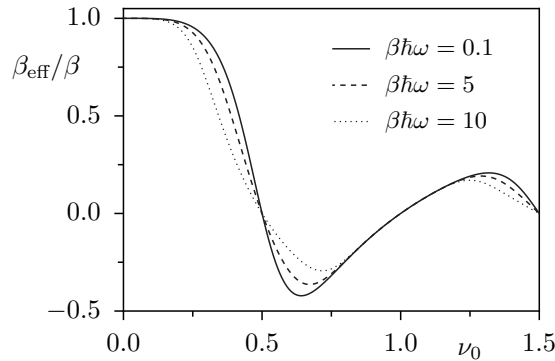


Figure 4.6: Inverse effective temperature β_{eff}/β according to Eq. (4.36) vs. winding number ν_0 for $\omega_c/\omega \gg 1$ and three different temperatures. Note that ν_0 could be replaced with $-E_{0,1}^{\text{reg}}/(\hbar\omega)$.

bath temperature, $\beta_{\text{eff}}/\beta \ll 1$, takes place around $|\nu_0| \approx 0.5$. In the limit $|\nu_0| \rightarrow 0$ on the other hand, where the kicked system approaches its static limit, the actual bath temperature $1/\beta$ is retained.

We recall from Section 2.3 that the winding number ν in kicked systems may be shifted by an integer q resulting in a new set of regular energies whose spacing is enlarged by the additional term $q\hbar\omega$. Conventionally ν is chosen in the interval $[-1/2, 1/2]$. By virtue of the property (4.31) the product $\beta_{\text{eff}}E_{0,1}^{\text{reg}}$ is however invariant under this shift and therefore leaves the rate ratio $R_{0,1}/R_{1,0}$ unchanged.

The parametrization $R_{0,1}/R_{1,0} = e^{\beta_{\text{eff}}E_{0,1}^{\text{reg}}}$ provides a useful analog to the rate ratio $R_{0,1}/R_{1,0} = e^{\beta E_{0,1}}$ of time-independent systems, with the eigenenergy spacing $E_{0,1}$. Beyond that, this parametrization is meaningful for the entire set of regular occupations, if β_{eff} is able to parametrize the other rate ratios $R_{m,m+1}/R_{m+1,m}$ as well. For that to hold the function $f(z, b)$ has to depend exponentially on z . In general this is not fulfilled. If however the regular energy spacing $E_{m,m+1}^{\text{reg}}$ does not change substantially throughout the island, which is often fulfilled even for generic islands of non-constant winding number, then $\ln f(z, b)/b$ may be treated as a constant with respect to z . That is why we further assume that the effective temperature defined in Eq. (4.36) from $R_{0,1}/R_{1,0}$ extends to the whole set of nearest-neighbor rate-ratios even beyond the two lowest states 0 and 1,

$$\frac{R_{m,m+1}}{R_{m+1,m}} \simeq e^{\beta_{\text{eff}}E_{m,m+1}^{\text{reg}}} . \quad (4.37)$$

Inserting this into the approximate detailed balance amongst the regular states, Eq. (4.6), this finally yields the occupation ratios

$$p_m/p_{m+1} = e^{-\beta_{\text{eff}}E_{m,m+1}^{\text{reg}}} , \quad (4.38)$$

analogously to the Boltzmann weights.

Figure 4.2(c) shows the regular Floquet occupations of the kicked rotor (4.3) vs. the regular energies E_m^{reg} and demonstrates excellent agreement with the above predicted exponential weights $e^{-\beta_{\text{eff}} E_m^{\text{reg}}}$ (red line) for almost all regular states. Deviations occur for the outermost regular states, $m \geq 20$, only. These have a stronger weight outside the regular island and are thus coupled stronger to the chaotic states. The additional rates between these regular states and the chaotic states in the rate equations (3.30), see Fig. 4.3, enforce a gradual adaptation between the outermost regular probabilities and the occupation level of the chaotic states. Besides, Fig. 4.2(c) shows the large discrepancy of the Boltzmann-like weights $e^{-\beta E_m^{\text{reg}}}$ with the true bath temperature $1/\beta$.

4.2.3 Quality of the detailed balance assumption

This supplementary section serves to critically discuss some of the approximations in the derivation of the Boltzmann-type distribution (4.38). An overview is given in Fig. 4.7, in column (a) for the kicked rotor corresponding to Fig. 4.2. The regular occupations p_m from the rate equations (3.30) (black dots) are shown in (a1) and the respective occupation ratios p_{m+1}/p_m of neighboring regular states in (a2). Furthermore, in order to probe the restriction of the total balance to the detailed balance (4.6), we solve Eq. (3.30) with a reduced rate matrix

$$R_{ij}^{(k)} := \begin{cases} 0 & i = m, j = n \text{ and } |m - n| > k \\ R_{ij} & \text{otherwise} \end{cases}, \quad (4.39)$$

which contains in the regular subspace only the neighboring rates R_{mn} with $|m - n| \leq k$, instead of the full rate matrix R_{ij} . For $k \geq 3$ the resulting regular occupations $p_m^{(k)}$ match the original occupations p_m very well, e.g. $p_m^{(3)}$ (orange circles), for which the difference to p_m is not even visible on the scale of Fig. 4.7(a1). We recall $R_{m,m\pm 2} = 0$, such that the $p_m^{(2)}$ are identical to the $p_m^{(1)}$ (green circles) and are not shown in Fig. 4.7. We also compare p_{m+1}/p_m in Fig. 4.7(a2) with the rate ratios $R_{m,m+1}/R_{m+1,m}$ (black crosses). Not surprisingly, the latter agree best with the occupation ratios of the $p_m^{(1)}$ (green circles), as these are based on the reduced rate matrix $R_{ij}^{(1)}$ with contributions from the nearest-neighbor rates $R_{m,m\pm 1}$ alone. The systematic deviation between p_{m+1}/p_m and $R_{m,m+1}/R_{m+1,m}$ originates from the existence of rates beyond the nearest-neighbor rates $R_{m,m\pm 1}$, in particular rates between the regular subspace and the chaotic states. These cause a gradual adaptation of the regular occupations to the mean value \bar{p}_{ch} of the chaotic occupations and are thus responsible for a deviation from the exponential Boltzmann-type prediction (4.38). Figure (a2) also shows the approximation of $R_{m,m+1}/R_{m+1,m}$ by Eq. (4.35) (black line), which performs excellently. Finally, Fig. 4.7(a) contains the predicted weights $e^{-\beta_{\text{eff}} E_m^{\text{reg}}}$ of Eq. (4.38) (red line). In contrast to the excellent approximation (4.35), the latter approximation agrees only in the leading order. The error of the approximation (4.38) compared to the approximation (4.35) is a consequence of the assumption that the parameter β_{eff} is independent of m . However,

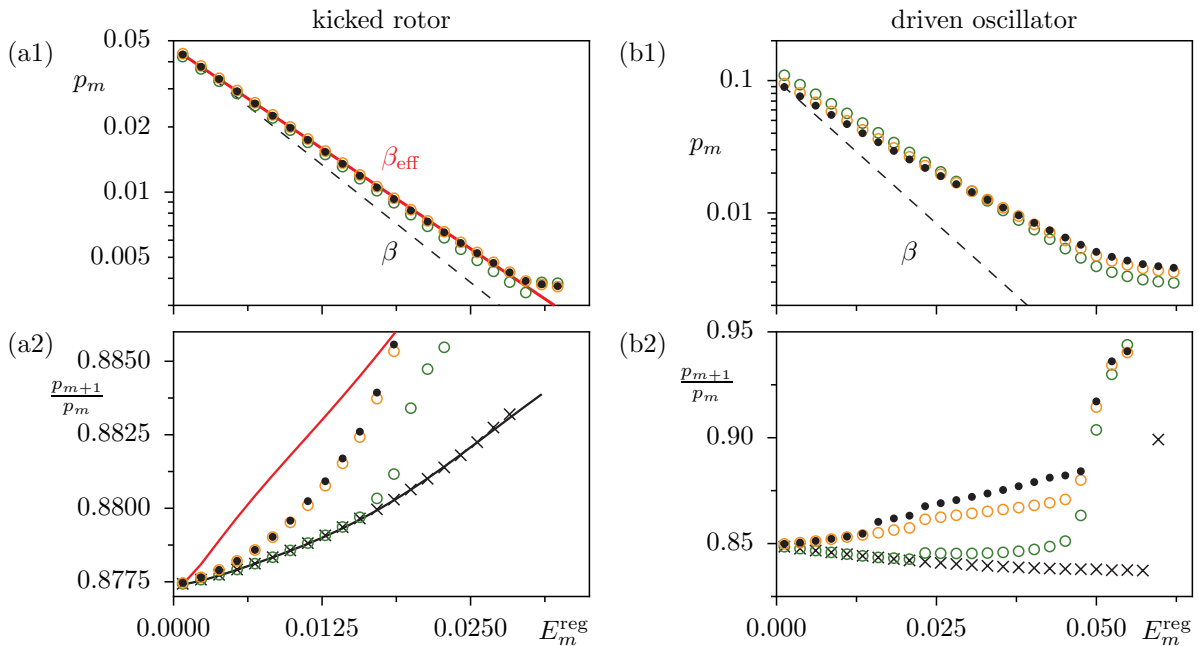


Figure 4.7: Illustration of some approximations leading to the prediction (4.38). (a1)-(b1) Regular occupations p_m vs. regular energies E_m^{reg} and (a2)-(b2) relative occupations p_{m+1}/p_m of neighboring regular states for (a) the kicked rotor of Fig. 4.2 and (b) the driven oscillator of Fig. 4.1. The occupations p_m are the solutions of Eq. (3.30) based on the full rate matrix R_{ij} (black dots) and on the reduced rate matrix $R_{ij}^{(k)}$ defined in Eq. (4.39), here with $k = 3$ (orange circles) and $k = 1$ (green circles), respectively. Further data in (a) are the analytical prediction $p_m \sim e^{-\beta E_m^{\text{reg}}}$ according to Eq. (4.38) (red line), in (a1) additionally compared to the Boltzmann-like weights $e^{-\beta E_m^{\text{reg}}}$ (dashed line). Moreover, (a2) shows the rate ratios $R_{m,m+1}/R_{m+1,m}$ (black crosses) as well as their approximation by Eq. (4.35) (black line).

the deviations are tiny on the scale of the absolute occupations p_m in Fig. 4.7(a1), especially in comparison to the Boltzmann-like weights $e^{-\beta E_m^{\text{reg}}}$ (dashed line).

For the continuously driven oscillator (4.2) the regular Floquet occupations p_m are shown in Fig. 4.1(c) vs. the regular energies E_m^{reg} . We fit an inverse temperature $\beta_{\text{fit}} \approx 0.66\beta$, again corresponding to a higher temperature than the actual bath temperature. Equation (4.36) however fails with a prediction of $\beta_{\text{eff}} = 0.06\beta$. This is not surprising, because the derivation of β_{eff} contains assumptions which are justified for the kicked systems only. For the driven oscillator Fig. 4.7(b) presents the same quantities as for the kicked rotor in (a), with the exception of β_{eff} . Qualitatively, the same observations and conclusions can be made. Quantitatively, the stronger deviations between p_{m+1}/p_m and $R_{m,m+1}/R_{m+1,m}$ can be noticed and are to be attributed to the rather strong influence of rates $R_{m,m\pm n}$ with $n > 1$, compare Fig. 4.3. We conclude that this absence of a detailed balance is responsible for the comparably poor quality of the exponential fit for the regular occupations p_m with respect to both E_m^{reg} and $\langle E_m \rangle_\tau$, as illustrated in Fig. 4.4(b) by the rather fast deviation of the factors w_m from 1. Note, that in other examples of continuously driven systems, e.g. the driven double well potential of Chapter 5, a strong dominance of the nearest-neighbor rates can

again be recorded and the detailed-balance assumption is justified far better there. Also the exponential fit based on the regular energies E_m^{reg} performs better, compared to the mean energies $\langle E_m \rangle_\tau$. A systematic investigation, under which circumstances the dominance of the nearest-neighbor rates allows to neglect the other rates between regular states, is still lacking.

Coming back to the kicked systems, we can report that the weights of Eq. (4.38) accurately parametrize the regular Floquet occupations in typical situations. However, being based on the assumptions of detailed balance, Eq. (4.6), and m -independence of the parameter β_{eff} , Eq. (4.37), there are a couple of circumstances, where the prediction (4.38) must fail:

- (i) For instance, they are limited to the semiclassical regime, where already a series of regular states exists. In the deep quantum regime on the contrary, the few existing regular states are strongly coupled to the chaotic states, comparable to the outermost regular states in Fig. 4.2(c). Besides, the semiclassical eigenfunction hypothesis does not necessarily apply in this regime: Floquet states that spread over regular as well as chaotic parts of the classical phase space may exist.
- (ii) Another situation, where (4.38) is not well-adapted is that of a strong internal variation of the winding number and thus also of the regular energy spacing. Then, $\ln f(z, b)/b$ cannot be treated as a constant and the parameter β_{eff} is not well-adapted to states $m > 1$. This can also happen, if ν varies only moderately around $|\nu| \approx 0.5$, where β_{eff} is particularly sensitive to variations of ν , see Fig. 4.6. For the kicked rotor this happens e.g. at $\kappa \approx 4$, where the central periodic orbit bifurcates and the regular island hence splits into two islands. If on the other hand ν is constant throughout the island, which is fulfilled if $T'(p)$ and $V'(x)$ are linear functions, the parametrization (4.37) works particularly well and the occupations are well characterized by Eq. (4.38).
- (iii) Yet another local disturbance of the exponential scaling (4.38) takes place as a consequence of avoided crossings. We will discuss this point in detail in Section 5.

4.2.4 Dependence of β_{eff} on the winding number ν

Figure 4.6 suggests that the effective temperature $1/\beta_{\text{eff}}$ can assume values very different from the true temperature $1/\beta$ of the heat bath. To verify this, we consider a linearized

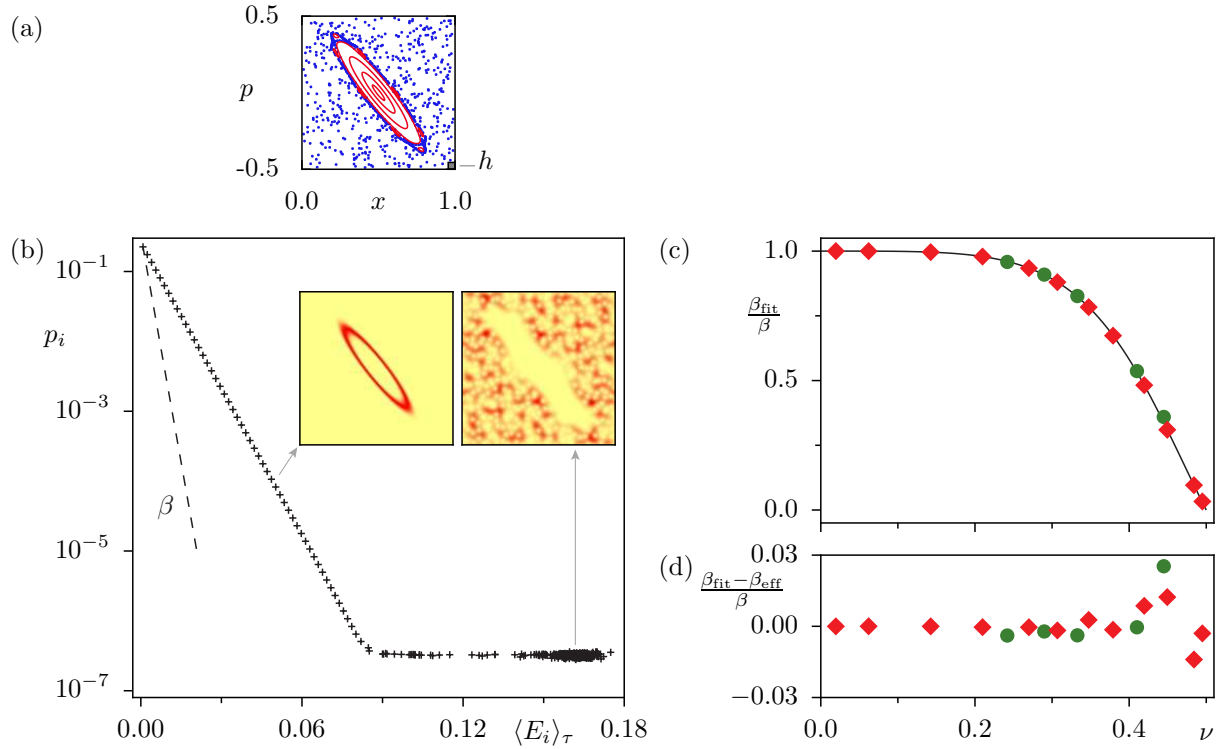


Figure 4.8: (a) Stroboscopic Poincaré-section for the kicked map with the kinetic energy (4.40) and the stepwise defined potential (4.41). (b) Floquet occupations p_i vs. $\langle E_i \rangle_\tau$ and insets with Husimi representations of the regular state $m = 30$ and a chaotic state. (c) Inverse fit temperature β_{fit} according to Eq. (4.43) (red diamonds) vs. winding number ν of the island, compared to the effective inverse temperature β_{eff} (black line) for $\beta\hbar\omega = 1$. (d) Relative deviation between β_{eff} and β_{fit} . The variation of ν is done with the system parameters $s = 1.5$, $\epsilon = 0.05$, and $r = 0.01, 0.1, 0.5, 1.0, 1.5, 1.8, 2.1, 2.3, 2.5, 2.6, 2.66, 2.666$. The additional data points (green dots) are for the kicked rotor with $\kappa = 1.9, 2.5, 3.0, 3.7, 3.9$. Other parameters are $h = 1/500$, $\beta = 500$, and $\omega_c/\omega = 100$.

kicked system with the kinetic energy and the kick potential

$$T(p) = \frac{s}{2} \cdot p^2 \quad (4.40)$$

$$V(x) = \begin{cases} \frac{r}{2} \cdot \left(x - \frac{1}{2}\right)^2 - \frac{2r}{25} & \frac{1}{10} < x < \frac{9}{10} \\ 0 & \text{otherwise} \end{cases} \quad (4.41)$$

$$(4.42)$$

which is smoothed with a Gaussian of variance ϵ^2 to avoid non-smooth behavior at the points $x = 1/10$ and $9/10$. Periodic boundary conditions are imposed in both position and momentum.

The stroboscopic Poincaré-section in Fig. 4.8(a) is dominated by a regular island centered at the fixed point $(1/2, 0)$ for parameters $r = 2.3$, $s = 1.5$, and $\epsilon = 0.05$. As $V'(x)$ and $T'(p)$ are linear functions in a wide region around the fixed point, the winding number is constant

throughout the regular island, $\nu = \nu_0$. By variation of the harmonic frequency r of the potential, ν is tunable in the range $0 < \nu < 1/2$. Note, however, that the island size shrinks to 0 for $r \rightarrow 0$ (implying $\nu \rightarrow 0$), as well as for $r \rightarrow 8/3$ (implying $\nu \rightarrow 1/2$), where the limit of stability, $|r \cdot s| = 4$, is encountered. Figure 4.8(b) presents the set of Floquet occupations for $h = 1/500$. Due to the constant winding number ν , the occupations excellently match the exponential prediction of Eqs. (4.38) and (4.36). This is additionally demonstrated in Figs. 4.8(c) and (d), which compares the fit parameter (red diamonds)

$$\beta_{\text{fit}} := \frac{\ln p_1 - \ln p_0}{E_0^{\text{reg}} - E_1^{\text{reg}}} \quad (4.43)$$

of the regular occupations p_m to the inverse effective temperature β_{eff} (black line).

Besides, Fig. 4.8(c) includes the fit parameter β_{fit} for several parameter realizations of the kicked rotor (4.3) (green dots). In contrast to the kicked system of Eqs. (4.40) and (4.41), the winding number in the regular island of the latter is not constant inside the island. Although this may lead to small deviations from the exponential scaling of the p_m , the fit parameter β_{fit} in the center of the island agrees very well with the value of β_{eff} and confirms the leading order dependence of β_{eff} on the winding number ν .

4.3 Additional classical phase-space structures

The set of Floquet states in the examples of the last sections are dominated by regular states in large regular islands on the one hand and chaotic states on the other hand. Apart from these, other types of Floquet states can exist, depending on the structures in the classical phase space and the size of the effective Planck constant h . The following sections give an overview about the fingerprints of such additional types of Floquet states on the distribution of the Floquet occupations p_i .

4.3.1 Independent islands

In Sec. 4.2 the prediction $p_m \sim e^{-\beta_{\text{eff}} E_m^{\text{reg}}}$ for the occupations of the regular island states has been derived, with an effective temperature β_{eff} that depends on the properties of the regular island, in leading order on the winding number ν_0 of the lowest regular state. This dependence is best illustrated in a kicked system with independent regular islands of different winding number. We construct such a system by replacing the potential energy of the kicked rotor by a stepwise quadratic potential

$$V(x) = \begin{cases} \frac{r_L}{2} \left(x - \frac{1}{4}\right)^2 + \frac{r_R - r_L}{32} & 0 \leq x \leq \frac{1}{2} \\ \frac{r_R}{2} \left(x - \frac{3}{4}\right)^2 & \frac{1}{2} \leq x < 1 \end{cases}, \quad (4.44)$$

which is smoothed with a Gaussian of variance ϵ^2 to avoid non-smooth behavior at the points $x = 0$ and $1/2$, see Fig. 4.9(a). The kinetic energy is generalized to read $T(p) = sp^2/2$. Like in the kicked rotor, periodic boundary conditions in position and momentum are imposed. The potential and the stroboscopic Poincaré-section with two dominant regular islands at $x_L = 1/4$ and $x_R = 3/4$ of the sizes $A_L = 0.053$ and $A_R = 0.028$, respectively, are shown Fig. 4.9(a) for the parameter values $r_L = 0.2$, $r_R = 2.0$, $s = 1.95$, and $\epsilon = 0.005$. The kicked map with the kick potential (4.44) may also serve as a model system for a driven bistable potential, as it is considered in Chapter 5. In contrast to a continuously driven system, it is relatively easy to generate two regular islands of strongly differing winding numbers $\nu_{L,R}$. To this end, the independent harmonic frequencies $r_{L,R}$ have to be chosen at very different values. The winding numbers of the two islands are both constant, $\nu_L = 0.10$ and $\nu_R = 0.45$, as a consequence of the linear behavior of $V'(x)$ and $T'(p)$ in the domains of the islands.

The Floquet occupations are shown in Fig. 4.9(b) for $h = 1/500$. The prevailing features are the two distinct, monotonous occupation branches with very different slopes. These belong to the regular subsets each of which consists of the regular states localized in either of the two islands, $\alpha = L, R$. This feature can be retraced from the different orders of magnitude of the involved rates. The spatial overlap between the states of different islands is exponentially small and hence also the inter-island rates are negligible in comparison to the intra-island rates, especially those between neighboring states $m_\alpha, m_{\alpha+1}$ of the same island.

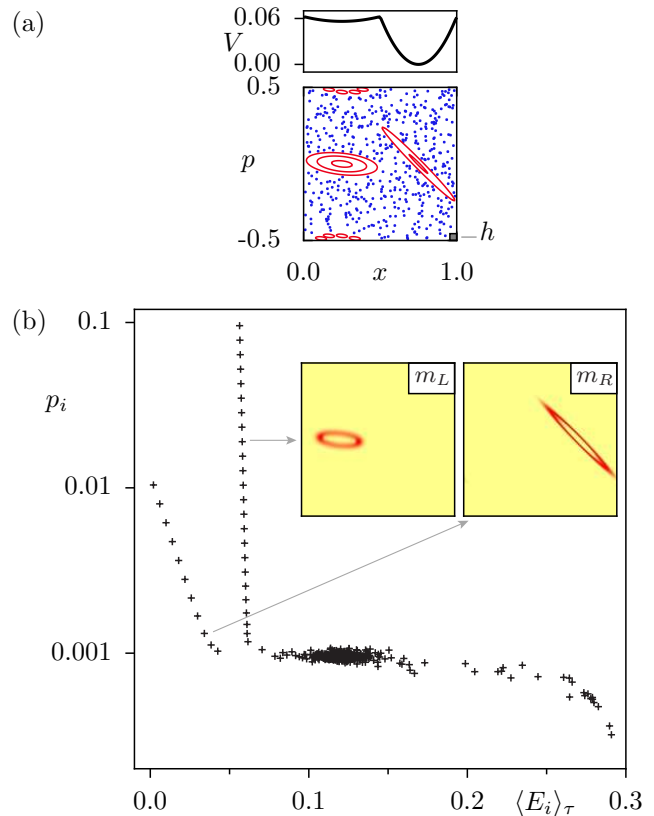


Figure 4.9: (a) Stepwise defined potential $V(x)$ of Eq. (4.44) and stroboscopic Poincaré-section for the kicked map with $V(x)$ and $T(p) = sp^2/2$. (b) Floquet occupations p_i vs. $\langle E_i \rangle_\tau$ and insets with Husimi representations of the regular states $m_R = 8$ and $m_L = 8$. The parameters are $r_L = 0.2$, $r_R = 2.0$, $s = 1.95$, $\epsilon = 0.005$, $h = 1/500$, $\beta = 1000$, and $\omega_c/\omega = 100$.

The equilibration process, whose asymptotic state is described by the rate balance (3.30), therefore takes place almost independently in the two islands. The main interaction between the two occupation branches is mediated only by a coupling of the outermost regular states with notably higher weight in the other island, or indirectly via the coupling to chaotic states. The latter ensures that both occupation branches are ‘smoothly’ attached to the chaotic occupation plateau. With the analysis of Section 4.2.2 we find the inverse effective temperatures $\beta_{\text{eff},L}/\beta \approx 1.0$ for the left island and $\beta_{\text{eff},R}/\beta \approx 0.29$ for the right island, both in excellent agreement with the corresponding inverse fit temperatures.

Around $(x, p) = (1/4, 1/2)$ there exists a third regular region in phase space. It consists of several nonlinear resonance chains, which host states of high average energy $\langle E_i \rangle_\tau \gtrsim 0.2$. In Fig. 4.9 these are found in a separate interval at small values of p_i . However, no distinct occupation hierarchy is visible among them, since the Floquet states are localized on several different resonance island chains. The effective Planck constant h is not small enough to support resonance states with principal quantum numbers $m > 2$ even in the biggest of them. The occupations of resonance states for a better suited example are discussed in the following section.

4.3.2 Nonlinear resonances

Apart from the islands centered at stable elliptic fixed points of period one, island chains consisting of r regular islands are found in phase space around stable periodic orbits of

period r . These are generated at nonlinear $r:s$ -resonances, where the r -periodic trajectory has the rational winding number $\nu = s/r$ with respect to the central fixed point in the Poincarè-section. A trajectory on the secondary tori of the resonance passes from island to island and returns after r periods to the island, where it initially started. Considering the r -fold iterated map instead of the map itself, the trajectory always remains on one and the same island. That is why the semiclassical quantization is done with respect to this map of period $r \cdot \tau$.

To each principal quantum number m there exist r regular Floquet states $|\psi_{(ml)}\rangle$ of different quantum numbers $l = 0, \dots, r-1$. We refer to these states as resonance states. Each of them has equal weights in each of the dynamically connected resonance islands, but different phases, according to the semiclassical approximation. The associated semiclassical quasienergies $\varepsilon_{(ml)}$ are spaced equidistantly in $[0, \hbar\omega)$ with spacing $\hbar\omega/r$. In Section 2.3 we have introduced the semiclassical energies of the resonance states $|\psi_{(ml)}\rangle$

$$E_m^{\text{reg}} = \hbar\omega \frac{\nu_m^{(r)}}{r} \left(m + \frac{1}{2} \right) + \hbar\omega \frac{s}{2r} - \langle L \rangle_m, \quad (4.45)$$

which are independent of the quantum number l . The winding number $\nu_m^{(r)}$ refers to the iterates of the r -fold iterated map instead of the stroboscopic map itself.

Figure 4.10(b) shows the Floquet occupations p_i vs. the average energy for the kicked rotor with $\kappa = 2.35$, where the phase space features in addition to the main regular island a 4:1-resonance around the periodic orbit of period 4, see Fig. 4.10(a). The area of a single resonance island is $A \approx 0.015$ and the entire resonance chain hosts $N_{\text{reg}} = 4 \cdot 15$ resonance states for $h = 1/1000$. The Floquet occupations of both the regular states of the central island and the chaotic states resemble those of Fig. 4.2(b). In addition, one finds an occupation branch belonging to the resonance states. Interestingly, it has a positive slope stemming from the fact that the average energies $\langle E_{(ml)} \rangle_\tau$ of the resonance states $|\psi_{(ml)}\rangle$ decrease with increasing quantum number m , in contrast to the regular states of the central island. This is due to the asymmetry of the resonance tori around their respective island center in phase space. This is another clear evidence, that the cycle-averaged energy does not serve as a suitable measure to quantify the regular occupations by exponential weights in analogy to the Boltzmann distribution.

The r resonance states $|\psi_{(ml)}\rangle$ of fixed quantum number m have almost the same average energy $\langle E_{(ml)} \rangle_\tau$. Small deviations from this semiclassical prediction exist only for the outermost resonance states. These can be attributed to the occurrence of avoided crossings, which break the degeneracy of the $\varepsilon_{(ml)} \bmod (\hbar\omega/r)$ for $l = 0, \dots, r-1$ and fixed m , as well as the degeneracy of the $\langle E_{(ml)} \rangle_\tau$. As long as the coupling to the heat bath does not disturb the equivalence of the resonance islands, the occupations $p_{(ml)}$ of the r resonance states of

fixed principal quantum number m are also degenerate,

$$p_{(ml)} = p_m, \quad (4.46)$$

independent of the quantum number l . In Fig. 4.10(b) the corresponding 4 branches of the resonance state occupations $p_{(ml)}$ therefore lie on top of each other and cannot be distinguished from each other.

Now we want to explain, that the occupations $p_{(ml)}$ of the resonance states are likewise distributed as $p_{(ml)} \sim e^{-\beta_{\text{eff}} E_m^{\text{reg}}}$, according to the exponential weights (4.38) with the effective temperature $1/\beta_{\text{eff}}$ of Eq. (4.36). First we note that all arguments of Section 4.2.2, which lead to the approximation (4.29) for the rate ratio of two regular states, apply without restriction also to the resonance states, in particular Eq. (4.27) for the coupling matrix elements $x_{ij}(K) = x_{(ml)(nk)}(K)$. The assumed detailed balance relation (4.6), however, is no longer adapted to the structure of the rate matrix, since here also ‘internal’ rates exist, i.e. rates in the subspace of the r equivalent resonance states $l = 0 \dots r - 1$ with fixed quantum number m , in addition to the nearest-neighbor rates $R_{(ml)(m\pm 1, l)}$. Nonetheless, the total rate balance approximately decouples for each principal quantum number m into the r redundant balance relations

$$\frac{p_{(m+1, l)}}{p_{(ml)}} = \frac{R_{(ml)(m+1, l)}}{R_{(m+1, l)(ml)}} \quad (4.47)$$

for the degenerate occupations $p_{(ml)}$. They have the same structure as Eq. (4.6). A motivation for this approximation is deferred to Appendix F. Figure 4.10(d) shows the rate matrix $R_{(ml)(m'l')}$ restricted to the subspace of the $4 \cdot 15$ resonance states. The entries to the rate matrix are sorted in such a way, that the semiclassical quasienergies $\varepsilon_{(ml)} = E_m^{\text{reg}} + (ls/r)\hbar\omega$ are monotonously increasing functions of $m + ls/r$. By that measure, the rate matrix becomes approximately block-diagonal with 15 similar submatrices $R_{(ml)(ml')}$, each for a fixed value of the principal quantum number m . Besides, the four subfigures of Fig. 4.10(e) show the four submatrices $R_{(ml)(m'l')}$, each for a fixed value of the quantum number l , indicating the equivalence of these rate matrices.

The decoupling into the r equivalent balance relations (4.47), each of which involves the same rate ratio $R_{(ml)(m+1, l)}/R_{(m+1, l)(ml)}$ independent of l , can be hold responsible for the degeneracy (4.46) of the occupations $p_{(ml)}$. At the same time, it allows to make use of Eq. (4.37) and to approximate the $p_{(ml)}$ by the exponential weights $e^{-\beta_{\text{eff}} E_m^{\text{reg}}}$ of Eq. (4.38) with the effective temperature $1/\beta_{\text{eff}}$ of Eq. (4.36). Figure 4.10(c) shows the occupations $p_{(ml)}$ of the resonance states vs. the regular energies E_m^{reg} . Even on the magnified scale of this subfigure, compared to subfigure (b), the tiny differences of the $p_{(ml)}$ with different quantum numbers l are not visible. The effective temperature $1/\beta_{\text{eff}}$ is nearly indistinguishable from the actual temperature $1/\beta$, because the winding number $\nu_{m=0}^{(r)}/r = 0.79/4 \approx 0.2$ of the resonance islands is small and yields a value of β_{eff}/β very close to 1, compare Fig. 4.6. Note

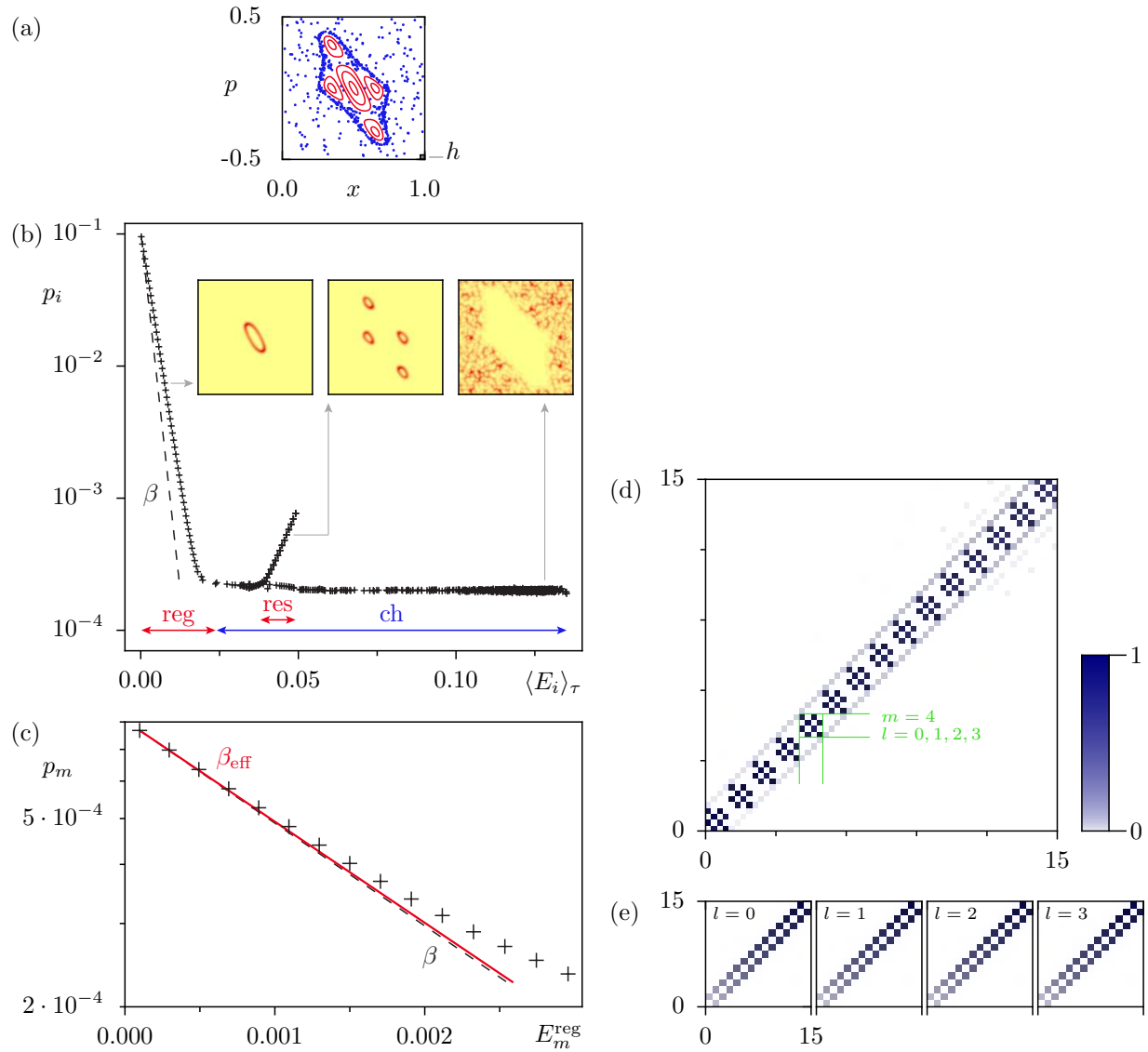


Figure 4.10: (a) and (b) analogously to Fig. 4.2 for the kicked rotor in presence of a 4:1-resonance. The insets in (b) show Husimi representations of a regular state from the main island, a resonance state and a chaotic state. (c) Floquet occupations $p_{(ml)} \approx p_m$ of the resonance states vs. regular energies E_m^{reg} , the exponential prediction (4.38) with $\beta_{\text{eff}} \approx 0.98\beta$ (solid line), and the Boltzmann-like prediction $p_m \sim \exp(-\beta E_m^{\text{reg}})$ (dashed line). (d) Rate matrix $R_{(ml)(m'l')}$ in the subspace of the resonance Floquet states, with $(ml) \neq (m'l')$ sorted firstly by increasing principal quantum number m . For fixed m the r different values of the quantum number l are sorted in such a way, that the semiclassical quasienergies $\varepsilon_{(ml)} = (E_m^{\text{reg}} + (ls/r)\hbar\omega) \bmod \hbar\omega$ increase monotonously. (e) The 4 equivalent rate matrices $R_{(ml)(m'l')}$, each for a fixed value of the quantum number l and $m \neq m'$. The parameters are $\kappa = 2.35$, $h = 1/1000$, $\beta = 500$, and $\omega_c/\omega = 100$.

that it still differs, though weakly, from $\beta_{\text{eff}} \approx 0.93$ of the main island. The parameter β_{eff} is the same for each of the four independent occupation branches $p_{(ml)}$. In contrast, the regular states localized on dynamically unconnected islands constitute separate occupation branches with respectively independent values β_{eff} , as demonstrated in the example of Section 4.3.1.

A similar example, where a 4:1-resonance is situated inside the regular island, is shown

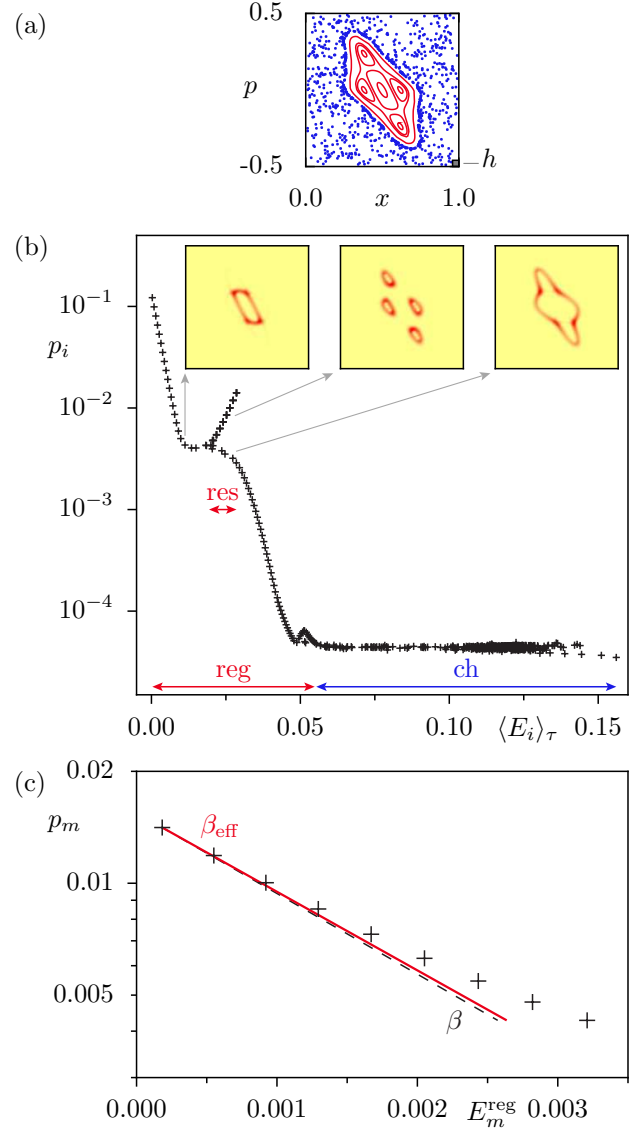


Figure 4.11: (a) and (b) analogously to Fig. 4.2 for the kicked rotor in presence of a 4:1-resonance inside the main regular island. The insets in (b) show Husimi representations of a regular state below the resonance region, a resonance state and a regular state between the resonance region and the chaotic sea. (c) Floquet occupations $p_{(ml)} \approx p_m$ of the resonance states vs. regular energy E_m^{reg} , the prediction (4.38) with the effective temperature $\beta_{\text{eff}} \approx 0.97\beta$ (solid line), and the Boltzmann-like prediction $p_m \sim \exp(-\beta E_m^{\text{reg}})$ (dashed line). The parameters are $\kappa = 2.2$, $h = 1/600$, $\beta = 500$, and $\omega_c/\omega = 100$.

in Fig. 4.11. Accordingly, the four superposed occupation branches of the $4 \cdot 9$ resonance states appear within the range of the regular occupations. The monotonous behavior of the regular occupations is locally disrupted due to the finite rates of the outermost resonance states to adjacent regular states of the main island. A further disruption of the monotonous behavior is visible for states in the transition region to the chaotic states. This phenomenon is related to an avoided crossing and will be explained in Section 5.2.

Another remark refers to the semiclassical limit: since the phase space of a generic time-periodic system contains a hierarchy of nonlinear resonance chains and islands of all scales, which host Floquet states if h is sufficiently small, we expect that the entire set of regular Floquet occupations becomes increasingly structured by the corresponding occupation branches from nonlinear resonances.

4.3.3 Beach states

The transition between regular phase-space regions and the chaotic sea is usually not sharp, but shaped by a multitude of small island chains and cantori, the fractal remains of broken KAM tori. These additional phase-space structures can strongly inhibit the classical flux of trajectories towards and away from the regular island and, depending on the size of h , can eventually give rise to the formation of quantum beach states, a term introduced in Ref. [82]. These reside on the transition layer around the regular islands and have little overlap with the remaining chaotic sea. Typically, beach states have very similar appearance and properties like the regular states of the adjacent island. Due to the proximity they partly even allow a quantization similar to the EBK-quantization rules [82, 83].

At $\kappa = 4$ the central island of the kicked rotor bifurcates into a resonance around a stable periodic orbit of period 2. It is accompanied by a series of partial barriers with a reduced classical flux towards and away from the islands. This is indicated for $\kappa = 4.415$ in the stroboscopic Poincaré-section of Fig. 4.12(a) by the comparatively high density of the chaotic orbit in the vicinity of the island. Figure 4.12(b) shows the Floquet occupations p_i vs. the average energy $\langle E_i \rangle_\tau$. The highest occupations belong to the regular states of the resonance. Figure 4.12(c) shows the regular occupations $p_{(ml)}$ vs. E_m^{reg} . In this example the winding number $\nu_{m=0}^{(r)}/r = 0.71/2 \approx 0.35$ in the resonance islands yields a rather strong deviation between β and β_{eff} , with $\beta_{\text{eff}}/\beta \approx 0.76$. Furthermore, Fig. 4.12(b) demonstrates that also the occupations of the beach states form a separate, nearly monotonous set in the transition region between the occupations of the resonance states on the one hand and of the chaotic states on the other hand. This is a consequence of a comparable structure in the coupling matrix R_{ij} , where also typically the nearest-neighbor rates dominate. At the same time, due to the exponentially decaying overlap of the resonance states with the chaotic phase-space region, the rates to the chaotic states are typically small as opposed to the rates to the proximately localized beach states. Thus, the beach states mediate the transition between the regular and the chaotic occupations. However, the occupations of the beach states are not strictly monotonous as functions of $\langle E_i \rangle_\tau$ as a result of avoided crossings, especially with chaotic states.

4.3.4 Hierarchical States

As mentioned above, in the vicinity of regular islands typically a lot of partial barriers with a limited classical flux towards and away from the island can be found, e.g. in the form of cantori or based on stable and unstable manifolds [84, 85]. Depending on the ratio of h to the classical flux, partial barriers can prevent Floquet states from spreading over the entire chaotic domain, apart from tunneling tails. If the phase-space area enclosed by the island and the partial barrier exceeds h , these states locally resemble chaotic states. For decreasing values of h they resolve and occupy the hierarchy of the classical phase space better and

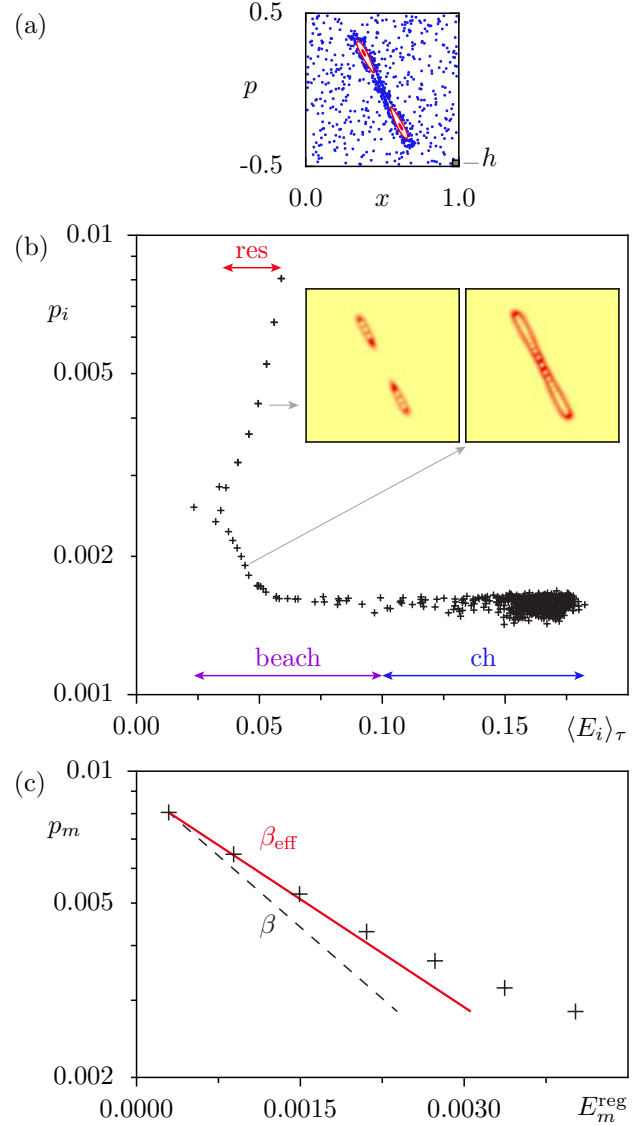


Figure 4.12: (a) and (b) analogously to Fig. 4.2 for the kicked rotor in presence of a 2:1-resonance surrounded by a series of strong partial barriers. The insets in (b) show Husimi representations of a resonance state ($m = 3$) and a beach state. (c) Floquet occupations $p_{(ml)} \approx p_m$ of the resonance states vs. regular energies E_m^{reg} , the exponential prediction (4.38) with $\beta_{\text{eff}} \approx 0.76 \beta$ (solid line), and the Boltzmann-like prediction $p_m \sim \exp(-\beta E_m^{\text{reg}})$ (dashed line). The parameters are $\kappa = 4.415$, $h = 1/600$, $\beta = 500$, and $\omega_c/\omega = 100$.

better and are therefore called hierarchical states [86]. The existence of these states does not contradict the quantum-classical correspondence as their fraction vanishes with $\mathcal{O}(h^\alpha)$ in the semiclassical limit. We apply the overlap criterion from Ref. [86] to determine, whether a Floquet state is hierarchical or not: it is identified as a hierarchical state, if it is not a regular state but comparably strongly localized, such that the Husimi weight $\iint_{\Omega} dx_0 dp_0 H_\psi(x_0, p_0)$ within a large chaotic phase-space area Ω away from the regular island falls below 0.7. The normalization is done, such that the Husimi weight assumes the value 1 for a state that is uniformly spread over the entire phase space.

Figure 4.13(a) shows the Poincaré-section and Fig. 4.13(b) the Floquet occupations for the kicked rotor with $\kappa = 2.5$, where the fraction of hierarchical states is comparatively high [86]. In Fig. 4.13(c) the occupations of the hierarchical states are emphasized. The figure indicates that their occupations are distributed analogously to the chaotic states which explore the entire chaotic phase-space region. Again, the corresponding fluctuation pattern of the occupations p_i has its origin in the randomly fluctuating rates R_{ij} in the subspace of

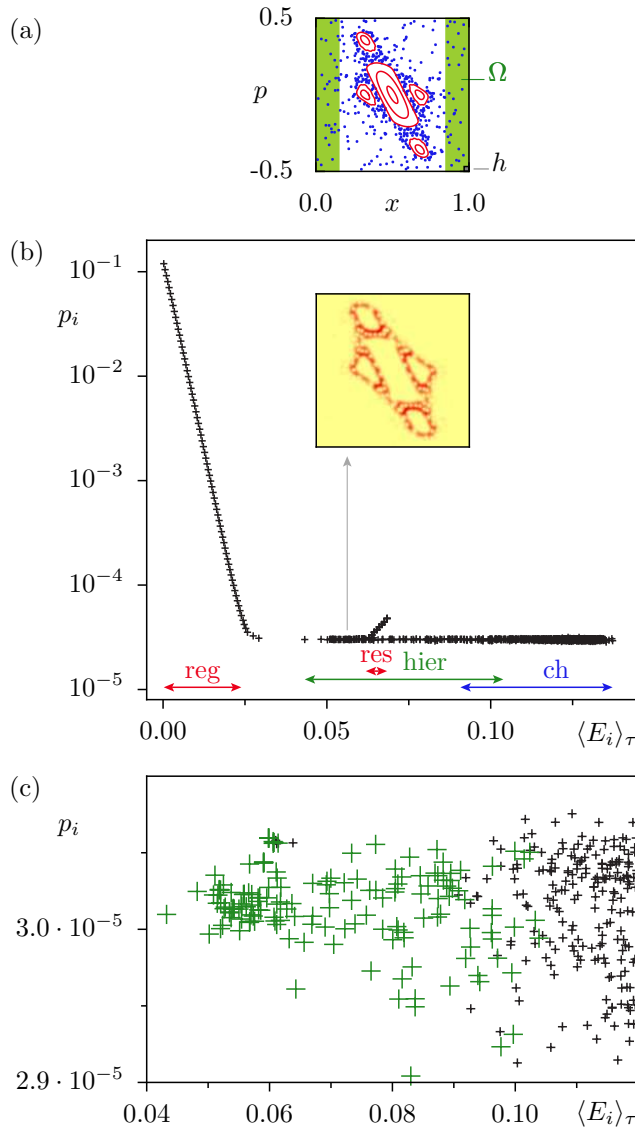


Figure 4.13: (a) and (b) analogously to Fig. 4.2 for the kicked rotor in presence of a 4:1-resonance surrounded by a series of strong partial barriers. The inset in (b) is the Husimi representation of a hierarchical state. (c) Magnification of (b) with emphasized data points of the hierarchical states (large green crosses), which are determined by the overlap criterion from the shaded phase-space area Ω in (a). The parameters are $\kappa = 2.5$, $h = 1/1000$, $\beta = 500$, and $\omega_c/\omega = 100$.

the hierarchical states, which resemble those amongst the other chaotic states.

To conclude, the occupation characteristics of the beach states and the hierarchical states again confirm the influence of the classical phase structure not only on the spectrum and on the Floquet states, but eventually also on the Floquet occupations and hence on the asymptotic state.

Note, that in the above examples, Figs. 4.12 and 4.13, either of the two types is predominant, but still representatives of the other are present. In general, hierarchical states and beach states are found in coexistence. For example, a few of the states of intermediate energy $\langle E_i \rangle_\tau$ that are indicated in Fig. 4.13 as hierarchical by the above overlap criterion had rather to be classified as beach states or as states with scarring behavior, i.e. localized on hyperbolic fixed points or on a family of parabolic fixed points.

4.4 Chaotic states

The examples of the previous sections give evidence that the occupations p_i of the chaotic states fluctuate around a mean value \bar{p}_{ch} with a very small variance σ_{ch}^2 compared to the range of occupations of the regular states, see e.g. Figs. 4.1 and 4.2. In particular, the individual occupations of the chaotic states are uncorrelated with the cycle-averaged energy $\langle E_i \rangle_\tau$. In this section the distribution of the chaotic Floquet occupations is analyzed in more detail. In particular, the scaling behavior of the relative width $\sigma_{\text{ch}}/\bar{p}_{\text{ch}}$ is investigated in the semiclassical limit $h \rightarrow 0$.

4.4.1 Distribution of the chaotic Floquet occupations

The chaotic occupations are characterized by the mean value $\bar{p}_{\text{ch}} = \frac{1}{N_{\text{ch}}} \sum_{i=0}^{N_{\text{ch}}-1} p_i$ and the standard deviation σ_{ch} from \bar{p}_{ch}

$$\sigma_{\text{ch}} = \sqrt{\frac{1}{N_{\text{ch}}} \sum_{i=0}^{N_{\text{ch}}-1} p_i^2 - (\bar{p}_{\text{ch}})^2}. \quad (4.48)$$

With N_{ch} we denote the number of chaotic states. If the area A_{reg} of the regular regions in phase space is larger than $h = 1/N$, they are resolved by the quantum system and therefore host $N_{\text{reg}} = \lfloor A_{\text{reg}} \cdot N + 1/2 \rfloor$ regular states. The number of chaotic states $N_{\text{ch}} = N - N_{\text{reg}}$ is then smaller than the Hilbert dimension N .

We solve the rate equations (3.30) for the quantum kicked rotor and other kicked systems with fully or dominantly chaotic spectrum. The statistical quality of the statistical parameters is improved by accumulating the solutions of Eq. (3.30) based on several realizations of the rates (3.31). These are obtained by a variation of the Bloch phase θ_p in the interval $[0, 1/2]$. In the insets (a) and (b) of Fig. 4.14 the distribution of the chaotic occupations is shown for the kicked rotor in the absence of regular states ($\kappa = 6.0$) for two different values of h . The distribution of the chaotic occupations is roughly Gaussian, compare the Gaussian fit in inset (b), provided that $\sigma_{\text{ch}} \ll \bar{p}_{\text{ch}}$. Otherwise, if $\sigma_{\text{ch}} \gtrsim \bar{p}_{\text{ch}}$, the Gaussian character of the distribution is distorted, because the positivity of the occupations p_i enforces a repulsion from 0 and thus entails an asymmetric distribution as in inset (a).

We want to study, how the characteristic parameters of the distribution, \bar{p}_{ch} and σ_{ch} , behave in the semiclassical limit $h \rightarrow 0$. The following paragraphs give a survey.

A. Mean chaotic occupation \bar{p}_{ch}

If only chaotic states exist, $\bar{p}_{\text{ch}} = 1/N_{\text{ch}} = 1/N$ is an immediate consequence of the normalization $1 = \sum_{i=0}^{N-1} p_i$, and \bar{p}_{ch} decreases as $\bar{p}_{\text{ch}} = 1/N = h$ in the semiclassical limit. In the

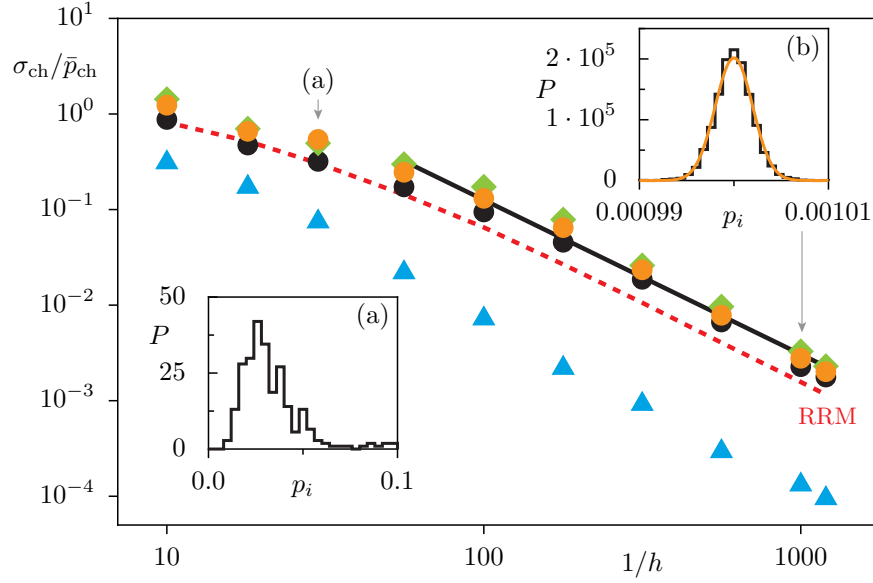


Figure 4.14: Relative standard deviation $\sigma_{\text{ch}}/\bar{p}_{\text{ch}} = \sigma_{\text{ch}}N_{\text{ch}}$ from the mean value \bar{p}_{ch} of the chaotic occupations vs. $1/h = N$ for the kicked rotor with a mixed regular-chaotic phase space ($\kappa = 2.9$: black dots), a macroscopically chaotic phase space ($\kappa = 6.0$: orange dots), and for the linearized kicked system (4.40), (4.41) ($r = 3.0, s = 1.5, \epsilon = 0.05$: green diamonds). In contrast to these results for the coupling operator $A = x$, we compare with σ_{ch} based on the spatially periodic coupling operator $A = \sin(2\pi x)/(2\pi)$ for the kicked rotor ($\kappa = 2.9$: blue triangles). The solid line indicates a power-law fit $\sigma_{\text{ch}}/\bar{p}_{\text{ch}} \sim h^b$ with $b = 1.6$ and the dashed line is taken from the random-rate model (RRM) of Section 4.4.2. The insets represent two of the underlying occupation distributions $P(p_i)$ for the kicked rotor in absence of regular states, $\kappa = 6.0$, with (a) $h = 1/30$ and (b) $h = 1/1000$. In (b) the distribution is compared to a Gaussian fit (orange line). Other parameters are $\beta = 100$ and $\omega_c/\omega = 100$.

presence of regular states, the mean chaotic occupation \bar{p}_{ch} is approximately

$$\bar{p}_{\text{ch}} = \frac{1}{N_{\text{ch}}} \left(1 - \sum_{m=0}^{N_{\text{reg}}-1} p_m \right) \leq \frac{1}{N_{\text{ch}}} \quad (4.49)$$

and can be estimated with the help of the approximate exponential distribution (4.38) as

$$\bar{p}_{\text{ch}} \approx \frac{1}{N - N_{\text{reg}}} \left(1 - p_0 e^{\beta_{\text{eff}} E_0^{\text{reg}}} \sum_{m=0}^{N_{\text{reg}}-1} e^{-\beta_{\text{eff}} E_m^{\text{reg}}} \right). \quad (4.50)$$

It can be shown, that \bar{p}_{ch} in the presence of regular states also scales proportional to h , where more and more regular states emerge for $h \rightarrow 0$. However, the exact value of \bar{p}_{ch} depends on θ_p , as the chaotic states and their quasienergies depend sensitively on θ_p . By variation of θ_p a multitude of avoided crossings occurs in the spectrum, among them also avoided crossings between chaotic and regular states. As will be discussed in Chapter 5, these are responsible for modifications of the entire set of Floquet occupations, and consequently \bar{p}_{ch} fluctuates

around the above-estimated value. In order to eliminate this side-effect of the θ_p -variation and make the occupation distributions from different values of θ_p comparable, we shift in the following analysis the actual mean chaotic occupation \bar{p}_{ch} to the renormalized mean value $\bar{p}_{\text{ch}} = 1/N_{\text{ch}}$, whenever the spectrum is not purely chaotic.

B. Relative standard deviation $\sigma_{\text{ch}}/\bar{p}_{\text{ch}}$

Together with \bar{p}_{ch} also the standard deviation σ_{ch} of the chaotic occupations p_i decreases in the semiclassical limit. Figure 4.14 illustrates the dependence of the relative standard deviation $\sigma_{\text{ch}}/\bar{p}_{\text{ch}} = \sigma_{\text{ch}}N_{\text{ch}}$ on $1/h = N$. Firstly for the kicked rotor with a mixed phase space ($\kappa = 2.9$: black points) and in the absence of regular states ($\kappa = 6.0$: orange points), as well as for the kicked quantum system with the kinetic energy (4.40) and the kick potential (4.41) ($r = 3.0, s = 1.5$ and $\epsilon = 0.05$: green diamonds). Each of these realizations results in similar distributions of the chaotic occupations. The measured values of $\sigma_{\text{ch}}/\bar{p}_{\text{ch}}$ are fairly insensitive to the details of the dynamical system and suggest universality of the power-law scaling behavior

$$\frac{\sigma_{\text{ch}}}{\bar{p}_{\text{ch}}} = \sigma_{\text{ch}}N_{\text{ch}} \approx a \cdot h^b \quad (4.51)$$

with the exponent $b = 1.6$. The prefactor a depends on the temperature and especially on the specific model employed to describe the heat bath and the system-bath coupling: in particular, $\sigma_{\text{ch}}/\bar{p}_{\text{ch}}$ can be considerably smaller, if instead of the conventional coupling operator $A = x$ the spatially periodic operator $A = \sin(2\pi x)/(2\pi)$ (compare $A^{(2)}$ in Section 4.5) is employed (kicked rotor at $\kappa = 2.9$: blue triangles).

C. Statistical properties of the rates R_{ij} and explanation for the power-law scaling of $\sigma_{\text{ch}}/\bar{p}_{\text{ch}}$

Interestingly, $\sigma_{\text{ch}}/\bar{p}_{\text{ch}} \sim h^b = N^{-b}$ with $b = 1.6 > 0.5$ drops faster than the error $N^{-1/2}$ in the determination of the mean value of a random variable by N independent measurements. Starting from this comparison to the theory of random variables one might assess, that a scaling behavior of $\sigma_{\text{ch}}/\bar{p}_{\text{ch}}$ with an exponent $1/2$ reflects merely the increasing dimension $N = h^{-1}$ of the underlying rate equation system (3.30). The decrease with an exponent $b > 1/2$ can hence only be explained by a further h -dependence of the rates R_{ij} in the rate equations (3.30).

To validate this assumption, we firstly consider the distribution of the rates R_{ij} ($i \neq j$), for which we observe in Fig. 4.15 an exponential distribution

$$P(R) = \lambda e^{-\lambda R} \quad (4.52)$$

with mean $\bar{R} = 1/\lambda$ and variance $\sigma_R^2 = 1/\lambda^2$. Although $1/\lambda$ decreases in the semiclassical limit, compare e.g. $1/\lambda = 3 \cdot 10^{-7}$ for $h = 1/30$ in Fig. 4.15(a) with $1/\lambda = 8 \cdot 10^{-9}$ for $h = 1/1000$ in Fig. 4.15(b), this is irrelevant for the distribution of the Floquet occupations.

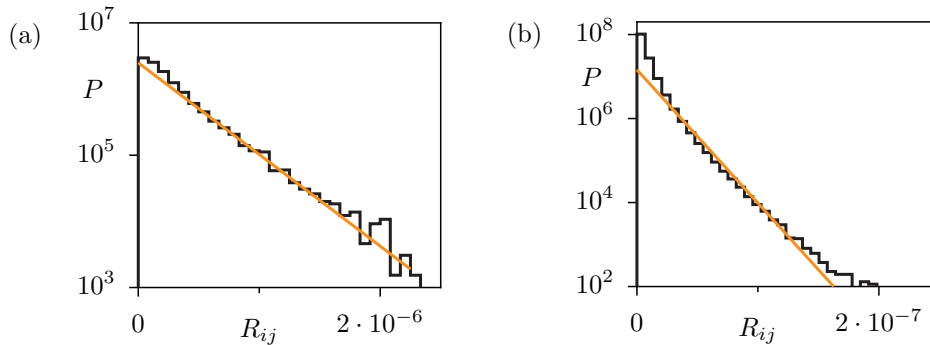


Figure 4.15: Distribution of the rates R_{ij} for the kicked rotor in absence of regular states, $\kappa = 6.0$, for (a) $h = 1/30$ and (b) $h = 1/1000$ and with $\beta = 100$, and $\omega_c/\omega = 100$. The orange lines indicate the exponential fits (4.52) with the standard deviations $1/\lambda = 3 \cdot 10^{-7}$ in (a) and $1/\lambda = 8 \cdot 10^{-9}$ in (b).

To verify this, we consider a change of the parameter λ in Eq. (4.52) to a value λ' . The rescaled random variable $R' = \lambda/\lambda'R$ is then distributed according to the transformed density $P_{\lambda'}(R') = \lambda'e^{-\lambda'R'} = \lambda'e^{-\lambda R} = \lambda'/\lambda P_{\lambda}(R)$. That means, changing the parameter λ is equivalent to rescaling R by a global factor. However, such a factor to the rates R_{ij} eventually cancels in the homogeneous rate equations (3.30). Thus, the changing width σ_R of the R_{ij} -distribution does not affect $\sigma_{\text{ch}}/\bar{p}_{\text{ch}}$ and cannot account for the unexpected scaling behavior⁵.

Which other statistical parameters can be hold responsible for $b > 1/2$? In a second step we consider the distribution of the quantity

$$\eta_{ij} := \max\left(\frac{R_{ij}}{R_{ji}}, \frac{R_{ji}}{R_{ij}}\right) - 1 > 0 \quad (i \neq j), \quad (4.53)$$

where the maximum value out of the rate ratio R_{ij}/R_{ji} and its inverse R_{ji}/R_{ij} is chosen, such that η_{ij} is always positive definite. This quantity is found to be distributed roughly exponentially, as indicated in the insets of Fig. 4.16 by the individual distributions $P(\eta_{ij})$ for (a) $h = 1/30$ and (b) $h = 1/1000$. The distributions are compared with the exponential fits

$$P(\eta) = (1/\sigma_{\eta})e^{-\eta/\sigma_{\eta}} \quad (4.54)$$

(orange lines). Note, that in the distributions the contributions of $\theta_p = 0.0, 0.5$ are omitted, since in these cases the Floquet states are parity eigenstates: the coupling matrix elements x_{ij} between states of the same parity vanish, and the distribution would then acquire an additional contribution at $\ln(\eta) \ll -1$, i.e. for small η .

The width of the η_{ij} -distribution, estimated by the standard deviation σ_{η} of the expo-

⁵Note, that this argument equally holds for a Porter-Thomas distribution $P(R) = (\sqrt{2\pi}\sigma)^{-1}R^{-1/2}\exp(-R/(2\sigma^2))$, which due to the enhanced weight at small R is somewhat better suited to describe the R_{ij} -distribution. However, the deviations to the exponential fit are only weak and, as we find confirmed by random-rate model of the next section, have only marginal effect on the distribution $P(p_i)$ of the occupations.

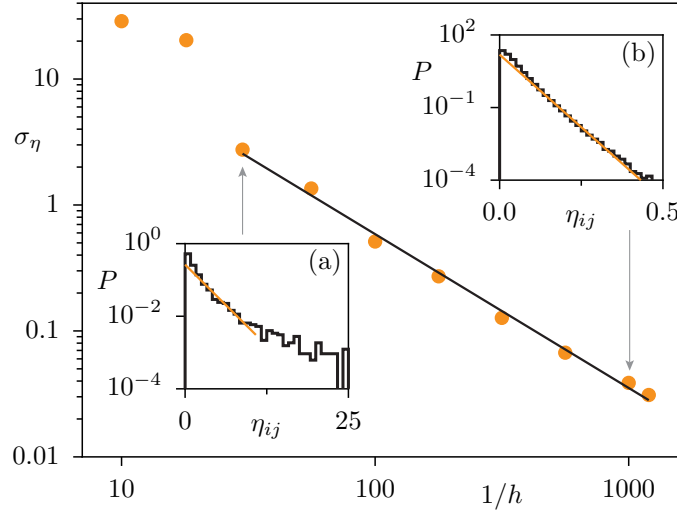


Figure 4.16: Standard deviation σ_η of the quantities η_{ij} according to Def. (4.53) vs. $1/h = N$ for the kicked rotor in absence of regular states, $\kappa = 6.0$. The solid line indicates a power-law fit $\sigma_\eta \sim h^\alpha$ with $\alpha = 1.2$. The insets represent two of the underlying distributions $P(\eta_{ij})$ for (a) $h = 1/30$ and (b) $h = 1/1000$, each compared to an exponential fit (orange lines). Other parameters are $\beta = 100$ and $\omega_c/\omega = 100$.

ponential distribution (4.54), decreases in the semiclassical limit, as is illustrated in Fig. 4.16. More specifically, σ_η describes a power-law scaling

$$\sigma_\eta \sim h^\alpha \quad \text{with } \alpha = 1.2. \quad (4.55)$$

For the moment we consider the limit $\sigma_\eta = 0$, which is here approached for $h \rightarrow 0$. Independent of h , this limit would also be fulfilled, if the rates were ‘non-thermal’, i.e. if the correlation function were energy-independent, $g(E) \equiv g_0$. In that case, the rate R_{ij} of a transition and the rate R_{ji} of the reverse transition would be exactly equal,

$$R_{ij} = \frac{2\pi\gamma^2}{\hbar} g_0 \sum_K |x_{ij}(K)|^2 = \frac{2\pi\gamma^2}{\hbar} g_0 \sum_K |x_{ij}(-K)|^2 = \frac{2\pi\gamma^2}{\hbar} g_0 \sum_K |x_{ji}(K)|^2 = R_{ji}, \quad (4.56)$$

and therefore $\eta = 0$ would be fixed. It is instructive to compare this behavior with the case of detailed balance, where $\eta_{ij} = p_j/p_i - 1$ holds: in the high-temperature limit $1/\beta \rightarrow \infty$, where all states acquire the same probability $p_i \rightarrow 1/N$, the widths of both distributions $P(p_i)$ and $P(\eta_{ij})$ approach zero.

For the actual Floquet rates R_{ij} with energy-dependent $g(E)$ and accordingly finite variance of the η_{ij} , the following arguments explain the observed decrease of σ_η in the semiclassical limit:

- (i) The domain $-\hbar\omega K_{\max} \leq E \leq \hbar\omega K_{\max}$, from which $g(E)$ is evaluated in the rates (3.31), decreases due to the factor $\hbar\omega$ in the semiclassical limit $h \rightarrow 0$. Here K_{\max} is the Fourier index that limits the Fourier expansion of x_{ij} to values $|K| \leq K_{\max}$, beyond which the

matrix elements $x_{ij}(K)$ are negligible. With the energy domain of $g(E)$ also its range of values decreases.

- (ii) Thus, when summing the Fourier contributions K , the values $\sum_K |x_{ij}(K)|^2 g(\varepsilon_{ji} - K\hbar\omega)$ in the rate R_{ij} and $\sum_K |x_{ij}(-K)|^2 g(\varepsilon_{ij} - K\hbar\omega)$ in the reverse rate R_{ji} approach each other.
- (iii) With $R_{ij}/R_{ji} \rightarrow 1$ for all i and j , the width σ_η of the distribution of η_{ij} goes to zero.

Finally, to come back to the starting point of our question, we relate the h -dependence of σ_η to the h -dependence of $\sigma_{\text{ch}}/\bar{p}_{\text{ch}}$: since the parameter σ_η decreases in the semiclassical limit, the solutions of the rate equations adopt this additional h -dependence on top of the trivial dependence on the dimension $N = 1/h$ of the rate equation system. The decrease of $\sigma_{\text{ch}}/\bar{p}_{\text{ch}} \sim h^b$ therefore scales with an exponent $b > 1/2$. In order to validate and to further elucidate these conclusions, a random-rate model is introduced in the following section.

4.4.2 A random-rate model for the chaotic occupations

The universal scaling behavior of $\sigma_{\text{ch}}/\bar{p}_{\text{ch}}$ suggests that it should be reproducible by a random-rate model. To verify this hypothesis, we replace the Floquet rates R_{ij} in Eq. (3.30) by independent random rates r_{ij} , which we assume to be exponentially distributed according to Eq. (4.52). As mentioned above, the parameter λ does not affect the solutions of Eq. (3.30) and can be chosen arbitrarily. The diagonal rates r_{ii} , which cancel in Eq. (3.30), can be set zero.

To improve the statistical quality of the statistical parameters we accumulate the solutions p_i from $10000/N_{\text{ch}}$ independent realizations of the random matrices of dimension N_{ch} . The dimension N_{ch} takes the role of the Hilbert dimension $N = N_{\text{ch}}$ of the modelled quantum dynamical system, provided that the latter has only chaotic states. It is thus implicitly related to the effective Planck constant $h = 1/N$ of the quantum system. It is the only parameter of the isolated quantum system that is introduced to the random-rate model.

To incorporate also thermal properties into the random-rate model, we impose statistical boundary conditions to the random rates r_{ij} on top of their exponential distribution. To this end, the rates r_{ij} have to be correlated with their reverse rates r_{ji} . This is done by either keeping r_{ij} unchanged and setting $r_{ji} = (1 + \eta_{ji}) \cdot r_{ij}$ or keeping r_{ji} unchanged and setting $r_{ij} = (1 + \eta_{ij}) \cdot r_{ji}$, where the decision between these two options is made randomly. The η_{ij} are independent random variables, which are uncorrelated to the original random rates, and which by the above transformation rule are consistent with Def. (4.53). After this transformation the rates are still found to be roughly exponentially distributed, though with a different variance, provided that the η_{ij} do not assume too high values $\eta_{ij} \gg 1$. As mentioned before, an altered variance $1/\lambda^2$ in Eq. (4.52) is irrelevant for the resulting occupations.

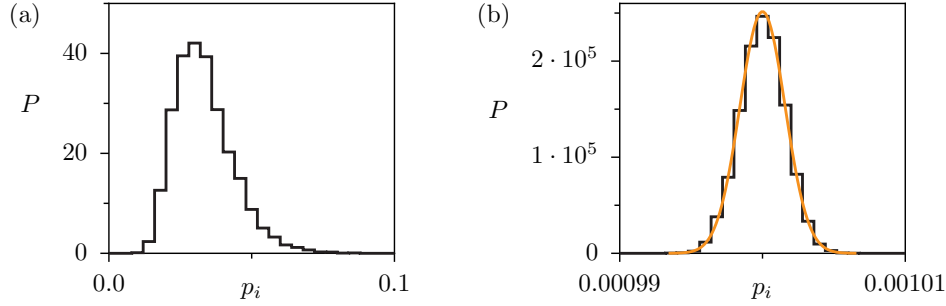


Figure 4.17: Random-rate model: Occupation distributions $P(p_i)$ based on exponentially distributed random rates r_{ij} simulating (a) $N_{\text{ch}} = 30$ and (b) $N_{\text{ch}} = 1000$ chaotic Floquet occupations. The second parameter of the model is $\sigma_\eta = 100/30^{1.2} \approx 1.7$ in (a) and $\sigma_\eta = 100/1000^{1.2} \approx 0.03$ in (b), respectively. In (b) the distribution is compared to a Gaussian fit (orange line).

Based on the observed behavior of η_{ij} for the kicked rotor, we determine the η_{ij} from the exponential distribution (4.54), whose standard deviation σ_η enters as a second parameter into the random-rate model. Moreover, again based on the corresponding observation of h -dependent scaling of σ_η in the true Floquet system (Fig. 4.16), we treat σ_η as N_{ch} -dependent with the scaling

$$\sigma_\eta(N_{\text{ch}}) \sim N_{\text{ch}}^{-\alpha} \quad (4.57)$$

and with $\alpha = 1.2$.

On the basis of the so constructed random rates r_{ij} , the solution vector p_i of the rate equations (3.30) assumes an equally random character. Starting from a uniform distribution in the interval $[0, 1]$ for $N_{\text{ch}} = 2$, the distribution $P(p_i)$ develops with increasing dimension N_{ch} a Gaussian shape with an ever smaller variance σ_{ch}^2 . Two examples for $P(p_i)$ are shown in Fig. 4.17 for the dimensions (a) $N_{\text{ch}} = 30$ and (b) $N_{\text{ch}} = 1000$. These figures correspond to the insets (a) and (b) of Fig. 4.14, based on the true Floquet rate matrix R_{ij} with the same Hilbert dimension $N = N_{\text{ch}}$. The distributions are quite similar, even though the prefactor 100 used in the presumed scaling (4.57) of σ_η only roughly equals the corresponding prefactor of the power-law fit (4.55) of σ_η .

Figure 4.18 shows the resulting N_{ch} -dependent scaling of the relative standard deviation $\sigma_{\text{ch}}/\bar{p}_{\text{ch}}$ for the described realization of the random-rate model (highlighted red dots). The N_{ch} -dependence of $\sigma_{\text{ch}}/\bar{p}_{\text{ch}}$ is best parametrized by the power law

$$\frac{\sigma_{\text{ch}}}{\bar{p}_{\text{ch}}} \sim N_{\text{ch}}^{-b} \quad (4.58)$$

(red line) and with the exponent $b = 1.6$ it accords with the observed power law (4.51) in the Floquet system. For comparison, we have added the $\sigma_{\text{ch}}/\bar{p}_{\text{ch}}$ -values from the random-rate model in Fig. 4.14 (red dashed line).

Figure 4.18 contains additional data, which serve to visualize the connection between

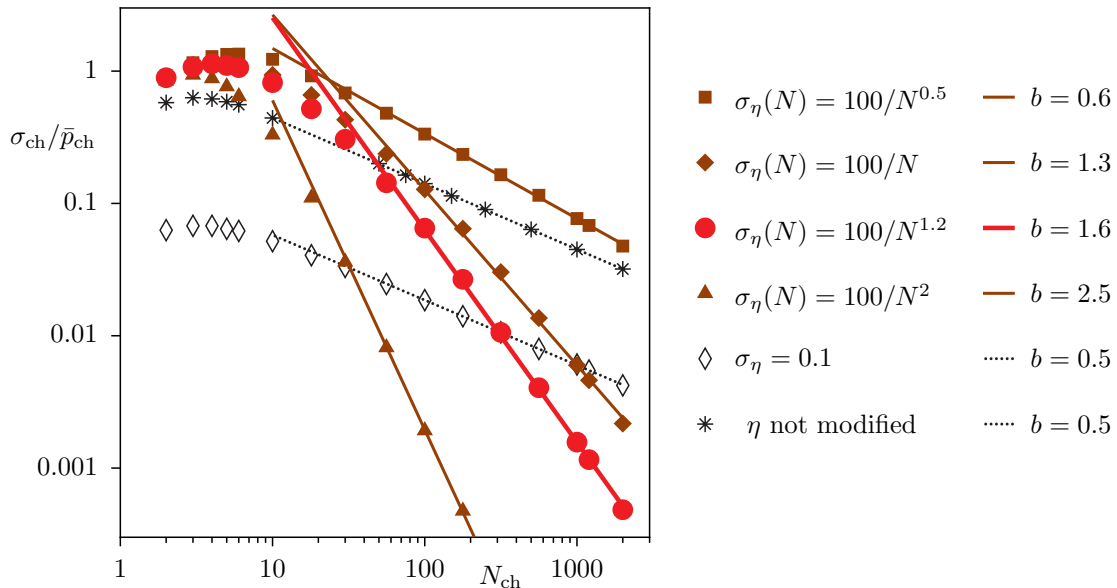


Figure 4.18: Random-rate model: N_{ch} -scaling behavior of $\sigma_{\text{ch}}/\bar{p}_{\text{ch}}$, based on exponentially distributed random rates r_{ij} for a system consisting of N_{ch} chaotic states. With one exception (black stars), the rates r_{ij} are additionally correlated, such that the η_{ij} of Def. (4.53) become exponentially distributed with the standard deviation σ_{η} . The latter is chosen according to the scaling (4.57) (solid symbols) with $\alpha = 0.5$ (brown squares), $\alpha = 1$ (brown diamonds), $\alpha = 1.2$ (highlighted red dots), and $\alpha = 2$ (brown triangles). A further realization (black diamonds) assumes fixed $\sigma_{\eta} = 0.01$. The lines represent algebraic fits (4.58) with exponents b listed on the right side.

the scaling behavior of σ_{η} and the exponent b in Eq. (4.58). The data marked by brown symbols refer to three further realizations of the scaling (4.57), but with different exponents $\alpha = 0.5, 1,$ and 2 , where the resulting power-law fits (brown lines) indicate a monotonous dependence of the exponents b on α . Note, that the exponent b appears to be insensitive to the use of other distributions for the random variables η_{ij} , which are not presented here. The only relevant dependence is established by α .

Secondly, if σ_{η} is treated as a fixed quantity, $\sigma_{\eta} = 0.1$ (black diamonds), instead of the scaling (4.57), the resulting exponent $b = 0.5$ merely originates from the increasing dimension N_{ch} , as has been pointed out in the previous section. The exponent $b = 0.5$ is even identically obtained, when no statistical boundary conditions at all are imposed on η_{ij} , i.e. for independent rates r_{ij} and r_{ji} (black stars). These last two realizations correspond to h -independent behavior of the rates in the Floquet system of the previous section and clearly confirm our hypothesis, that the h -dependent scaling of σ_{η} is responsible for the power-law scaling (4.51) with an exponent $b > 1/2$.

In conclusion, the random-rate model confirms the universality of the power-law behavior (4.51), as well as the arguments, used in the last section to explain the unexpected scaling exponent $b = 1.6 > 0.5$.

4.4.3 Influence of dynamical localization

Up to this point we have considered quantum kicked systems quantized on the two-torus \mathbb{T}^2 with the unit cell $[0, 1) \times [-1/2, 1/2)$. The Husimi representation shows almost all chaotic states as more or less uniformly spread over the chaotic phase-space domain. As discussed in Section 2.2, for a resonant value $h = 1/N$ of the effective Planck constant the quantum system automatically complies with the corresponding periodic boundary conditions in p -direction. If in contrast the periodic boundary conditions in p -direction are abandoned, such that the quantum dynamics takes place in the cylindrical phase space, the chaotic Floquet states are known to be exponentially localized [53, 87–90]. This property is paraphrased as *dynamical localization* in contrast to the Anderson localization observed for the eigenstates of a static random potential. As a consequence of the localization a quantum wave packet does not follow the diffusive growth of the kinetic energy $\langle p \rangle^2 \sim t$ of the classical system for arbitrarily long times. The reason is, that only those Floquet states can be excited during the evolution, that overlap with the finite momentum range of the initial wave packet.

The localized wave functions

$$|\psi_i(p)| \sim \exp\left(-\frac{|p - p^{(i)}|}{\xi}\right), \quad (4.59)$$

decay roughly exponentially with a characteristic localization length ξ around a state-dependent value $p^{(i)}$, see Fig. 4.19(a). For the kicked rotor, it has been shown that ξ is proportional to the classical diffusion constant D in phase space [87, 91], which itself is a function of the kick strength [44, 52, 53],

$$D := \lim_{t \rightarrow \infty} \frac{1}{t} \langle (p(t) - p(0))^2 \rangle = \frac{1}{2} \left(\frac{\kappa}{2\pi} \right)^2. \quad (4.60)$$

The increase of ξ with κ is qualitatively illustrated in Fig. 4.19(a) by typical eigenstates $|\psi(p)|$ for three different values of κ . In order to examine the influence of localization on the distribution of the chaotic occupations, we therefore vary the kick strength κ of the kicked rotor.

To observe localization at all, we have to generalize the periodic boundary conditions in p -direction to $p \rightarrow p + M_p$, and by that extend the unit cell to $[0, 1) \times [-M_p/2, M_p/2)$. If M_p is larger than the localization length ξ , this allows the wave functions to develop its localized form, similarly as if it were computed on the cylindrical phase space. The new periodic boundary conditions are compatible with the quantum system only for the adapted resonant values $h = M_p/N$ of the effective Planck constant, Eq. (2.52), with incommensurate values of M_p and N . These are chosen according to a rational approximate of the golden mean $\phi = (\sqrt{5} - 1)/2 \approx Q/P$, here in particular $M_p = P = 233$, $N = N_0 \cdot P + Q = N_0 \cdot 233 + 144$. The value of the effective Planck constant in the extended cell with $M_p = 233$ is then

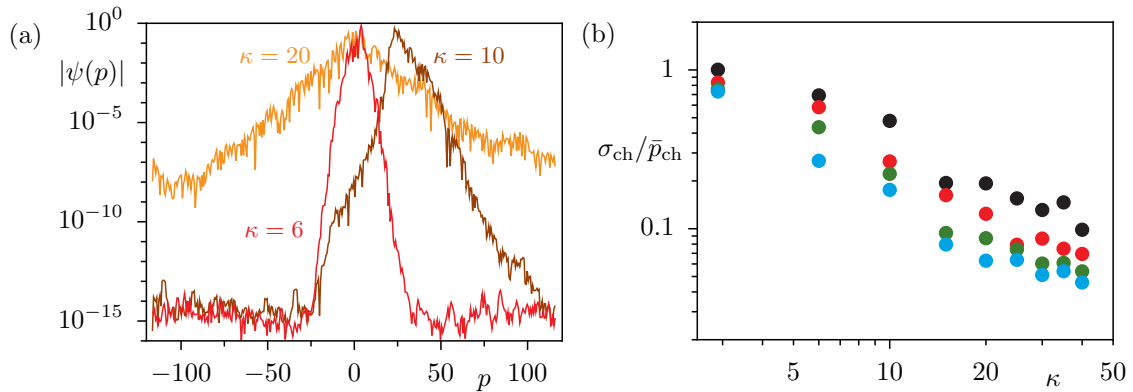


Figure 4.19: (a) Chaotic states in momentum representation $|\psi(p)|$ vs. p for $h = 233/377$ and three values of the kick strength $\kappa = 6, 10,$ and 20 of the kicked rotor. (b) Relative standard deviation $\sigma_{\text{ch}}/\bar{p}_{\text{ch}}$ of the chaotic occupations vs. κ for the kicked rotor with four different values of $h = M_p/N$: $h = 233/377 \approx 1$ (black), $233/610 \approx 1/2$ (red), $233/843 \approx 1/3$ (green), and $233/1076 \approx 1/4$ (blue).

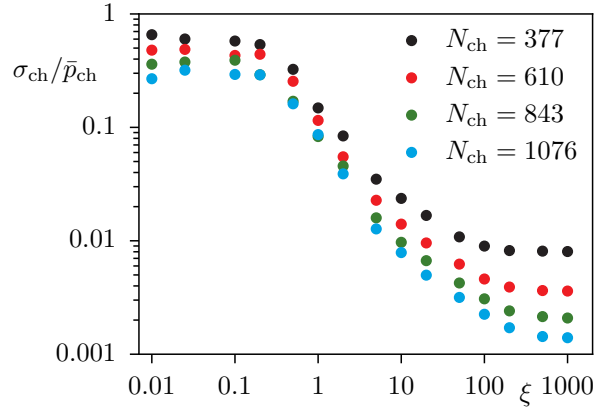
comparable to the value $1/N_0$ in the original cell with $M_p = 1$, i.e. $h = M_p/N \approx 1/N_0$. This specific choice of M_p and N is motivated by the requirement, to be far from a commensurable combination of M_p and N , where the quantum system would behave as if quantized on a two-torus with effectively smaller size of the unit cell.

Figure 4.19(b) demonstrates that the distribution of the chaotic occupations, in particular their relative standard deviation $\sigma_{\text{ch}}/\bar{p}_{\text{ch}}$, in the presence of localized chaotic states is not independent of κ . This is in contrast to the case $M_p = 1$ of Fig. 4.14 without localization. As the reason we identify the localization length ξ , which increases proportional to κ^2 . At small localization length ξ the values of $\sigma_{\text{ch}}/\bar{p}_{\text{ch}}$ are largest. We explain this by the different orders of magnitude of the involved rates R_{ik} : the largest rates are between those states that are closely localized in phase space and hence have a large overlap. States with small mutual overlap on the contrary have only tiny rates. This situation is qualitatively similar to the pronounced band structure of the rate matrix in the subspace of the regular states. In contrast to the regular states in a regular island, however, the localization centers $p^{(i)}$ of the localized chaotic wave functions $\psi_i(p)$ are irregularly spread over the entire momentum-axis. That is why the chaotic occupations still fluctuate irregularly around the mean value \bar{p}_{ch} , without monotonous branches as formed by the regular occupations. Note, that in the example of the kicked rotor localization occurs in momentum-space whereas the system-bath coupling operator is x .

For increasing κ the value of $\sigma_{\text{ch}}/\bar{p}_{\text{ch}}$ drops, because ξ grows and even separated states tend to have a larger overlap. Compared to the strongly localized states, the number of negligibly small rates shrinks. Finally, if ξ comes into the order of M_p , the size of the unit cell is insufficient to resolve the localization. The rates then have similar properties as for $M_p = 1$ and $\sigma_{\text{ch}}/\bar{p}_{\text{ch}}$ decreases no longer.

These conclusions are further supported by the random-rate model introduced in the

Figure 4.20: Random-rate model: Relative standard deviation $\sigma_{\text{ch}}/\bar{p}_{\text{ch}}$ vs. localization length ξ for exponentially distributed random rates r_{ij} for a system of dimension N_{ch} . The rates r_{ij} are correlated by the use of exponentially distributed quantities η_{ij} , Def. (4.53) becomes with a standard deviation $\sigma_{\eta} = 100/N_{\text{ch}}^{1.2}$. In accordance with Fig. 4.18 the saturation plateaus for $\xi \gg N_{\text{ch}}$ scale proportional to $N_{\text{ch}}^{-1.6}$.



previous section. It is here extended by the aspect of localization. The localization length is introduced by the exponential cut-off

$$r_{ij} \rightarrow r_{ij} e^{-|i-j|/\xi}, \quad (4.61)$$

superimposed on the distributions of the random rates r_{ij} and of the η_{ij} . By that, the indices i play the role of the quantization grid points in p -direction with the period N_{ch} instead of M_p . To ensure the periodic boundary conditions, i.e. the invariance of r_{ij} for the shifts $i \rightarrow i + N_{\text{ch}}$ and $j \rightarrow j + N_{\text{ch}}$, the spacings $|i - j|$ in Eq. (4.61) are replaced by $|i - j| \rightarrow |i - j + (N_{\text{ch}} - 1)/2| \bmod (N_{\text{ch}} - (N_{\text{ch}} - 1)/2)$.

Figure 4.20 shows the relative standard deviation $\sigma_{\text{ch}}/\bar{p}_{\text{ch}}$ of the resulting random occupations vs. the new model parameter ξ for several matrix dimensions N_{ch} , which are directly comparable to the Hilbert dimensions of Fig. 4.19. The ξ -dependence of $\sigma_{\text{ch}}/\bar{p}_{\text{ch}}$ discussed for Fig. 4.19 is clearly confirmed. The occupations are independent of ξ , as long as ξ is smaller than the fundamental scale that is resolved by the quantum system, $\xi \ll 1$. This limit is not observed in the true Floquet system of Fig. 4.19, as there the localization length is always larger than the fundamental quantized momentum scale M_p/N . For larger values of ξ the random-rate model qualitatively reproduces the decrease of $\sigma_{\text{ch}}/\bar{p}_{\text{ch}}$ and saturates when ξ exceeds the system size, $\xi \gg N$.

As a concluding remark we would like to relate these findings with the destruction of quantum localization reported in the literature. The authors of Ref. [92] study the time evolution of a wave packet in the damped quantum kicked rotor on the cylinder. Its mean squared displacement $\langle p^2 \rangle$ does not saturate any more for high values of the damping constant. Although we do not explicitly study time dependent phenomena here, we come to a similar conclusion: All chaotic Floquet states are asymptotically occupied with almost the same probability \bar{p}_{ch} , independent of their center of localization. An evolving wave packet must therefore explore the entire available phase space in the course of time and is hence not localized any more.

We conclude this section about the occupations of the chaotic states with a remark about Floquet systems with a purely chaotic spectrum. The truncation of the eigenbasis of a time-independent system is a familiar concept, which is indispensable in numerical implementations. It basically relies on the hierarchy of the statistical weights: only a finite number of states acquires sufficient probability to contribute appreciably to the dynamics of the system, whereas the other, high-energetic states can be neglected. As the findings of this section indicate, there is no such occupation hierarchy among the chaotic states. Thus, if there are only chaotic states in a Floquet system, no truncation of the Hilbert dimension seems possible. Reliable studies on the occupation statistics of a system with purely chaotic spectrum can thus only be made for systems with a finite Hilbert space, like the kicked rotor on the two-torus.

4.5 System-bath interaction and symmetry

The Floquet occupations studied so far are based on the linear coupling operator $A = x$ to the heat bath, as it is suggested by the Caldeira-Leggett model [71]. To a kicked system that is quantized on the two-torus \mathbb{T}^2 according to Section 2.2 it has to be applied with caution: the unbound linear coupling operator breaks the spatial periodicity of the quantum kicked system and is therefore not uniquely defined on \mathbb{T}^2 , while it is well-defined in the Hilbert space of square-integrable functions over \mathbb{R} , e.g. the eigenfunctions of a one-dimensional bound system. However, this seeming discrepancy is resolved once x is represented in the basis of the Floquet states of the quantum kicked system: they are spatially quasi-periodic and, by the quantization on \mathbb{T}^2 , they need to be evaluated only on a finite grid x_l in the unit interval $0 \leq x_l < 1$, see Eq. (2.47). The coupling matrix in the Floquet representation is hence also evaluated solely at these values x_l ,

$$x_{ij}(t) = \langle u_i(t) | x | u_j(t) \rangle = \sum_{l=0}^{N-1} \langle u_i(t) | x_l \rangle x_l \langle x_l | u_j(t) \rangle \quad (4.62)$$

with $x|x_l\rangle = x_l|x_l\rangle$. In this representation the matrix elements of x are indistinguishable from the matrix elements of its periodized counterpart $x' = (x \bmod 1)$. The linear coupling operator x of the Caldeira-Leggett model is thus adapted to the periodicity of the quantum kicked system.

However, the discontinuity of x' at the borders of the unit cell might cause unwanted artefacts. These can be only of marginal influence for the regular states of a regular island situated well inside the unit cell, because of the only exponentially small tunneling tails outside the island. Note, that the action of x' does not depend on the position x_c of the regular island. This can be seen from the fact, that a shifted coupling operator $\bar{x} = x - x_c$ merely introduces a diagonal term in the matrix elements, $\bar{x}_{ij}(t) = \langle u_i(t) | \bar{x} | u_j(t) \rangle = x_{ij}(t) - x_c \delta_{ij}$, which cancels in the systems of rate equations, Eqs. (3.26) and (3.30).

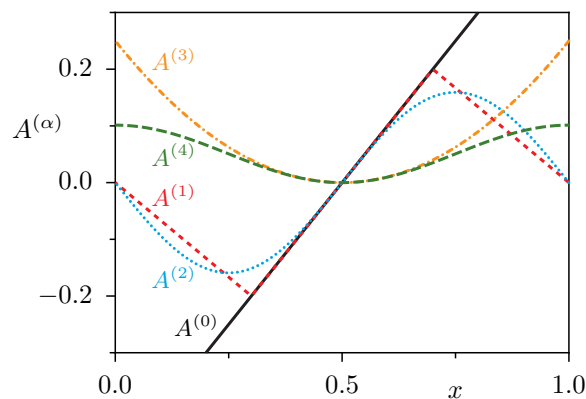


Figure 4.21: Coupling operators $A^{(\alpha)}$ vs. x for $\alpha = 0 - 4$ according to Defs. (4.63)-(4.66).

The chaotic states, which on the other hand typically have strong weights at the borders of the unit cell, directly map the discontinuity of $x' = (x \bmod 1)$ to the matrix elements. It can therefore be expected that the choice of a different, smoothly continued coupling operator would mainly affect the distribution of the chaotic states. To confirm this assumption we compare the action of $A^{(0)} = (x - 1/2)$ to the following four coupling operators, shown in Fig. 4.21:

$$A^{(1)}(x) := \begin{cases} -(2/3)x & x \leq 3/10 \\ (x - 1/2) & 3/10 < x < 7/10 \\ -(2/3)(x - 1) & 7/10 \leq x \end{cases} \quad (4.63)$$

$$A^{(2)}(x) := -\sin(2\pi x)/(2\pi) \quad (4.64)$$

$$A^{(3)}(x) := (x - 1/2)^2 \quad (4.65)$$

$$A^{(4)}(x) := (\cos(2\pi x) + 1)/(2\pi^2) . \quad (4.66)$$

These enter the definition (3.31) The original correlation function (3.9) in Def. (3.31) is kept, on the grounds of the assumption that the interaction operator $\gamma B = \sum_n c_n x_n$ of the heat bath remains unchanged in the interaction Hamiltonian $H_{sb} = \gamma A \otimes B$.

A comment on the coupling operators (4.63)-(4.66) seems necessary: we are aware that these coupling operators appear questionable from the point of view of the Caldeira-Leggett model, where the linearity of the coupling operator x accounts for the weakness of the interaction with the heat bath. Moreover, x is appropriate to generate a velocity-proportional damping force in the corresponding quantum Langevin equation, see Appendix A. The additionally introduced operators (4.63)-(4.66) would reproduce corresponding versions of the quantum Langevin equation with non-conventional functional dependences of the damping force.

The operators $A^{(1,2)}$ generalize $A^{(0)}$ in a natural way: they keep the local linearity of the Caldeira-Leggett model around $x_c = 1/2$, of course only approximately in case of $A^{(2)}$, and are at the same time continuous on \mathbb{T}^2 and thus adapt the periodicity of the quantum map. The two other coupling operators on the contrary are even functions with respect to the center $x_c = 1/2$ of the regular island.

The situation is in particular clear for the values $\theta_q = 0$ and $\theta_p = (n + 1)/2$ ($n \in \mathbb{Z}$) of the Bloch phases, where the Floquet states are eigenstates of a parity operator with either even or odd parity⁶. The regular states m are of alternating parity, giving rise to ‘selection rules’ for the matrix elements of the coupling operator: for the operators $A^{(0,1,2)}$, which are odd with respect to x_c , this implies $A_{m,m\pm 2\nu}^{(0,1,2)} = 0$ ($\nu \in \mathbb{N}$), as the involved Floquet states

⁶The kicked rotor possesses a parity symmetry with respect to the island center $x_c = 1/2$ due to its symmetric kick potential. However, a parity operator with respect to the values of the quantization grid (2.47) exists only, if the inversion point x_I is located at a grid point, $x_I = x_c - n/N$. This happens for the values $\theta_p = (n + 1)/2$ of the Bloch phase.

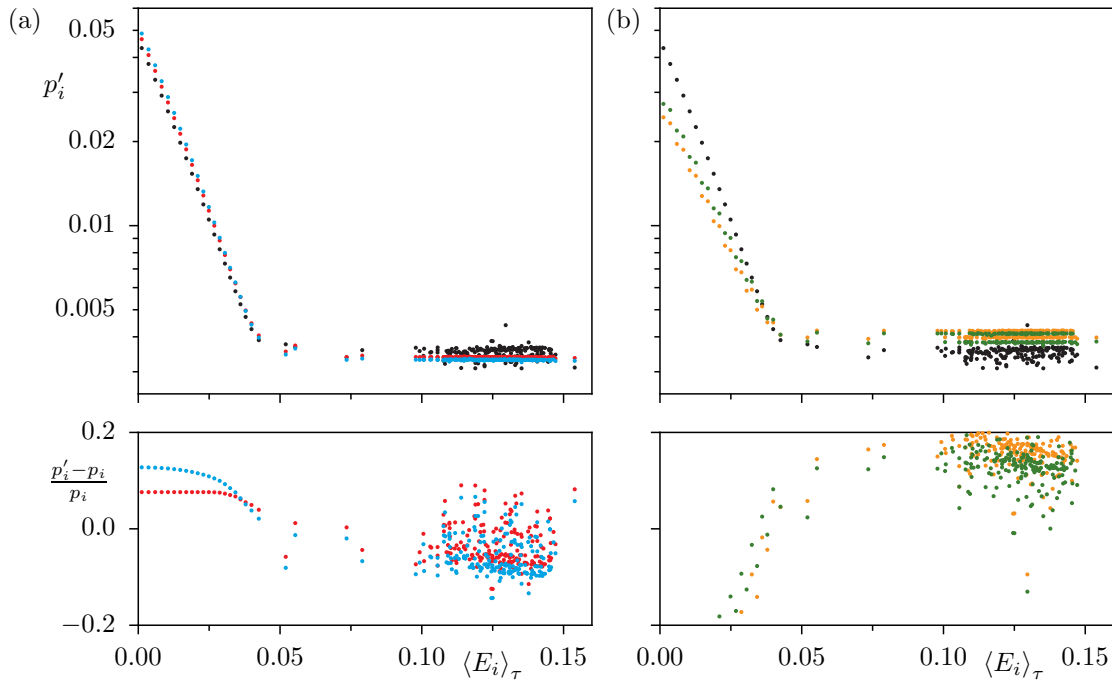


Figure 4.22: Floquet occupations p'_i vs. $\langle E_i \rangle_\tau$ based on (a) the odd system-bath coupling operators $A^{(1)}$ (red) and $A^{(2)}$ (blue) on the one hand, and on (b) the even coupling operators $A^{(3)}$ (orange) and $A^{(4)}$ (green) of Defs. (4.63)-(4.66). In both subfigures these are compared to the corresponding occupations p_i stemming from $A^{(0)} = (x-1/2)$ (black). Besides, the relative deviations $(p'_i - p_i)/p_i$ from the occupations p_i are shown in the lower subfigures. See Fig. 4.2 for parameters.

have equal parity. In this case also the corresponding rates are zero. As the matrix elements $A_{m,m\pm\nu}^{(0,1,2)}$ at the same time decrease with ν due to increasing spatial separation of the states, this realizes a distinctly dominant rate $R_{m,m\pm 1}$ between the neighboring regular states, as discussed in Section 4.2. Since identical selection rules apply to each of the operators $A^{(0,1,2)}$ and since $A^{(0)}$ is identical to $A^{(1)}$ within the island and is also a good approximation for $A^{(2)}$ there, the resulting occupations p_m of the regular states should be similar. This is confirmed in Fig. 4.22(a) showing the Floquet occupations p_i for the quantum kicked rotor at $\kappa = 2.9$, where the rates are based on $A^{(1)}$ (red) and $A^{(2)}$ (blue), in comparison to those based on $A^{(0)}$ (black). The latter are the same as in Fig. 4.2. The shift between the occupations of the inner regular states is a mere normalization effect. Besides, the similar occupations p_m for the discontinuous operator $A^{(0)}$ and the continuous operators $A^{(1,2)}$ confirm the anticipated insensitivity of the regular states on the behavior of the coupling operator at the borders of the unit cell. On the other hand, if the regular island would cross the unit cell border, the use of the coupling operator $A^{(0)}$ is certainly questionable.

In contrast, these operators make a difference for the chaotic occupations, with a considerably smaller variance σ_{ch}^2 of the occupation distribution for $A^{(1,2)}$ than for $A^{(0)}$. This indicates that the variance of the chaotic occupations, as observed in Section 4.4, is to some extent enhanced by the discontinuous jump of the coupling operator $A^{(0)}$.

Now we consider the coupling operators $A^{(3,4)}$, which are even with respect to x_c . For their matrix elements the alternating parity of the regular states implies $A_{m,m\pm(2\nu+1)}^{(3,4)} = 0$ and thus the rates between states of different parity vanish, irrespective of whether they are regular or chaotic. This results in a decoupling of the rate equations (3.30) into the two independent subsystems of even and odd states. In other words, the null space of the matrix $M_{ii;kk}$ in Eq. (3.30) is of dimension two, supporting two linearly independent solutions⁷. Hence, the states of different parity form independent occupation branches, which are separated by a small gap, as can be seen in Fig. 4.22(b) for the even operators $A^{(3)}$ (orange) and $A^{(4)}$ (green), again in comparison to $A^{(0)}$ (black). The occupations stemming from $A^{(3)}$ and $A^{(4)}$ are similar, as $A^{(3)}$ is the leading term in the expansion of $A^{(4)}$ around $x_c = 1/2$.

While the above stated is exactly true for the values $\theta_q = 0$ and $\theta_p = (n+1)/2$, the Floquet states are no longer exact eigenstates of the parity operator for all other phases $\theta_p \neq (n+1)/2$ and the matrix elements $A_{m,m\pm 2\nu}^{(0,1,2)}$ as well as $A_{m,m\pm(2\nu+1)}^{(3,4)}$ become finite. Nonetheless, at least the lowest regular states remain to be approximate eigenstates of a parity operator and the corresponding matrix elements are still found to be strongly suppressed.

In reference to Section 4.2.2 the observations of this section indicate that the prediction of exponentially distributed regular occupations, Eq. (4.38), which relies on a nearest-neighbor assumption for the rates between regular states, can be justifiable in an even broader context, e.g. for generalized models of the system-bath coupling.

To summarize, the present chapter has given diverse examples for the occupation distribution in the asymptotic state of time-periodic quantum systems coupled to a heat bath. Each of them fits in a quite general picture, by which the Floquet occupations are characterized from a semiclassical perspective. The different classes of Floquet states follow very different types of occupation distributions. The regular states have exponentially scaling occupations, which in the case of kicked systems can be quantified by weights $e^{\beta_{\text{eff}} E_m^{\text{reg}}}$ of the Boltzmann type, depending on their regular energy E_m^{reg} and the effective temperature β_{eff} . The same applies to the regular states of nonlinear resonances. The chaotic and hierarchical Floquet states on the contrary form a plateau of almost equal occupations with only small fluctuations, which are uncorrelated with the cycle-averaged energies $\langle E_i \rangle_\tau$.

⁷Since there exists only a single normalization condition for the entire set of occupations, the relative weight between the two independent solutions $p_i^{(\text{even})}$ and $p_i^{(\text{odd})}$ is then in principle arbitrary. However, since neither of the subsets is physically distinguished, both should be weighted equal, i.e. $p_i = p_i^{(\text{even})}/Z$ if $u_i(x)$ is even and $p_i = p_i^{(\text{odd})}/Z$ if $u_i(x)$ is odd, with $Z = \sum_i p_i^{(\text{even})} + \sum_i p_i^{(\text{odd})}$.

5 Occupations at avoided crossings and bath-induced switching

The spectrum of a Floquet system is bounded within a finite interval $0 \leq \varepsilon < \hbar\omega$ and typically features a multitude of avoided level crossings under variation of a parameter. These can give rise to complex behavior, when the dimension of the Hilbert space is successively increased. This issue is discussed in some more detail in the introduction of Section 3.2. In contrast to time-independent systems, where the energy provides a natural measure to truncate the basis of the (in general infinite) Hilbert space, *a priori* there does not exist any such means of truncation in time-periodic systems. However, if the system interacts with a thermal reservoir and certain Floquet states are singled out by their dominant occupation, a physically reasonable truncation criterion is then re-established by the Floquet occupations. It is especially instructive to ask, how the occupation hierarchy behaves at points of near degeneracy encountered at avoided crossings. As shown in Ref. [25], the asymptotic density ρ is not affected by a small avoided crossing, provided that it is smaller than a specific effective coupling strength. Thus, the complex behavior in a dense quasienergy spectrum arising from the avoided crossings is eventually resolved by the interaction with the heat bath.

In this section we study the implications of large avoided crossings on the Floquet occupations. A remarkable consequence appears to be the possibility of a novel bath-induced switching, i.e. a macroscopic change of the asymptotic state into an almost orthogonal state compared to the original equilibrium state [37]. One might relate this behavior to the class of *non-equilibrium steady states* [93, 94], which are enabled by the permanent pumping of energy into the system by the external field and the properly counterbalancing dissipation of energy into the thermal bath. In contrast to such situations, where the statistical physical parameters describing the system on macroscopic scales are constant in time, however, the asymptotic state of the switching which we will study still varies periodically in time.

In Ref. [37] the switching is demonstrated between the wells of a bistable potential, where a weak periodic driving switches the cycle-averaged asymptotic probability density from the ground state of the undriven system in the left well to the right well. The double well potential, the archetype of a switchable system, is experimentally realized in superconducting quantum interference devices (SQUIDs) [95], atom-optical potentials [40, 96], spin tunneling in condensed matter [97], or in the transfer of protons along chemical bonds [98]. In some cases the model can be restricted to a two-level system. Different approaches for switching by a population inversion in driven two-level systems have been proposed, e.g. induced by symmetry-breaking [99], structured environments [100], strong non-equilibrium noise [101], or strong driving [102]. However, the restriction to a two- or a three-level system limits the possible switching mechanisms and the existence of more than two states is even indispensable for the switching mechanism presented in the following section.

This Chapter is organized as follows: Firstly, in Section 5.1, the switching in the double-well potential is demonstrated and explained with the help of the effective rate equations of Section 3.2. In the same section also a displacement of the switching effect is introduced, where the avoided crossing significantly influences the asymptotic state far away from its actual position in parameter space. An explanation is given with the help of the *Lamb shifts* discussed in Section 3.3. Furthermore, the insight from the study of the driven double well facilitates the interpretation of certain phenomena in the occupation distribution, which clearly deviate from our observations in Chapter 4. Such phenomena are quite generally encountered in driven systems and are here again discussed for the kicked rotor (Section 5.2). These studies for the kicked rotor in turn help to put the switching mechanism in a broader context (Section 5.3). Finally, the chapter is closed by the introduction of a simplified, analytically solvable rate model, which can retrace the characteristic occupation phenomena caused by avoided crossings.

5.1 Switching in a double well potential

We study a particle in an asymmetric double well potential in the quantum regime, where the ground state is in the left well and the first excited state is in the right well, see Fig. 5.1(a). It is driven by an additive time-periodic force, leading to the system Hamiltonian

$$H(t) = \frac{p^2}{2} + x^4 - x^2 + x(\mu + A \cos \omega t) . \quad (5.1)$$

The two quantum wells of the potential render macroscopically distinguishable states that are probed via the spatial probability density $\rho(x, t)$. After a phase of relaxation this quantity adopts the system's time-periodicity in the long-time limit and the asymptotic spatial probability density averaged over one period of the driving

$$\rho(x) := \lim_{t \rightarrow \infty} \frac{1}{T} \int_t^{t+T} dt' \langle x | \rho(t') | x \rangle \quad (5.2)$$

$$= \sum_{i,j} \rho_{ij} \frac{1}{T} \int_0^T dt u_j^*(x, t) u_i(x, t) \quad (5.3)$$

is then of particular interest. In the second line this quantity is expressed in terms of the asymptotic Floquet density matrix ρ_{ij} .

Figure 5.1(b) shows that for the undriven double well, $A = 0$, at low temperatures almost all probability is concentrated in the left well. This reflects the dominant occupation of the ground state in thermodynamic equilibrium. In contrast, for a small driving amplitude, $A_0 \approx 0.008$, the probability density is almost completely transferred to the right well, as Fig. 5.1(c) demonstrates. Note, that the driving amplitude is much weaker than the asymmetry, $A_0 \ll \mu$, such that at all times the right well is energetically higher than the left well

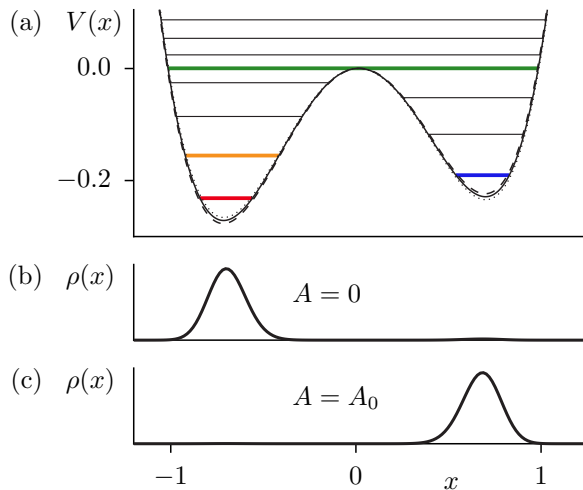


Figure 5.1: (a) Asymmetric double well potential and its eigenenergies without driving, $A = 0$ (solid line). The variations of the potential for a small driving amplitude $A_0 \approx 0.008$ (dashed and dotted line) are almost indistinguishable. (b) Asymptotic probability density $\rho(x)$ for $A = 0$ and a small temperature $1/\beta = 1/100$, with almost all probability in the left well. (c) Cycle-averaged asymptotic probability density $\rho(x)$ according to Eq. 5.3 for $A = A_0$, with more than 99 % of probability in the right well, demonstrating a switching to a macroscopically different state, that is induced by a weak driving. See Fig. 5.2 for parameters.

(Fig. 5.1(a)). The observed switching phenomenon is therefore unrelated to previous studies on hysteretic switching in a driven dissipative double well [103–105].

This example demonstrates that even a weak periodic driving not only alters the static Boltzmann occupation probabilities slightly [25, 74], but can switch to an almost orthogonal and macroscopically different asymptotic state of the system by only a small parameter variation. This is in sharp contrast to time-independent systems, where the asymptotic occupations are determined by Boltzmann weights and vary slowly with a parameter.

5.1.1 Inspection of the Floquet occupations

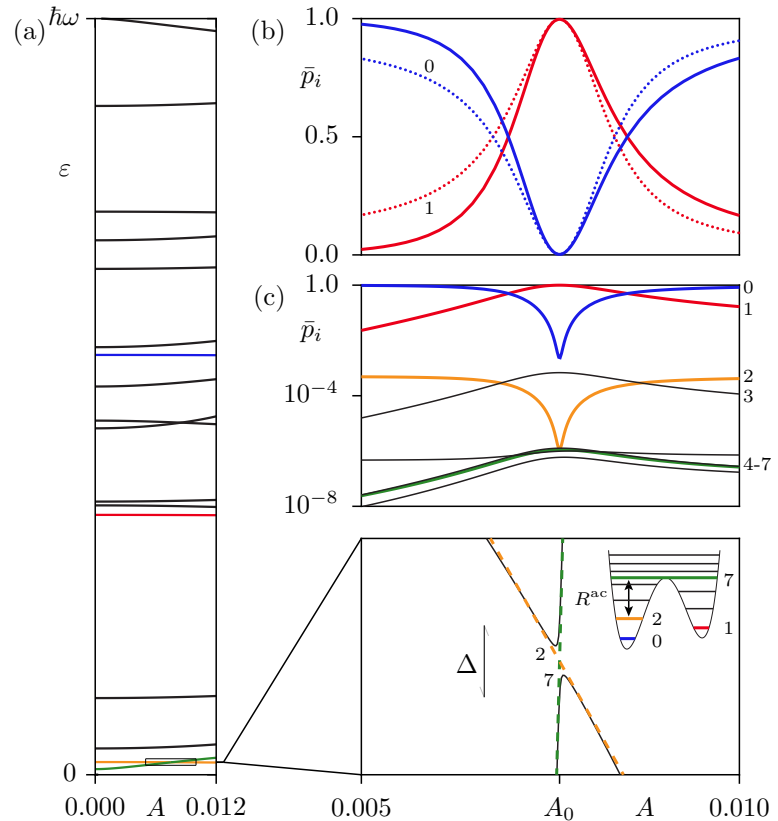
We get a first insight into this dramatic phenomenon from Fig. 5.2. In Fig. 5.2(a) one can see that under the variation of the driving amplitude A the quasienergy spectrum has an isolated avoided around $A = A_0$ ⁸. The involved states originate from the second and the 7th excited state of the undriven system. With an energy above the potential barrier the latter is not confined to one of the wells, while the second excited state is localized in the left well. We emphasize, that both the ground state, which is dominantly populated at $A = 0$, and the first excited state, which will turn out to be dominantly populated at $A = A_0$, are not involved in this avoided crossing.

An intuitive understanding of the switching from the rate equations (3.26) or (3.30) themselves seems impossible: tuning through the avoided crossing, the two involved Floquet states 2 and 7 hybridize and eventually exchange their character. This hybridization affects a large number of rates $R_{lj;ki}$ in Eq. (3.26), where one of the four indices is 2 or 7.

It is convenient to express $\rho(t)$ in a basis that does not significantly change in the neighborhood of the avoided crossing. Such a basis uses the diabatic states instead of the two adiabatic Floquet states themselves. The former are determined by the locally linear transformation (3.42). The diabatic states 2 and 7 do not hybridize and, like all the other states

⁸Note, that Δ , indicated by an arrow, is indeed the minimal spacing, albeit it might appear somewhat oversized due to the aspect ratio.

Figure 5.2: (a) Quasienergy spectrum for the 17 lowest Floquet states vs. driving amplitude A and magnification of the avoided crossing at $A = A_0$ (solid lines) with $\Delta = |\varepsilon_2(A_0) - \varepsilon_7(A_0)| \approx 1.82 \cdot 10^{-6}$, the quasienergies corresponding to diabatic states 2 and 7 (dashed lines), and eigenenergies of the undriven potential (inset). (b) Asymptotic occupations \bar{p}_i in the diabatic basis (solid lines) and their approximation based on the effective rate R^{ac} , Eqs.(3.43) and (3.45) (dotted lines). (c) same as (b) with logarithmic axis for \bar{p}_i . The parameters are $\mu = 0.03$, $\hbar = 0.04$, $1/\omega = 0.768$, $\beta = 100$, $\gamma = 10^{-3}$ and $\omega_c/\omega = 100$.



not involved in the avoided crossing, do not significantly change in the neighborhood of the avoided crossing. Changes of ρ along the parameter A can therefore be visualized without the trivial consequences of the hybridization and state exchange. Besides, the states in this basis are nearly identical to the eigenstates 2 and 7 of the undriven system (Fig. 5.2(a), inset), since the driving amplitude is indeed very weak, $A \ll \mu$. This allows to identify the Floquet indices, which in general are arbitrary, with the quantum numbers of eigenstates in the undriven system.

As a basis we have chosen the Floquet states arising from the 17 lowest eigenstates and computed the Floquet density matrix from Eq. (3.26). The diagonal densities $\bar{p}_i \equiv \bar{\rho}_{ii}$ are shown vs. A in Fig. 5.2(b) and, with a logarithmic scale, in (c). One observes that \bar{p}_0 , which corresponds to being in the ground state of the undriven system, drops from close to one to almost zero for $A = A_0$. In contrast, the probability \bar{p}_1 increases almost to one, which corresponds to the first excited state being dominantly populated. The tiny occupations \bar{p}_2 and \bar{p}_7 , i.e. the probabilities to be in one of the states of the avoided crossing, become equal. These observations for the \bar{p}_i are consistent with the spatial probability density observed in Fig. 5.1(c) and can indeed be exploited for a switching between the wells: tuning the driving amplitude from outside the avoided crossing into its center is accompanied by a probability transfer from the former ground state in the left well to the first excited state localized in the right well.

These observations demonstrate that in the presence of avoided crossings the occupations

not only of the two involved states are affected, but a whole set of states are repopulated. While the equality $\bar{p}_2 \simeq \bar{p}_7$ at the center of an avoided crossing of states 2 and 7 is quite plausible, the main question is still unanswered: how can states 0 and 1, which are not involved in the avoided crossing, interchange their probability?

5.1.2 Explanation based on the effective rate R^{ac}

We will answer the above question by using the effective approximate rate equations (3.45) of Section 3.2. Therein, the rates \bar{R}_{ik} are expressed in the diabatic basis and the direct rates \bar{R}_{27} , \bar{R}_{72} acting between the diabatic states 2 and 7 of the avoided crossing are replaced by the new rate of Def. (3.43)

$$R^{\text{ac}} = \frac{\Gamma}{(\hbar\Gamma/\Delta)^2 + 4d^2}, \quad (5.4)$$

see Fig. 5.3. The dimensionless distance d from the center A_0 is $d = (A - A_0) \cdot (\sigma_1 - \sigma_2)/\Delta$ with the characteristic quantities of the avoided crossing, $A_0 = 7.62 \cdot 10^{-3}$, $\Delta = 1.82 \cdot 10^{-6}$, $\sigma_2 = -3.41 \cdot 10^{-3}$, and $\sigma_7 = 7.48 \cdot 10^{-6}$. The composite rate $\Gamma = \sum_k (\bar{R}_{2k} + \bar{R}_{7k}) - 2\bar{R}_{22;77}$ is specific to the considered avoided crossing. The rate $\bar{R}_{22;77}$ is real-valued due to $H_s(-t) = H_s(t)$, as is shown in Appendix D.

As γ is chosen sufficiently small, the main assumption in the derivation of Eqs. (3.43) and (3.45) is fulfilled: the quasienergy spacings exceed the rates in Eq. (3.26), with the possible exception of $|\bar{\varepsilon}_7 - \bar{\varepsilon}_2|$ in the vicinity of the avoided crossing. Accordingly, the dotted lines in Fig. 5.2(b), which indicate the solutions of the approximate rate equations (3.45), reproduce the solutions of the full rate equations (3.26). The approximation is especially accurate near the center of the avoided crossing, since there the absolute dominance of R^{ac} compared to all other rates ensures that all in Eq. (3.45) neglected terms are indeed negligible.

The approximate rate equations (3.45) with R^{ac} facilitate the interpretation of the switching effect. Firstly, the observed equality of \bar{p}_2 and \bar{p}_7 at the center of the avoided crossing is in line with the arguments in Section 3.2: for the small value of γ the criterion $\hbar\Gamma \ll \Delta$ holds and the rate R^{ac} therefore exceeds Γ as well as the other rates at $A \approx A_0$. This enforces

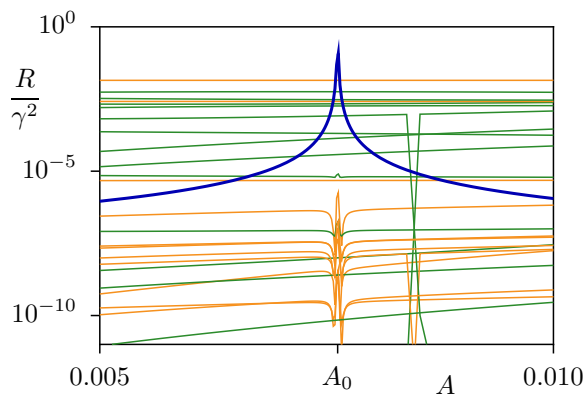


Figure 5.3: Effective rate $R = R^{\text{ac}}$ (blue) vs. driving amplitude A , as well as several rates appearing in Eq. (3.45), in particular $R = \bar{R}_{7k}$ (green) and $R = \bar{R}_{2k}$ (orange), which are constituents of Γ . Note, that there is an additional avoided crossing among two other unrelated states at $A > A_0$ in the presented range of A , which is the same as in Fig. 5.2. See Fig. 5.2 for parameters.

almost equal occupations $\bar{p}_2 \simeq \bar{p}_7$ in the solution of the rate equations (3.45). The dominant occupation of state 1 around A_0 has to be attributed to the combination of the following facts:

- (i) The overall probability flux between any two states is in general nonzero, even in the asymptotic state, as detailed balance is broken by the periodic driving.
- (ii) The rates between neighboring states localized in the same well are much larger than other intra-well rates as well as inter-well rates. The latter is due to the small spatial overlap between the states of different wells. Therefore, among the states confined to the same well, detailed balance approximately holds true, e.g. between state 0 and 2 or state 1 and 3.
- (iii) R^{ac} is the dominating rate around A_0 with the maximum value $R^{\text{ac}}(A_0) = \Delta^2 \hbar^{-2} \Gamma^{-1}$, see Fig. 5.3, and induces occupation equality of states 2 and 7. In Fig. 5.2(c) the resulting depopulation of state 2 towards state 7 can be observed.
- (iv) The relative occupation of state 0 and 2 remains constant due to the approximate detailed balance among the states in the left well. That is why \bar{p}_0 decreases together with \bar{p}_2 .
- (v) The states in the right well still equilibrate likewise as away from the avoided crossing, but with respectively increased weights due to probability conservation, see Fig. 5.2(c).

In conclusion, this reasoning explains the dominant occupation of state 1 around A_0 and hence the localization of $\rho(x)$ in the right potential well, observed in Fig. 5.1(c).

A minimal example, where one of the partners of the avoided crossing is the ground state 0 in the left well, is shown in Fig. 5.4. The hybridization partner, state 3, is again not confined in one of the wells. The above discussion simplifies, since step (iv) is eliminated and essentially just three states are involved. For this example the non-diagonal density element $\bar{\rho}_{03}$ is presented in Fig. 5.5. According to the presumptions of the approximate rate equations at the avoided crossing, this is given by $\bar{\rho}_{03} = (2d + i\hbar\Gamma/\Delta) (R^{\text{ac}}/\Gamma) \cdot (\bar{p}_0 - \bar{p}_3)$ (compare Eq. (3.47)). The real part $\text{Re}\bar{\rho}_{03}$ is always zero at $A = A_0$, whereas the imaginary part $\text{Im}\bar{\rho}_{03}$ is finite there and scales with $R^{\text{ac}}(A_0) \cdot (\bar{p}_0(A_0) - \bar{p}_3(A_0)) \sim \gamma^2$. Figure 5.5 demonstrates the excellent agreement between this approximation at the avoided crossing (dotted line) and the solutions of Eqs. (3.26) (solid line).

5.1.3 Switching efficiency and parameter study

What are the optimal parameters for this switching effect? To measure the switching efficiency we consider the probability in the right potential well

$$P_r(A) = \int_0^\infty dx \rho(x). \quad (5.5)$$

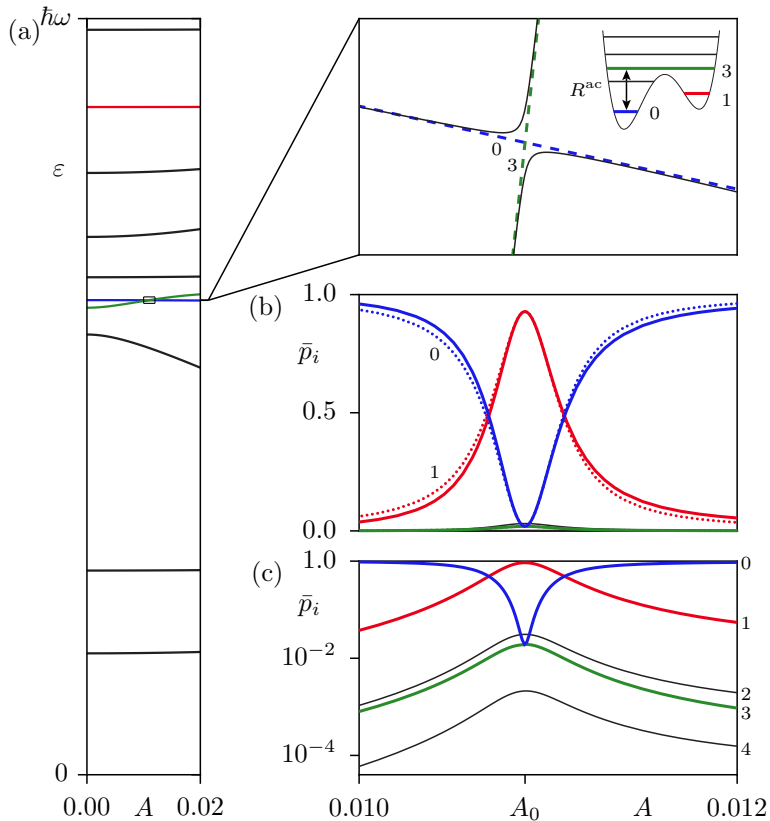


Figure 5.4: (a) Quasienergy spectrum for the ten lowest Floquet states vs. driving amplitude A and magnification of the avoided crossing at $A = A_0$ (solid lines) with $\Delta = |\varepsilon_0(A_0) - \varepsilon_3(A_0)| \approx 3.57 \cdot 10^{-6}$, the quasienergies corresponding to diabatic states 0 and 3 (dashed lines), and eigenenergies of the undriven potential (inset). (b) Asymptotic occupations \bar{p}_i in the diabatic basis (solid lines) and their approximation based on the effective rate R^{ac} , Eqs. (3.45) and (3.43) (dotted lines). (c) same as (b) with logarithmic axis for \bar{p}_i . The parameters are $\mu = 0.08$, $\hbar = 0.1$, $\omega = 0.8165$, $\beta = 60$, $\gamma = 10^{-4}$, and $\omega_c/\omega = 100$.

This quantity is shown in Fig. 5.6(a). Figures 5.6(b) and (c) illustrate the dependence on the parameters of the heat bath and the coupling for the individual occupations $\bar{p}_i(A_0)$ at $A = A_0$ and the resulting value of $P_r(A_0)$.

A. Coupling strength Γ

Firstly, Figs. 5.6(b1)-(b2) study the influence of the coupling strength Γ specific to the considered avoided crossing. This composite rate is like all other rates proportional to the damping constant γ^2 . If the coupling to the heat bath is larger than the minimal splitting of the avoided crossing, $\hbar\Gamma > 100\Delta$, almost no probability is switched to the right well. (Note, that even for the largest values of $\hbar\Gamma$ in Figs. 5.6(b1)-(b2) the assumption of weak coupling of the Floquet-Markov approach is still fulfilled.) This is due to the fact that in this limit R^{ac} becomes negligible compared to the other rates and thus the influence of the avoided crossing vanishes [25]. Qualitatively speaking, the avoided crossing is not resolved by the heat bath. Together with the smallness of the driving amplitude A this explains that the occupations $\bar{p}_i(A_0)$ are roughly comparable to the Boltzmann weights $e^{-\beta E_i}$, indicated at the right side of Fig. 5.6(b2).

In contrast, for small coupling $\hbar\Gamma < \Delta$ the increased influence of R^{ac} leads to a reduced occupation imbalance $\bar{p}_2 - \bar{p}_7$ of states 2 and 7 and eventually, by Arguments (iv)-(v), causes a high value of $P_r(A_0)$. In the limit $\hbar\Gamma/\Delta \rightarrow 0$ the effective rate diverges in the center of the avoided crossing, $R^{\text{ac}}(A_0) = \Delta^2 \hbar^{-2} \Gamma^{-1} \sim \gamma^{-2}$, whereas the other rates grow smaller and

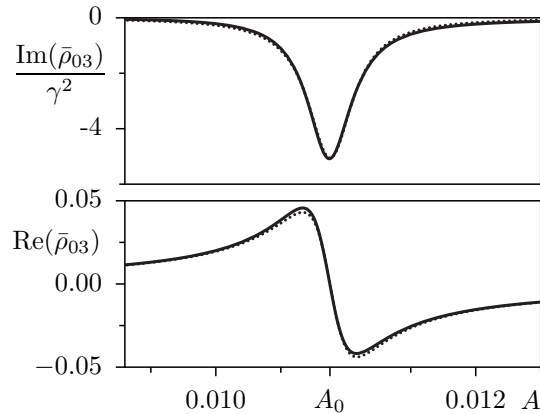


Figure 5.5: Real and imaginary part of the non-diagonal density matrix elements $\bar{\rho}_{03}$ vs. A . The solid line represents the corresponding part of the solution vector of Eq. (3.26), subsequently transformed to the diabatic basis via the transformation (3.42). The dotted line represents the approximation (3.47) based on the effective rate R^{ac} . See Fig. 5.4 for parameters.

smaller, $\bar{R}_{ik} \sim \gamma^2$. To fulfill the set of equations (3.45) for all values of γ , the occupation imbalance $\bar{p}_2 - \bar{p}_7$ has to approach zero in this limit, scaling proportional to γ^4 , as is seen e.g. from the equation for $i = 2$:

$$0 = (\bar{p}_2 - \bar{p}_7)R_0^{\text{ac}} + \bar{p}_2 \sum_{k \neq 7} \bar{R}_{2k} - \sum_{k \neq 7} \bar{p}_k \bar{R}_{k2}. \quad (5.6)$$

The occupations $\bar{p}_i(A_0)$ are then independent of $\hbar\Gamma/\Delta$ and consequently also $P_r(A_0)$. Note, that the γ -independent occupations are identical to the solutions of the reduced rate equations (3.30). The latter is applicable here, since the limit $\hbar\Gamma/\Delta \ll 1$ is achieved by assuming a small value of the coupling constant γ , whereas the spacing Δ is fixed for the chosen avoided crossing.

B. Temperature $1/\beta$

Figures 5.6(c1)-(c2) show the influence of the temperature $1/\beta$ on the $\bar{p}_i(A_0)$ and on $P_r(A_0)$. The values of β can be related to the level spacing $E_1 - E_0$ of the undriven system. At high temperatures, $1/\beta \gg E_1 - E_0$, the Floquet states are almost equally occupied, both away from the avoided crossing as well as at its center, resulting in $P_r(A_0) \approx 0.5$. For temperatures $1/\beta < E_1 - E_0$ the probability in the right well becomes dominant, while, of course, it vanishes in the undriven case $A = 0$. At these low temperatures, states 0 and 1 have a large occupation imbalance at $A \ll A_0$. Only thereby the avoided crossing can induce a macroscopically relevant change of occupations and thus entail a maximum value of $P_r(A_0)$. For even lower temperatures, however, $P_r(A_0)$ drops to zero. The occupation equality $\bar{p}_2 \simeq \bar{p}_7$ at $A = A_0$ originates here from an increase of \bar{p}_7 towards \bar{p}_2 , in contrast to the decrease of \bar{p}_2 towards \bar{p}_7 observed in Fig. 5.2(c2). By Argument (iv), also \bar{p}_0 remains

therefore constant together with \bar{p}_2 and switching does not take place. The origin of this low-temperature dependence lies in the normalization, which imposes an additional boundary condition. At very low temperatures a massive decline of \bar{p}_0 and \bar{p}_2 is no longer compensable by an increase of the tiny occupations of other states, if at the same time the relative occupations, determined by the temperature and the arguments (i)-(v), are to be satisfied. This dependence at very low temperatures is traceable with a simplified, analytically solvable rate model, which we introduce in Section 5.4.

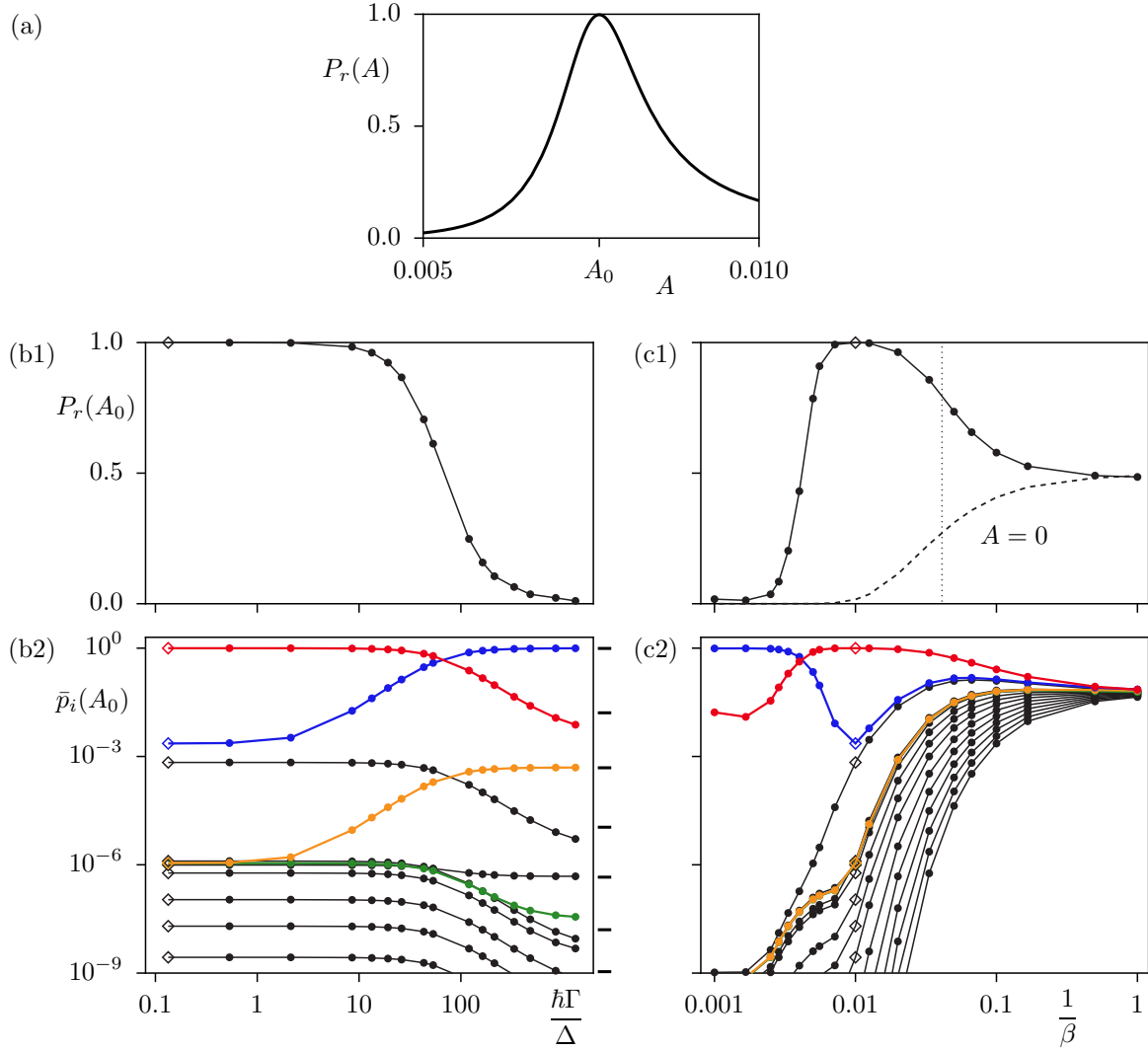


Figure 5.6: (a) Total probability in the right well P_r vs. driving amplitude A . (b1) Peak height $P_r(A_0)$ of total probability in the right well at $A = A_0$ vs. effective coupling strength $\hbar\Gamma/\Delta$ and (b2) corresponding occupations $\bar{p}_i(A_0)$ in the diabatic basis with highlighted values of $\bar{p}_0 = p_0$ (blue), $\bar{p}_1 = p_1$ (red), \bar{p}_2 (orange), and \bar{p}_7 (green). The same quantities are shown in (c1)-(c2) vs. the temperature $1/\beta$. Diamonds indicate the parameters of Fig. 5.2. The bars at the right side of (b2) indicate the Boltzmann weights $e^{-\beta E_i}$ of the seven lowest eigenstates in the undriven system. The dashed line in (c1) represents $P_r(A = 0)$, the probability in the right well without driving. The dotted line at $1/\beta = E_1 - E_0$ indicates the transition between the high and the low-temperature regimes.

C. Correlation time $1/\omega_c$

For the parameters of Fig. 5.4 the dependence on the coupling strength Γ and on the temperature $1/\beta$ is presented in Figs. 5.7(a) and (b). The characteristics are widely similar, but $P_r(A_0)$ does not drop to zero for $1/\beta \rightarrow 0$, i.e. the switching is maintained even for low temperatures. In addition, we allow for a variation of the spectral cut-off parameter ω_c of the heat bath, which is considered in column (c). The behavior of $P_r(A_0)$ on a varying cor-

relation time τ_c , which we approximate as $1/\omega_c$, is similar to that for varying temperature. A strong influence of ω_c is detected only for $\tau_c \gtrsim 1/\omega$. Such high values of τ_c , being of the order of the driving period $2\pi/\omega$, may not necessarily be compatible with the assumptions underlying the Floquet-Markov master equation. In the present case, we have checked that the Born-Markov criterion of Eq. (3.10) is still fulfilled, as well as the alternative condition of Eq. (B.51). Notwithstanding the questionableness of the small ω_c -values in Figs. 5.7(c1)-(c3), these shed some light on the sensitivity to the structure of the heat bath: although the rate equations assume a huge heat bath with a quasi-continuous spectral density, the crude limitation of spectral modes to values smaller than ω_c mimics a finite heat bath, or even a structured heat bath with only few bath modes. As Fig. 5.7(c3) indicates, all Floquet states tend to have similar occupations in the limit $\omega_c \ll \omega$.

An additional surprising phenomenon is observed in Figs. 5.2(b)-(c) and in Figs. 5.4(b)-(c): the influence of the avoided crossing on the occupations occurs within a significantly broader range of the driving amplitude A compared to the width of the avoided crossing. For example, with the parameters of Fig. 5.4 the full width at half maximum $\text{fwhm}(P_r)$ of $P_r(A)$ is a factor of 5 larger than the width of the avoided crossing $\Delta_{ac} = 2\Delta/(\sigma_3 - \sigma_0)$, and for the parameters of Fig. 5.2 even a factor of 30 larger. The occupations are sensitive to the rate R^{ac} , if its magnitude is larger than or comparable to other significant rates \bar{R}_{ik} in Eq. (3.45). Since these rates vary over many orders of magnitude, see Fig. 5.3, this criterion may be fulfilled even beyond the avoided crossing, $|A - A_0| > \Delta_{ac}/2$. This gives qualitative insight into the enlarged parameter range of influence of the avoided crossing as observed in $\text{fwhm}(P_r)$. For an implementation of the switching mechanism this feature is desirable, as it reduces the necessary parameter resolution. The second row of Fig. 5.7 shows the dependence of the width of $\text{fwhm}(P_r)$ on the parameters. The increase of $\text{fwhm}(P_r)$ at enhanced correlation time $1/\omega_c$ is particularly large, but is accompanied by a decrease of the switching efficiency $P_r(A_0)$.

For a clear presentation we have chosen examples in the limit of a small driving amplitude A , where the Floquet states are not very different from the eigenstates of the undriven system. In this case an avoided crossing requires near-resonant driving, $E_7 - E_2 \approx 3\hbar\omega$ in Fig. 5.2 and $E_3 - E_0 \approx 3\hbar\omega$ in Fig. 5.4. This is not an exclusion criterion: we have observed switching also in the case of strong driving, supporting the generality of the proposed switching mechanism. However, at strong driving $A \geq \mu$ the regular islands, which originate from the presence of the potential wells, are dissolved and their regular states do not exist any more. As the chaotic states tend to carry occupations of similar size, any change of occupations between them will be hardly detectable. Besides, the chaotic states are macroscopically not distinguishable. In that sense, only the switching between the regular states of different regular islands is desirable.

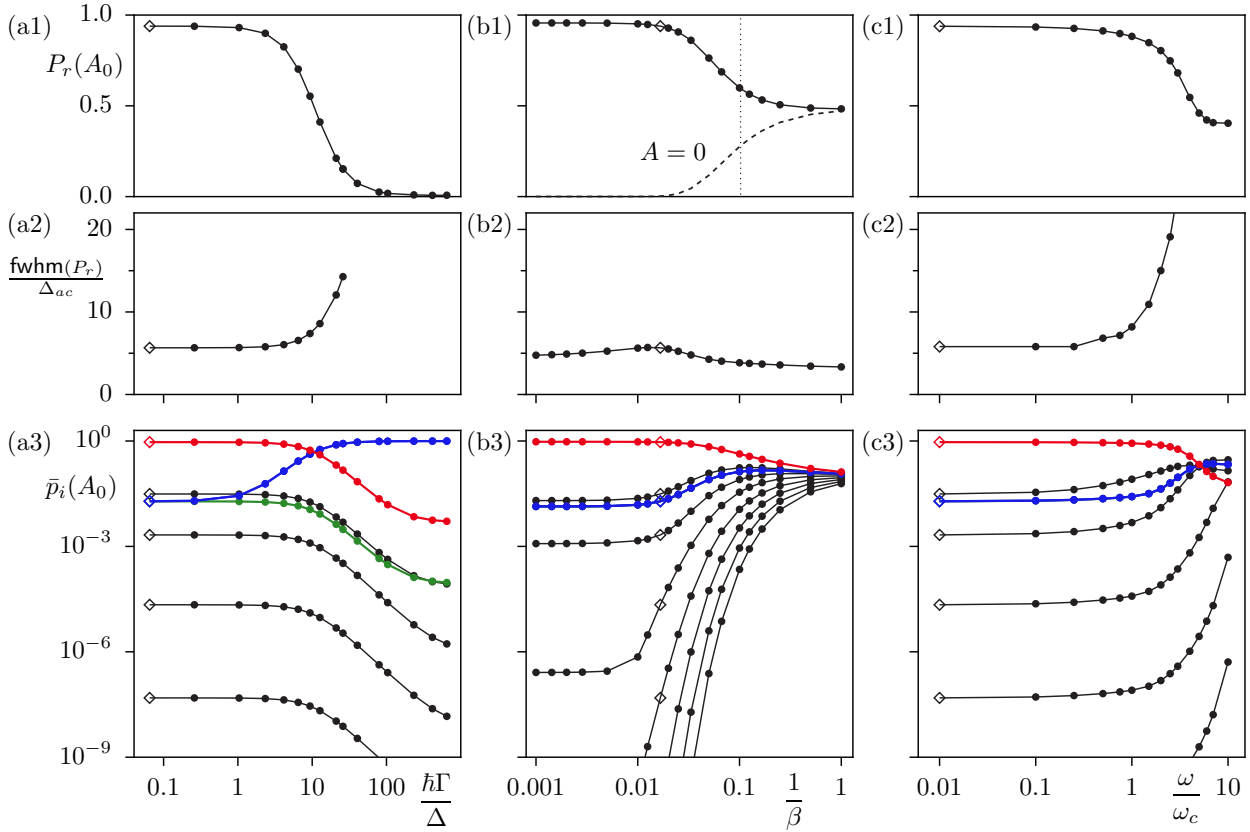


Figure 5.7: (a1) Peak height $P_r(A_0)$ of total probability in the right well at $A = A_0$ and (a2) full width at half maximum $\text{fwhm}(P_r)$ of $P_r(A)$ vs. effective coupling strength $\hbar\Gamma/\Delta$. (a3) Occupations $\bar{p}_i(A_0)$ in the diabatic basis with highlighted values of $\bar{p}_0 = p_0$ (blue), $\bar{p}_1 = p_1$ (red), and \bar{p}_3 (green). The same quantities are shown in (b1)-(b3) vs. the temperature $1/\beta$ and in (c1)-(c3) vs. the spectral cut-off parameter ω/ω_c . Diamonds indicate the parameters of Fig. 5.4. The dashed line in (b1) represents the probability in the right well without driving, $P_r(A = 0)$. The dotted line at $1/\beta = E_1 - E_0$ indicates the transition between the high and the low-temperature regimes.

We now briefly discuss possible advantages of the switching mechanism in applications: (i) If one uses a laser for the periodic driving, the amplitude dependence of the switching mechanism and the beam profile allow switching at a 3D spatially localized position with a resolution smaller than the focus width. (ii) In situations where a theoretical modeling of the system, e.g. a complex molecule, is not achievable and no other switching mechanism is known, the generic appearance of avoided crossings in periodically driven systems suggests the existence of driving parameters for the desired switching.

5.1.4 Displaced signatures of avoided crossings

As the studies of the previous sections demonstrate, the Floquet occupations p_i in the vicinity of an avoided crossing are very sensitive to the values of the involved quasienergies $\varepsilon_{a,b}$, especially the minimal spacing Δ and the asymptotic slopes $\sigma_{1,2}$ of the quasienergies. That is why any modifications of the spectrum may lead to severe changes of the p_i . A candidate

for such spectral modifications would be e.g. a disturbed time-periodicity, as resulting from the finite duration of the driving or from a pulse-shaped driving. A different, inevitable cause of spectral renormalizations are the Lamb shifts, that arise from the back action of the bath on the system energies, see Section 3.3.

We have modified the Floquet-Markov master equation to a form that includes the Lamb shift contributions. The rate equation (3.49) for its asymptotic solutions p_i^{LS} is formally identical to the original rate equation (3.26) neglecting the Lamb shifts. In contrast, however, the rates $R_{lj;ki}$ have to be replaced by the modified rates $\hat{R}_{lj;ki}$, which we introduce in Appendix C.

In Fig. 5.8 we study the influence of the Lamb shifts on the density matrix in the double well with an avoided crossing between states 0 and 2, similar to the minimal example of Fig. 5.4. Firstly, the first row shows the diabatic occupations. The solid lines represent the solutions \bar{p}_i^{LS} of the modified rate equations (3.49), properly transformed into the diabatic representation of states 0 and 2. The three subfigures compare the \bar{p}_i^{LS} for three different values of the coupling strength γ . Each of them is sufficiently small to guarantee $\hbar\Gamma/\Delta < 1$, such that the occupation transfer at the avoided crossing takes place at all. Besides, each of the subfigures compares with the original occupations \bar{p}_i (dash-dotted lines), which are based on the solution of Eq. (3.26), where no Lamb shifts are taken into account.

As a most remarkable result we observe that the Lamb shifts displace the influence range of the avoided crossing in parameter space away from its actual position A_0 . In particular, the value of A , where the occupation imbalance $|\bar{p}_0 - \bar{p}_2|$ is minimal as a signature of the maximum change of occupations, differs strongly from A_0 in Figs. 5.4(b) and (c). The distance to A_0 increases proportional to γ^2 .

How can an avoided crossing influence the Floquet occupations at a parameter value far away from its actual position? The answer is yet again given by the system of effective rate equations at the avoided crossing, with the additional rate R^{ac} . In contrast to the approach of Section 3.2 leading to the definition (3.43) of R^{ac} , we have to take into account the Lamb shifts in the derivation of R^{ac} . This is done in Appendix E and leads to the modified definition (3.53) of R^{ac} ,

$$R^{ac} = \frac{\Gamma}{(\hbar\Gamma/\Delta)^2 + (2d - \hbar\Sigma/\Delta)^2}. \quad (5.7)$$

It differs from Def. (3.43) by the contribution of Σ , an effective rate, which is defined similarly to Γ , see Eq. (E.7). This quantity shifts the maximum value of R^{ac} away from $A = A_0$ to the remote value

$$A_0^* = A_0 + \frac{d^*\Delta}{\sigma_1 - \sigma_2} = A_0 + \frac{\hbar\Sigma}{2(\sigma_1 - \sigma_2)}. \quad (5.8)$$

We have recorded this parameter value in Figs. 5.8(b) and (c), where it is in excellent agreement with the position of minimal occupation imbalance $\bar{p}_0 - \bar{p}_2$.

Apart from the modified definition of R^{ac} , the form (3.45) of the approximate rate equations is unchanged, compare Eq. (3.52). The dotted lines in Fig. 5.4 represent its solutions and are in good agreement with the \bar{p}_i^{LS} . Note, that the small bumps observed at A_0 in Figs. 5.8(b) and (c) occur due to the transformation from the adiabatic to the diabatic basis, which is determined by the locally linear model (3.33) of Section 3.2. Since Eq. (3.52) is already represented in the diabatic basis, these deviations are seen in its entire solution vector (dotted lines), whereas in the solutions of Eq. (3.49) they are only present in the two occupations \bar{p}_0^{LS} (blue) and \bar{p}_2^{LS} (green), which are transformed from the adiabatic occupations at the avoided crossing.

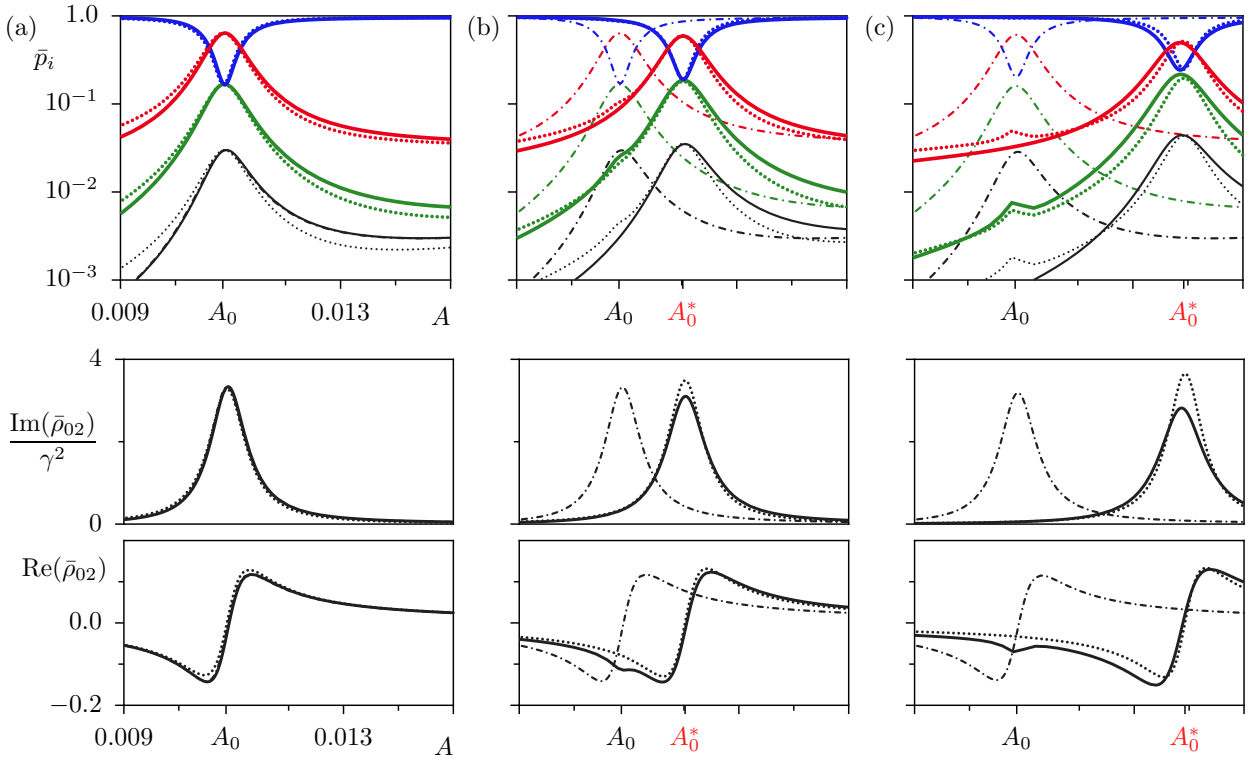


Figure 5.8: Asymptotic occupations \bar{p}_i^{LS} (solid lines) vs. A under the influence of an increasing effective coupling strength $\hbar\Gamma/\Delta = 4.72 \cdot 10^{-3}$ (a), $3.02 \cdot 10^{-1}$ (b), and $7.98 \cdot 10^{-1}$ (c). The \bar{p}_i^{LS} are compared to the occupations \bar{p}_i (dash-dotted lines) neglecting the Lamb shift. Besides, the dotted lines indicate the approximation based on the effective rate R^{ac} , Eq. (5.7). All occupations are represented in the diabatic basis. The second and third row show the real and imaginary part of the non-diagonal density matrix elements $\bar{\rho}_{02}^{LS}$ (solid lines) and $\bar{\rho}_{02}$ (dash-dotted lines) in the diabatic basis, as well as their respective approximations based on the effective rate R^{ac} (dotted lines). The other parameters are $\mu = 0.09$, $\hbar = 0.13$, $\omega = 10.16/13$, $\beta = 70$, and $\omega_c/\omega = 100$.

5.2 General occupation characteristics at avoided crossings

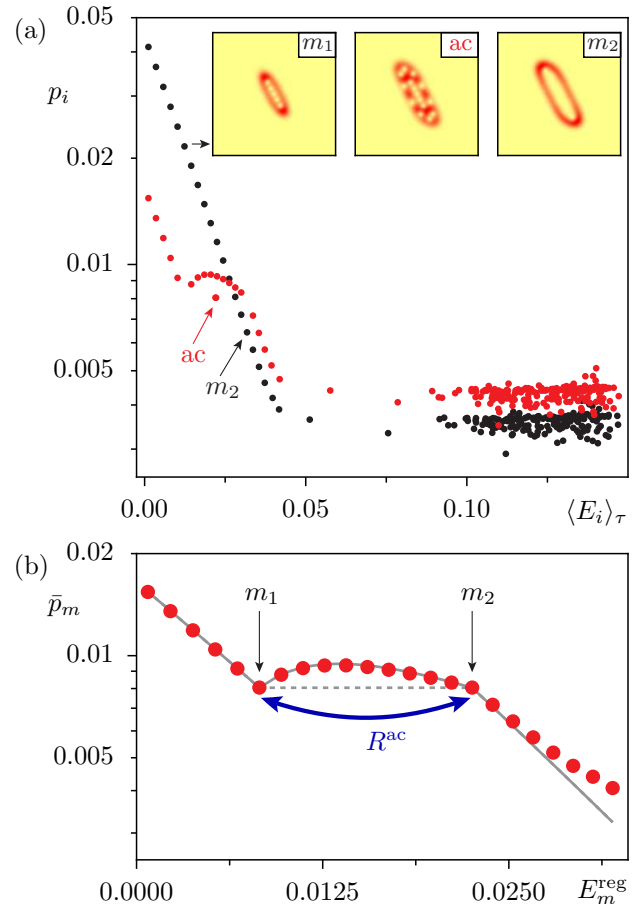
This section continues the study of Floquet occupations under the influence of avoided crossings. In contrast to the previous section, it focusses on the semiclassical regime that has been under consideration in Chapter 4. We consider the quantum kicked rotor with a kick strength $\kappa \approx 2.9$, very close to the parameter realization in Fig. 4.2. Figure 5.9(a) shows the Floquet occupations p_i vs. the mean energies $\langle E_i \rangle_\tau$ for two different values of the kick strength κ . The difference of these κ -values is sufficiently small, such that the classical phase space and almost all regular states vary only marginally. For two of the regular Floquet states, which we denote a and b , this is however not the case, as they undergo under variation of κ an avoided crossing centered at $\kappa_0 \approx 2.857$. The avoided crossing is shown in the magnification of the Floquet spectrum in Fig. 5.10(a). In contrast to the hybridizing states a and b , the corresponding diabatic states change only slightly throughout the avoided crossing and are identical to the semiclassical modes with the quantum numbers $m_1 = 5$ and $m_2 = 15$.

The avoided crossing strongly influences the Floquet occupations, and most prominently the regular occupations: firstly, away from the avoided crossing at $\kappa_1 \ll \kappa_0$ (black dots in Fig. 5.9(a)), the regular occupations monotonously decrease with $\langle E_i \rangle_\tau$, similar as in Fig. 4.2. When approaching the center of the avoided crossing, $\kappa_3 \approx \kappa_0$ (red dots), the occupations p_i are locally disturbed. The gradual transition of the occupation characteristics from $\kappa_1 \ll \kappa_0$ to $\kappa_3 \approx \kappa_0$ is illustrated in further detail in the sequence of subfigures of Fig. 5.10(c), showing p_i vs. $\langle E_i \rangle_\tau$ for κ_1 , κ_3 , and three further values of κ in the vicinity of the avoided crossing. For a better comparison, the data points from the first subfigure referring to κ_1 are repeated in each of the subsequent figures (gray points).

The hybridization of the states a and b near κ_3 results in an adjustment of their mean energies $\langle E_a \rangle_\tau$ and $\langle E_b \rangle_\tau$, illustrated in Fig. 5.10(b), as well as of their occupations p_a and p_b . In Fig. 5.9(a) the data points of the states a and b at κ_3 (marked as ‘ac’) are therefore found indistinguishable on top of each other. Beyond that, also the occupations p_m of all regular states with quantum numbers m from the interval $[m_1, m_2]$ change severely. More specifically, they tend to the value of occupation $p_a \approx p_b$ of the hybridized states. In contrast, their mean energies $\langle E_m \rangle_\tau$ do not change notably under the tiny κ -variation, like those of the diabatic states m_1 and m_2 . The relative occupations p_m/p_n among the regular states with quantum numbers outside the range $[m_1, m_2]$ are also not affected. Only the absolute values of their occupations p_m are shifted as a compelling consequence of the normalization $\sum_i p_i = 1$. The latter is also the origin of a shift of the chaotic occupation plateau.

These observations are in line with the massive influence of an avoided crossing observed in the previous section for a driven bistable potential. In the present example, however, \hbar is far smaller than in the examples of Section 5.1 and in particular supports more regular states. Thereby it is clearer to see, how the character of the set of Floquet occupations changes as a

Figure 5.9: (a) Floquet occupations p_i vs. mean energies $\langle E_i \rangle_\tau$ for two different values of κ , namely $\kappa_1 = 2.856350$ (black) and $\kappa_3 = 2.857175$ (red) close to the center of the avoided crossing between the states $m_1 = 5$ and $m_2 = 15$. The insets show Husimi representations of the states m_1 and m_2 at κ_1 and of a corresponding hybridized state at κ_3 . (b) Occupations \bar{p}_m of the regular states vs. regular energies E_m^{reg} at κ_3 and comparison to the analytical solution (5.13) of the rate model with $R_{m,m+1}/R_{0,1} = (m+1)$ (solid gray line) and with $R_{m,m+1}/R_{0,1} \equiv 1$ (dashed gray line), respectively. The effective rate R^{ac} between the states m_1 and m_2 is indicated. Note, that \bar{p}_{m_1} and \bar{p}_{m_2} are represented in the diabatic basis by means of the transformation (3.42), in contrast to the Floquet occupations p_i in (a). The parameters are $h = 1/210$, $\beta = 100$, and $\omega_c/\omega = 100$.



whole in the presence of the avoided crossing. The interpretation of the observed phenomenon is very similar in both cases and is again made intuitive by the use of the approximate rate equations (3.45). In the examples of Figs. 5.9 and 5.10 the occupations p_i are the solutions of the reduced rate equations (3.30), where the non-diagonal elements ρ_{ij} are neglected. For this to hold, all rates are required to be small compared to all quasienergy spacings, and in particular $\hbar\Gamma < \Delta$ is assumed. That is why, according to the discussion in Section 3.2, the additional rate R^{ac} exceeds all the other rates at κ_0 and so generates the balanced population between the diabatic states, $\bar{p}_{m_1} \simeq \bar{p}_{m_2}$. Likewise, the non-monotonous behavior of the occupations of regular states from the interval $[m_1, m_2]$, as well as the unchanged relative occupations outside of this interval, can be qualitatively explained by similar arguments as those in Section 5.1.2. A quantitative account is however intricate, but it is possible to model the observed behavior by a simplified and analytically solvable rate model. This is done in Section 5.4.

Apart from avoided crossings between two regular states m_1 and m_2 , avoided crossings between a regular state m_1 on the one hand and a chaotic state on the other hand are found in the Floquet spectrum. An example for the resulting Floquet occupations is shown in Fig. 5.11(a), again for $\kappa \approx 2.857$ and with $m_1 = 10$. Again, the occupations far away from the avoided crossing (black dots) are compared to those close to its center (red dots).

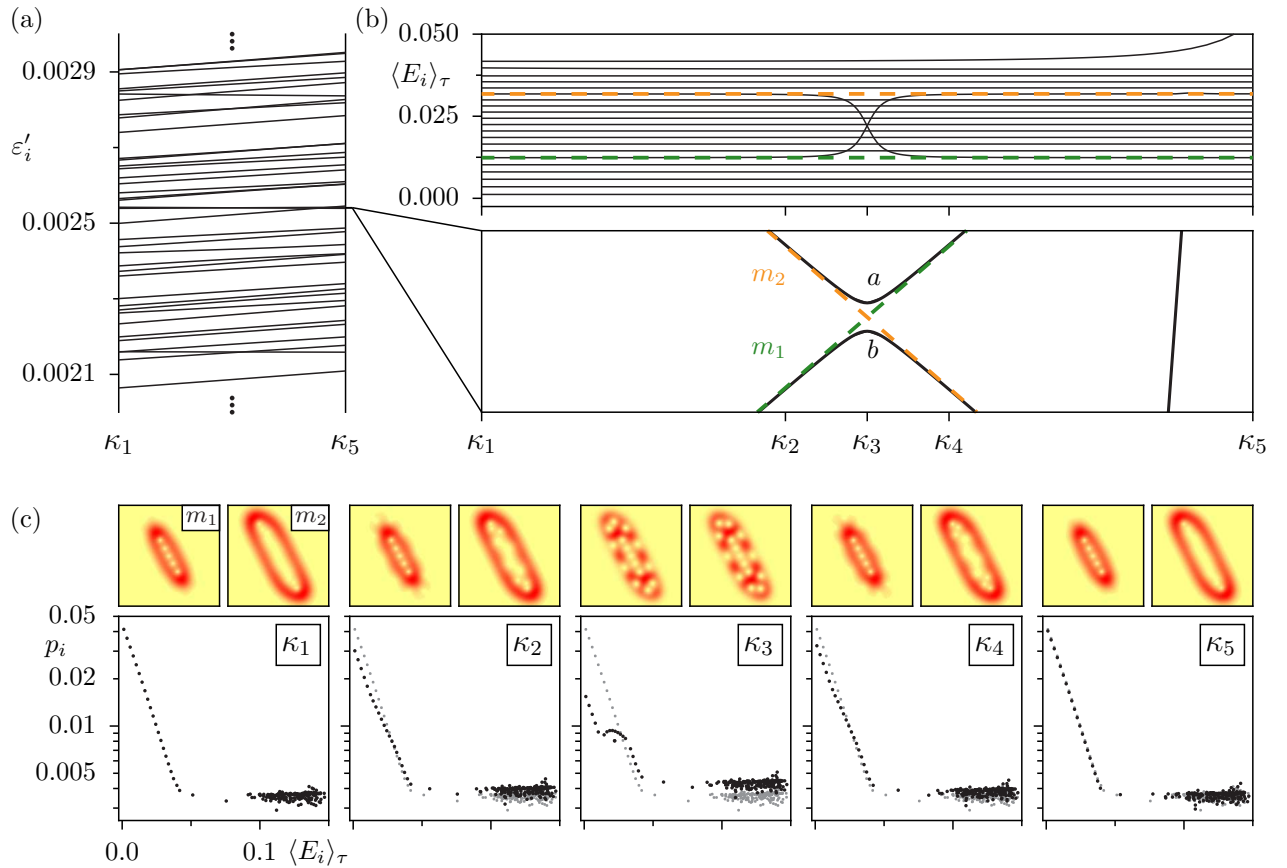


Figure 5.10: (a) Extract from the quasienergy spectrum ε'_i vs. kick strength κ in the interval $[2.85635, 2.85800]$ and magnification of the avoided crossing of the regular states $m_1 = 5$ and $m_2 = 15$. The ε'_i are renormalized to eliminate the huge slope difference between $\bar{\varepsilon}_5$ and $\bar{\varepsilon}_{15}$, $\varepsilon'_i = \varepsilon_i - (\kappa - \kappa_0) \cdot (\sigma_5 + \sigma_{15})/2$. (b) Mean energies $\langle E_i \rangle_\tau$ of the 21 lowest regular states. (c) Floquet occupations p_i vs. $\langle E_i \rangle_\tau$ for a sequence of five κ -values indicated in (a) and (b). For each of the subfigures the Husimi functions of the adiabatic states a and b are represented within the phase-space area $[0.2, 0.8] \times [-0.3, 0.3]$.

In the latter case, the occupation of the regular state m_1 is forced down to the chaotic occupation level. At the same time, the occupations p_m of the entire subset of regular states $m > m_1$ changes in a nontrivial way, but similarly as in the example of Fig. 5.9(a) and can be quantitatively explained with the model proposed in Section 5.4.

We emphasize that the remarkable influence of an avoided level crossing on the entire set of Floquet occupations is bounded to the non-equilibrium character of the driven system. In a time-independent system on the contrary, an avoided crossing entails only a local shift in the occupations of the two involved states and leaves the Boltzmann-distribution of the entire set of occupations unchanged.

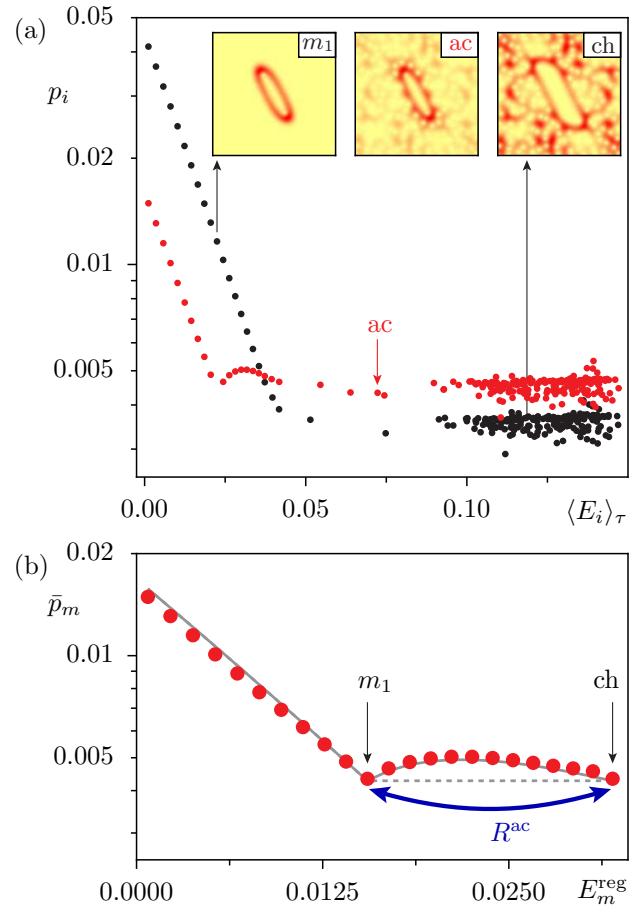


Figure 5.11: Floquet occupations in presence of an avoided crossing between the regular state $m_1 = 10$ and a chaotic state in analogy to Fig. 5.9. Here, κ assumes the values 2.856400 (black) and 2.856897 (red) close to the center of the avoided crossing. Note in (b), that we have simulated the avoided crossing of m_1 with a chaotic state in the rate model (5.13) by an avoided crossing between m_1 and $m = 22$, the last regular state. The parameters are $h = 1/210$, $\beta = 100$, and $\omega_c/\omega = 100$.

5.3 Switching between independent islands

The previous section shed further light on the switching effect of Section 5.1. We want to explain this relation with the series of subfigures in Fig. 5.12, showing the Floquet occupations p_i vs. the mean energies $\langle E_i \rangle_\tau$ for three different driving amplitudes A of the double well potential, starting with $A = 0$ in Fig. 5.12(a). The corresponding classical phase space, where the motion in the two wells is separated by a separatrix, is shown as an inset. The effective Planck constant $\hbar = 0.025$ is sufficiently small to support several states in either of the regular regions left and right of the separatrix. Of course, at $A = 0$ the Boltzmann distribution determines the occupations, which depend solely on their energy but not on their localization in the different wells. For $A > 0$ a small chaotic layer emerges between the islands corresponding to the two wells of the potential, see the insets in Figs. 5.12(b)-(c). Still, there are several regular states in both islands, states 0,2,4, and 6 in the left and states 1,3,5, and 7 in the right island. Figures 5.12(b)-(c) show that the regular states of the different regular islands form separate branches in the $p_i - \langle E_i \rangle_\tau$ representation, with a separation that increases over orders of magnitude, when A approaches the value $A \approx 0.0292432$ in (c).

The explanation is similar to the arguments of Section 5.1.2 and is sketched in the following paragraphs. The spatial overlap between the states of different islands is exponentially small and hence also the inter-island rates are negligible in comparison to the intra-island

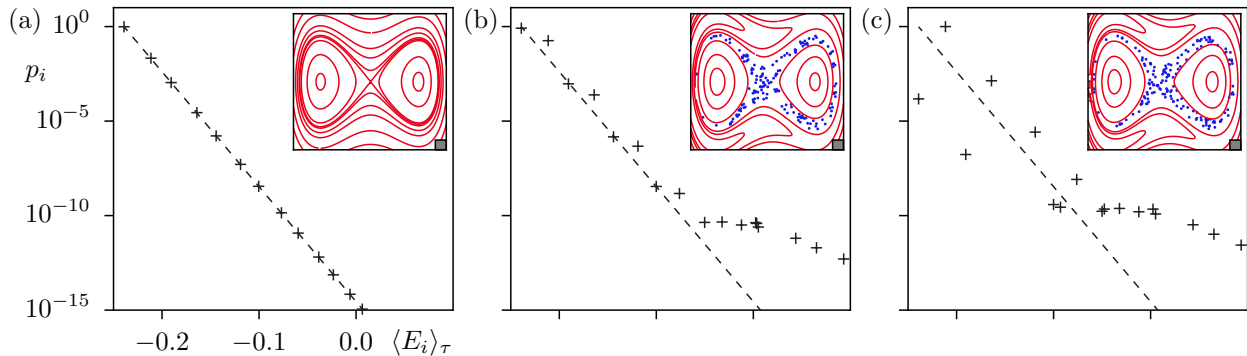


Figure 5.12: Floquet occupations p_i vs. mean energies $\langle E_i \rangle_\tau$ of the driven double well potential (5.1) for the driving amplitudes (a) $A = 0$, (b) $A = 0.029$, and (c) $A = 0.0292432$. The insets show the corresponding stroboscopic Poincaré-sections. The other parameters are $\mu = 0.02$, $1/\omega = 0.900995$, $\hbar = 0.025$, $\beta = 140$, and $\omega_c/\omega = 100$.

rates, especially those between neighboring states in the same island. The equilibration process, whose asymptotic state is described by the rate balance (3.26), therefore takes place almost independently in the two islands. An interaction between the independent occupation branches is only indirectly mediated via the weak rates between the outermost regular states and the chaotic states. As these rates depend sensitively on the parameters and as they are different in the two islands, separate occupation branches are generated.

If a regular state in one of the islands undergoes an avoided crossing, e.g. with a chaotic state, the dominating rate R^{ac} induces occupation equality of the two involved states. The values of A in Figs. 5.12(b)-(c) are not arbitrary, but lie in the vicinity of the avoided crossing between state 4 in the left well and the delocalized state 11 with $\langle \bar{E}_{11} \rangle > 0$. Upon approach to the avoided crossing, \bar{p}_4 is shifted down to the value of \bar{p}_{11} . Since its relative occupation \bar{p}_4/p_n to the other regular states $n = 0$ and 2 in the left island remains the same due to the approximate detailed balance there, the entire left occupation branch decreases together with \bar{p}_4 . This explains, why the separation to the right occupation branch grows significantly. Eventually, the states in the right island hold the dominant occupations. By these arguments it is clear that the largest probability transfer is achieved, if the avoided crossing is between a chaotic state and the ground state 0 , instead of state 4 . However, the parameter range supporting such an avoided crossing is generally very small in contrast to the outer regular states. The reason is the exponentially decreasing spatial overlap of the regular states in the chaotic region.

From the discussed example we can conclude, that the application of the bath-induced switching is not restricted to the driven double well system (5.1). Any system with independent, i.e. not dynamically connected islands, is capable of this mechanism upon variation of a parameter, provided that these islands host regular states. A counterexample are Floquet states, which have comparably high overlap with both islands, e.g. as a consequence of strong dynamical tunneling or as in the case of the resonance states in Section 4.3.2.

5.4 Analytical model for the signatures of avoided crossings

To account for the local modifications of the occupations p_m , which are entailed by an avoided crossing, we apply a simplified, analytically solvable model for the rate equations (3.45). It is based on the nearest-neighbor rate model in Ref. [25]. We restrict it to the chain of N_{reg} regular states and, at first in absence of an avoided crossing, assume that each of them is coupled only to its directly neighboring states. Under this circumstance detailed balance is fulfilled. The primary parameter of the model is the rate ratio of the first two states, $g := R_{0,1}/R_{1,0} = e^{\beta_{\text{eff}} E_{0,1}^{\text{reg}}}$. We approximate the rate ratio $R_{m,m+1}/R_{m+1,m}$ as independent of m , i.e. $R_{m,m+1}/R_{m+1,m} \equiv g$ for all m , and from that obtain the solution $p_m = p_0 g^m = \frac{1-g}{1-g^{N_{\text{reg}}}} g^m$ of Eq. (3.45). The approximation is especially suited for regular islands with a constant winding number ν_m and, thereby, also nearly m -independent $E_{m,m+1}^{\text{reg}}$ in Eq. (4.37).

The rates themselves however differ from state to state. In contrast to Ref. [25], where $R_{m,m+1}/R_{0,1}$ is presumed as constant, we make use of the approximation

$$\frac{R_{m,m+1}}{R_{0,1}} = m + 1. \quad (5.9)$$

This relation holds exactly for the regular states of a harmonic oscillator-like island with constant winding number and elliptic tori. Their coupling-matrix elements have the property $x_{m,m+1}/x_{0,1} = \sqrt{m+1}$, which has already been shown in Section 4.2.2 with the help of the associated algebra of creation and annihilation operators. Beyond the application to elliptic islands of constant winding number we presume relation (5.9) for arbitrary islands, which seems to be in general a good approximation.

To account for an avoided crossing between the states m_1 and m_2 , the model introduces as the second free parameter the additional rate R^{ac} to the direct rates R_{m_1,m_2} and R_{m_2,m_1} . By that, the flux

$$F_{m,m-1} := p_m R_{m,m-1} - p_{m-1} R_{m-1,m} \quad (5.10)$$

is rendered non-zero for all $m_1 < m \leq m_2$. The rate equations (3.45) translate to the flux equations

$$\begin{aligned} 0 &= F_{1,0} \\ 0 &= F_{m+1,m} - F_{m,m-1} \quad m \neq 0, m_1, m_2 \\ (p_{m_1} - p_{m_2}) R^{\text{ac}} &= F_{m_1+1,m_1} - F_{m_1,m_1-1} \\ -(p_{m_1} - p_{m_2}) R^{\text{ac}} &= F_{m_2+1,m_2} - F_{m_2,m_2-1} \end{aligned} \quad (5.11)$$

which have the solution $F_{m,m-1} = F$ with

$$F := (p_{m_1} - p_{m_2}) R^{\text{ac}} \quad (5.12)$$

for $m_1 < m \leq m_2$, and $F_{m,m-1} = 0$ otherwise. The occupations assume the values

$$p_m = \begin{cases} p_0 g^m & m \leq m_1 \\ p_{m_1} \left[(1 - g^{m_2 - m_1}) \frac{r_m}{1 + r_{m_2}} + g^{m - m_1} \right] & m_1 < m \leq m_2 \\ p_{m_2} g^{m - m_2} & m_2 \leq m \end{cases} \quad (5.13)$$

with

$$r_m := R^{\text{ac}} \sum_{k=1}^{m-m_1} \frac{g^{m-m_1-k}}{R_{m_1+k, m_1+k-1}}. \quad (5.14)$$

For $R^{\text{ac}} \gg R_{1,0}$ the parameter r_{m_2} diverges and $p_{m_2}/p_{m_1} = (1 - g^{m_2 - m_1}) \frac{r_{m_2}}{1 + r_{m_2}} + g^{m_2 - m_1}$ then approaches 1.

Note, that the model solution (5.13) relies on the nearest-neighbor coupling and on the m -independence of $R_{m,m+1}/R_{m+1,m}$, whereas $R_{m,m+1}/R_{0,1}$ is still unspecified therein. The latter only comes into play in the evaluation of the r_m . With the assumption (5.9) these adopt the values $r_m = \frac{R^{\text{ac}}}{R_{1,0}} \sum_{k=1}^{m-m_1} \frac{g^{m-m_1-k}}{m_1+k}$. With the further simplified assumption of entirely m -independent rates, as in Ref. [25],

$$\frac{R_{m,m+1}}{R_{0,1}} = 1, \quad (5.15)$$

these are $r_m = \frac{R^{\text{ac}}}{R_{1,0}} \sum_{k=1}^{m-m_1} g^{m-m_1-k} = \frac{R^{\text{ac}}}{R_{1,0}} \frac{1-g^{m-m_1}}{1-g}$ leading to a solution with the occupations $p_m = p_{m_1} \frac{r_{m_2} + g^{m-m_1}}{r_{m_2} + 1}$ of the states $m_1 < m \leq m_2$. In this simplified model, even all occupations of the states $m_1 < m \leq m_2$ assume degenerate values in the limit $R^{\text{ac}} \gg R_{1,0}$.

Figure 5.13 shows the analytical solutions (5.13) on the basis of both assumptions (5.9) (filled dots and solid lines) and (5.15) (open circles and dotted lines) for a series of values $R^{\text{ac}}/R_{1,0}$. It indicates that R^{ac} can lead to notable deviations from the exponential scaling of the p_m already for small values of $R^{\text{ac}}/R_{1,0} \ll 1$. With increasing values of $R^{\text{ac}}/R_{1,0}$ the gradual formation of a plateau-like pattern of the occupations p_m with $m_1 \leq m \leq m_2$ is observed. An accompanying shift of the entire set of occupations ensures the normalization. The size of this shift depends firstly on the size of g and secondly on the separation $m_2 - m_1$ of the states involved in the avoided crossing.

In Figs. 5.9(b) and 5.11(b) we apply the analytical model to the respective subsets of regular states and compare its solution (5.13) for the assumptions (5.9) (solid gray line) and (5.15) (dashed gray line) to the occupations \bar{p}_m from the solution of the rate equations (3.30). In both figures the kick strength κ is close to the center of an avoided crossing. The regular energies E^{reg} are not well defined for the hybridizing states of the avoided crossing, but well-defined for the respective diabatic states m_1 and m_2 . That is why the occupations in these subfigures are represented in the diabatic basis by means of the transformation (3.42). The comparison indicates that the analytical model succeeds to reconstruct the local disturbance

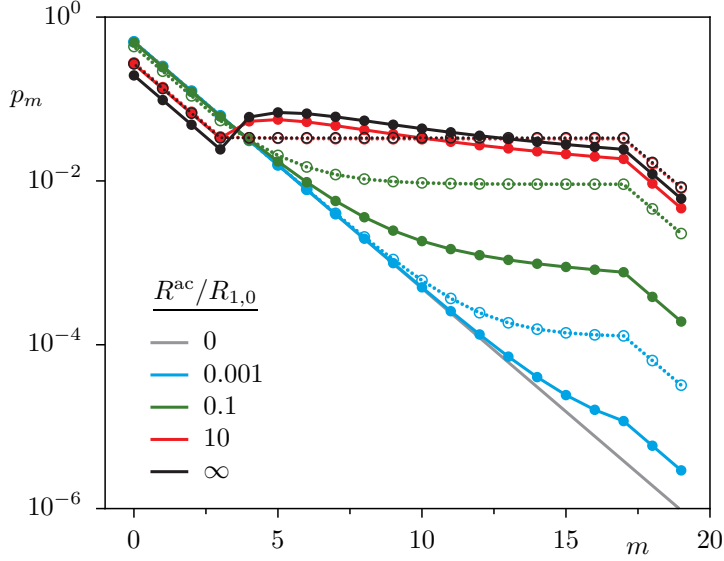


Figure 5.13: Analytical solutions of the rate model for $N_{\text{reg}} = 20$ states. The nearest-neighbor rates $R_{m,m+1}$ scale according to Eqs. (5.9) (solid line and filled symbols) and (5.15) (dotted line and open symbols). Without an avoided crossing, $R^{\text{ac}} = 0$, both yield the same exponential scaling (gray line). An avoided crossing between the states $m_1 = 3$ and $m_2 = 17$ is modelled by the rate R^{ac} , with the values $R^{\text{ac}}/R_{1,0} = 0.001, 0.1, 10$, and the limit $R^{\text{ac}}/R_{1,0} \rightarrow \infty$. The parameters $R_{1,0} = 1$ and $g = 0.5$ are fixed.

of the exponential scaling for the states $m_1 < m < m_2$. In particular the model solutions based on the assumption (5.9) agrees accurately with the numerical solutions.

In the example of Fig. 5.11(b) the analytical model is not perfectly adapted, since it does not account for chaotic states. As a way out, we have applied the model as if the avoided crossing were between the regular states $m_1 = 10$ and the outermost regular state, $m = 22$. Note also, that in both presented examples R^{ac} is indeed the dominant rate, where the approximate rate equations (3.45) are in excellent agreement with the rate equations (3.30). In a case, where R^{ac} is no longer the largest rate, the solutions of Eqs. (3.45) and (3.30) may differ noticeably, and by construction the analytical model based on the assumption (3.45) yields better agreement.

To summarize, the present chapter has given diverse examples for the signatures of avoided crossings in the asymptotic state of a time-periodic quantum system coupled to a heat bath. Avoided crossings as inherently quantum properties lead to new phenomena in the distribution of the Floquet occupations, going beyond the characterizations in Chapter 4, which are based on the semiclassical character of the Floquet states. Still, these features can be explained and quantified by a set of approximate rate equations with an effective rate R^{ac} , and are accessible by analytically solvable models. Their presence can be exploited for the proposed switching mechanism, which is most impressively demonstrated in a weakly driven double well potential, but is also applicable in a broader context.

6 Summary and outlook

A core question of statistical mechanics is the characterization of the asymptotic state approached by a quantum system, when it interacts with a thermal reservoir. In the familiar equilibrium thermodynamics of time-independent systems in the weak-coupling limit it is answered by the canonical distribution, where the eigenstates of the isolated quantum system are occupied with the statistical weights $p_i \sim e^{-\beta E_i}$. In non-equilibrium situations, where external fields permanently pump energy into the system and prevent its relaxation to equilibrium, this is in general an intricate question, that cannot be answered by deduction from the time-independent case.

A special situation is present in a *non-equilibrium steady state*, where the statistical physical parameters that describe the system on macroscopic scales are constant in time, despite the fact that the system is not in thermal equilibrium. This constancy in time is no longer guaranteed in quantum systems driven by a time-periodic field. Here the asymptotic state ρ under a weak coupling to the thermal reservoir becomes time-periodic. Such systems are the object of investigation of this thesis. The asymptotic state is studied in terms of the Floquet occupations $p_i = \rho_{ii}$, i.e. the statistical weights which the Floquet states acquire asymptotically. They are evaluated from the rate equations (3.26) with time-independent rates $R_{lj;ki}$, describing probability flows between the individual Floquet states and decoherence processes. The obtained occupations of the Floquet states can be classified according to their semiclassical character. This is demonstrated for several types of time-periodic systems, which feature the characteristic mixed phase space of non-integrable systems with coexistent regular and chaotic dynamics. The occupations of the chaotic Floquet states fluctuate weakly around a mean value \bar{p}_{ch} . The regular Floquet states on the contrary acquire probabilities that are roughly exponentially distributed.

In contrast to previous studies of a driven particle in a box [23], where the regular states carry occupations close to the Boltzmann weights, we observe that in general the regular occupations can considerably deviate from the Boltzmann result. This observation is possible as we focus on time-periodic systems where the classical phase space and the Floquet states are strongly perturbed compared to the originally time-independent system. This is in particular true for the kicked systems under consideration. In many cases the distribution of the regular occupations can still be well approximated by weights of the Boltzmann type, $p_m \sim e^{-\beta_{\text{eff}} E_m^{\text{reg}}}$, depending on the regular energies E_m^{reg} . The effective temperature $1/\beta_{\text{eff}}$ is evaluated as a function of the winding number in the regular island. Of course, as the driven system is not in an equilibrium state, this temperature might not be directly comparable to the true temperature $1/\beta$ of the heat bath. The proper definition of such a non-equilibrium temperature is a subtle problem [106–108], and the critical question for future investigations is, whether the quantity β_{eff} is accessible by a measurement. As we are not aware of any counterarguments at the present stage, we claim that this is indeed the case. Besides,

as detailed balance can be only approximately fulfilled in driven systems, the quantitative predictive power of the established Boltzmann-type distribution for the regular states is of course not comparable to time-independent systems. In particular for the continuously driven systems other approximation techniques have to be developed in future work.

For the chaotic states we report for $\hbar \rightarrow 0$ a decreasing relative width $\sigma_{\text{ch}}/\bar{p}_{\text{ch}}$ of the occupation distribution, with a power-law scaling that hints to universal behavior. If the chaotic states are dynamically localized in phase space, the distribution of the rates R_{ik} is broadened, and the chaotic occupation distribution consequently tends to an increasing width σ_{ch} for small localization length ξ . Our interpretations about the behavior of the chaotic occupation distribution are supported by the insight of a random-rate model.

Apart from the regular and chaotic states, other types of Floquet states can be found in time-periodic systems. We find that the occupation characteristics of such states still reflects their regular or chaotic nature: beach states, which are very similar to the regular states and situated close, but outside of the regular island, form a correlated set of occupations, which is qualitatively comparable to the regular occupations. In contrast, the occupations of hierarchical states, which have the properties of chaotic states, but live in a restricted region of the chaotic phase space, are distributed analogously to the chaotic states.

A situation, where such purely classical information is of course no longer sufficient to account for the observed occupations, is present at avoided crossings, which are ubiquitous in the quasienergy spectra of Floquet systems. Avoided crossings can give rise to prominent changes in the set of Floquet occupations. As an impressive demonstration we propose a switching between the wells of an asymmetric double well potential. This new switching mechanism is intuitively explained by the effective rate equations (3.45) at the avoided crossing which introduce an additional rate R^{ac} . This rate becomes important once the characteristic coupling strength Γ at the avoided crossing is small compared to its size Δ , $\hbar\Gamma < \Delta$, and might then severely influence the whole set of Floquet occupations. A macroscopic probability transfer is facilitated, if in particular the initially dominantly occupied state is involved in the avoided crossing. However, the switching works even if the Floquet states involved in the avoided crossing have only small probabilities both in the initial and in the final state. This is possible, because firstly the equilibration in the two potential wells takes place almost independently, and secondly detailed balance is approximately fulfilled in both of them. We emphasize that the remarkable impact of an avoided level crossing on the entire set of Floquet occupations is a consequence of the non-equilibrium character of the driven system. In a time-independent system on the contrary, an avoided crossing entails only a local shift in the occupations of the two involved states and of course leaves the Boltzmann-distribution of the entire set of occupations unchanged. At the same time, the new switching mechanism is very different from standard techniques which allow to transfer a wave packet from one well to the other by resonant or near resonant driving and negligible

coupling to a heat bath. In those cases a specific initial wave packet has to be prepared and the driving has to be applied for a specific duration. In contrast, for the here presented switching the initial state of the system is arbitrary and the duration of the driving is arbitrary, if it is only longer than the relaxation time. The presence of the heat bath is essential for the switching.

In conclusion, with the presented characterizations of the Floquet occupations we demonstrate that ubiquitous signatures of the classical dynamics are reflected in the asymptotic density matrix of the open quantum system. In this way it is feasible to draw an intuitive and coherent picture of the asymptotic state, shedding new light on the statistical mechanics of time-periodic quantum systems. We claim that the phase-space characterization provides a generic picture. An accurate and reliable quantitative prediction of the asymptotic state is difficult, e.g. for a strongly structured phase space. This is not surprising, since the interplay of the time-periodic driving and the dissipation does not only generate interesting phenomena in the relaxation dynamics, but can also make the asymptotic state susceptible to the details of the interactions. Besides, the insight gained from the classical phase-space analysis is a mainly semiclassical perspective, whereas states in the deep quantum regime do not necessarily adhere to the phase-space classification scheme. On the other hand, we expect the semiclassical picture to be consistent with the corresponding analysis of the classical regime. For a verification in future work, the Floquet density matrix has to be transformed into an appropriate phase-space representation, which has to be compared to the asymptotic solution of a Fokker-Planck equation for the classical density. The implementation of a Fokker-Planck equation for general time-periodic systems is highly nontrivial and still deserves further studies [109–111].

A The harmonic oscillator heat bath

A.1 Quantum Langevin equation

The damped motion of a Brownian particle in a fluctuating environment is a paradigmatic model of classical mechanics. The equation of motion is the Langevin equation

$$\ddot{x} + \eta\dot{x} + V'(x) = \xi(t) \quad (\text{A.1})$$

with a damping force proportional to the velocity \dot{x} and the damping constant η as proportionality factor, and with the fluctuating force $\xi(t)$. In this section we briefly sketch the derivation of a quantum version of the Langevin equation, starting from the microscopic description of the quantum system interacting with the bath of independent harmonic oscillators of Section 3.1. The derivation is based on Refs. [70, 72, 73]. The Hamiltonian of the composite system

$$H_{\text{tot}} = H_s + H_b + H_{sb} = \frac{p^2}{2} + V(x) + \sum_n \left(\frac{p_n^2}{2m_n} + \frac{m_n\omega_n^2}{2} \left(x_n - \frac{c_n}{m_n\omega_n^2} x \right)^2 \right) \quad (\text{A.2})$$

(Eq. (3.5)) with $H_b = p_n^2/(2m_n) + m_n\omega_n^2 x_n^2/2$ and $H_s = p^2/2 + V(x)$ rules the Heisenberg equations of motion for the coordinate operators x and x_n of the relevant subsystem and the bath oscillators, respectively,

$$\ddot{x} + V'(x) = \sum_n c_n \left(x_n - \frac{c_n}{m_n\omega_n^2} x \right) \quad (\text{A.3})$$

$$\ddot{x}_n + \omega_n^2 x_n = \frac{c_n}{m_n} x. \quad (\text{A.4})$$

The solution of Eq. (A.4) is

$$x_n(t) = x_n^{(h)}(t) + \frac{c_n}{m_n\omega_n} \int_{t_0}^t dt' \sin(\omega_n(t-t')) x(t') \quad (\text{A.5})$$

with the solution of the homogeneous part

$$x_n^{(h)}(t) = x_n(t_0) \cos(\omega_n(t-t_0)) + \frac{p_n(t_0)}{m_n\omega_n} \sin(\omega_n(t-t_0)). \quad (\text{A.6})$$

These solutions $x_n(t)$ are inserted into Eq. (A.3),

$$\begin{aligned} \ddot{x} + V'(x) + \sum_n \frac{c_n^2}{m_n\omega_n^2} x &= \sum_n c_n \left(x_n(t_0) \cos(\omega_n(t-t_0)) + \frac{p_n(t_0)}{m_n\omega_n} \sin(\omega_n(t-t_0)) \right) \\ &+ \sum_n \frac{c_n^2}{m_n\omega_n} \int_{t_0}^t dt' \sin(\omega_n(t-t')) x(t'), \end{aligned} \quad (\text{A.7})$$

where one makes use of

$$\int_{t_0}^t dt' \sin(\omega_n(t-t'))x(t') = \frac{1}{\omega_n} \cos(\omega_n(t-t'))x(t') \Big|_{t_0}^t - \frac{1}{\omega_n} \int_{t_0}^t dt' \cos(\omega_n(t-t'))\dot{x}(t') \quad (\text{A.8})$$

to obtain

$$\begin{aligned} \ddot{x} + \int_{t_0}^t dt' \sum_n \frac{c_n^2}{m_n \omega_n^2} \cos(\omega_n(t-t'))\dot{x}(t') + V'(x) = & \quad (\text{A.9}) \\ & \sum_n c_n \left(x_n(t_0) \cos(\omega_n(t-t_0)) + \frac{p_n(t_0)}{m_n \omega_n} \sin(\omega_n(t-t_0)) \right) \\ & - \sum_n \frac{c_n^2}{m_n \omega_n^2} \cos(\omega_n(t-t_0))x(t_0). \end{aligned}$$

With the definitions

$$\eta(t) := \sum_n \frac{c_n^2}{m_n \omega_n^2} \cos(\omega_n t) \quad (\text{A.10})$$

$$\xi(t) := \sum_n c_n \left(x_n(t_0) \cos(\omega_n(t-t_0)) + \frac{p_n(t_0)}{m_n \omega_n} \sin(\omega_n(t-t_0)) \right) \quad (\text{A.11})$$

the Heisenberg equation of motion for the system coordinate reads

$$\ddot{x} + \int_{t_0}^t dt' \eta(t-t')\dot{x}(t') + V'(x) = \xi(t) - \eta(t-t_0)x(t_0). \quad (\text{A.12})$$

The second term on the lhs acts as a damping force, whereas the first term on the rhs plays the role of a fluctuating force.

The damping kernel $\eta(t)$ can be expressed using the spectral density of the heat bath

$$J(\omega) := \frac{\pi}{2} \sum_n \frac{c_n^2}{m_n \omega_n} \left(\delta(\omega - \omega_n) - \delta(\omega + \omega_n) \right), \quad (\text{A.13})$$

compare Eq. (3.11), where the contributions of the bath modes are weighted with the individual coupling strength. When invoking Def. (A.13), it is cast into the form

$$\begin{aligned} \eta(t) &= \frac{1}{2} \sum_n \frac{c_n^2}{m_n \omega_n} \left(\int_0^\infty d\omega \frac{\cos(\omega t)}{\omega} \delta(\omega - \omega_n) + \int_{-\infty}^0 d\omega \left(-\frac{\cos(\omega t)}{\omega} \right) \delta(\omega + \omega_n) \right) \\ &= \frac{1}{\pi} \int_{-\infty}^\infty d\omega J(\omega) \frac{\cos(\omega t)}{\omega} = \frac{2}{\pi} \int_0^\infty d\omega J(\omega) \frac{\cos(\omega t)}{\omega}, \end{aligned} \quad (\text{A.14})$$

where the last step uses $J(-\omega) = -J(\omega)$. In the continuum limit the spectral density is

treated as a continuous function. With the ansatz

$$J_o(\omega) = \eta\omega \quad (\text{A.15})$$

the damping kernel becomes

$$\eta_o(t) = \frac{\eta}{\pi} \int_{-\infty}^{\infty} d\omega \cos(\omega t) = \frac{2\eta}{2\pi} \int_{-\infty}^{\infty} d\omega \frac{1}{2} (e^{i\omega t} + e^{-i\omega t}) = 2\eta\delta(t) \quad (\text{A.16})$$

and, using $\int_{t_0}^t dt' \delta(t-t') = 1/2$, the Heisenberg equation of motion finally adopts the form

$$\ddot{x} + \eta\dot{x} + V'(x) = \xi(t) - 2\eta\delta(t-t_0)x(t_0). \quad (\text{A.17})$$

This quantum Langevin equation is identical to the classical version (A.1), except for the term $2\eta\delta(t-t_0)x(t_0)$, which is relevant only within the initial relaxation step. This correspondence is the motivation for Assumption (A.15) on the spectral density. In particular it ensures that the Langevin equation becomes Markovian, i.e. memoryless: the evolution at time t does not depend on the state $x(t')$ at times $t' < t$, as is still the case in Eq. (A.12) for a general time-dependent damping kernel $\eta(t)$.

A.2 Correlation function

Here we want to evaluate the correlation function

$$G(t-t') := \langle \tilde{B}(t)\tilde{B}(t') \rangle_b = \text{Tr}_b \left(\tilde{B}(t)\tilde{B}(t')\rho_b \right) \quad (\text{A.18})$$

of the bath coupling operator $B = \sum_n c_n x_n$ in the interaction term H_{sb} of the Hamiltonian (A.2). Note, that the supplementing term, $\sim x^2$, in the Hamiltonian (A.2) is diagonal in the Hilbert space of the heat bath. It serves to remove a coupling induced renormalization of the system energies and is therefore absorbed in H_s .

The operators in Def. (A.18) are required in the interaction picture, where the unperturbed system has the Hamiltonian $H_0 = H_s + H_b$. As this is in contrast to the Heisenberg picture of the preceding section, it explains that the time-dependent oscillator coordinates $\tilde{x}_n(t)$ are here given by the homogeneous part of Eq. (A.6) alone and $\tilde{B}(t)$ is hence identical to $\xi(t)$ defined in Eq. (A.11). Setting $t_0 = 0$ for simplicity and with $\tilde{x}_n(0) \equiv x_n$ and $\tilde{p}_n(0) \equiv p_n$ the correlation function reads

$$G(t-t') = \langle \tilde{B}(t)\tilde{B}(t') \rangle_b = \left\langle \sum_{n,m} c_n c_m \left(x_n \cos(\omega_n t) + \frac{p_n}{m_n \omega_n} \sin(\omega_n t) \right) \cdot \left(x_m \cos(\omega_m t') + \frac{p_m}{m_m \omega_m} \sin(\omega_m t') \right) \right\rangle. \quad (\text{A.19})$$

The individual bosonic correlations at equal time $t_0 = 0$ and with respect to the Hamiltonian H_b and the equilibrium density $\rho_b \sim e^{-\beta H_b}$ of the heat bath are

$$\frac{1}{2}m_n\omega_n^2 \langle x_n x_m \rangle = \frac{1}{2m_n} \langle p_n p_m \rangle = \frac{\hbar\omega_n}{4} \coth\left(\frac{\hbar\omega_n}{2k_B T}\right) \delta_{nm} \quad \text{and} \quad (\text{A.20})$$

$$\langle x_n p_m \rangle = -\langle p_m x_n \rangle = \frac{1}{2}i\hbar\delta_{nm}. \quad (\text{A.21})$$

They are related to the bosonic occupation number of the bath modes

$$n_\beta(\omega_n) = (e^{\beta\hbar\omega_n} - 1)^{-1} \quad (\text{A.22})$$

by the identity $\coth(\beta\hbar\omega_n/2) = 2n_\beta(\omega_n) + 1$. Besides, the bosonic occupation number has the property $n_\beta(-\omega_n) = -(n_\beta(-\omega_n) + 1)$. With the individual correlations $G(t-t')$ becomes

$$G(t-t') = \sum_n c_n^2 \left(\frac{\hbar}{2m_n\omega_n} \coth\left(\frac{\hbar\omega_n}{2k_B T}\right) \left(\cos(\omega_n t) \cos(\omega_n t') + \sin(\omega_n t) \sin(\omega_n t') \right) + \frac{i\hbar}{2m_n\omega_n} \left(\cos(\omega_n t) \sin(\omega_n t') - \sin(\omega_n t) \cos(\omega_n t') \right) \right) \quad (\text{A.23})$$

$$= \sum_n \frac{\hbar c_n^2}{2m_n\omega_n} \left(\coth\left(\frac{\hbar\omega_n}{2k_B T}\right) \cos(\omega_n(t-t')) - i \sin(\omega_n(t-t')) \right) \quad (\text{A.24})$$

$$= \sum_n \frac{\hbar c_n^2}{2m_n\omega_n} \left(n_\beta(\omega_n) e^{i\omega_n(t-t')} - n_\beta(-\omega_n) e^{-i\omega_n(t-t')} \right) \quad (\text{A.25})$$

$$= \sum_n \frac{\hbar c_n^2}{2m_n\omega_n} \left(n_\beta(\omega_n) e^{i\omega_n(t-t')} + (n_\beta(\omega_n) + 1) e^{-i\omega_n(t-t')} \right). \quad (\text{A.26})$$

Now the correlation function of Eq. (A.25) is expressed with the spectral density $J(\omega)$,

$$G(t) = \sum_n \frac{\hbar c_n^2}{2m_n\omega_n} \left(\frac{1}{2} \int_0^\infty d\omega \delta(\omega - \omega_n) \left(n_\beta(\omega) e^{i\omega t} - n_\beta(-\omega) e^{-i\omega t} \right) + \frac{1}{2} \int_{-\infty}^0 d\omega \delta(\omega + \omega_n) \left(n_\beta(-\omega) e^{-i\omega t} - n_\beta(\omega) e^{i\omega t} \right) \right) \quad (\text{A.27})$$

$$= \frac{\hbar}{2\pi} \int_{-\infty}^\infty d\omega J(\omega) \left(n_\beta(\omega) e^{i\omega t} - n_\beta(-\omega) e^{-i\omega t} \right) \quad (\text{A.28})$$

$$= \frac{\hbar}{2\pi} \int_{-\infty}^\infty d\omega J(\omega) \left(n_\beta(\omega) e^{i\omega t} + (n_\beta(\omega) + 1) e^{-i\omega t} \right). \quad (\text{A.29})$$

Finally, the Fourier-transformed correlation function reads

$$g(\omega) = \frac{1}{2\pi} \int_{-\infty}^{\infty} dt G(t) e^{-i\omega t} \quad (\text{A.30})$$

$$\stackrel{(\text{A.28})}{=} \frac{\hbar}{2\pi} \frac{1}{2\pi} \int_{-\infty}^{\infty} dt \int_{-\infty}^{\infty} d\omega' J(\omega') \left(n_{\beta}(\omega') e^{i(\omega' - \omega)\tau} - n_{\beta}(-\omega') e^{-i(\omega' + \omega)\tau} \right) \quad (\text{A.31})$$

$$= \frac{\hbar}{2\pi} \int_0^{\infty} d\omega' J(\omega') \left(n_{\beta}(\omega') \delta(\omega' - \omega) - n_{\beta}(-\omega') \delta(\omega' + \omega) \right) \quad (\text{A.32})$$

$$= \frac{\hbar}{2\pi} \left(J(\omega) n_{\beta}(\omega) - J(-\omega) n_{\beta}(\omega) \right) = \frac{\hbar}{\pi} J(\omega) n_{\beta}(\omega), \quad (\text{A.33})$$

where $J(-\omega) = -J(\omega)$ has been used in the last line. Correctly scaled to energy-units it is

$$g(E) := \frac{1}{2\pi\hbar} \int_{-\infty}^{\infty} dt G(t) e^{-iEt/\hbar} = \frac{g(E/\hbar)}{\hbar} = \frac{1}{\pi} J(E/\hbar) n_{\beta}(E). \quad (\text{A.34})$$

With that, the relation (3.15) between the Fourier-transformed correlation function $g(E)$ and the spectral density $J(\omega)$ of the heat bath is established.

B Derivation of the Floquet-Markov master equation and its asymptotics

This section recapitulates the derivation of the Floquet-Markov master equation, i.e. the equation of motion for the reduced density operator $\rho(t)$ in the Born-Markov approximation, appropriately conditioned to time-periodic systems. For time-independent systems this is a standard technique, see e.g. [68, 77]. In the context of time-periodic systems the master equation is completely analogous, but special care has to be taken when considering the different time scales of the relevant microscopic processes [20–22, 25].

B.1 Evolution of the density operator

The microscopic description of an open quantum system in contact with a heat bath is based on the composite Hamiltonian

$$H_{\text{tot}}(t) = H_s(t) \otimes \mathbb{1}_b + H_{sb} + \mathbb{1}_s \otimes H_b \quad (\text{B.1})$$

with the Hamiltonian $H_s(t)$ of the system of interest and the Hamiltonian H_b of the heat bath, where both are in mutual interaction via the coupling term H_{sb} . The combined degrees of freedom of system and bath are characterized in terms of the density operator ρ_{tot} of the composite system, whose evolution is ruled by the Liouville-von Neumann equation

$$i\hbar \frac{\partial}{\partial t} \rho_{\text{tot}}(t) = [H_{\text{tot}}(t), \rho_{\text{tot}}(t)] . \quad (\text{B.2})$$

With the objective of a perturbation expansion, where the interaction term H_{sb} is understood as a weak perturbation of the uncoupled system, $H_0(t) = H_s(t) + H_b$, an evaluation in the interaction picture is convenient. The unitary transformation

$$\tilde{W}(t, t_0) = U_0^{-1}(t, t_0) W(t) U_0(t, t_0) , \quad (\text{B.3})$$

mediated by the propagator

$$U_0(t, t_0) = \hat{T} \exp \left(-i \int_{t_0}^t dt' H_0(t') / \hbar \right) \quad (\text{B.4})$$

of the uncoupled system, transforms an operator $W(t)$ into the interaction picture. We denote operators in the interaction picture by a tilde and introduce the short-hand notation $\tilde{W}(t) \equiv \tilde{W}(t, 0)$. The propagator $U_0(t, t_0)$ is a solution to the Schrödinger equation $i\hbar(\partial/\partial t)U_0(t, t_0) = H_0(t)U_0(t, t_0)$ with the initial condition $U_0(t_0, t_0) = \mathbb{1}_s \otimes \mathbb{1}_b$. In the

interaction picture the Liouville-von Neumann equation becomes

$$i\hbar \frac{\partial}{\partial t} \tilde{\rho}_{\text{tot}}(t, t_0) = - \left[\tilde{H}_0(t, t_0), \tilde{\rho}_{\text{tot}}(t, t_0) \right] + U_0^{-1}(t, t_0) i\hbar \frac{\partial}{\partial t} \rho_{\text{tot}}(t, t_0) U_0(t, t_0) \quad (\text{B.5})$$

$$= \left[\tilde{H}_{sb}(t, t_0), \tilde{\rho}_{\text{tot}}(t, t_0) \right]. \quad (\text{B.6})$$

By integration

$$\tilde{\rho}_{\text{tot}}(t) \equiv \tilde{\rho}_{\text{tot}}(t, 0) = \rho_{\text{tot}}(0) - \frac{i}{\hbar} \int_0^t dt' \left[\tilde{H}_{sb}(t'), \tilde{\rho}_{\text{tot}}(t') \right] \quad (\text{B.7})$$

and reinsertion in Eq. (B.6) the equation of motion becomes

$$\frac{\partial}{\partial t} \tilde{\rho}_{\text{tot}}(t) = -\frac{i}{\hbar} \left[\tilde{H}_{sb}(t), \rho_{\text{tot}}(0) \right] - \frac{1}{\hbar^2} \int_0^t dt' \left[\tilde{H}_{sb}(t), \left[\tilde{H}_{sb}(t'), \tilde{\rho}_{\text{tot}}(t') \right] \right]. \quad (\text{B.8})$$

While the density operator $\rho_{\text{tot}}(t)$ contains the statistical information of the composite system, one is generally only interested in the degrees of freedom of the relevant system, whose statistical information subsumes in the reduced density operator

$$\rho(t) := \text{Tr}_b \left(\rho_{\text{tot}}(t) \right), \quad (\text{B.9})$$

where the degrees of freedom in the Hilbert space of the bath are traced out. Since the propagator $U_0(t, t_0)$ factorizes,

$$U_0(t, t_0) = \hat{\mathcal{T}} \exp \left(-\frac{i}{\hbar} \int_{t_0}^t dt' H_s(t') \right) \otimes e^{-\frac{i}{\hbar} H_b(t-t_0)} = U_s(t, t_0) \otimes U_b(t, t_0), \quad (\text{B.10})$$

the trace in Def. (B.9) commutes with the unitary transformation (B.3), such that

$$\tilde{\rho}(t, t_0) = U_0^{-1}(t, t_0) \text{Tr}_b \left(\rho_{\text{tot}}(t) \right) U_0(t, t_0) = U_s^{-1}(t, t_0) \text{Tr}_b \left(\rho_{\text{tot}}(t) \right) U_s(t, t_0) \quad (\text{B.11})$$

$$= \text{Tr}_b \left(U_s^{-1}(t, t_0) \rho_{\text{tot}}(t) U_s(t, t_0) \right) = \text{Tr}_b \left(U_0^{-1}(t, t_0) \rho_{\text{tot}}(t) U_0(t, t_0) \right) \quad (\text{B.12})$$

$$= \text{Tr}_b \left(\tilde{\rho}_{\text{tot}}(t, t_0) \right). \quad (\text{B.13})$$

The equation of motion for the reduced density operator in the interaction picture $\tilde{\rho}(t, t_0)$ is hence obtained from Eq. (B.8) by tracing over the bath degrees of freedom,

$$\frac{\partial}{\partial t} \tilde{\rho}(t) = -\frac{i}{\hbar} \text{Tr}_b \left[\tilde{H}_{sb}(t), \rho_{\text{tot}}(0) \right] - \frac{1}{\hbar^2} \int_0^t dt' \text{Tr}_b \left[\tilde{H}_{sb}(t), \left[\tilde{H}_{sb}(t'), \tilde{\rho}_{\text{tot}}(t') \right] \right]. \quad (\text{B.14})$$

B.2 Born-Markov approximation

The equation of motion (B.14) for $\tilde{\rho}(t, t_0)$, though still exact, is not suitable for integration in practical applications. It still contains the density operator $\rho_{\text{tot}}(t)$ of the composite system. Besides, the integrand on the rhs of the integro-differential equation depends on its solution at earlier times $t' \leq t$. That is why Eq. (B.14) is often treated in the limit of weak system-bath interaction, where the effective strength γ of the interaction term H_{sb} is small compared to that of $H_0(t)$, and a series of approximations are feasible.

With a first assumption, that the interaction Hamiltonian $\tilde{H}_{sb}(t)$ in the Hilbert space of the heat bath is zero on average, $\text{Tr}_b(\tilde{H}_{sb}(t)\rho_b) = 0$, the first term on the rhs of Eq. (B.14) is eliminated. Technically, this can always be achieved by adding $\text{Tr}_b(H_{sb}\rho_b)$ to the system Hamiltonian $H_s(t)$ [77]. Secondly, according to the Feynman-Vernon initial condition [112], system and heat bath are assumed to be initially uncorrelated,

$$\rho_{\text{tot}}(0) = \rho(0) \otimes \rho_b . \quad (\text{B.15})$$

Herein, the reduced density operator of the heat bath ρ_b is assumed to be of the canonical form $\rho_b \sim e^{-\beta H_b}$, since the heat bath is understood to be in equilibrium at the temperature $1/\beta$. Despite of the initially uncorrelated state (B.15), correlations between system and bath may arise during evolution. These, being of the order $\mathcal{O}(H_{sb})$, are neglected in the course of the *Born approximation*

$$\tilde{\rho}_{\text{tot}}(t) \approx \tilde{\rho}(t) \otimes \rho_b . \quad (\text{B.16})$$

The factorization (B.16) moreover acts on the assumption that the heat bath due to its mere dimension and the weak interaction with the system on average remains unaffected by processes in the system and for all times retains the equilibrium state ρ_b . By virtue of the Born approximation, Eq. (B.14) becomes a closed integro-differential equation of second order in H_{sb} ,

$$\frac{\partial}{\partial t} \tilde{\rho}(t) = -\frac{1}{\hbar^2} \int_0^t dt' \text{Tr}_b \left[\tilde{H}_{sb}(t), \left[\tilde{H}_{sb}(t'), \tilde{\rho}(t') \otimes \rho_b \right] \right] . \quad (\text{B.17})$$

The second approximation, the *Markov approximation*, replaces $\tilde{\rho}(t')$ in Eq. (B.17) by $\tilde{\rho}(t)$ and moreover removes the distinction of the preparation time $t = 0$. The state $\tilde{\rho}(t)$ then depends no longer on its history, i.e. on $\tilde{\rho}(t')$ at times $t' < t$. Qualitatively speaking, the Markov approximation is reasonable for the premised huge dimension of the reservoir, which is constantly held in equilibrium: Any minor modifications of the bath stemming from the weak interaction with the system decay faster than the time between successive interaction events and information about a previous interaction event can therefore not return to the system. The appropriateness of the Markov approximation is hence a question whether the bath correlation time is small compared to the typical time of changes in the system. The explicit implementation of the Markov approximation requires some care and is sketched in

the following paragraphs. The resulting equation of motion for $\rho(t)$ is Eq. (B.29).

Firstly, the coupling operator H_{sb} can be specified to be

$$H_{sb} = \gamma A \otimes B \quad (\text{B.18})$$

with an operator A acting in the Hilbert space of the system and an operator B acting in the Hilbert space of the heat bath, or, more generally, a sum of such coupling terms. The coupling parameter γ is a measure for the strength of the interaction. It serves as the small parameter in the perturbation expansion, leading to the rhs of Eq. (B.17), which is of the order $\mathcal{O}(\gamma^2)$. Equation (B.17) now becomes

$$\frac{\partial}{\partial t} \tilde{\rho}(t) = -\frac{\gamma^2}{\hbar^2} \int_0^t dt' \text{Tr}_b \left[\tilde{A}(t) \otimes \tilde{B}(t), \left[\tilde{A}(t') \otimes \tilde{B}(t'), \tilde{\rho}(t') \otimes \rho_b \right] \right] \quad (\text{B.19})$$

$$= -\frac{\gamma^2}{\hbar^2} \int_0^t dt' \left(G(t-t') \left(\tilde{A}(t) \tilde{A}(t') \tilde{\rho}(t') - \tilde{A}(t') \tilde{\rho}(t') \tilde{A}(t) \right) + G(t'-t) \left(\tilde{\rho}(t') \tilde{A}(t') \tilde{A}(t) - \tilde{A}(t) \tilde{\rho}(t') \tilde{A}(t') \right) \right). \quad (\text{B.20})$$

In the second line the correlation function of the bath coupling operator B

$$G(t-t') := \langle \tilde{B}(t) \tilde{B}(t') \rangle_b = \text{Tr}_b \left(\tilde{B}(t) \tilde{B}(t') \rho_b \right) \quad (\text{B.21})$$

is defined, which refers to the thermal equilibrium state ρ_b of the heat bath and whose time-dependence is generated by the free bath Hamiltonian H_b . Besides, the property $G(-t) = G^*(t)$ has been used in Eq. (B.20).

To perform the Markov approximation, Eq. (B.20) is retransferred into the Schrödinger picture via

$$\frac{\partial}{\partial t} \rho(t) = -\frac{i}{\hbar} [H_s(t), \rho(t)] + U_s(t, 0) \frac{\partial}{\partial t} \tilde{\rho}(t, 0) U_s^{-1}(t, 0). \quad (\text{B.22})$$

With the help of $U_s(t, 0) \tilde{A}(t, 0) \tilde{A}(t', 0) \tilde{\rho}(t', 0) U_s^{-1}(t, 0) = A(t) \tilde{A}(t', t) \tilde{\rho}(t', t)$ and three equivalent relations it becomes

$$\frac{\partial}{\partial t} \rho(t) = -\frac{i}{\hbar} [H_s(t), \rho(t)] \quad (\text{B.23})$$

$$- \frac{\gamma^2}{\hbar^2} \int_0^t dt' \left(G(t-t') \left(A(t) \tilde{A}(t', t) \tilde{\rho}(t', t) - \tilde{A}(t', t) \tilde{\rho}(t', t) A(t) \right) + G(t'-t) \left(\tilde{\rho}(t', t) \tilde{A}(t', t) A(t) - A(t) \tilde{\rho}(t', t) \tilde{A}(t', t) \right) \right) \quad (\text{B.24})$$

and with the substitution $t' \rightarrow t - t'$

$$\begin{aligned} \frac{\partial}{\partial t} \rho(t) &= -\frac{i}{\hbar} [H_s(t), \rho(t)] \\ &\quad - \frac{\gamma^2}{\hbar^2} \int_0^t dt' \left(G(t') \left(A(t) \tilde{A}(t-t', t) \tilde{\rho}(t-t', t) - \tilde{A}(t-t', t) \tilde{\rho}(t-t', t) A(t) \right) \right. \\ &\quad \left. + G^*(t') \left(\tilde{\rho}(t-t', t) \tilde{A}(t-t', t) A(t) - A(t) \tilde{\rho}(t-t', t) \tilde{A}(t-t', t) \right) \right). \end{aligned} \quad (\text{B.25})$$

The correlation function $G(t)$ decays on the characteristic time scale τ_c . Ideally, one might even think of a δ -correlation $G(t) \sim \delta(t)$. This property of the correlation function is the key to the Markov approximation: under the assumption, that any essential changes in the state of the system occur only on time scales larger than τ_c , the contribution $\tilde{\rho}(t-t', t)$ to the integrands in Eq. (B.25) can be replaced by $\rho(t)$ in the time interval $0 \leq t' \leq \tau_c$:

$$\tilde{\rho}(t-t', t) \approx \tilde{\rho}(t, t) = \rho(t) \quad \text{for } 0 \leq t' \leq \tau_c. \quad (\text{B.26})$$

As a consequence of the approximation, the equation of motion becomes local in time, i.e. the evolution at the time t depends only on the current state $\rho(t)$. The action of the heat bath is now coarse-grained on the scale τ_c , meaning that changes on time scales smaller than τ_c are not resolved any more. Times larger than τ_c , in contrast, do not contribute to the integration in Eq. (B.25), since the correlation function $G(t')$ is assumed to be zero there. For this reason the upper integration borders in Eq. (B.25) can just as well be extended to infinity, thereby abolishing the explicit dependence on the preparation time in Eq. (B.25).

An estimate of the error brought about by the Markov approximation can be found e.g. in Ref. [68] in the case of time-independent systems and, generalized to the case of Floquet systems, in Ref. [25]: in the expansion (B.25) $\tilde{\rho}(t)$ changes with the characteristic rate

$$\Gamma^{(2)} = \frac{\gamma^2}{\hbar^2} \tau_c \langle A^2 \rangle \langle B^2 \rangle. \quad (\text{B.27})$$

The Markov presumption, that the influence of these second-order terms is small on the time scale τ_c , thus requires⁹

$$\tau_c \Gamma^{(2)} \ll 1. \quad (\text{B.28})$$

At this point we emphasize, that the Markov approximation is done with respect to the interaction picture: the correlation time τ_c is compared to the characteristic time scale $1/\Gamma^{(2)}$ of changes in $\tilde{\rho}(t)$. Being an operator in the interaction picture, its evolution is not ruled by the coherent, possibly fast contributions $-i[H_s(t), \rho(t)]/\hbar$. That is why apart from the criterion (B.28) no conditions specific to the time-periodicity of the system have to be

⁹An equivalent criterion (B.51), based on the relaxation rate of the fastest decaying eigensolution of the Floquet-Markov master equation, is stated below in Eq. (B.51).

imposed. The authors of Ref. [25] in particular point out that the more restrictive condition $\hbar\Gamma^{(2)} < \varepsilon_{ij}$ for all i and j , as stated in Refs. [22,74], is in general not mandatory for the Born-Markov approximation. Note besides, that the condition (B.28) at the same time entails the condition of validity for the Born approximation, i.e. that the contribution of the next order of the perturbation expansion is weak compared to the second order in γ .

To summarize the last paragraphs, the master equation in Born-Markov approximation reads

$$\begin{aligned} \frac{\partial}{\partial t}\rho(t) = & -\frac{i}{\hbar}[H_s(t), \rho(t)] \\ & -\frac{\gamma^2}{\hbar^2} \int_0^\infty dt' \left(G(t') \left(A(t)\tilde{A}(t-t', t)\rho(t) - \tilde{A}(t-t', t)\rho(t)A(t) \right) \right. \\ & \left. + G^*(t') \left(\rho(t)\tilde{A}(t-t', t)A(t) - A(t)\rho(t)\tilde{A}(t-t', t) \right) \right). \end{aligned} \quad (\text{B.29})$$

The first term represents the evolution of the isolated system. The second term accounts for dissipative effects originating from the interaction with the reservoir. Equation (B.29) is however not of the Lindblad form. A Markovian master equation of the Lindblad form,

$$\frac{\partial\rho}{\partial t} = -\frac{i}{\hbar}[H_s, \rho] + \frac{1}{2} \sum_{\alpha} \left([L_{\alpha}\rho, L_{\alpha}^{\dagger}] + [L_{\alpha}, \rho L_{\alpha}^{\dagger}] \right) \quad (\text{B.30})$$

with constant operator coefficients L_{α} , generates a completely positive semigroup [113], i.e. it conserves the intrinsic properties of ρ as a density operator, namely

$$\rho^{\dagger} = \rho \quad \text{Hermiticity,} \quad (\text{B.31a})$$

$$\text{Tr}\rho = 1 \quad \text{normalization} \quad (\text{B.31b})$$

$$0 \leq \rho_{ii} \leq 1 \quad \text{positivity.} \quad (\text{B.31c})$$

In particular the conservation of positivity is not ensured by Eq. (B.29), and it could in general generate unphysical solutions with violated positivity of the diagonal density matrix elements ρ_{ii} . This is however a transient effect, whereas Eq. (B.29) is by definition valid, only after an initial time span has elapsed.

B.3 Master equation in Floquet representation

Adapted to the relevant degrees of freedom of the isolated Floquet system, the master equation is represented in the periodic parts $|u_i(t)\rangle$ of the Floquet states. We recall that those constitute a complete orthonormal set of basis states. Applying the eigenequation (2.25) of the Floquet operator $\mathcal{H}(t) = H(t) - i\hbar\partial/\partial t$, the lhs of Eq. (B.29) combined with the first

term on the rhs reads in this basis

$$\begin{aligned}
\left\langle u_i(t) \left| \frac{\partial \rho}{\partial t} + \frac{i}{\hbar} [H_s(t), \rho(t)] \right| u_j(t) \right\rangle &= \left\langle u_i(t) \left| \frac{\partial \rho}{\partial t} \right| u_j(t) \right\rangle + \frac{i}{\hbar} \left\langle u_i(t) \left| \left(\varepsilon_i - i\hbar \frac{\partial}{\partial t} \right) \rho(t) \right| u_j(t) \right\rangle \\
&\quad - \frac{i}{\hbar} \left\langle u_i(t) \left| \rho(t) \left(\varepsilon_j + i\hbar \frac{\partial}{\partial t} \right) \right| u_j(t) \right\rangle \\
&= \frac{\partial}{\partial t} \rho_{ij}(t) + \frac{i}{\hbar} \varepsilon_{ij} \rho_{ij}(t). \tag{B.32}
\end{aligned}$$

We have introduced the short-hand notation $\varepsilon_{ij} = \varepsilon_i - \varepsilon_j$ for the quasienergy spacings. Secondly, with $U_s(t, t_0) |u_j(t_0)\rangle = e^{-i\varepsilon_j(t-t_0)/\hbar} |u_j(t)\rangle$, the matrix elements for the rhs of Eq. (B.29) become

$$\langle u_i(t) | A(t) \tilde{A}(t-t', t) \rho(t) | u_j(t) \rangle = \sum_{k,l} A_{ik}(t) A_{kl}(t-t') \rho_{lj}(t) e^{i\varepsilon_{lk}t'/\hbar} \tag{B.33a}$$

$$\langle u_i(t) | \tilde{A}(t-t', t) \rho(t) A(t) | u_j(t) \rangle = \sum_{k,l} A_{ik}(t-t') \rho_{kl}(t) A_{lj}(t) e^{i\varepsilon_{ki}t'/\hbar} \tag{B.33b}$$

$$\langle u_i(t) | \rho(t) \tilde{A}(t-t', t) A(t) | u_j(t) \rangle = \sum_{k,l} \rho_{ik}(t) A_{kl}(t-t') A_{lj}(t) e^{i\varepsilon_{lk}t'/\hbar} \tag{B.33c}$$

$$\langle u_i(t) | A(t) \rho(t) \tilde{A}(t-t', t) | u_j(t) \rangle = \sum_{k,l} A_{ik}(t) \rho_{kl}(t) A_{lj}(t-t') e^{i\varepsilon_{jl}t'/\hbar}. \tag{B.33d}$$

The time-periodic matrix elements $A_{ij}(t) = \langle u_i(t) | A | u_j(t) \rangle$ are expanded in a Fourier series

$$A_{ij}(t) = \sum_{K,M} e^{i(M-K)\omega t} \langle u_i(K) | A | u_j(M) \rangle \tag{B.34}$$

$$= \sum_L e^{iL\omega t} \sum_K \langle u_i(K) | A | u_j(K+L) \rangle = \sum_L e^{iL\omega t} A_{ij}(L) \tag{B.35}$$

based on the expansion of the periodic states $|u_i(t)\rangle = \sum_K e^{iK\omega t} |u_i(K)\rangle$. The coefficients $A_{ij}(L)$ have the property $A_{ij}(-L) = A_{ji}^*(L)$. The Floquet representation of the master equation becomes

$$\begin{aligned}
\left(\frac{\partial}{\partial t} + \frac{i}{\hbar} \varepsilon_{ij} \right) \rho_{ij}(t) &= -\frac{\gamma^2}{\hbar^2} \sum_{k,l,M,L} e^{i(M+L)\omega t} \\
&\cdot \left(\begin{aligned}
&A_{ik}(M) A_{kl}(L) \rho_{lj}(t) \int_0^\infty dt' G(t') e^{i(\varepsilon_{lk} - L\hbar\omega)t'/\hbar} \\
&- A_{ik}(L) \rho_{kl}(t) A_{lj}(M) \int_0^\infty dt' G(t') e^{i(\varepsilon_{ki} - L\hbar\omega)t'/\hbar} \\
&+ \rho_{ik}(t) A_{kl}(L) A_{lj}(M) \int_0^\infty dt' G^*(t') e^{i(\varepsilon_{lk} - L\hbar\omega)t'/\hbar} \\
&- A_{ik}(M) \rho_{kl}(t) A_{lj}(L) \int_0^\infty dt' G^*(t') e^{i(\varepsilon_{jl} - L\hbar\omega)t'/\hbar}
\end{aligned} \right). \tag{B.36}
\end{aligned}$$

The correlation function $G(t)$ appears in Eq. (B.36) in terms of its Laplace transform, which is related to the Fourier transform

$$G(t) = \int_{-\infty}^{\infty} dE g(E) e^{iEt/\hbar} \quad \text{with} \quad (\text{B.37})$$

$$g(E) = \frac{1}{2\pi\hbar} \int_{-\infty}^{\infty} dt G(t) e^{-iEt/\hbar} \quad (\text{B.38})$$

via the relation

$$\int_0^{\infty} dt' G(t') e^{-iEt'/\hbar} = \lim_{\delta \rightarrow 0} \int_{-\infty}^{\infty} dE' \int_0^{\infty} dt' g(E') e^{i(E'-E+i\delta)t'/\hbar} \quad (\text{B.39})$$

$$= i\hbar \lim_{\delta \rightarrow 0} \int_{-\infty}^{\infty} dE' \frac{g(E')}{E' - E + i\delta} \quad (\text{B.40})$$

$$= \pi\hbar g(E) + i\hbar \mathcal{P} \int_{-\infty}^{\infty} dE' \frac{g(E')}{E' - E}. \quad (\text{B.41})$$

Inserted in Eq. (B.36), the first term of (B.41) implicitly describes thermal transition processes between individual Floquet states. The other term, the Cauchy principal value, is responsible for shifts of the quasienergies with respect to the original spectrum of the isolated system, which are known as the *Lamb shifts* in quantum optics [77]. In Appendix C we explicitly take into account the Lamb shifts in the master equation. Especially at avoided crossings their influence on the asymptotic state of time-periodic systems can be important, as is demonstrated in Appendix E. However, in many applications their contribution is usually disregarded, being of the order $\mathcal{O}(\gamma^2)$. In time-independent systems in the weak-coupling limit they only influence the non-diagonal density matrix elements, but not the asymptotic occupations [77]. Without the Lamb shifts, the equation of motion reads

$$\begin{aligned} \left(\frac{\partial}{\partial t} + \frac{i}{\hbar} \varepsilon_{ij} \right) \rho_{ij}(t) &= -\pi \frac{\gamma^2}{\hbar} \sum_{k,l,M,L} e^{i(M+L)\omega t} \left(A_{ik}(M) A_{kl}(L) \rho_{lj}(t) g(L\hbar\omega - \varepsilon_{lk}) \right. \\ &\quad - A_{ik}(L) \rho_{kl}(t) A_{lj}(M) g(L\hbar\omega - \varepsilon_{ki}) \\ &\quad + \rho_{ik}(t) A_{kl}(L) A_{lj}(M) g(-L\hbar\omega + \varepsilon_{lk}) \\ &\quad \left. - A_{ik}(M) \rho_{kl}(t) A_{lj}(L) g(-L\hbar\omega + \varepsilon_{jl}) \right). \end{aligned} \quad (\text{B.42})$$

These terms can be simplified by the thermodynamic transition rates

$$R_{lj;ki}(t) := \sum_L R_{lj;ki}(L) e^{iL\omega t} \quad \text{with} \quad (\text{B.43})$$

$$R_{lj;ki}(L) := \sum_K R_{lj;ki}^{(K)}(L) = 2\pi \frac{\gamma^2}{\hbar} \sum_K A_{lj}(K+L) A_{ki}^*(K) g(\varepsilon_{ik} - K\hbar\omega), \quad (\text{B.44})$$

($L, K \in \mathbb{Z}$) which allow to simplify e.g.

$$\pi \frac{\gamma^2}{\hbar} \sum_K A_{ik}(K+L) \underbrace{A_{kl}(-K)}_{A_{ik}^*(K)} g(\varepsilon_{kl} - K\hbar\omega) = \frac{1}{2} R_{ik;lk}(L) \quad (\text{B.45})$$

$$\pi \frac{\gamma^2}{\hbar} \sum_K \underbrace{A_{lj}(-K+L)}_{A_{jl}^*(K-L)} A_{kl}(K) g(\varepsilon_{lk} - K\hbar\omega) = \frac{1}{2} R_{jl;kl}^*(-L) \quad (\text{B.46})$$

and the final form of the *Floquet-Markov master equation* is obtained:

$$\left(\frac{\partial}{\partial t} + \frac{i}{\hbar} \varepsilon_{ij} \right) \rho_{ij}(t) = \quad (\text{B.47})$$

$$- \frac{1}{2} \sum_{k,l} \left(\rho_{lj}(t) R_{ik;lk}(t) + \rho_{il}(t) R_{jk;lk}^*(t) - \rho_{kl}(t) \left(R_{lj;ki}(t) + R_{ki;lj}^*(t) \right) \right).$$

B.4 Rate equations for the asymptotic state

The elements

$$M_{ij;kl} := \frac{1}{2} \left(\sum_m R_{im;km} \delta_{jl} + \sum_m R_{jm;lm}^* \delta_{ik} - R_{lj;ki} - R_{ki;lj}^* \right) + \frac{i}{\hbar} \varepsilon_{ij} \delta_{ik} \delta_{jl} \quad (\text{B.48})$$

of the coefficient matrix $\mathbf{M}(t)$ in the coupled set (B.47) of linear first-order differential equations,

$$\dot{\rho}_{ij} = - \sum_{k,l} M_{ij;kl}(t) \rho_{kl}, \quad (\text{B.49})$$

are periodic with the period τ and therefore employ the Floquet theorem. Accordingly, Eq. (B.49) has a complete set of solutions, each of which can be factorized into a product of a relaxation factor $e^{\sigma_n t}$ and a periodic function $p_{ij;n}(t)$. The general solution of Eq. (B.47) is

$$\rho_{ij}(t) = \sum_n a_n e^{\sigma_n t} p_{ij;n}(t). \quad (\text{B.50})$$

If $\mathbf{U}(t+\tau, t) = \hat{\mathcal{T}} \exp \left(\int_t^{t+\tau} dt' \mathbf{M}(t') \right)$ is diagonalizable, all functions $p_{ij;n}(t)$ are periodic with period τ . Otherwise, these are in general ‘polynoms’ with periodic coefficients [46, 47].

The general solution (B.50) has to fulfil the properties (B.31) of a density matrix at all times t . Positive real parts of the Floquet exponents, $\text{Re}(\sigma_n) > 0$, are incompatible with these requirements, as well as the combination of $\text{Re}(\sigma_n) = 0$ with a finite order of the ‘polynoms’ $p_{ij;n}(t)$, i.e. for $\text{Re}(\sigma_n) = 0$ the functions $p_{ij;n}(t)$ are truly periodic. Solutions with a finite imaginary part of the Floquet exponent, $\text{Im}(\sigma_n) \neq 0$, can only occur in complex conjugate pairs to ensure real-valued diagonal elements $\rho_{ii}(t)$. For the same reason, the trace $\sum_i p_{ii;n}$ vanishes, if $\text{Im}(\sigma_n)$ is incommensurable with the frequency $\omega = 2\pi/\tau$.

Solutions with $\text{Re}(\sigma_n) < 0$ decay in the course of time. Among these, the fastest decaying eigensolution $e^{\sigma_1 t} p_{ij;1}(t)$ is of particular interest for the Markov approximation, as its decay rate $-\text{Re}(\sigma_1) = |\text{Re}(\sigma_1)| = \max_n(|\text{Re}(\sigma_n)|)$ determines the upper bound for the relaxation rate of the system. Thus,

$$-\text{Re}(\sigma_1)\tau_c \ll 1 \quad (\text{B.51})$$

is an alternative formulation of the Markov criterion.

As shown in the following section, Eq. (B.47) preserves the norm of ρ and so at least one solution with $\text{Re}(\sigma_0) = 0$ exists. This is the asymptotic solution ruling the long-time behavior of the system. It holds the preserved trace $\sum_i p_{ii;0}(t) = 1$. Consequently, the traces of the transient solutions on the contrary are zero. The question, whether $\text{Im}(\sigma_0) \neq 0$ in the asymptotic solution is allowed, cannot be answered by implication. In principle, a solution pair with finite imaginary parts $\pm i\omega_0$,

$$\rho_{ij}(t) = a_0 p_{ij;0}(t) + a_1 e^{i\omega_0 t} p_{ij;\alpha}(t) + a_2 e^{-i\omega_0 t} p_{ij;\beta}(t) \quad (\text{B.52})$$

with vanishing traces $\sum_i p_{ii;\alpha}(t) = \sum_i p_{ii;\beta}(t) = 0$ is compatible with the aforementioned requirements. Notwithstanding their possible existence, we have not detected such solution types and we will here regard the periodic density matrix

$$\rho_{ij}(t) \equiv p_{ij;0}(t) = \sum_K e^{iK\omega t} \rho_{ij}(K) \quad (\text{B.53})$$

as the general asymptotic solution of Eq. (B.47). This equates to a suited choice of initial conditions. Note, that the asymptotic solution might be even denoted as stationary, in reference to its vanishing relaxation rate $\text{Re}(\sigma_0) = 0$.

Using the Fourier expansions (B.53) and (B.43) of the density matrix and of the rates, the differential equations (B.47) are cast into a system of linear equations for the Fourier components,

$$\begin{aligned} \frac{i}{\hbar} (K\hbar\omega + \varepsilon_{ij}) \rho_{ij}(K) &= -\frac{1}{2} \sum_{k,l,L} \left(\rho_{lj}(K-L) R_{ik;lk}(L) + \rho_{il}(K-L) R_{jk;lk}^*(-L) \right. \\ &\quad \left. - \rho_{kl}(K-L) \left(R_{lj;ki}(L) + R_{ki;lj}^*(-L) \right) \right). \end{aligned} \quad (\text{B.54})$$

The rates on the rhs of this equation are of the order $\mathcal{O}(\gamma^2)$, whereas the lhs is of the order $\mathcal{O}(\gamma^0)$. In the spirit of the weak-coupling assumption, the rates are regarded small with respect to the relevant rates of change in the isolated system, in particular to the driving frequency ω on the lhs. Consequently, the leading Fourier coefficients

$$\rho_{ij} := \rho_{ij}(K=0) \quad (\text{B.55})$$

dominate all other contributions $\rho_{ij}(K \neq 0)$, which account for small temporal oscillations about the average value ρ_{ij} . When neglecting them and consistently also the rates $R_{lj;ki}(K \neq 0)$, the system of homogeneous linear equations for the time-independent ρ_{ij} remains

$$0 = \frac{1}{2} \sum_{k,l} \left(\rho_{lj} R_{ik;lk} + \rho_{il} R_{jk;lk}^* - \rho_{kl} \left(R_{lj;ki} + R_{ki;lj}^* \right) \right) + \frac{i}{\hbar} \varepsilon_{ij} \rho_{ij}, \quad (\text{B.56})$$

with the rates

$$R_{lj;ki} := R_{lj;ki}(K = 0) = \frac{1}{\tau} \int_0^\tau dt R_{lj;ki}(t). \quad (\text{B.57})$$

B.5 Some properties of Eqs. (B.47) and (B.56)

Equation (B.47) preserves the norm of ρ ,

$$\begin{aligned} \frac{\partial}{\partial t} \sum_i \rho_{ii} &= -\frac{1}{2} \sum_{k,l,i} \left(R_{ik;lk}(t) \rho_{li} + R_{ik;lk}^*(t) \rho_{il} - (R_{li;ki}(t) + R_{ki;li}^*(t)) \rho_{lk} \right) \\ &= -\frac{1}{2} \sum_{l,i} \left(\rho_{li} \sum_k R_{ik;lk}(t) + \rho_{il} \sum_k R_{ik;lk}^*(t) \right) + \frac{1}{2} \sum_{k,l} \left(\rho_{kl} \sum_i R_{li;ki}(t) + \rho_{kl} \sum_i R_{ki;li}^*(t) \right) \\ &= -\frac{1}{2} \sum_{k,l} \left(\rho_{kl} \sum_i R_{li;ki}(t) + \rho_{kl} \sum_i R_{ki;li}^*(t) \right) + \frac{1}{2} \sum_{k,l} \left(\rho_{kl} \sum_i R_{li;ki}(t) + \rho_{kl} \sum_i R_{ki;li}^*(t) \right) \\ &= 0, \end{aligned}$$

as well as its Hermiticity,

$$\begin{aligned} \frac{\partial}{\partial t} (\rho_{ij}^* - \rho_{ji}) &= \sum_{k,l} (M_{ij;kl}^*(t) \rho_{kl}^* - M_{ji;kl}(t) \rho_{kl}) = \sum_{k,l} (M_{ji;lk}(t) \rho_{lk} - M_{ji;kl}(t) \rho_{kl}) \\ &= 0, \end{aligned}$$

where in the second line the initial condition $\rho_{kl}^*(0) = \rho_{lk}(0)$ has been used. Using the Hermiticity of ρ , the equations (B.56) for the complex valued ρ_{ij} can be transformed into equivalent equations for the quantities $\{\rho_{ii}, \text{Re}\rho_{ij}, \text{Im}\rho_{ij} \ (i < j)\}$,

$$0 = \sum_k M_{ii;kk} \rho_{kk} + \sum_{k,l,k < l} \left(2\text{Re}(M_{ii;kl}) \text{Re}\rho_{kl} - 2\text{Im}(M_{ii;kl}) \text{Im}\rho_{kl} \right) \quad (\text{B.58a})$$

$$0 = \sum_k \text{Re}M_{ij;kk} \rho_{kk} + \sum_{k,l,k < l} \left(\text{Re}(M_{ij;kl} + M_{ij;lk}) \text{Re}\rho_{kl} - \text{Im}(M_{ij;kl} - M_{ij;lk}) \text{Im}\rho_{kl} \right)$$

$$0 = \sum_k \text{Im}M_{ij;kk} \rho_{kk} + \sum_{k,l,k < l} \left(\text{Im}(M_{ij;kl} + M_{ij;lk}) \text{Re}\rho_{kl} + \text{Re}(M_{ij;kl} - M_{ij;lk}) \text{Im}\rho_{kl} \right).$$

The coefficients $M_{ij;kl}$ have the following properties

$$M_{ii;kl}^*(t) = M_{ii;lk}(t) \quad (\text{B.59a})$$

$$M_{ij;kk}^*(t) = M_{ji;kk}(t) \quad (\text{B.59b})$$

$$M_{ij;kl}^*(t) = M_{ji;lk}(t) \quad (\text{B.59c})$$

$$(M_{ij;kl}(t) \pm M_{ij;lk}(t))^* = \pm(M_{ji;kl}(t) \pm M_{ji;lk}(t)) . \quad (\text{B.59d})$$

C Lamb shifts in the Floquet-Markov master equation

The interaction between the relevant system and the heat bath induces a renormalization of the original spectrum of the isolated system. As a consequence, the heat bath experiences a perturbed spectrum that deviates from the original spectrum by the *Lamb shifts*. In this section we explicitly include the Lamb shifts in the Floquet-Markov master equation and the rate equation for its asymptotic solution. The starting point is Eq. (B.36), where we no longer neglect the contributions of the Cauchy principal values originating from the Laplace transformations,

$$\int_0^\infty dt' G(t') e^{-iEt'/\hbar} \stackrel{\text{(B.41)}}{=} \pi\hbar g(E) + i\hbar\mathcal{P} \int_{-\infty}^\infty dE' \frac{g(E')}{E' - E} \quad (\text{C.1})$$

$$= \pi\hbar g(E) - i\hbar^2 (\Delta'(E) + \Delta_2(E)) \quad (\text{C.2})$$

$$\int_0^\infty dt' G^*(t') e^{-iEt'/\hbar} \stackrel{\text{(B.41)}}{=} \pi\hbar g(-E) + i\hbar\mathcal{P} \int_{-\infty}^\infty dE' \frac{g(-E')}{E' - E} \quad (\text{C.3})$$

$$= \pi\hbar g(-E) - i\hbar^2 (\Delta'(E) + \Delta_1(E)) . \quad (\text{C.4})$$

Herein the following Lamb shift terms have been introduced

$$\Delta_1(E) := -\frac{1}{\pi\hbar}\mathcal{P} \int_0^\infty dE' J(E'/\hbar) \frac{1}{E' - E} \quad (\text{C.5a})$$

$$\Delta_2(E) := \frac{1}{\pi\hbar}\mathcal{P} \int_0^\infty dE' J(E'/\hbar) \frac{1}{E' + E} \quad (\text{C.5b})$$

$$\Delta'(E) := -\frac{1}{\pi\hbar}\mathcal{P} \int_0^\infty dE' J(E'/\hbar) \frac{n_\beta(E')}{E' - E} + \frac{1}{\pi\hbar}\mathcal{P} \int_0^\infty dE' J(E'/\hbar) \frac{n_\beta(E')}{E' + E} , \quad (\text{C.5c})$$

where the relation $g(E) = n_\beta(E)J(E/\hbar)/\pi$ between the correlation function $g(E)$, the thermal occupation number $n_\beta(E)$ and the spectral density $J(\omega)$ of the boson bath is employed. Including these terms, Eq. (B.36) becomes

$$\left(\frac{\partial}{\partial t} + \frac{i}{\hbar}\varepsilon_{ij} \right) \rho_{ij}(t) = -\frac{\gamma^2}{\hbar^2} \sum_{k,l,M,L} e^{i(M+L)\omega t} \quad (\text{C.6})$$

$$\cdot \left(\begin{aligned} & A_{ik}(M)A_{kl}(L)\rho_{lj}(t) \left(\pi\hbar g(\zeta_{klL}) - i\hbar^2 (\Delta'(\zeta_{klL}) + \Delta_2(\zeta_{klL})) \right) \\ & - A_{ik}(L)\rho_{kl}(t)A_{lj}(M) \left(\pi\hbar g(\zeta_{ikL}) - i\hbar^2 (\Delta'(\zeta_{ikL}) + \Delta_2(\zeta_{ikL})) \right) \\ & + \rho_{ik}(t)A_{kl}(L)A_{lj}(M) \left(\pi\hbar g(-\zeta_{klL}) - i\hbar^2 (\Delta'(\zeta_{klL}) + \Delta_1(\zeta_{klL})) \right) \\ & - A_{ik}(M)\rho_{kl}(t)A_{lj}(L) \left(\pi\hbar g(-\zeta_{ljL}) - i\hbar^2 (\Delta'(\zeta_{ljL}) + \Delta_1(\zeta_{ljL})) \right) \end{aligned} \right) .$$

We have introduced the short-hand notation $\zeta_{klL} = \varepsilon_k - \varepsilon_l + L\hbar\omega$ and define the quantities

$$S_{lj;ki}(t) := \sum_L S_{lj;ki}(L) e^{iL\omega t} \quad \text{with} \quad (\text{C.7})$$

$$S_{lj;ki}(L) := 2\gamma^2 \sum_K A_{lj}(K+L) A_{ki}^*(K) (\Delta'(-\zeta_{kiK}) - \Delta_1(\zeta_{kiK})) \quad (\text{C.8})$$

($L, K \in \mathbb{Z}$) in close analogy to the definitions of the rates $R_{lj;ki}(t)$ in Eqs. (B.43) and (B.44). The individual Lamb shift terms in Eq. (C.6) can be simplified with the help of the relations $\Delta_2(-E) = -\Delta_1(E)$ and $\Delta'(-E) = -\Delta'(E)$,

$$i\gamma^2 \sum_L A_{ik}(K+L) A_{lk}^*(L) (\Delta'(-\zeta_{lkL}) + \underbrace{\Delta_2(-\zeta_{lkL})}_{-\Delta_1(\zeta_{lkL})}) = \frac{i}{2} S_{ik;lk}(K) \quad (\text{C.9a})$$

$$i\gamma^2 \sum_L A_{lj}(L+K) A_{ki}^*(L) (\Delta'(-\zeta_{kiL}) + \underbrace{\Delta_2(-\zeta_{kiL})}_{-\Delta_1(\zeta_{kiL})}) = \frac{i}{2} S_{lj;ki}(K) \quad (\text{C.9b})$$

$$i\gamma^2 \sum_L A_{jl}^*(L-K) A_{kl}(L) (\underbrace{\Delta'(\zeta_{klL})}_{-\Delta'(-\zeta_{klL})} + \Delta_1(\zeta_{klL})) = -\frac{i}{2} S_{jl;kl}^*(-K) \quad (\text{C.9c})$$

$$i\gamma^2 \sum_L A_{ki}^*(L-K) A_{lj}(L) (\underbrace{\Delta'(\zeta_{ljL})}_{-\Delta'(-\zeta_{ljL})} + \Delta_1(\zeta_{ljL})) = -\frac{i}{2} S_{ki;lj}^*(-K). \quad (\text{C.9d})$$

Finally, replacing the rates $R_{lj;ki}$ by the extended rates

$$\hat{R}_{lj;ki} := R_{lj;ki} - iS_{lj;ki}, \quad (\text{C.10})$$

the form of the Floquet-Markov master equation is recovered in the same form as Eq. (B.47),

$$\left(\frac{\partial}{\partial t} + \frac{i}{\hbar} \varepsilon_{ij} \right) \rho_{ij}(t) = -\frac{1}{2} \sum_{k,l} \left(\rho_{lj}(t) \hat{R}_{ik;lk}(t) + \rho_{il}(t) \hat{R}_{jk;lk}^*(t) - \rho_{kl}(t) \left(\hat{R}_{lj;ki}(t) + \hat{R}_{ki;lj}^*(t) \right) \right). \quad (\text{C.11})$$

Since the coefficients $S_{lj;ki}(t)$ are also time-periodic, the Floquet theorem still applies to this differential equation and the reasoning of Appendix B for its asymptotic solution still holds: it is time-periodic and satisfies an extended system of rate equations for the individual Fourier components $\rho_{ij}(K)$. Again, we neglect the small temporal oscillations about the average values $\rho_{ij} \equiv \rho_{ij}(K=0)$ by setting the components $\rho_{ij}(K \neq 0)$ zero. This approximation requires the extended rates $\hat{R}_{lj;ki}(K) \sim \mathcal{O}(\gamma^2)$ to be small against ω . We obtain the already known form (B.56) for the rate equation,

$$0 = \frac{1}{2} \sum_{k,l} \left(\rho_{lj} \hat{R}_{ik;lk} + \rho_{il} \hat{R}_{jk;lk}^* - \rho_{kl} \left(\hat{R}_{lj;ki} + \hat{R}_{ki;lj}^* \right) \right) + \frac{i}{\hbar} \varepsilon_{ij} \rho_{ij}, \quad (\text{C.12})$$

but wherein now the original rates $R_{lj;ki}$ replaced by the extended rates $\hat{R}_{lj;ki} := \hat{R}_{lj;ki}(K=0)$. In the short-hand notation $0 = \sum_{k,l} \hat{M}_{ij;kl} \rho_{kl}$ the coefficient matrix $\hat{M}_{ij;kl} = M_{ij;kl} - iN_{ij;kl}$ differs from the original $M_{ij;kl}$ of Def. (B.48) by the additional term

$$N_{ij;kl} := \frac{1}{2} \left(\sum_m S_{im;km} \delta_{jl} + \sum_m S_{jm;lm}^* \delta_{ik} - S_{lj;ki} - S_{ki;lj}^* \right). \quad (\text{C.13})$$

Note, that the $N_{ij;kl}$ behave opposite to the $M_{ij;kl}$ under complex conjugation, such that the properties (B.59) of the latter are passed to $\hat{M}_{ij;kl}$:

$$N_{ij;kl}^* = -N_{ji;lk} \quad (\text{C.14a})$$

$$\stackrel{(\text{B.59c})}{\Rightarrow} \hat{M}_{ij;kl}^* = \hat{M}_{ji;lk} \quad (\text{C.14b})$$

$$(N_{ij;kl} \pm N_{ij;lk})^* = \mp (N_{ji;kl} \pm N_{ji;lk}) \quad (\text{C.14c})$$

$$\stackrel{(\text{B.59d})}{\Rightarrow} (\hat{M}_{ij;kl} \pm \hat{M}_{ij;lk})^* = \pm (\hat{M}_{ji;kl} \pm \hat{M}_{ji;lk}) \quad (\text{C.14d})$$

Hence, also the conversion of Eq. (C.12) into a system of equations for the quantities $\{\rho_{ii}, \text{Re}\rho_{ij}, \text{Im}\rho_{ij} \ (i < j)\}$ is analogous to Eq. (B.58).

We now ask for the reduction of the rate equations (C.12) to a system of rate equations for the diagonal densities $p_i := \rho_{ii}$, under the assumption that the rates $|\hat{R}_{lj;ki}|$ are small compared to all quasienergy spacings. If the spacings ε_{ij} are dominant in the coefficient matrix of the rate equations (C.12), the corresponding non-diagonal densities ρ_{ij} can be neglected. Remarkably, in the remaining rate equations for the diagonal densities the contributions of the Lamb shifts vanish:

$$0 = \frac{1}{2} \sum_k \left(\rho_{ii} (R_{ik} - iS_{ik}) + \rho_{ii} (R_{ik}^* + iS_{ik}^*) - \rho_{kk} (R_{ki} - iS_{ki} + R_{ki}^* + iS_{ki}^*) \right) \quad (\text{C.15})$$

$$= p_i \sum_k R_{ik} - \sum_k p_k R_{ki}, \quad (\text{C.16})$$

using that the quantities $S_{ik} := S_{ik;ik}$ are real-valued, like the original rates $R_{ik} = R_{ik;ik}$. That means, in this limit of very weak coupling the Lamb shifts have no influence on the asymptotic state. This is similar to the situation in time-independent systems in the weak-coupling limit, where the Lamb shifts only influence the non-diagonal density matrix elements, but not the asymptotic occupations [77]. On the other hand, if the effective coupling strength exceeds certain quasienergy spacings, which is especially likely to happen at avoided crossings, the reduction to Eq. (C.16) is not allowed, since certain non-diagonal elements ρ_{ij} of the Floquet density matrix cannot be neglected and influence the diagonal elements. Then the Lamb shifts can cause significant changes in the asymptotic state, compared to the asymptotic solution of the original Floquet-Markov master equation. The rate equations for such a situation are analyzed in Appendix E.

D Rate equations at avoided crossings

The Floquet basis is the appropriate representation for the time-periodic asymptotic state $\rho(t)$ of the driven system. As it already contains the explicit time-dependence, the Floquet density matrix elements ρ_{ij} are approximately constant in the asymptotic state and then satisfy the rate equations (3.26) (Eq. (B.56)) with time-independent rates $R_{lj;ki}$. However, in the vicinity of avoided crossings this representation is not perfectly suited, because the hybridization of the two involved Floquet states, the adiabatic states $|u_{a,b}\rangle$, affects a multitude of rates $R_{lj;ki}$ in Eq. (3.26), where one of the indices is a or b . In order to remove the resulting sensitive parameter dependence, the rate equations (3.26) have to be represented in the local diabatic basis of the avoided crossing. We recall that the terms diabatic and adiabatic basis refer not only to the two states of the avoided crossing, but to the entire basis including the diabatic states $|\bar{u}_{1,2}\rangle$ in the first case, and containing the adiabatic states $|u_{a,b}\rangle$ in the latter case. All quantities in the diabatic basis are designated with an overbar.

The following derivation is taken from Ref. [25], with some of the transformations performed explicitly here. The starting point is the still representation-independent form (B.29) of the master equation. Firstly, we consider its lhs combined with the first term of the rhs. For all matrix elements omitting the states of the avoided crossing one recovers the same form as in Eq. (B.32),

$$\left\langle \bar{u}_i(t) \left| \frac{\partial \rho}{\partial t} + \frac{i}{\hbar} [H_s(t), \rho(t)] \right| \bar{u}_j(t) \right\rangle = \frac{\partial \rho_{ij}}{\partial t} + \frac{i}{\hbar} \bar{\varepsilon}_{ij} \bar{\rho}_{ij} \quad i, j \notin \{1, 2\}. \quad (\text{D.1})$$

In the subspace of the avoided crossing, we make use of the matrix (3.33) of the Floquet operator \mathcal{H}^{ac} in the basis of the diabatic states, e.g. $(H_s(t) - i\hbar\partial/\partial t) |\bar{u}_1(t)\rangle = \mathcal{H}^{\text{ac}}(t) |\bar{u}_1(t)\rangle = \bar{\varepsilon}_1 |\bar{u}_1(t)\rangle + \Delta/2 |\bar{u}_2(t)\rangle$ with the minimal spacing Δ of the avoided crossing. Thus, instead of Eq. (B.32) one obtains

$$\left\langle \bar{u}_i(t) \left| \frac{\partial \rho}{\partial t} + \frac{i}{\hbar} [H_s(t), \rho(t)] \right| \bar{u}_j(t) \right\rangle = \begin{cases} \frac{\partial \rho_{1j}}{\partial t} + \frac{i}{\hbar} (\bar{\varepsilon}_{1j} \bar{\rho}_{1j} + \frac{\Delta}{2} \bar{\rho}_{2j}) & i = 1, j \notin \{1, 2\} \\ \frac{\partial \rho_{2j}}{\partial t} + \frac{i}{\hbar} (\bar{\varepsilon}_{2j} \bar{\rho}_{2j} + \frac{\Delta}{2} \bar{\rho}_{1j}) & i = 2, j \notin \{1, 2\} \end{cases} \quad (\text{D.2})$$

and

$$\left\langle \bar{u}_i(t) \left| \frac{\partial \rho}{\partial t} + \frac{i}{\hbar} [H_s(t), \rho(t)] \right| \bar{u}_j(t) \right\rangle = \frac{\partial}{\partial t} \begin{pmatrix} \bar{\rho}_{11} & \bar{\rho}_{12} \\ \bar{\rho}_{21} & \bar{\rho}_{22} \end{pmatrix} + \frac{i}{\hbar} \begin{pmatrix} -i\Delta \text{Im} \bar{\rho}_{12} & -\frac{\Delta}{2} (\bar{\rho}_{11} - \bar{\rho}_{22} - 2d\bar{\rho}_{12}) \\ \frac{\Delta}{2} (\bar{\rho}_{11} - \bar{\rho}_{22} - 2d\bar{\rho}_{21}) & i\Delta \text{Im} \bar{\rho}_{12} \end{pmatrix}. \quad (\text{D.3})$$

We recall the definition (3.37) of the dimensionless distance d to the center of the avoided crossing. The remaining density matrix elements are determined by the Hermiticity of ρ .

To represent the remaining terms on the rhs of Eq. (B.29), the same transformations are made as from Eq. (B.33) to Eq. (B.47). However, in the diabatic basis the evaluation needs to be founded on the assumption, that the quasienergies $\varepsilon_{a,b}$ and their linearized branches $\bar{\varepsilon}_{1,2}$ differ only weakly, $\varepsilon_a \approx \varepsilon_b \approx \bar{\varepsilon}_1 \approx \bar{\varepsilon}_2$, and are consequently all set equal in the occurring phase factors $e^{-i\varepsilon_i t/\hbar}$. By that, the phase factors $e^{-i\varepsilon_i t/\hbar}$, which occur due to the action of the propagator on the diabatic states, can be set equal:

$$U_s(t, t_0) |\bar{u}_1(t_0)\rangle = (\alpha^2 e^{-i\varepsilon_a(t-t_0)/\hbar} + \beta^2 e^{-i\varepsilon_b(t-t_0)/\hbar}) |\bar{u}_1(t)\rangle \quad (\text{D.4})$$

$$+ \alpha\beta (e^{-i\varepsilon_a(t-t_0)/\hbar} - e^{-i\varepsilon_b(t-t_0)/\hbar}) |\bar{u}_2(t)\rangle \\ \approx e^{-i\bar{\varepsilon}_1(t-t_0)/\hbar} |\bar{u}_1(t)\rangle, \quad (\text{D.5})$$

making the respective matrix elements formally identical to those in Eqs. (B.33). The rhs of Eq. (B.36) is thereby reproduced form invariant. This consideration also indicates the limit of validity for the above approximation: the maximum error in the exponents is Δ . If $G(t)$ has already dropped to zero on the corresponding time scale \hbar/Δ , i.e. for $\tau_c \ll \hbar/\Delta$, the approximation is well-grounded. As we here take $\tau_c < 2\pi/\omega$ for granted, this presumption is fulfilled anyway. Eventually, the coupling-induced terms on the rhs of Eq. (B.29) have form invariant representations in the diabatic basis as compared to the Floquet basis,

$$-\frac{1}{2} \sum_{k,l} \left(\bar{\rho}_{lj} \bar{R}_{ik;lk} + \bar{\rho}_{il} \bar{R}_{jk;lk}^* - \bar{\rho}_{kl} \left(\bar{R}_{lj;ki} + \bar{R}_{ki;lj}^* \right) \right), \quad (\text{D.6})$$

compare the rhs of Eq. (B.47). The rates are defined according to Defs. (B.44) and (B.57), but now refer to the diabatic representation.

We ask for the asymptotic solution of the resulting differential equation, whose lhs is given by the differentiation (D.1)-(D.3) and whose rhs is (D.6). The same arguments as in Appendix B.4 apply, in particular we again neglect the small temporal oscillations of $\rho_{ij}(t)$ about the mean value $\bar{\rho}_{ij}$ and obtain a system of rate equations similar to those in Eq. (3.26), but with modified coherent terms:

$$0 = \frac{1}{2} \sum_{k,l} \left(\bar{\rho}_{lj} \bar{R}_{ik;lk} + \bar{\rho}_{il} \bar{R}_{jk;lk}^* - \bar{\rho}_{kl} \left(\bar{R}_{lj;ki} + \bar{R}_{ki;lj}^* \right) \right) \quad (\text{D.7})$$

$$+ \frac{i}{\hbar} \begin{cases} \bar{\varepsilon}_{ij} \bar{\rho}_{ij} & i, j \notin \{1, 2\} \\ (\bar{\varepsilon}_{1j} \bar{\rho}_{1j} + \frac{\Delta}{2} \bar{\rho}_{2j}) & i=1, j \notin \{1, 2\} \\ (\bar{\varepsilon}_{2j} \bar{\rho}_{2j} + \frac{\Delta}{2} \bar{\rho}_{1j}) & i=2, j \notin \{1, 2\} \\ -i\Delta \text{Im} \bar{\rho}_{12} & i=j=1 \\ i\Delta \text{Im} \bar{\rho}_{12} & i=j=2 \\ -\frac{\Delta}{2} (\bar{\rho}_{11} - \bar{\rho}_{22} - 2d\bar{\rho}_{12}) & i=1, j=2 \end{cases}$$

To further evaluate the rate terms in Eq. (D.7), the following presumptions are made in the parameter range throughout the avoided crossing:

- (i) The diabatic states $|\bar{u}_{1,2}\rangle$ are assumed to be independent of the parameter distance d from the center of the avoided crossing.
- (ii) Almost all quasienergy spacings are taken to be larger than the effective coupling strength to the heat bath, with the exception of the single quasienergy spacing ε_{ab} . The separation of the non-diagonal densities $\bar{\rho}_{ij}$ ($i \neq j$) in analogy to Eq. (3.26) is then possible, except of $\bar{\rho}_{12}$.
- (iii) The deviations between $\varepsilon_{a,b}$ and $\bar{\varepsilon}_{1,2}$ as well as the spacings ε_{ab} and $|\bar{\varepsilon}_{12}|$ are assumed to be tiny compared to the mean quasienergy spacing. All of them are treated as equal, $\varepsilon_a \approx \varepsilon_b \approx \bar{\varepsilon}_1 \approx \bar{\varepsilon}_2$, in the arguments of the correlation function $g(E)$ with the maximum error in $g(E)$ being Δ . Provided that $g(E)$ does not vary significantly on the scale Δ , i.e. $\Delta \ll \hbar/\tau_c$, the approximation is not critical. This is automatically satisfied since we restrict the consideration to cases $\hbar/\tau_c > \hbar\omega$.
- (iv) The matrix elements $\bar{A}_{12}(K)$ and $\bar{A}_{21}(K)$ as well as combinations like $\bar{A}_{1j}(K)\bar{A}_{2j}(K)$ or $\bar{A}_{j1}(K)\bar{A}_{2j}(K)$ are neglected. This approximation is possible, if the spatial structure of the states $|\bar{u}_1\rangle$ and $|\bar{u}_2\rangle$ is fundamentally different, e.g. if they arise from energetically widely separated states of the undriven system. Then, the matrix elements \bar{A}_{12} are very small and the matrix elements \bar{A}_{1j} and \bar{A}_{2j} have well-separated maxima in K -space. It follows that all rates like $\bar{R}_{12;ij}$, $\bar{R}_{1j;2j}$ are negligible. Only the real-valued rates \bar{R}_{11} , $\bar{R}_{1i} = \bar{R}_{i1}$, $\bar{R}_{1i;i1}$, $\bar{R}_{i1;1i}$ remain out of all the rates involving the state $|\bar{u}_1\rangle$. The same holds for the accordant rates referring to state $|\bar{u}_2\rangle$. Besides, $\bar{R}_{11;22}$ and $\bar{R}_{22;11}$ are still maintained.

By virtue of the assumption (ii) the non-diagonal densities $\bar{\rho}_{ij}$ ($i \neq j$) apart from $\bar{\rho}_{12}$ are neglected and only the following rate terms remain in Eqs. (D.7):

$$\begin{aligned}
& \frac{1}{2} \sum_{k,l} \left(\bar{\rho}_{lj} \bar{R}_{ik;lk} + \bar{\rho}_{il} \bar{R}_{jk;lk}^* - \bar{\rho}_{kl} (\bar{R}_{lj;ki} + \bar{R}_{ki;lj}^*) \right) \\
& = \begin{cases} \frac{1}{2} \sum_{k,l} \left(\bar{\rho}_{li} \bar{R}_{ik;lk} + \bar{\rho}_{il} \bar{R}_{ik;lk}^* - \bar{\rho}_{kl} (\bar{R}_{li;ki} + \bar{R}_{ki;li}^*) \right) & i=j \notin \{1,2\} \\ \frac{1}{2} \sum_{k,l} \left(\bar{\rho}_{l1} \bar{R}_{1k;lk} + \bar{\rho}_{1l} \bar{R}_{1k;lk}^* - \bar{\rho}_{kl} (\bar{R}_{l1;k1} + \bar{R}_{k1;l1}^*) \right) & i=j=1 \\ \frac{1}{2} \sum_{k,l} \left(\bar{\rho}_{l2} \bar{R}_{2k;lk} + \bar{\rho}_{2l} \bar{R}_{2k;lk}^* - \bar{\rho}_{kl} (\bar{R}_{l2;k2} + \bar{R}_{k2;l2}^*) \right) & i=j=2 \\ \frac{1}{2} \sum_{k,l} \left(\bar{\rho}_{l2} \bar{R}_{1k;lk} + \bar{\rho}_{1l} \bar{R}_{2k;lk}^* - \bar{\rho}_{kl} (\bar{R}_{l2;k1} + \bar{R}_{k1;l2}^*) \right) & i=1, j=2 \end{cases} \quad (\text{D.8})
\end{aligned}$$

and further

$$\begin{aligned} & \frac{1}{2} \sum_{k,l} \left(\bar{\rho}_{lj} \bar{R}_{ik;lk} + \bar{\rho}_{il} \bar{R}_{jk;lk}^* - \bar{\rho}_{kl} (\bar{R}_{lj;ki} + \bar{R}_{ki;lj}^*) \right) \\ &= \begin{cases} \bar{\rho}_{ii} \sum_k \bar{R}_{ik} - \sum_k \bar{\rho}_{kk} \bar{R}_{ki} & i=j \notin \{1,2\} \\ \bar{\rho}_{11} \sum_k \bar{R}_{1k} - \sum_k \bar{\rho}_{kk} \bar{R}_{k1} & i=j=1 \\ \bar{\rho}_{22} \sum_k \bar{R}_{2k} - \sum_k \bar{\rho}_{kk} \bar{R}_{k2} & i=j=2 \\ \frac{\bar{\rho}_{12}}{2} \left(\sum_k (\bar{R}_{1k} + \bar{R}_{2k}) - \bar{R}_{22;11} - \bar{R}_{11;22}^* \right) & i=1, j=2 \end{cases} \end{aligned} \quad (\text{D.9})$$

In combination with the coherent terms in Eqs. (D.7) these take the forms

$$0 = \bar{\rho}_{ii} \sum_k \bar{R}_{ik} - \sum_k \bar{\rho}_{kk} \bar{R}_{ki} \quad (\text{D.10a})$$

$$0 = \bar{\rho}_{11} \sum_k \bar{R}_{1k} - \sum_k \bar{\rho}_{kk} \bar{R}_{k1} + \frac{\Delta}{\hbar} \text{Im} \bar{\rho}_{12} \quad (\text{D.10b})$$

$$0 = \bar{\rho}_{22} \sum_k \bar{R}_{2k} - \sum_k \bar{\rho}_{kk} \bar{R}_{k2} - \frac{\Delta}{\hbar} \text{Im} \bar{\rho}_{12} \quad (\text{D.10c})$$

$$0 = \frac{1}{2} \bar{\rho}_{12} (\Gamma - i\Sigma) - i \frac{\Delta}{2\hbar} (\bar{\rho}_{11} - \bar{\rho}_{22} - 2d\bar{\rho}_{12}), \quad (\text{D.10d})$$

where the following definitions are used

$$\Gamma := \sum_k (\bar{R}_{1k} + \bar{R}_{2k}) - 2\text{Re} \bar{R}_{11;22} \quad (\text{D.11})$$

$$= \sum_{k \notin \{1,2\}} (\bar{R}_{1k} + \bar{R}_{2k}) + 2\pi \frac{\gamma^2}{\hbar} \sum_K |\bar{A}_{11}(K) - \bar{A}_{22}(K)|^2 g(-K\hbar\omega) > 0 \quad (\text{D.12})$$

$$\Sigma := -2\text{Im} \bar{R}_{11;22} \quad (\text{D.13})$$

The effective rate Γ basically measures the total probability flow away from the subspace of the avoided crossing. The quantity Σ is zero in the case of a symmetric driving, as is explained by the following arguments: for the symmetric Hamiltonian $H_s(-t) = H_s(t)$ the Schrödinger equation is invariant under time reversal and the periodic parts $|u_i(t)\rangle$ of the Floquet states can hence be chosen as even or odd functions of the time. This implies $A_{ii}(t) = A_{ii}(-t)$ for the diagonal matrix elements, and further $A_{ii}^*(K) = A_{ii}(-K) = A_{ii}(K)$ for their Fourier coefficients and eventually $R_{ii;jj} = R_{ii;jj}^*$. Thus, the rate $\bar{R}_{11;22}$ is real-valued, if $H_s(-t) = H_s(t)$ holds. Otherwise, the term Σ has a similar effect as the analogous term (E.7) originating from the Lamb shifts, see Appendix E.

Equation (D.10d) establishes the relation

$$\bar{\rho}_{12} = \frac{i\hbar\Gamma/\Delta + 2d}{(\hbar\Gamma/\Delta)^2 + 4d^2} (\bar{\rho}_{11} - \bar{\rho}_{22}) \quad (\text{D.14})$$

between the non-diagonal density $\bar{\rho}_{12}$ and the occupation imbalance $(\bar{\rho}_{11} - \bar{\rho}_{22})$. Inserting this into Eqs. (D.10b) and (D.10c) yields

$$0 = \bar{\rho}_{11} \left(R^{\text{ac}} + \sum_k \bar{R}_{1k} \right) - \sum_k \bar{\rho}_{kk} \bar{R}_{k1} + \bar{\rho}_{22} R^{\text{ac}} \quad (\text{D.15a})$$

$$0 = \bar{\rho}_{22} \left(R^{\text{ac}} + \sum_k \bar{R}_{2k} \right) - \sum_k \bar{\rho}_{kk} \bar{R}_{k2} + \bar{\rho}_{11} R^{\text{ac}} \quad (\text{D.15b})$$

with the effective rate R^{ac} defined as

$$R^{\text{ac}} := \frac{\Gamma}{(\hbar\Gamma/\Delta)^2 + 4d^2}. \quad (\text{D.16})$$

It replaces the direct rates between the two states of the avoided crossing, which under the above premises are negligible, $\bar{R}_{12} \approx \bar{R}_{21} \approx 0$. Finally, by means of the substitutions $\bar{R}_{12} \rightarrow R^{\text{ac}}$ and $\bar{R}_{21} \rightarrow R^{\text{ac}}$ the equations (D.15) and (D.10a) can be formally combined to

$$0 = \bar{\rho}_{ii} \sum_k \bar{R}_{ik} - \sum_k \bar{\rho}_{kk} \bar{R}_{ki}. \quad (\text{D.17})$$

Note, that if Σ is not zero, Def. (D.16) has to be slightly modified by the displacement $2d \rightarrow 2d - \hbar\Sigma/\Delta$ and then reads

$$R^{\text{ac}} = \frac{\Gamma}{(\hbar\Gamma/\Delta)^2 + (2d - \hbar\Sigma/\Delta)^2}. \quad (\text{D.18})$$

Note also, that if the additional phase factor χ in the non-diagonal terms of the Floquet matrix (3.33) at the avoided crossing are considered, this has an effect only on the non-diagonal density, which is then modified by the factor χ^* , i.e. $\bar{\rho}_{12} \rightarrow \chi^* \bar{\rho}_{12}$.

Equations (D.10b) and (D.10c) suggest that the maximum of $\text{Im}\bar{\rho}_{12}$ scales with γ^2 like the rates. From the comparison with (D.14) it follows that the occupation imbalance $(\bar{\rho}_{11} - \bar{\rho}_{22})$ at $d = 0$ scales with γ^4 , whereas $\text{Re}\bar{\rho}_{12}$ is exactly zero at $d = 0$.

E Rate equations at avoided crossings including Lamb shifts

In this section we derive the modified version of the effective rate equations at an avoided crossing. In contrast to Appendix D we explicitly include the Lamb shifts here. We take the rate equations (C.12) as our starting point, which take full account of the Lamb shifts, but are still represented in the adiabatic basis of the Floquet states $|u_i(t)\rangle$. Following the lines of Appendix D these equations are now expressed in the diabatic basis of states $|\bar{u}_i(t)\rangle$. By this change of representation, the last, coherent term of Eq. (C.12) has to be chosen according to the last, coherent term of Eq. (D.7). Under the same assumptions as in Appendix D, also the rate terms in Eqs. (D.7) are recovered, but now have to be extended by the corresponding Lamb shift terms (compare Eq. (B.56) with Eq. (C.12)), i.e. the rates $\bar{R}_{lj;ki}$ have to be replaced by the extended rates $\hat{R}_{lj;ki} = \bar{R}_{lj;ki} - i\bar{S}_{lj;ki}$, now of course referring to the diabatic representation. Under the assumptions of Appendix D several rates can again be neglected, such that the rate terms simplify, namely for $i = j \notin \{1, 2\}$ according to

$$\frac{1}{2} \sum_{k,l} \left(\bar{\rho}_{li} \hat{R}_{ik;lk} + \bar{\rho}_{il} \hat{R}_{ik;lk}^* - \bar{\rho}_{kl} \left(\hat{R}_{li;ki} + \hat{R}_{ki;li}^* \right) \right) \quad (\text{E.1})$$

$$\begin{aligned} &= \frac{1}{2} \sum_k \left(\bar{\rho}_{ii} (\bar{R}_{ik} - i\bar{S}_{ik}) + \bar{\rho}_{ii} (\bar{R}_{ik}^* + i\bar{S}_{ik}^*) - \bar{\rho}_{kk} (\bar{R}_{ki} - i\bar{S}_{ki} + \bar{R}_{ki}^* + i\bar{S}_{ki}^*) \right) \\ &= \bar{\rho}_{ii} \sum_k \bar{R}_{ik} - \sum_k \bar{\rho}_{kk} \bar{R}_{ki} \end{aligned} \quad (\text{E.2})$$

and for $i = j = 1$ and $i = j = 2$ according to

$$\frac{1}{2} \sum_{k,l} \left(\bar{\rho}_{l1} \hat{R}_{1k;lk} + \bar{\rho}_{1l} \hat{R}_{1k;lk}^* - \bar{\rho}_{kl} \left(\hat{R}_{l1;k1} + \hat{R}_{k1;l1}^* \right) \right) = \bar{\rho}_{11} \sum_k \bar{R}_{1k} - \sum_k \bar{\rho}_{kk} \bar{R}_{k1} \quad (\text{E.3})$$

$$\frac{1}{2} \sum_{k,l} \left(\bar{\rho}_{l2} \hat{R}_{2k;lk} + \bar{\rho}_{2l} \hat{R}_{2k;lk}^* - \bar{\rho}_{kl} \left(\hat{R}_{l2;k2} + \hat{R}_{k2;l2}^* \right) \right) = \bar{\rho}_{22} \sum_k \bar{R}_{2k} - \sum_k \bar{\rho}_{kk} \bar{R}_{k2} . \quad (\text{E.4})$$

Note, that in these equations for the diagonal densities the original rates \bar{R}_{ik} are recovered instead of the extended \hat{R}_{ik} . Solely in the remaining equation for $i = 1$ and $j = 2$, which determines the non-diagonal density $\bar{\rho}_{12}$, the Lamb shift contributions \bar{S}_{ik} are sustained,

$$\frac{1}{2} \sum_{k,l} \left(\bar{\rho}_{l2} \hat{R}_{1k;lk} + \bar{\rho}_{1l} \hat{R}_{2k;lk}^* - \bar{\rho}_{kl} \left(\hat{R}_{l2;k1} + \hat{R}_{k1;l2}^* \right) \right) \quad (\text{E.5})$$

$$\begin{aligned} &= \frac{1}{2} \sum_k \left(\bar{\rho}_{12} (\bar{R}_{1k} - i\bar{S}_{1k}) + \bar{\rho}_{12} (\bar{R}_{2k} + i\bar{S}_{2k}) - \bar{\rho}_{12} (\bar{R}_{22;11} - i\bar{S}_{22;11} + \bar{R}_{11;22}^* + i\bar{S}_{11;22}^*) \right) \\ &= \frac{1}{2} \bar{\rho}_{12} (\Gamma - i\Sigma) . \end{aligned} \quad (\text{E.6})$$

We have introduced the effective rates

$$\Gamma := \sum_k (\bar{R}_{1k} + \bar{R}_{2k}) - 2\text{Re}\bar{R}_{11;22} \quad (\text{E.7a})$$

$$\Sigma := \sum_k (\bar{S}_{1k} - \bar{S}_{2k}) - 2\text{Im}\bar{R}_{11;22} \quad (\text{E.7b})$$

and used $\bar{R}_{12} \approx \bar{R}_{21} \approx \bar{S}_{12} \approx \bar{S}_{21} \approx 0$ according to the premise (iv) in Appendix D. Besides, the properties $\bar{S}_{22;11} = \bar{S}_{11;22}^*$ and $\bar{R}_{22;11} + \bar{R}_{11;22}^* = 2\text{Re}\bar{R}_{11;22} - 2i\text{Im}\bar{R}_{11;22}$ have been employed in Eqs. (E.3)-(E.6). Combining the expressions (E.2)-(E.6) with the last, case-differentiated terms of Eq. (D.7) yields the set of equations

$$0 = \bar{\rho}_{ii} \sum_k \bar{R}_{ik} - \sum_k \bar{\rho}_{kk} \bar{R}_{ki} \quad (\text{E.8a})$$

$$0 = \bar{\rho}_{11} \sum_k \bar{R}_{1k} - \sum_k \bar{\rho}_{kk} \bar{R}_{k1} + \frac{\Delta}{\hbar} \text{Im}\bar{\rho}_{12} \quad (\text{E.8b})$$

$$0 = \bar{\rho}_{22} \sum_k \bar{R}_{2k} - \sum_k \bar{\rho}_{kk} \bar{R}_{k2} - \frac{\Delta}{\hbar} \text{Im}\bar{\rho}_{12} \quad (\text{E.8c})$$

$$0 = \frac{1}{2}\bar{\rho}_{12}\Gamma - i\frac{\Delta}{2\hbar} \left(\bar{\rho}_{11} - \bar{\rho}_{22} - \left(2d - \frac{\hbar\Sigma}{\Delta} \right) \bar{\rho}_{12} \right). \quad (\text{E.8d})$$

The last equation establishes the relation

$$\bar{\rho}_{12} = \frac{i\hbar\Gamma/\Delta + (2d - \hbar\Sigma/\Delta)}{(\hbar\Gamma/\Delta)^2 + (2d - \hbar\Sigma/\Delta)^2} (\bar{\rho}_{11} - \bar{\rho}_{22}) \quad (\text{E.9})$$

between the non-diagonal density $\bar{\rho}_{12}$ and the occupation imbalance $(\bar{\rho}_{11} - \bar{\rho}_{22})$ and suggests the modification of the effective rate to

$$R^{\text{ac}} := \frac{\Gamma}{\left(\frac{\hbar\Gamma}{\Delta}\right)^2 + \left(2d - \frac{\hbar\Sigma}{\Delta}\right)^2}. \quad (\text{E.10})$$

Substituting the negligible rates $\bar{R}_{12} \approx \bar{R}_{21} \approx 0$ by R^{ac} , the rate equations are again cast into the form

$$0 = \bar{\rho}_{ii} \sum_k \bar{R}_{ik} - \sum_k \bar{\rho}_{kk} \bar{R}_{ki}, \quad (\text{E.11})$$

where no case differentiation is needed. A comparison between the present definition (E.10) of R^{ac} and the definition (D.16) in the absence of Lamb shifts demonstrates, that the latter effectively displace the maximum of R^{ac} from $d = 0$ to $d = d^* := \hbar\Sigma/(2\Delta)$.

F Rate balance among the resonance states

This section aims to demonstrate the decoupling of the balance relation among the regular states $|\psi_{(ml)}\rangle$ of a nonlinear r : s -resonance leading to the independent detailed balance relations (4.47). The original detailed balance relation (4.6) is not adequate for the occupations $p_{(ml)}$ of the resonance states, since in addition to the nearest-neighbor rates $R_{(ml)(m\pm 1,l)}$ also the ‘internal’ rates $R_{(ml)(ml')}$ in the subspace of the r resonance states $l = 0, 1, \dots, r-1$ of fixed principal quantum number m are non-negligible. In analogy to Eq. (4.6) we consider only the dominant rates between states of successive principal quantum numbers, m and $m+1$, with the reduced balance condition

$$p_{(ml)} \left(\sum_{l'=0}^{r-1} R_{(ml)(ml')} + R_{(ml)(m+1,l)} \right) = \sum_{l'=0}^{r-1} p_{(ml')} R_{(ml')(ml)} + p_{(m+1,l)} R_{(m+1,l)(ml)}. \quad (\text{F.1})$$

Note, that the tiny rates $R_{(ml)(m+1,l')}$ and $R_{(m+1,l')(ml)}$ with $l \neq l'$ are already neglected in Eq. (F.1).

We recall that the r resonance states $l = 0, 1, \dots, r-1$ of fixed principal quantum number m have near degenerate values of the mean energy $\langle E_{(ml)} \rangle_\tau$ as well as of the occupation $p_{(ml)}$. Deviations from exact degeneracy of these values can be traced back to the influence of avoided crossings. Under the premise $p_{(ml)} \equiv p_m$, compare Eq. (4.46), the balance (F.1) can be cast into the form

$$\frac{p_{(m+1,l)}}{p_{(ml)}} = \frac{R_{(ml)(m+1,l)}}{R_{(m+1,l)(ml)}} + \frac{\sum_{l'=0}^{r-1} (R_{(ml)(ml')} - R_{(ml')(ml)})}{R_{(m+1,l)(ml)}}. \quad (\text{F.2})$$

We want to show that the second term, containing the ‘internal’ rates, vanishes. Firstly, the period r of the central periodic orbit of the resonance is assumed to be odd. The numerator in the last term of Eq. (F.2) can then be rewritten as

$$\begin{aligned} & \sum_{l'=0}^{r-1} (R_{(ml)(ml')} - R_{(ml')(ml)}) \\ &= \sum_{k=1}^{(r-1)/2} (R_{(ml)(m,l+k)} - R_{(m,l+k)(ml)} + R_{(ml)(m,l-k)} - R_{(m,l-k)(ml)}) \end{aligned} \quad (\text{F.3})$$

$$=: \sum_{k=1}^{(r-1)/2} G_{(mk)}, \quad (\text{F.4})$$

where the indices $k \pm l$ have to be taken modulo r . Since all rates in this expression refer to a fixed value of m , we omit the index m in the following. Inserting approximation (4.27) for the matrix elements $x_{ij}(K)$ into Def. (3.31) for the rates and using $g(-E) = g(E)e^{\beta E}$ the

G_k thus evaluate as

$$\begin{aligned}
\frac{4\pi^3}{(\hbar\omega)^2} G_k &= |x_{l,l+k}^0|^2 \left(1 - \cos 2\pi \frac{\varepsilon_{l,l+k}}{\hbar\omega}\right)^2 \sum_K \zeta_{l,l+k,K}^{-4} g(\zeta_{l,l+k,K}) e^{\beta\zeta_{l,l+k,K}} \\
&- |x_{l+k,l}^0|^2 \left(1 - \cos 2\pi \frac{\varepsilon_{l+k,l}}{\hbar\omega}\right)^2 \sum_K \zeta_{l+k,l,K}^{-4} g(\zeta_{l+k,l,K}) e^{\beta\zeta_{l+k,l,K}} \\
&+ |x_{l,l-k}^0|^2 \left(1 - \cos 2\pi \frac{\varepsilon_{l,l-k}}{\hbar\omega}\right)^2 \sum_K \zeta_{l,l-k,K}^{-4} g(\zeta_{l,l-k,K}) e^{\beta\zeta_{l,l-k,K}} \\
&- |x_{l-k,l}^0|^2 \left(1 - \cos 2\pi \frac{\varepsilon_{l-k,l}}{\hbar\omega}\right)^2 \sum_K \zeta_{l-k,l,K}^{-4} g(\zeta_{l-k,l,K}) e^{\beta\zeta_{l-k,l,K}} .
\end{aligned} \tag{F.5}$$

Since the resonance states $l = 0 \dots r-1$ have equidistant quasienergies with mutual spacing $\varepsilon_{l+1,l} = \hbar\omega s/r$, i.e. $\varepsilon_{l,l+k} = \varepsilon_{l-k,l} = -\varepsilon_{l,l-k} = -\varepsilon_{l+k,l}$ each of the cos-terms take the same value. Besides, $\zeta_{l,l+k,K} = \varepsilon_{l,l+k} + K\hbar\omega = \zeta_{l-k,l,K}$ and likewise $\zeta_{l+k,l,K} = \zeta_{l,l-k,K}$.

The matrix elements fulfill $|x_{l\pm k,l}^0|^2 = |x_{l,l\pm k}^0|^2$ and $|x_{l,l+k}^0|^2 = |x_{l,l-k}^0|^2$. The last identity follows from the semiclassical character of the resonance states

$$|u_{(ml)}(t)\rangle = \left(\sum_{j=0}^{r-1} |\tilde{u}_m^{(j)}(t)\rangle e^{i2\pi jls/r} \right) e^{ils/r\omega t}, \tag{F.6}$$

compare Eq. (2.79), which are linear combinations of the states $|\tilde{u}_m^{(j)}(t)\rangle$ localized on the r islands of the resonance chain. Since these have only exponentially small overlap for $j \neq j'$, one may presume $\langle \tilde{u}_m^{(j')}(t) | x | \tilde{u}_m^{(j)}(t) \rangle \sim \delta_{jj'}$ and finds

$$x_{l,l+k}(t) = \langle u_{(ml)}(t) | x | u_{(m,l+k)}(t) \rangle \tag{F.7}$$

$$= \left(\sum_{j,j'} \langle \tilde{u}_m^{(j')}(t) | x | \tilde{u}_m^{(j)}(t) \rangle e^{i2\pi(j(l+k)-j'l)s/r} \right) e^{iks/r\omega t} \tag{F.8}$$

$$\approx \left(\sum_j \langle \tilde{u}_m^{(j)}(t) | x | \tilde{u}_m^{(j)}(t) \rangle e^{i2\pi jks/r} \right) e^{iks/r\omega t} = x_{l,l-k}^*(t) \tag{F.9}$$

This confirms the above stated equality $|x_{l,l+k}^0|^2 = |x_{l,l-k}^0|^2$ and thus the first term in Eq. (F.5) cancels with the last, and likewise the two inner terms with each other, leading to $G_k = 0$.

Secondly, for a resonance stemming from a periodic orbit of even period r , the sum

$$\sum_{l'=0}^{r-1} (R_{(ml)(ml')} - R_{(ml')(ml)}) = \sum_{k=1}^{(r-1)/2} G_{(mk)} + (R_{(ml)(m,l+r/2)} - R_{(m,l+r/2)(ml)}) \tag{F.10}$$

contains an additional contribution, which also vanishes¹⁰: the relevant quasienergy spacings

¹⁰For the resonance with $s = 1, r = 4$, as discussed in Section 4.3.2, already the matrix element $|x_{l,l+r/2}^0|$ vanishes for symmetry reasons.

are $\varepsilon_{l+r/2,l} = \hbar\omega r/2 = \varepsilon_{l,l+r/2} + \hbar\omega$ and $\zeta_{l+r/2,l,K} = \zeta_{l,l+r/2,K+1}$. Defining $K' = K + 1$ in the rate $R_{(m,l+r/2)(ml)}$ this implies

$$(R_{l,l+r/2} - R_{l+r/2,l}) = |x_{l,l+r/2}^0|^2 \left(1 - \cos 2\pi \frac{\varepsilon_{l,l+r/2}}{\hbar\omega}\right)^2 \quad (\text{F.11})$$

$$\begin{aligned} & \cdot \left(\sum_K \zeta_{l,l+r/2,K}^{-4} g(\zeta_{l,l+r/2,K}) e^{\beta\zeta_{l,l+r/2,K}} \right. \\ & \quad \left. - \sum_{K'} \zeta_{l,l+r/2,K'}^{-4} g(\zeta_{l,l+r/2,K'}) e^{\beta\zeta_{l,l+r/2,K'}} \right) \\ & = 0 \end{aligned} \quad (\text{F.12})$$

In conclusion, the second term in Eq. (F.2) vanishes irrespective of r , such that the balance relation among the resonance states reduces to the r redundant detailed balance relations

$$\frac{p_{(m+1,l)}}{p_{(ml)}} = \frac{R_{(ml)(m+1,l)}}{R_{(m+1,l)(ml)}} \quad (\text{F.13})$$

for the occupations $p_{(m,l)} = p_m$, as used in Chapter 4 in Eq. (4.47).

References

- [1] S. Chu: *Laser manipulation of atoms and particles*, Science **253** (1991) 861–866.
- [2] F. Grossmann, T. Dittrich, P. Jung and P. Hänggi: *Coherent Destruction of Tunneling*, Phys. Rev. Lett. **67** (1991) 516–519.
- [3] S. A. Rice and M. Zhao: *Optical Control of Molecular Dynamics*, Wiley, New York, (2000).
- [4] A. Sethi and S. Keshavamurthy: *Bichromatically driven double well: Parametric perspective of the strong field control landscape reveals the influence of chaotic states*, J. Chem. Phys. **128** (2008) 164117 [8 pages].
- [5] J. L. Krause, M. Shapiro and P. Brumer: *Coherent control of bimolecular chemical reactions*, J. Chem. Phys. **92** (1990) 1126–1131.
- [6] A. Assion, T. Baumert, M. Bergt, T. Brixner, B. Kiefer, V. Seyfried, M. Strehle and G. Gerber: *Control of Chemical Reactions by Feedback-Optimized Phase-Shaped Femtosecond Laser Pulses*, Science **282** (1998) 919–922.
- [7] P. Brumer and M. Shapiro: *Principles of the Quantum Control of Molecular Processes*, Wiley-VCH, Berlin, (2003).
- [8] R. T. Philips, ed.: *Coherent Optical Interactions in Semiconductors*, vol. 330 of *NATO ASI Ser. B*, Plenum Press, New York, (1994).
- [9] A. P. Heberle, J. J. Baumberg and K. Köhler: *Ultrafast Coherent Control and Destruction of Excitons in Quantum Wells*, Phys. Rev. Lett. **75** (1995) 2598–2601.
- [10] T. Flissikowski, A. Betke, I. A. Akimov and F. Henneberger: *Two-Photon Coherent Control of a Single Quantum Dot*, Phys. Rev. Lett. **92** (2004) 227401 [4 pages].
- [11] M. B. Plenio and P. L. Knight: *The quantum-jump approach to dissipative dynamics in quantum optics*, Rev. Mod. Phys. **70** (1998) 101–144.
- [12] C. W. Gardiner and P. Zoller: *Quantum Noise*, Springer Series in Synergetics, Springer, Berlin, 3rd edn., (2004).
- [13] H.-P. Breuer and F. Petruccione: *Dissipative quantum systems in strong laser fields: Stochastic wave-function method and Floquet theory*, Phys. Rev. A **55** (1997) 3101–3116.
- [14] M. Grifoni, M. Sassetti, J. Stockburger and U. Weiss: *Nonlinear response of a periodically driven damped two-state system*, Phys. Rev. E **48** (1993) 3497–3509.

- [15] M. Grifoni, M. Sasseti, P. Hänggi and U. Weiss: *Cooperative effects in the nonlinearly driven spin-boson system*, Phys. Rev. E **52** (1995) 3596–3607.
- [16] R. Graham and R. Hübner: *Generalized Quasi-Energies and Floquet States for a Dissipative System*, Ann. Phys. (N.Y.) **234** (1994) 300–315.
- [17] C. Zerbe and P. Hänggi: *Brownian parametric quantum oscillator with dissipation*, Phys. Rev. E **52** (1995) 1533–1543.
- [18] P. A. Miller and S. Sarkar: *Entropy production, dynamical localization and criteria for quantum chaos in the open quantum kicked rotor*, Nonlinearity **12** (1999) 419–442.
- [19] J. Shao, M.-L. Ge and H. Cheng: *Decoherence of quantum-nondemolition systems*, Phys. Rev. E **53** (1996) 1243–1245.
- [20] M. Grifoni and P. Hänggi: *Driven Quantum Tunneling*, Phys. Rep. **304** (1998) 229–354.
- [21] R. Blümel, A. Buchleitner, R. Graham, L. Sirko, U. Smilansky and H. Walther: *Dynamical localization in the microwave interaction of Rydberg atoms: The influence of noise*, Phys. Rev. A **44** (1991) 4521–4540.
- [22] S. Kohler, T. Dittrich and P. Hänggi: *Floquet-Markovian description of the parametrically driven, dissipative harmonic quantum oscillator*, Phys. Rev. E **55** (1997) 300–313.
- [23] H.-P. Breuer, W. Huber and F. Petruccione: *Quasistationary distributions of dissipative nonlinear quantum oscillators in strong periodic driving fields*, Phys. Rev. E **61** (2000) 4883–4889.
- [24] W. Kohn: *Periodic Thermodynamics*, J. Stat. Phys. **103** (2001) 417–423.
- [25] D. W. Hone, R. Ketzmerick and W. Kohn: *Statistical mechanics of Floquet systems: the pervasive problem of near degeneracies*, Phys. Rev. E **79** (2009) 051129 [13 pages].
- [26] M. Thorwart, M. Grifoni and P. Hänggi: *Strong Coupling Theory for Tunneling and Vibrational Relaxation*, Phys. Rev. Lett. **85** (2000) 860–863.
- [27] M. Thorwart, M. Grifoni and P. Hänggi: *Strong coupling theory for tunneling and vibrational relaxation in driven bistable systems*, Ann. Phys. (N.Y.) **293** (2001) 15–66.
- [28] K. Husimi: *Miscellanea in Elementary Quantum Mechanics, II*, Progress of Theoretical Physics **9** (1953) 381–402.

- [29] T. Dittrich, P. Hänggi, G.-L. Ingold, B. Kramer, G. Schön and W. Zwerger: *Quantum Transport and Dissipation*, Wiley-VCH, Weinheim, (1998).
- [30] I. C. Percival: *Regular and irregular spectra*, J. Phys. B: Atomic and Molecular Physics **6** (1973) L229–L232.
- [31] M. V. Berry: *Regular and irregular semiclassical wavefunctions*, J. Phys. A **10** (1977) 2083–2091.
- [32] A. Voros: *Semi-classical ergodicity of quantum eigenstates in the Wigner representation*, in: *Stochastic Behavior in Classical and Quantum Hamiltonian Systems*, vol. 93 of *Lecture Notes in Physics*, Springer, Berlin, (1979).
- [33] M. V. Berry and M. Tabor: *Level clustering in the regular spectrum*, Proc. R. Soc. London Ser. A (1977) 356–375–394.
- [34] O. Bohigas, M.-J. Giannoni and C. Schmit: *Characterization of chaotic quantum spectra and universality of level fluctuation laws*, Phys. Rev. Lett. (1984) 52 1–4.
- [35] J. S. Howland: *Floquet operators with singular spectrum*, Ann. Inst. Henri Poincaré Phys. Theor. **49** (1989) 309–323.
- [36] D. W. Hone, R. Ketzmerick and W. Kohn: *Time-dependent Floquet theory and absence of an adiabatic limit*, Phys. Rev. A **56** (1997) 4045–4054.
- [37] R. Ketzmerick and W. Wustmann: *Switching mechanism in periodically driven quantum systems with dissipation*, Phys. Rev. E **80** (2009) 021117 [5 pages].
- [38] V. Romero-Rochin and I. Oppenheim: *Relaxation properties of two-level systems in condensed phases*, Physica A: Statistical and Theoretical Physics **155** (1989) 52–72.
- [39] E. Geva, E. Rosenman and D. Tannor: *On the second-order corrections to the quantum canonical equilibrium density matrix*, J. Chem. Phys. **113** (2000) 1380–1390.
- [40] E. Kierig, U. Schnorrberger, A. Schietinger, J. Tomkovic and M. K. Oberthaler: *Single-Particle Tunneling in Strongly Driven Double-Well Potentials*, Phys. Rev. Lett. **100** (2008) 190405 [4 pages].
- [41] J. H. Shirley: *Solution of the Schrödinger Equation with a Hamiltonian Periodic in Time*, Phys. Rev. **138** (1965) B979–B987.
- [42] G. Floquet: *Sur les équations différentielles linéaires à coefficients périodiques*, Ann. É. N. S. **12** (1883) 47–88.
- [43] M. Tabor: *Chaos and integrability in nonlinear dynamics*, Wiley, New York, (1989).

- [44] A. J. Lichtenberg and M. A. Leiberman: *Regular and Chaotic Dynamics*, vol. 38 of *Applied Mathematical Sciences*, Springer, New York, 2nd edn., (1992).
- [45] H.-J. Stöckmann: *Quantum Chaos*, Cambridge University Press, Cambridge, (1999).
- [46] J. K. Hale: *Ordinary differential equations*, vol. 21 of *Pure and applied mathematics*, Wiley-Interscience, New York, (1969).
- [47] G. Birkhoff and G.-C. Rota: *Ordinary differential equations*, Wiley, New York, 4th edn., (1989).
- [48] H. Sambé: *Steady States and Quasienergies of a Quantum-Mechanical System in an Oscillating Field*, Phys. Rev. A **7** (1973) 2203–2213.
- [49] K. Drese and M. Holthaus: *Floquet theory for short laser pulses*, The European Physical Journal D - Atomic, Molecular, Optical and Plasma Physics **5** (1999) 119–134.
- [50] P. Pfeifer and R. D. Levine: *A stationary formulation of time-dependent problems in quantum mechanics*, J. Chem. Phys **79** (1983) 5512–5519.
- [51] U. Peskin and N. Moiseyev: *The Solution of the Time-Dependent Schrödinger Equation by the (t, t') Method: Theory, Computational Algorithm and Applications*, J. Chem. Phys **99** (1993) 4590–4596.
- [52] B. V. Chirikov: *A universal instability of many-dimensional oscillator systems*, Phys. Rep. **52** (1979) 263–379.
- [53] G. Casati, B. V. Chirikov, F. M. Izraelev and J. Ford: *Stochastic behaviour of a quantum pendulum under a periodic perturbation*, in: *Stochastic Behaviour in Classical and Quantum Hamiltonian Systems* (Eds. C. Casati and J. Ford), vol. 93 of *Lecture Notes in Physics*, Springer, Berlin, (1979).
- [54] J. P. Keating, F. Mezzadri and J. M. Robbins: *Quantum boundary conditions for torus maps*, Nonlinearity **12** (1999) 579–591.
- [55] L. Schilling: *Direct dynamical tunneling in systems with a mixed phase space*, PhD dissertation, Technische Universität Dresden, (2006).
- [56] S. J. Chang and K. J. Shi: *Evolution and exact eigenstates of a resonant quantum system*, Phys. Rev. A **34** (1986) 7–22.
- [57] K. Husimi: *Some formal properties of the density matrix*, Proc. Phys. Math. Soc. Jpn. **22** (1940) 264–314.
- [58] W. P. Schleich: *Quantum Optics in Phase Space*, Wiley-VCH, Berlin, (2001).

- [59] H.-P. Breuer and M. Holthaus: *A Semiclassical Theory of Quasienergies and Floquet Wave Functions*, Ann. Phys. (N.Y.) **211** (1991) 249–291.
- [60] F. Bensch, H. J. Korsch, B. Mirbach and N. Ben-Tal: *EBK quantization of quasi-energies*, J. Phys. A: Math. Gen. **25** (1992) 6761–6777.
- [61] Tabor: *A semiclassical quantization of area-preserving maps*, Physica **6D** (1983) 195–210.
- [62] M. V. Berry, N. L. Balazs, M. Tabor and A. Voros: *Quantum Maps*, Ann. Phys. **122** (1979) 26–63.
- [63] V. P. Maslov and M. V. Fedoriuk: *Semi-classical approximation in quantum mechanics*, Reidel Publishing, Dordrecht, (1981).
- [64] R. G. Littlejohn: *The Van Vleck Formula, Maslov Theory, and Phase Space Geometry*, J. Stat. Phys. **68** (1992) 7–50.
- [65] J. Laskar, C. Froeschlé and A. Celletti: *The measure of chaos by the numerical analysis of the fundamental frequencies. Application to the standard mapping*, Physica D: Nonlinear Phenomena **56** (1992) 253–269.
- [66] B. Mirbach and H. J. Korsch: *Semiclassical quantization of KAM resonances in time-periodic systems*, J. Phys. A: Math. Gen. **27** (1994) 6579–6604.
- [67] R. Kubo, M. Toda and N. Hashitsume: *Statistical Physics II*, Springer, Berlin, (1985).
- [68] C. Cohen-Tannoudji: *Atoms in electromagnetic fields*, vol. 1 of *World Scientific series on atomic, molecular, and optical physics*, World Scientific, Singapore, (1994).
- [69] U. Weiss: *Quantum Dissipative Systems*, vol. 10 of *Series in Modern Condensed Matter Physics*, World Scientific, Singapore, 2nd edn., (1999).
- [70] G. W. Ford, J. T. Lewis and R. F. O’Connell: *Quantum Langevin equation*, Phys. Rev. A **37** (1988) 4419–4428.
- [71] A. O. Caldeira and A. J. Leggett: *Influence of Dissipation on Quantum Tunneling in Macroscopic Systems*, Phys. Rev. Lett. **46** (1981) 211–214.
- [72] R. Zwanzig: *Nonlinear Generalized Langevin Equations*, J. Stat. Phys. **9** (1973) 215–220.
- [73] G. W. Ford and M. Kac: *On the Quantum Langevin Equation*, J. Stat. Phys. **46** (1987) 803–810.

- [74] S. Kohler, R. Utermann, P. Hänggi and T. Dittrich: *Coherent and incoherent chaotic tunneling near singlet-doublet crossings*, Phys. Rev. E **58** (1998) 7219–7230.
- [75] S. Kohler: *The interplay of chaos and dissipation in driven quantum systems*, PhD dissertation, Universität Augsburg, (1999).
- [76] J. v. Neumann and E. Wigner: *Über das Verhalten von Eigenwerten bei adiabatischen Prozessen*, Physik. Zeitschrift **30** (1929) 467–470.
- [77] H. Carmichael: *An Open Systems Approach to Quantum Optics*, vol. 18 of *Lecture Notes in Physics: New Series M*, Springer, Berlin, (1993).
- [78] D. T. Gillespie: *Exact stochastic simulation of coupled chemical reactions*, J. Phys. Chem. **81** (1977) 2340–2361.
- [79] C. W. Gardiner: *Handbook of Stochastic Methods*, Springer Series in Synergetics, Springer, Berlin, 3rd edn., (2004).
- [80] L. D. Landau and E. M. Lifschitz: *Mechanik*, vol. 1 of *Lehrbuch der Theoretischen Physik*, Verlag Harri Deutsch, Frankfurt am Main, 14th edn., (1997).
- [81] L. D. Landau, E. M. Lifschitz and L. P. Pitajewski: *Statistische Physik, Teil 1*, vol. V of *Lehrbuch der Theoretischen Physik*, Akademie-Verlag, Berlin, 8th edn., (1987).
- [82] S. D. Frischat and E. Doron: *Dynamical tunneling in mixed systems*, Phys. Rev. E **57** (1998) 1421–1443.
- [83] O. Bohigas, S. Tomsovic and D. Ullmo: *Dynamical quasidegeneracies and separation of regular and irregular quantum levels*, Phys. Rev. Lett. **64** (1990) 1479–1482.
- [84] R. S. MacKay, J. D. Meiss and I. C. Percival: *Transport in Hamiltonian systems*, Physica **13D** (1984) 55–81.
- [85] J. D. Meiss: *Symplectic maps, variational principles, and transport*, Rev. Mod. Phys. **64** (1992) 795–848.
- [86] R. Ketzmerick, L. Hufnagel, F. Steinbach and M. Weiss: *New Class of Eigenstates in Generic Hamiltonian Systems*, Phys. Rev. Lett. **85** (2000) 1214–1217.
- [87] S. Fishman, D. R. Grempel and R. E. Prange: *Chaos, Quantum Recurrences, and Anderson Localization*, Phys. Rev. Lett. **49** (1982) 509–512.
- [88] D. R. Grempel, R. E. Prange and S. Fishman: *Quantum dynamics of a nonintegrable system*, Phys. Rev. A **29** (1984) 1639–1647.

- [89] D. L. Shepelyansky: *Localization of quasienergy eigenfunctions in action space*, Phys. Rev. Lett. **56** (1986) 677–680.
- [90] G. Casati, J. Ford, I. Guarneri and F. Vivaldi: *Search for randomness in the kicked quantum rotator*, Phys. Rev. A **34** (1986) 1413–1419.
- [91] B. V. Chirikov, F. M. Izrailev and D. L. Shepelyansky: *Dynamical stochasticity in classical and quantum mechanics*, Sov. Sci. Rev. C **2** (1981) 209–267.
- [92] T. Dittrich and G. Graham: *Long time behavior in the quantized standard map with dissipation*, Ann. Phys. (N.Y.) **200** (1990) 363–421.
- [93] S. R. de Groot and P. Mazur: *Non-equilibrium thermodynamics*, North Holland, Amsterdam, (1963).
- [94] R. Klages: *Microscopic Chaos, Fractals, and Transport in Nonequilibrium Steady States*, Habilitation, Max Planck Institut für Physik komplexer Systeme, Dresden, (2004).
- [95] Y. Makhlin, G. Schön and A. Shnirman: *Quantum-state engineering with Josephson-junction devices*, Rev. Mod. Phys. **73** (2001) 357–400.
- [96] I. H. Deutsch, P. M. Alsing, J. Grondalski, S. Ghose, D. L. Haycock and P. S. Jessen: *Quantum transport in magneto-optical double-potential wells*, J. Opt. B: Quantum Semiclass. Opt. **2** (2000) 633–644.
- [97] R. Lü and J. von Delft: *Angular-dependent spin tunneling in mesoscopic biaxial anti-ferromagnets*, Phys. Rev. B **67** (2003) 104425 [12 pages].
- [98] A. Douhal, F. Lahmani and A. H. Zewail: *Proton-transfer reaction dynamics*, Chem. Phys. **207** (1996) 477–498.
- [99] H. Adam, M. Winterstetter, M. Grifoni and U. Weiss: *Driving-Induced Symmetry Breaking in the Spin-Boson System*, Phys. Rev. Lett. **83** (1999) 252–255.
- [100] M. C. Goorden, M. Thorwart and M. Grifoni: *Entanglement Spectroscopy of a Driven Solid-State Qubit and Its Detector*, Phys. Rev. Lett. **93** (2004) 267005 [4 pages].
- [101] I. Goychuk and P. Hänggi: *Quantum dynamics in strong fluctuating fields*, Adv. in Physics **54** (2005) 525–584.
- [102] T. M. Stace, A. C. Doherty and S. D. Barrett: *Population Inversion of a Driven Two-Level System in a Structureless Bath*, Phys. Rev. Lett. **95** (2005) 106801 [4 pages].

-
- [103] M. Thorwart and P. Jung: *Dynamical Hysteresis in Bistable Quantum Systems*, Phys. Rev. Lett. **78** (1997) 2503–2506.
- [104] P. Thorwart, M. Reimann, P. Jung and R. F. Fox: *Dynamical Hysteresis in Bistable Quantum Systems*, Phys. Lett. A **239** (1998) 233–238.
- [105] P. Thorwart, M. Reimann, P. Jung and R. F. Fox: *Quantum hysteresis and resonant tunneling in bistable systems*, Chem. Phys. **235** (1998) 61–80.
- [106] J. Casas-Vázquez and D. Jou: *Temperature in non-equilibrium states: a review of open problems and current proposals*, Rep. Prog. Phys. **66** (2003) 1937–2023.
- [107] H. H. Rugh: *Dynamical Approach to Temperature*, Phys. Rev. Lett. **78** (1997) 772–774.
- [108] G. P. Morriss and L. Rondoni: *Definition of temperature in equilibrium and nonequilibrium systems*, Phys. Rev. E **59** (1999) R5–R8.
- [109] P. Jung and P. Hänggi: *Invariant measure of a driven nonlinear oscillator with external noise*, Phys. Rev. Lett. **65** (1990) 3365–3368.
- [110] S. Denisov, P. Hänggi and J. L. Mateos: *AC-driven Brownian motors: A Fokker-Planck treatment*, American Journal of Physics **77** (2009) 602–606.
- [111] L. E. Reichl: *A Delta-Kicked Brownian Rotor*, J. Stat. Phys. **70** (1993) 213–228.
- [112] R. P. Feynman and F. L. Vernon: *The theory of a general quantum system interacting with a linear dissipative system*, Ann. Phys.(N.Y.) **24** (1963) 118–173.
- [113] G. Lindblad: *On the Generators of Quantum Dynamical Semigroups*, Commun. math. Phys. **48** (1976) 119–130.

Acknowledgments

It is a pleasure to thank Prof. Dr. Roland Ketzmerick for entrusting me with the subject of this study. With many suggestions and instructive directions he gave important impulses to this work.

Among my colleagues in the Computational Physics group, whose friendly and encouraging atmosphere I highly appreciate, it is difficult to single out particular persons for acknowledgement. Many valuable discussions with Steffen Löck and Martin Richter have supported me, as well as helpful advice from Dr. Arnd Bäcker, Matthias Michler and Lars Bittrich. I am also grateful to Martin Richter, Steffen Löck, Matthias Michler, and Norman Mertig for proof-reading selected chapters. Besides, I thank Dr. Philip Brydon for encouragement and many suggestions to improve the English of this thesis.

As a participant of the International Max Planck Research School ‘Dynamical Processes in Atoms, Molecules and Solids’ I took advantage of the exchange with other fellow students and the participation in interesting summer schools.

Finally, I would especially like to thank my parents for their constant support and encouragement during the last years.

The graphics in this thesis were generated with the software P_YXGraph which simplifies the usage of P_YX (<http://pyx.sourceforge.net/>). The numerical computations were implemented in Python (<http://www.python.org>), in particular using NumPy and SciPy (<http://www.scipy.org>).

Erklärung

Hiermit versichere ich, dass ich die vorliegende Arbeit ohne unzulässige Hilfe Dritter und ohne Benutzung anderer als der angegebenen Hilfsmittel angefertigt habe; die aus fremden Quellen direkt oder indirekt übernommenen Gedanken sind als solche kenntlich gemacht. Die Arbeit wurde bisher weder im Inland noch im Ausland in gleicher oder ähnlicher Form einer anderen Prüfungsbehörde vorgelegt.

Die Dissertation wurde in der Zeit vom Januar 2007 bis zum Januar 2010 unter der Betreuung von Herrn Prof. Dr. Roland Ketzmerick am Institut für Theoretische Physik der Technischen Universität Dresden angefertigt. Es haben keine früheren erfolglosen Promotionsverfahren stattgefunden. Ich erkenne die Promotionsordnung der Fakultät Mathematik und Naturwissenschaften an der Technischen Universität Dresden vom 20. März 2000 an.

Dresden, den 3. Februar 2010

Waltraut Wustmann